The measurement of characteristics of a three dimensional density current. April 1966.

Author:
Fietz, T. R.

Publication details:
Report No. UNSW Water Research Laboratory Report No. 85

Publication Date:
1966

DOI:
https://doi.org/10.4225/53/5796cd56a778a

THE UNIVERSITY OF NEW SOUTH WALES

WATER RESEARCH LABORATORY

Manly Vale, N.S.W., Australia

REPORT No. 85

The Measurement of Characteristics of a Three Dimensional Density Current

by

T. R. Fietz

https://doi.org/10.4225/53/5796cd56a778a

APRIL, 1966

The University of New South Wales

School of Civil Engineering

THE MEASUREMENT OF CHARACTERISTICS OF A THREE DIMENSIONAL DENSITY CURRENT

by

T. R. Fietz

Report No. 85

April 1966.

PREFACE

The study of characteristics of a three dimensional density current is part of the more general field of the theory of flow of density currents with small density difference. Extension of fundamental knowledge of fluid flow of this kind has formed an integral part of the Water Research Laboratory programme of unsponsored research during the last four years.

R. T. Hattersley,
Senior Lecturer in Civil Engineering,
Officer-in-Charge,
Water Research Laboratory.

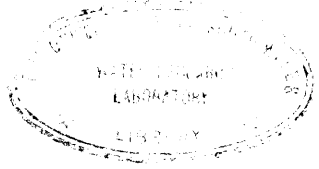

Summary

This report describes an experimental investigation of a three dimensional non-suspension type density current. The density current was modelled by releasing saltwater, as the denser fluid, from an orifice at the top of a downward sloping plane boundary which was immersed in a tank of freshwater. This freshwater served as the lighter miscible fluid.

The flow regime, lateral spread and normal spread has been examined for a range of cases on boundary slopes of 10^{o} and 20^{o}. When the flow is turbulent, and the difference in density between the injected and the ambient fluid is small, it is shown that the Richardson Number at the orifice is a sufficient criterion for predicting the behaviour of the flow.

The development of instruments for measuring the mean velocity and density at a point in the density current has been described in detail. These instruments have been used to obtain measurements at three cross sections of a turbulent density current on a boundary slope of 20^{o}.

The usual self preservation assumption for axisymmetric or two dimensional free turbulent flows has been extended to apply to the asymmetric cross section of a three dimensional density current. The velocity and density profiles for the three cross sections investigated have been presented on dimensionless diagrams on the basis of this extension. It is found that the velocity profiles are self preserving in the outer region of the flow while the density profiles are approximately self preserving in this region. Neither the velocity nor the density profiles are self preserving in the inner region adjacent to the boundary plane.

The variation of characteristic velocity, density, width and height scales at a cross section with distance from the orifice has been examined. The resulting relations have been compared with those predicted for a fully turbulent flow by dimensional analysis in conjunction with the self preservation assumption. It is suggested that the disparity between the measured and predicted relations may be due to the turbulence damping effect of the steep density gradient occurring in the inner region of the flow adjacent to the boundary plane.

The entrainment constant was found to decrease and the Local Richardson Number to increase in the direction of flow. This contrasts with the two dimensional case where both parameters remain constant throughout the flow.

Table of Contents

Table of Contents(cont'd.)

List of Illustrations

List of Illustrations (cont'd.)

List of Illustrations (cont'd.)

List of Illustrations (cont'd.)

List of Tables.

Acknowledgments

The investigation was carried out under the supervision of Mr. I. R. Wood at the Water Research Laboratory of the University of New South Wales. His guidance during the course of the project has been genuinely appreciated. Thanks are also extended to the other members of the Laboratory staff, and in particular to Mr. A. Baxter for making the instruments; Mrs. P. Decent for typing; Mrs. P. Auld for tracing; and Mr. W. T. Spurge for printing.

Mr. G. Johnson of the School of Electrical Engineering, advised on the design of the electronics. Mr. D. Hattersley advised on the use of epoxy resin.

Chapter I: Introduction and Theoretical Analysis.

1.1 Introduction

The term density current refers to the gravity induced flow of a fluid which is of slightly different density to its surroundings. The slight density difference may be due to dissolved chemical substances or a temperature difference in which case the density current is a "non-suspension" type. Ellison and Turner (Ref. 31) have reviewed some of the situations in nature where non-suspension density currents occur and these include the flow of katabatic winds in the atmosphere; the flow of cold water on the ocean floor from arctic to equatorial regions; and the flow of methane along the roof of a mine gallery. The spread of hot water on the surface of a power station cooling pond and the spread of fresh water over the ocean in the vicinity of the mouth of a flooded river represent a limiting case of a density current where the boundary plane is horizontal.

A density difference may also be caused by particles in suspension, giving rise to a "suspension" type density current or "turbidity current". Turbidity currents are more complex than non-suspension density currents in that the density difference may be large and also the current may deposit particles or gain particles by erosion. Johnson (Ref. 54) has argued that, in certain cases, data

from non-suspension density currents may be used to predict the flow of turbidity currents. Turbidity currents are of engineering interest in such problems as reservoir sedimentation and oceanic disposal of inert industrial wastes, for example power station ash (Ref. 34).

The present investigation is concerned with the three dimensional non-suspension density current formed by emission from a point source at the top of a downward sloping floor of a fluid which is slightly denser than its surrounding fluid. Alternatively a similar current is formed by release of a lighter fluid at the bottom of an upward sloping roof. The corresponding two dimensional case has been investigated by Ellison and Turner (Ref. 31) but to date no experimental investigation of the three dimensional case has been attempted.

The velocity and density are the physical quantities of most interest within the density current and the measurement of these quantities (particularly the velocity) is difficult in small laboratory experiments. Hence a considerable part of this investigation is concerned with development of suitable instruments for measuring velocity and density at a point in a laboratory model of a three dimensional density current. The remainder of the report describes detailed measurements of a typical turbulent density current and some exploratory measurements of flow regime, lateral spread etc. of several density currents on a gently sloping floor.

1.2 Review of Previous Related Work

Investigation of the present case of a three dimensional density current has not been previously attempted but it is appropriate to review the research on generally similar flows.

Rouse, Yih and Humphreys investigated an axisymmetric turbulent plume rising from a point source of buoyancy and a two dimensional plume from a line source (Ref. 88). The plumes were "neutral" in that the angle of spread was small so that the density gradient in the vertical direction across the interface between the plume and the ambient fluid was negligible and did not inhibit turbulent mixing. The virtual origin was assumed to coincide with the source of buoyancy. By commencing with the differential equations of motion and continuity and assuming dynamic or self-similarity for distribution of velocity, unit weight difference and shear stress Rouse et al showed for an axisymmetric plume that:

$$b \propto x$$

$$v_{x\,max} \propto x^{-1/3}$$

$$\Delta\gamma_{max} \propto x^{-5/3}$$

where:

(i) b is a linear characteristic of the velocity profile $v_x = v_x(r)$, such as the radius r where $\frac{v_x}{v_{x\,max}} = 0.5$ say;

(ii) x, r are cylindrical polar co-ordinates;

(iii) $v_{x\ max}$ is the maximum velocity at a cross section distance x from the virtual origin;

(iv) $\Delta\gamma_{max}$ is the maximum unit weight difference at cross section distance x from the virtual origin.

Measurements of velocity and temperature in several plumes verified the self similarity assumptions for the velocity and unit weight difference profiles. Rouse et al then fitted normal probability curves to the measured profiles and utilised the resulting expressions to plot dimensionless charts of $\frac{\Delta\gamma}{\bar{\gamma}}$ = constant and stream function ψ = constant curves. The latter streamlines within the plume proper are shown parallel to the x axis, that is the velocity has no radial component within the plume.

Morton, Taylor and Turner have investigated turbulent axisymmetric and line source plumes from maintained and instantaneous sources of buoyancy in both stably stratified and uniform density ambient fluid (Ref. 73). The axisymmetric plume in uniform ambient density fluid is of interest for the present project.

By commencing with the differential equations expressing conservation of volume, momentum and density deficiency at a height x above the point source of buoyancy, Morton et al showed that:

$$b = f_1(E)\, x$$

$$\bar{v}_x = f_2(E,G)\, x^{-1/3} \qquad (2)$$

$$\frac{\Delta\rho}{\rho} g = f_3(E,G)\, x^{-5/3}$$

where (i) b, $\bar{v}_x$ and $\frac{\Delta\rho}{\rho}$ are the width, velocity and density scales respectively at an x = constant cross section through the jet;

(ii) f_1, f_2, f_3 are known functions;

(iii) E is the entrainment constant relating the velocity of inflow of entrained ambient fluid to the velocity scale, and defined by:

$$E = \frac{\frac{d}{dx}(\pi b^2 \bar{v}_x)}{2\pi b \bar{v}_x} \qquad (3a)$$

(iv) G is the vertical flux of unit weight difference, defined by:

$$G = b^2 \bar{v}_x g \frac{\Delta\rho}{\rho} = \text{Constant} \qquad (3b)$$

Although Morton et al showed that $b \propto x$ (i.e. linear spread) etc. the angle of spread obtainable from $b = f_1(E)x$, can only be found by using experimentally determined values of E. Determination of exact values of E is very difficult.

On substituting the relations for b(x), $\bar{v}_x(x)$ etc. in the expression for E it is seen that $E \propto x^0$, that is E is constant throughout the plume. From experimental plumes formed by releasing dyed methylated spirits in a tank of saltwater Morton et al estimated that E = 0.085.

Morton (Ref. 74) extended the work of Morton, Taylor and Turner (Ref. 73) to include "forced plumes". He differentiated between three fields of motion: the jet, which is a flow of zero density difference and resulting from introduction of a momentum flux only; the plume, which is a density difference flow resulting from introduction of a flux of density difference only; and the forced plume where momentum effects predominate near the source while buoyancy effects predominate away from the source. This forcing of a plume was treated by Morton in terms of a shift in the virtual origin. His theoretical analysis for an axisymmetric plume was similar to that of Morton et al (Ref. 73) except that account was taken of the greater lateral spread of density difference than the vertical momentum at a jet cross section. The horizontal length scale b at a cross section was multiplied by a constant for the terms involving density difference. The constant was found to be 1.15 by analysing Rouse et al's (Ref. 88) data.

Probably the most pertinent work related to the present project is the investigation of a two dimensional turbulent wall plume by Ellison and Turner (Ref. 31). Using cartesian co-ordinates, with x in the direction of flow and y normal to the sloping floor, the velocity, length and density scales at a cross section were defined by:

$$Vh = \int_0^\infty v_x \, dy$$

$$V^2 h = \int_0^\infty v_x^2 \, dy$$

$$G = \int_0^\infty \frac{\Delta\rho}{\rho} g v_x \, dy = V h \Delta = \text{Constant} \qquad (4)$$

, where v(x), h(x) and $\frac{\Delta(x)}{g}$ are the velocity, length and density scales respectively, and G is the flux of unit weight difference, which is constant from continuity considerations. Other symbols are consistent with present notation.

The entrainment constant E is then given by:

$$E = \frac{1}{V} \frac{d}{dx}(hV) \qquad (5)$$

and from dimensional analysis:

$$E = \phi \ (R_{i-}, \ \frac{\Delta\rho}{\rho}, \ \text{Reynolds Number})$$

so that for $\frac{\Delta\rho}{\rho}$ small and a fully turbulent plume $E = \phi(R_{i-})$ only. R_{i-} is the Local Richardson number at a cross section defined by:

$$R_{i-} = \frac{\Delta h \cos S}{V^2} = \frac{G \cos S}{V^3} \qquad (6)$$

The expressions for E and R_{i-} were then substituted in the integrated equation of motion in the x direction and, after making the assumption of self similarity of velocity and density profiles, expressions for $\frac{dh}{dx}$ and $\frac{dR_{i-}}{dx}$ were obtained. Using measured values of $E(R_{i-})$ obtained subsequently in the expression for $\frac{dh}{dx}$ and $\frac{dR_{i-}}{dx}$ Ellison and Turner then showed that within a short distance of the source $\frac{dR_{i-}}{dx}$ becomes zero and thereafter $R_{i-} = R_{in}$, the Normal

Richardson Number, which is a function of the boundary slope and the boundary friction. Thus the zone of established flow of a two dimensional wall plume is analagous to gradually varied flow in a steep open channel in hydraulics; if the flow starts too fast it rapidly decelerates till the gravity component is exactly balanced by floor friction and the momentum spreading to the entrained ambient fluid. Similarly if the flow starts too slowly it rapidly accelerates till equilibrium is attained.

Rapid attainment of R_{in} has several implications:-

(i) From the definition of R_{i}- it is seen that for a given slope S the velocity V is constant throughout the plume and depends on the flux of unit weight difference G only. Hence from the definition of the entrainment constant E it follows $E = \frac{dh}{dx}$;

(ii) For fully developed turbulence $R_{in} = R_{in}(S)$ only and, as $E=E(R_{in})$, it follows that $E = E(S)$ only;

(iii) Constancy of E for a given slope results in $\frac{dh}{dx}$ = constant, (from $E = \frac{dh}{dx}$), that is the jet spreads linearly.

Following some inconclusive experiments with a surface jet of fresh water passing over a body of salt water the main experimental work was carried out in a tilting closed channel. The channel was filled with fresh water and a two dimensional plume formed by releasing saltwater through a rectangular slot at the upper end. "Make-up" fresh water was supplied under head through a long canvas sock in the

channel roof.

Velocity and density profiles were measured and these indicated that for low to moderate slopes an inner region of relatively undisturbed flow existed adjacent to the channel floor, even though the outer region was fully turbulent. This inner region was composed of much denser fluid than the outer region and the zone of maximum density gradient across the sharply defined interface between the two regions coincided with the zone of maximum velocity. The interface between the inner and outer regions became less distinct as the slope increased but the inner region was apparently still present in the limiting case of 90^{o} slope as Ellison and Turner claim to have measured the velocity of disturbances travelling along the interface in this case.

Ellison and Turner tried several methods to determine $E(R_{in})$. Firstly they integrated the measured velocity and density profiles and computed E and R_{in} at several cross sections for the small slopes of 9^{o}, 14^{o} and 23^{o}. There was no significant trend in $E(R_{in})$ and in fact widely different values of E and R_{in} were obtained for each slope. This latter variation in E was attributed to variation in the thickness of the inner region of concentrated salt water.

It was only when attention was confined to the outer turbulent region of the plume that a definite trend in $E(R_{in})$ was observed. The method finally adopted was to determine entrainment directly by

measuring the outflow of diluted salt water at the lower end of the channel and, on subtracting the input flow rate of salt water, the quantity of fresh water entrained over the length of the plume in unit time was known. Dividing this fresh water inflow rate by the length of entrainment gives $d\frac{(Vh)}{dx}$. The "layer velocity V_L" was determined by timing the passage between marks of a disturbance on the interface between the inner and outer regions of the plume. The layer velocity V_L was converted to the velocity scale V at a particular cross section by using a relation between V and V_L obtained from velocity profiles at one slope. Knowing V the entrainment constant $E = \frac{dh}{dx}$ was found from $d\frac{(Vh)}{dx}$. The Normal Richardson Number R_{in} was equal to $\frac{G \cos S}{V^3}$ where G is known from salt water input measurements.

The results obtained show a definite trend of decreasing E with increasing R_{in}, E varying from about 0.09 at $R_{in} = 0$, to 0 at $R_{in} = 0.8$. There was still some scatter in results on the $E(R_{in})$ curve for each floor slope investigated but this scatter was less than that obtained by the profile integration method of analysis. This scatter is probably due to variations in thickness of the inner region of denser salt water of the plume. The effect of the inner region was effectively ignored in Ellison and Turner's method of analysis but as the layer forms an appreciable part of the depth of flow at very low boundary slopes it is probable that the results obtained are not very reliable for such slopes.

Johnson has attempted to apply Ellison and Turner's results to prediction of the flow of oceanic turbidity currents (Ref. 54). He shows that, if settling of particles and bed erosion is negligible, then R_{in} for a turbidity current on an abyssal ocean plain is likely to exceed 0.8 in which case entrainment will be negligible.

Johnson also examines the lateral spread of a three dimensional turbidity current with the aid of Penney and Thornhill's work on the collapse of a rectangular column of heavier fluid on a horizontal plane in a body of lighter fluid. This analysis leads to a prediction of a lateral angle of spread of greater than 90^{o} for the Grand Banks turbidity current of 1929 while the observed angle of spread was considerably less than this.

Harris has analysed the case of a turbulent two dimensional wall plume using Birkhoffs' "method of inspectional analysis" (Ref. 47). He considered the equations of motion and continuity at a point and then integrated these over a cross section of the flow. The orders of magnitude of the terms in the equation of motion and in the integrated equation of motion were examined and one term of small value in each equation neglected as a first approximation. The profiles of velocity and density were assumed to be self preserving and, on substituting relations for velocity and density in the equation of motion, the integrated equation of motion and the integrated continuity equation,

it was shown that:

$$V \propto X^{0} \quad \text{i.e. constant}$$
$$\Delta\rho_m \propto X^{-1}$$
$$R_{in} \propto X^{0} \quad \text{i.e. constant} \qquad (7)$$
$$h \propto X \quad \text{i.e. linear spread}$$

, where V, $\Delta\rho_m$, and h are characteristic velocity, density and depth scales at a flow cross section, and X is the distance from the virtual origin.

Harris also replotted the published velocity and density profiles measured by Ellison and Turner (Ref. 31). By selecting the characteristic length scale as the height above the floor where $\frac{v_x}{v_{xmax}} = 0.5$ Harris showed that the velocity and density profiles appeared to be self preserving in the outer turbulent region of the plume, but not in the inner high density region.

1.3 General Description of the Phenomenon

The experimental density currents were produced by release of salt water at the top of a downward sloping floor which was submerged in a tank of fresh water, so the general description of a three dimensional density current will be in this context.

The relevant factors used in the following general description of the behaviour of a three dimensional jet are shown schematically in

Fig. 1A. The term "jet" has been loosely used throughout this report as synonymous with "three dimensional density current".

The pertinent independent variables are those describing:

(i) Boundary dimensions: Floor slope S, and roughness k

Orifice hydraulic radius R_h

(ii) Injected fluid: Density $\rho + \Delta\rho_o$

Flow rate Q_o

(iii) Ambient fluid: Density ρ

Viscosity μ

Within a short distance of the orifice there is a zone of unestablished flow where the fluid rapidly adjusts itself to its new surroundings. The zone of unestablished flow represents the change in the flow from a momentum controlled phenomenon at the orifice to a gravity controlled phenomenon in the zone of established flow. In the established flow zone there are several forces affecting the flow: the component of the submerged weight in the x direction tends to drive the jet down the plane while the unbalanced hydrostatic force due to the gradient of submerged weight in the y direction tends to cause the jet to spread laterally. The motion of the jet on the other hand is opposed by the friction of the boundary plane and, in the case of a turbulent jet, the spreading of momentum by the entrainment of ambient fluid.

The flow in the jet may be laminar or turbulent. Laminar or "slug" flows occur at low values of injection flow rate Q_o, high density difference $\Delta\rho_o$, and low bed slope S. Slug flows are small depth flows with slight lateral spreading; the interface between the saltwater in the jet and the ambient freshwater is well defined as the steep density gradient at the interface effectively damps any turbulence. With increase of injection flowrate Q_o well defined waves, travelling in the direction of flow, appear on the interface and, eventually, at high flow rates, the jet becomes "turbulent", with the intermittency of the interface which is characteristic of such free turbulent flows.

A turbulent jet is a relatively large depth flow with pronounced lateral spreading and considerable entrainment of ambient fresh water through the ill-defined interface. Turbulent jets are likely to occur with high injection flow rate Q_o, low density difference $\Delta\rho_o$, and a steeply sloping boundary. For the low slopes investigated, the flow in a turbulent jet appears to be composed of two parts; adjacent to the boundary plane is a boundary layer containing high density salt water, and which may be likened to the laminar sublayer of a constant pressure turbulent boundary layer on a flat plate. Above the boundary layer is a region of relatively dilute salt water which is fully turbulent and allows turbulent entrainment of the ambient fresh water because of its low density difference.

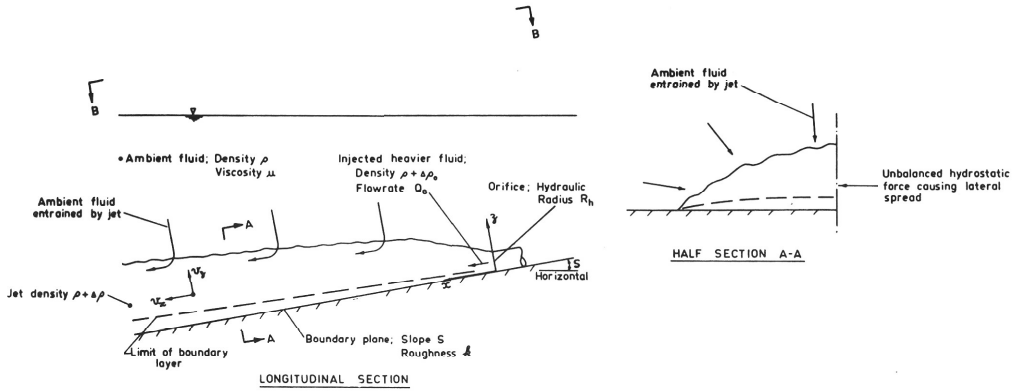

FIGURE 1A: NOTATION FOR GENERAL DESCRIPTION

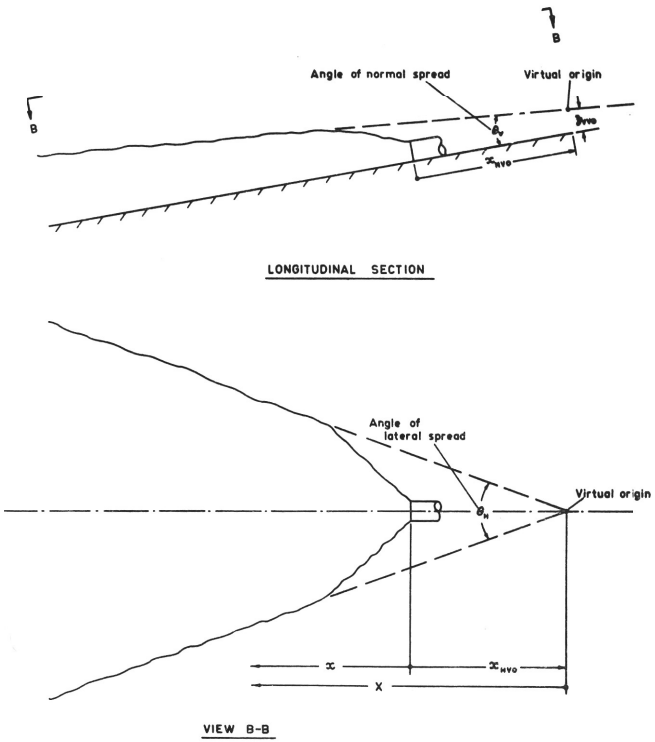

FIGURE 1B: NOTATION FOR OVERALL CHARACTERISTICS

FIGURE 1: SCHEMATIC DEFINITION OF NOTATION

Turbulent entrainment in the case of a three dimensional jet appears to be somewhat more complicated than that in the two dimensional case. Ellison and Turner (Ref. 31) refer to the commonly accepted view that where a density gradient occurs in the vertical direction, turbulence is suppressed and entrainment reduced. Where there is a density gradient in the horizontal direction, however, the turbulence damping effect is small and the entrainment relatively unaffected. For flat boundary slopes in the present case the entrainment of ambient fluid is substantially vertical for the central flat portion of the jet near the x axis, while in the outer regions the entrainment tends to be in the horizontal direction. Hence at any cross section through the jet the central flat portion near the x axis may behave as a two dimensional density current while the outer portion may behave similarly to a plume formed by release of a buoyancy from a point source in an unbounded medium.

Between the well defined slug and turbulent cases of flow is an ill-defined intermediate region of flows which have been termed "indeterminate" in this report.

Another independent variable influencing the onset of turbulence in a three dimensional jet is the turbulence level of the ambient fluid. If the turbulence level is high then the jet is likely to become turbulent at a lower injection flow rate than if the level is low, other factors being constant. This is an important factor to be kept in mind when

attempting to use model results to predict behaviour of prototype systems, such as jets in the atmosphere or the ocean.

For an exploratory investigation, it was decided to ignore the complication of turbulence in the ambient fluid and to carry out the experiments in a tank of freshwater of low turbulence level.

1.4 Dimensional Analysis

1.4.1 Overall Jet Characteristics

To systemise experimental data for the overall characteristics of the jet the pertinent independent variables are Q_o, $\Delta\rho_o$, g, ρ, μ, R_h, k and S, as defined schematically in Fig. 1A. It is assumed that the viscosity of the injected fluid is close to that of the ambient fluid.

If the zone of established flow is regarded as emanating from a virtual origin as shown in Fig. 1B, then the axial x location of the virtual origin x_{HVO} is given by:

$$x_{HVO} = f(Q_o, \Delta\rho_o, g, \rho, \mu, R_h, k, S) \qquad (8)$$

and, from the π theorem:

$$\frac{x_{HVO}}{R_h} = \phi_1\left(\frac{Q_o^2}{R_h^5 g}, \frac{\rho}{\Delta\rho_o}, \frac{Q_o \rho}{R_h \mu}, \frac{k}{R_h}, S\right) \qquad (9)$$

Assuming that $\frac{\Delta\rho_o}{\rho}$ is small and $\Delta\rho_o$ is only significant when combined with g, then:

$$\frac{x_{HVO}}{R_h} = \phi_2\left(\frac{Q_o^2 \rho}{R_h^5 \Delta\rho_o g}, \frac{Q_o \rho}{R_h \mu}, \frac{k}{R_h}, S\right) \qquad (10)$$

$\frac{Q_o^2 \rho}{R_h^5 \Delta\rho_o g}$ is a Richardson Number which may be regarded as a form

of Froude Number written in terms of unit weight excess for multi-density flows. For plotting convenience the Richardson Number at the orifice, R_{io}, is defined as:

$$R_{io} = \sqrt[3]{\frac{R_h^5 g \Delta\rho_o}{Q_o^2 \rho}} \tag{11}$$

Alternatively this parameter may be made independent of the orifice shape by noting that $Q_o \propto V R_h^2$, where V is the mean velocity at the orifice, then R_{io-} is defined as:

$$R_{io-} = \sqrt[3]{\frac{Q_o^{\frac{1}{2}} g \Delta\rho_o}{V^{5/2} \rho}} \tag{12}$$

Utilising the fact that the density of the injected fluid $\rho + \Delta\rho_o$ is close to the density of the ambient fluid, and also the assumption that the viscosities are almost equal, then $\frac{Q_o \rho}{R_h \mu}$ approximates closely the Reynolds Number at the orifice, R_{eo}. If the flow at the orifice is turbulent then variation of x_{Hvo} with variation of Reynolds Number is likely to be slow. Hence x_{Hvo} is given by:

$$\frac{x_{Hvo}}{R_h} = \phi_3\left(R_{io}, \frac{k}{R_h}, S\right) \tag{13}$$

Similarly the normal z location of the virtual origin z_{vvo} is given by:

$$\frac{z_{vvo}}{R_h} = \phi_4\left(R_{io}, \frac{k}{R_h}, S\right) \tag{14}$$

1. 4. 2 Variation of Velocity and Density Scales with Distance from the Virtual Origin

Regarding the virtual origin as a point source of mass flux $Q_o \rho$, of

momentum flux $Q_o \rho V$, and of flux of unit weight excess $Q_o \Delta\rho_o g$, then the velocity scale, taken as v_{xmax}, is in general given by:

$$v_{xmax} = f(Q_o \rho, Q_o \rho V, Q_o \Delta\rho_o g, \rho, \mu, X, S) \qquad (15)$$

where X is the distance from the virtual origin, as shown in Figs. 1B and 2A.

For a three dimensional plume in the zone of established flow the momentum flux $Q_o \rho V$ at the origin is neglected, as must be the mass flux $Q_o \rho$, which is of an order of magnitude less, and using the π theorem:

$$\frac{v_{xmax.}\, \rho^{\frac{1}{3}} X^{\frac{1}{3}}}{(Q_o \Delta\rho_o g)^{\frac{1}{3}}} = \phi_5\left(\frac{(Q_o \Delta\rho_o g)^{\frac{1}{3}} \rho^{\frac{2}{3}} X^{\frac{2}{3}}}{\mu}, S\right) \qquad (16)$$

The parameter $\dfrac{(Q_o \Delta\rho_o g)^{\frac{1}{3}} \rho^{\frac{2}{3}} X^{\frac{2}{3}}}{\mu}$ is a form of Reynolds Number which is likely to become insignificant at steep slopes and large fluxes of unit weight excess. Hence, in the limiting case of $S = 90^o$ and fully developed turbulence, v_{xmax} should vary as $X^{-1/3}$ fairly closely in the zone of established flow.

In a similar fashion it may be shown that in the same limiting case the density scale $\Delta\rho_{mean}$ should vary as $X^{-5/3}$ fairly closely.

In the zone of unestablished flow the momentum flux cannot be neglected but the mass flux may be neglected as it is of an order of magnitude less. In the limiting case of zero $\Delta\rho_o$ (that is, fresh water

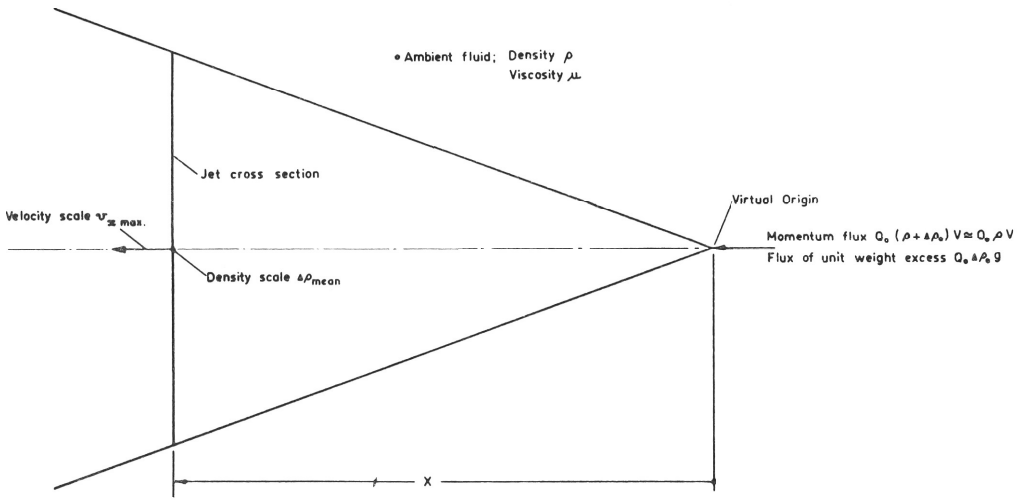

FIGURE 2 A: NOTATION FOR VELOCITY AND DENSITY SCALES

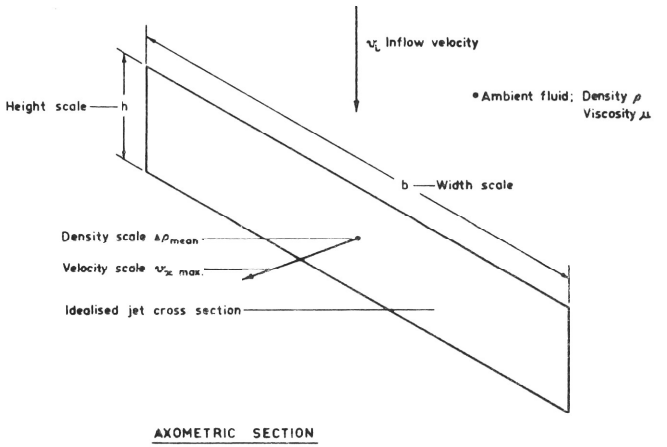

FIGURE 2 B: NOTATION FOR LOCAL STABILITY

FIGURE 2: SCHEMATIC DEFINITION OF NOTATION

into fresh water three dimensional wall jet) the mass flux tends to zero at the virtual origin (as shown by Morton, Ref. 74) and application of dimensional analysis yields:

$$\frac{v_{xmax.}^2 \rho X^2}{\rho_0 \rho V} = \phi_6\left(\frac{(\rho_0 \rho V)^{\frac{1}{2}} \rho^{\frac{1}{2}}}{\mu}\right) \tag{17}$$

This yields to the familiar result of $v_{xmax.} \propto X^{-1}$ for a turbulent jet Hence in the zone of unestablished flow of the present case where both buoyancy and momentum effects are significant, it might be expected that $v_{xmax} \propto X^{-a}$, where a lies between 1/3 and 1 and varies slowly.

1.4.3 Entrainment at a Jet Cross Section

The velocity of entrainment v_i at a particular jet cross section is given by:

$$v_i = f(v_{xmax.}, \Delta\rho_{mean} g, b, h, \rho, \mu, k) \tag{18}$$

, where $v_{x\ max}$, $\Delta\rho_{mean}$, b, and h are velocity, density, width and height scales respectively, as shown in Fig. 2B.

Applying the π theorem:

$$\frac{v_i}{v_{xmax.}} = \phi_7\left(\frac{\Delta\rho_{mean} g b}{v_{xmax.}^2 \rho}, \frac{b}{h}, \frac{k}{b}, \frac{v_{xmax.} b \rho}{\mu}\right) \tag{19}$$

$\frac{v_i}{v_{xmax}}$ is commonly called E, the entrainment constant. $\frac{\Delta\rho_{mean} g b}{v_{xmax}^2 \rho}$ is called the Local Richardson Number Ri-, and $\frac{v_{x\ max} b \rho}{\mu}$ is called the Local Reynolds Number R_{e-}.

For turbulent jets on steep slopes $\frac{b}{h}$ tends to unity and the

Reynolds Number is probably insignificant. Hence

$$E = \phi_8 (R_{i-}, \frac{k}{b}) \tag{20}$$

For a turbulent jet on a slight slope $\frac{b}{h}$ is greater than unity and the Reynolds Number effect cannot be ignored, hence

$$E = \phi_9 (R_{i-}, \frac{b}{h}, \frac{k}{b}, R_{e-}) \tag{21}$$

The $\frac{b}{h}$ term allows for the postulated difference in E between the central region of the jet and the outer regions discussed previously in Section 1.3.

Noting that R_{i-} is a type of Froude Number, it is seen that the entrainment constant E is a function of (Froude Number, Reynolds Number) and this foreshadows difficulty in using model data to predict prototype behaviour.

1.5 Additional Theory

While the variation of velocity and density scales with distance from the virtual origin may be obtained by dimensional analysis (as in Subsection 1.4.2 above) the prediction of width and height scale variation requires further data. The latter predictions may be made by utilising the equation for conservation of density excess in conjunction with a self preserving assumption.

1.5.1 Derivation of the Equations for Conservation of Density Excess and Conservation of Volume

The differential form of the equation of continuity for the portion

of the injected fluid causing the density excess $\Delta\rho$ is:

$$\frac{\partial(\Delta\rho v_x)}{\partial x} + \frac{\partial(\Delta\rho v_y)}{\partial y} + \frac{\partial(\Delta\rho v_z)}{\partial z} = 0 \qquad (22)$$

In equation (22) the salt in the injected saltwater is considered as a tracer, that is, $\frac{\Delta\rho}{\rho}$ is small. The terms involving velocity and density fluctuations have been ignored.

Integration of equation (22) over an x = constant section yields the equation expressing conservation of density excess:

$$\frac{d}{dx}\int_0^\infty\int_{-\infty}^{\infty} v_x \Delta\rho \, dy\, dz = 0 \qquad (23)$$

Equation (23) states that there is no change in the flux of density excess in the x direction, or, in other words if K slugs of salt per second are being injected at the source then the same mass flow rate must occur at each cross section in the flow.

Integration of equation (23) with respect to x gives the flux of density excess K:

$$K = \int_0^\infty\int_{-\infty}^{\infty} v_x \Delta\rho \, dy\, dz \quad = \text{Constant} \qquad (24)$$

The differential form of the equation of continuity for the fluid of density ρ (that is the freshwater portion of the injected fluid and the ambient fluid) is:

$$\frac{\partial v_x}{\partial x} + \frac{\partial v_y}{\partial y} + \frac{\partial v_z}{\partial z} = 0 \qquad (25)$$

Integration of equation (25) over an x = constant cross section yields

$$\frac{d}{dx}\int_0^\infty\int_{-\infty}^{\infty} v_x\,dy\,dz - 2\int_0^\infty v_{y\infty}\,dz - \int_{-\infty}^{\infty} v_{z\infty}\,dy = 0 \qquad (26)$$

Equation (26) expresses conservation of volume and states that the rate of change of volumetric flow rate in the x direction is equal to the rate at which fluid is being entrained in the y and z directions.

1.5.2 Introduction of the Self Preserving Assumption

It is often assumed (and has been verified experimentally in many free turbulent shear flows) that the transverse distribution functions of the mean flow variables (such as v_x, $\Delta\rho$ etc.) retain the same functional form and merely vary in scale from cross section to cross section through the flow. In the present case the transverse distribution function of the velocity v_x, for example, might be described in terms of a characteristic velocity scale, say $v_{x\,max}$, and characteristic width and height scales, b and h respectively; that is:

$$v_x = v_{x max} f(\eta, \epsilon), \quad \eta = \frac{z}{h}, \quad \epsilon = \frac{y}{b}$$

, where the unknown function f is independent of x. In other words, if v_x profiles are obtained by measurement at several x = constant planes and each is plotted on a transparent elastic sheet, then by careful stretching of the sheets the same velocity profile should result.

Transverse distribution functions for the quantities of interest in the present case are:-

$$\begin{aligned} v_x &= v_{x max} f(\eta, \epsilon) \\ \Delta\rho &= \Delta\rho_{mean}\,\phi(\eta, \epsilon) \end{aligned} \qquad (27)$$

, where $\eta = \frac{z}{h}$, $\epsilon = \frac{y}{b}$;

and v_{xmax} and $\Delta\rho_{mean}$ are the characteristic velocity and density scales at a cross section and are functions of x only.

The height scale h is defined by:

$$h = \frac{\left| \int_0^\infty v_x \, dz \right|_{y \text{ at } v_{xmax}}}{v_{xmax}} \tag{28}$$

, where $\left| \int_0^\infty v_x \, dz \right|_{y \text{ at } v_{xmax}}$ means that the integral is taken over the y = constant plane where v_{xmax} occurs. This will coincide with the x axis for a plume spreading laterally in both the $\pm$ y directions.

The width scale b is related to the height scale h by using the expression for the volumetric flow rate at a cross section:

$$b = \frac{\int_0^\infty \int_{-\infty}^\infty v_x \, dy \, dz}{h \, v_{xmax}} \tag{29}$$

Equation (29) indicates that the $bhv_{xmax} = Q$, where Q is the volumetric flow rate at a cross section.

The density scale $\Delta\rho_{mean}$ at a cross section is defined with the aid of equation (24):

$$\Delta\rho_{mean} = \frac{\int_0^\infty \int_{-\infty}^\infty v_x \, \Delta\rho \, dy \, dz}{\int_0^\infty \int_{-\infty}^\infty v_x \, dy \, dz} = \frac{K}{Q} \tag{30}$$

It is important to note at this stage that description of the transverse distribution functions in terms of two characteristic length scales b and h is an extension of the usual self preservation assumption. Self preservation is usually applied to axisymmetric or two dimensional

flows where only one length scale is necessary to describe the transverse distribution function of a variable at a cross section. In the present case, however, the distribution function is asymmetric so that two mutually perpendicular length scales are required to describe the distribution function.

1.5.3 Variation of Width and Height Scales with Distance from the Virtual Origin

Rearranging equation (30) and utilising the relation $Q = bhv_{xmax}$:

$$\Delta\rho_{mean}\, bh\, v_{xmax.} = K = \text{Constant} \tag{31}$$

In Subsection 1.4.2 it was shown that for a fully turbulent plume then $v_{xmax} \propto X^{-1/3}$ and $\Delta\rho_{mean} \propto X^{-5/3}$, where X is the distance from the virtual origin. Substituting these relations in equation (31):

$$\text{Constant}.\, X^{-\frac{5}{3}} . X^{a} . X^{c} . X^{-\frac{1}{3}} = \text{Constant} \tag{32}$$

, where a and c are the exponents associated with b and h respectively.

Thus, for dimensional homogeneity of equation (31):

$$a + c = 2 \tag{33}$$

But as b and h are length scales it follows that for self preservation $\frac{b}{h}$ must be constant, (that is, independent of X), so that $a = c = 1$. Hence both b and h should vary as X^1, or, in other words, the jet should spread linearly both laterally across and normally to the boundary plane.

1.6 Variation of Entrainment Constant and Local Richardson Number with Distance from the Virtual Origin

In Subsection 1.4.3 the entrainment constant E is defined as:

$$E = \frac{v_i}{v_{xmax.}} \tag{34}$$

For conservation of volume of the elementary volume between the x and x + dx idealised cross section planes similar to the plane shown in Fig. 2B:

$$v_i (b+h)\, dx = dQ \tag{35}$$

Equation (35) is consistent with equation (26) and using equations (29) and (34) it follows

$$E = \frac{\frac{d}{dx}(v_{xmax.}\, bh)}{v_{xmax.}} \tag{36}$$

As discussed previously in Section 1.3, for flat boundary slopes at least, it may be necessary to distinguish between the entrainment in the $\pm$ y directions, through the interface represented by hdx, and the entrainment in the -z direction through the interface represented by bdx. In this case two entrainment constants E_y and E_z may be defined by:

$$E_z b + E_y h = \frac{\frac{d}{dx}(v_{xmax}\, bh)}{v_{xmax.}} \tag{37}$$

Substitution of the predicted equations for $v_{x\,max}$ (X), b(X) and h(X) in equations (36) and (37) shows that E, E_y and E_z should all be independent of X.

The local Richardson Number Ri- is defined in equation (19) as $R_{i-} = \frac{\Delta\rho_{mean}\, g b}{v_{xmax}^2 \rho}$, and substitution of the predicted equations for $v_{xmax}(X)$ $\Delta\rho_{mean}(X)$ and b(X) indicates that R_{i-} should be independent of X.

1.7 Summary of Predictions from Dimensional Analysis and Additional Theory

The dimensional analysis indicated that observations of the overall jet characteristics might be processed systematically by plotting in terms of a Richardson Number at the orifice R_{io}, a boundary relative roughness $\frac{k}{R_h}$ and the boundary slope S. This assumes that the flow at the orifice is turbulent and hence variations with change in Reynolds Number at the orifice R_{eo} are slight: It is also assumed that the density difference of the injected fluid $\Delta\rho_o$ is slight.

In the zone of established flow of a fully turbulent jet, (which is likely to occur at steep boundary slopes and large fluxes of unit weight excess), then v_{xmax} should vary as $X^{-1/3}$ and $\Delta\rho_{mean}$ as $X^{-5/3}$. This assumes that buoyancy effects only are responsible for the motion and the momentum flux at the source may be neglected.

For turbulent jets on steep slopes E should be a function of R_{i-} and $\frac{k}{b}$ only. For a jet on a slight slope turbulence may not be fully developed and E is probably a function of $(R_{i-}, \frac{b}{h}, \frac{k}{b}, Re_-)$.

For small density differences and self preservation of velocity, and density profiles from cross section to cross section of a fully

turbulent jet, the lateral and normal spread are predicted to be linear in the zone of established flow and E and R_{i-} are predicted to be constant.

1.8 Summary

The practical importance of three dimensional density currents has been discussed and previous related work reviewed. The literature cited describes an experimental investigation of a two dimensional density current but it appears that the three dimensional case has not yet received serious attention.

A general description of the behaviour of three dimensional density current has been given and a dimensional analysis of the problem undertaken. The dimensional analysis will allow systematic processing of experimental data and also yields predictions of variation of velocity and density scales with distance from the virtual origin in certain limiting cases. Further assumptions requiring experimental verification allowed prediction of variation of width and height scales, entrainment constant and Local Richardson Number with distance from the virtual origin.

Chapter 2: Experimental Investigations.

2. 1 Introduction

The experimental program was comprised of two sections; firstly experiments were performed to determine the overall characteristics of a three dimensional density current, such as lateral and normal spread, flow regime etc. Secondly, a typical turbulent jet was investigated in detail by making measurements of velocity and density at three cross sections of the flow. These latter measurements were used to check the instrumentation, investigate the self preservation hypothesis, and to determine relationships for variation of velocity, density etc. scales with distance from the orifice.

2. 2 Choice of Working Fluids

Two miscible fluids of slightly different density were required. The fluids may be gases, such as air and heated air, or liquids such as fresh water and salt water.

Rouse et al used gas jets to provide a source of heated air in specially constructed rooms for a plume investigation (Ref. 88). In the present case it would be necessary to locate a gas burner at the lower end of a variable pitch upward sloping roof of a room of a size adequate to prevent side wall effects. With such an arrangement temperature measurements by thermocouple would allow

estimation of point densities in the flow while velocity could be measured by hot wire anemometer - both types of instrument are commercially available. Alternatively, instead of using air and heated air, air and another gas may be used. Davar and Cermak released anhydrous ammonia gas in a wind tunnel and measured density by analysing samples withdrawn through a small probe placed in the flow (Ref. 26). The ammonia concentration was determined by passing the sample through an absorption tube containing dilute acid and the density of precipitate formed was measured by a photoelectric colorimeter. Velocity measurement was by hot wire anemometer. Davar and Cermak were not concerned with buoyancy effects, but it is possible that a similar gas system could be used in the present case by selection of injected gases to yield the desired density differences with air as the ambient fluid.

Although a gas system has the advantage that density and velocity measurements are readily made with commercially available instruments, it has been pointed out by Ellison and Turner (Ref. 31) that, for the same Richardson and Reynolds Numbers and density difference, the apparatus for use of air as the working fluid must be six times as big as that for use of water as the working fluid. Hence, for an exploratory investigation, a liquid system was preferable.

Morton et al investigated plumes by releasing dyed methylated spirits in a tank of salt water (Ref. 73). They were interested in spread measurements only and did not attempt to measure velocity or density within the plume. Ellison and Turner used salt water and fresh water as the working fluids in an investigation of two dimensional inclined plumes (Ref. 31). Salt water was released as the heavier fluid at the top of a downward sloping floor in a closed channel filled with fresh water as the lighter ambient fluid. This is probably the most economical choice of working liquids. Unfortunately instruments for measuring density and velocity within the salt water jet are not commercially available. Frankel and Cumming injected a jet of fresh water (containing a small amount of salt as a tracer) into a tank of sugar solution in an ocean outfall model (Ref. 35). They claimed that this liquid system was superior to that of injecting fresh water into a tank of salt water as density measurement by directly exposed conductivity probe was made more reliable. On the other hand, sugar solutions are more expensive than saltwater, take an excessive time to clear after mixing, and are subject to clouding bacterial growths. Also, to use a fresh water - sugar solution liquid system for the present project, a closed tilting tank would be required so that the jet of fresh water could be released at the bottom of an upward sloping roof in a tank of sugar solution. A tilting closed tank was

not available, but a small open tank, (which could be fitted with a downward sloping floor), was available, so it was decided to use salt water as the injected heavier fluid and fresh water as the ambient lighter fluid.

2.3 Experimental Equipment

The general arrangement of experimental equipment is shown in Fig. 3. The equipment is comprised of the experimental tank and an ancillary salt water system. The instrumentation for measuring velocity and density at a point in the three dimensional density current is described in detail in Chapters 3 and 4 respectively.

2.3.1 The Experimental Tank

Details of the experimental tank are shown in Fig. 4. It was convenient to use a perspex tank approximately 4 ft. x 3 ft. x 2 ft. deep which had been made for a previous investigation. The tank was fitted with a downward sloping plywood floor which could be adjusted to angles of inclination to the horizontal between 0° and 20°. The salt water solution was introduced through a semicircular orifice adjacent to a side wall so that in effect half of a three dimensional jet was produced (the reason for using this arrangement will be discussed subsequently when the experiments to determine the overall characteristics of the jet are described).

One of the major difficulties in using a small laboratory tank to model a large body of ambient fluid is the introduction of "make-up" water to keep the water level in the tank steady. Ideally, the make-up water should be introduced so that it just satisfies the "entrainment appetite" at all cross sections of the jet. In the present case an attempt to do this was made by introducing the make-up water through the boxes shown in Fig. 4. These boxes ran laterally across the tank and were fitted with a weir and a hessian bottom to provide uniform inflow. In Chapter 1 it was predicted that the flow rate of a three dimensional turbulent jet increases with distance from the orifice so that the inflow of ambient fresh water must also increase in the direction of flow. To allow for this increase the make-up boxes were partially blanked off at the bottom, as shown in the plan view of Fig. 4, and the number of make-up water supply points was increased with distance from the orifice.

With careful adjustment of the make-up inflow rate and the tank outflow rate the system performed reasonably satisfactorily. The make-up inflow and waste outflow valves were adjusted so that flow over the fresh water overflow weir was slight and the level of the pool of diluted salt water at the bottom of the sloping floor was constant. The entrainment of fresh water was then checked by observing the movement of the dye trails left by crystals of potassium permanganate

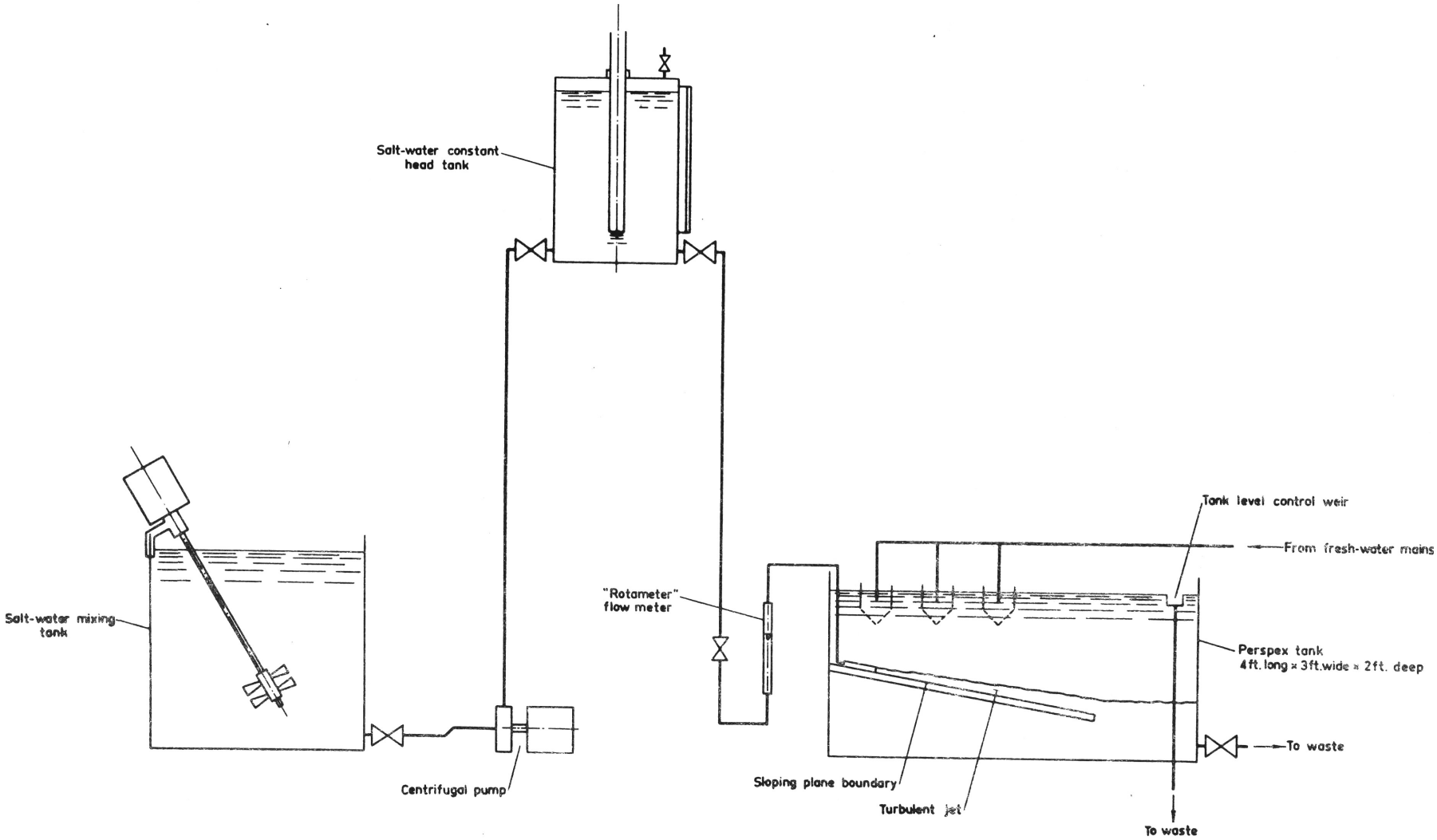

FIGURE 3: EQUIPMENT DETAILS

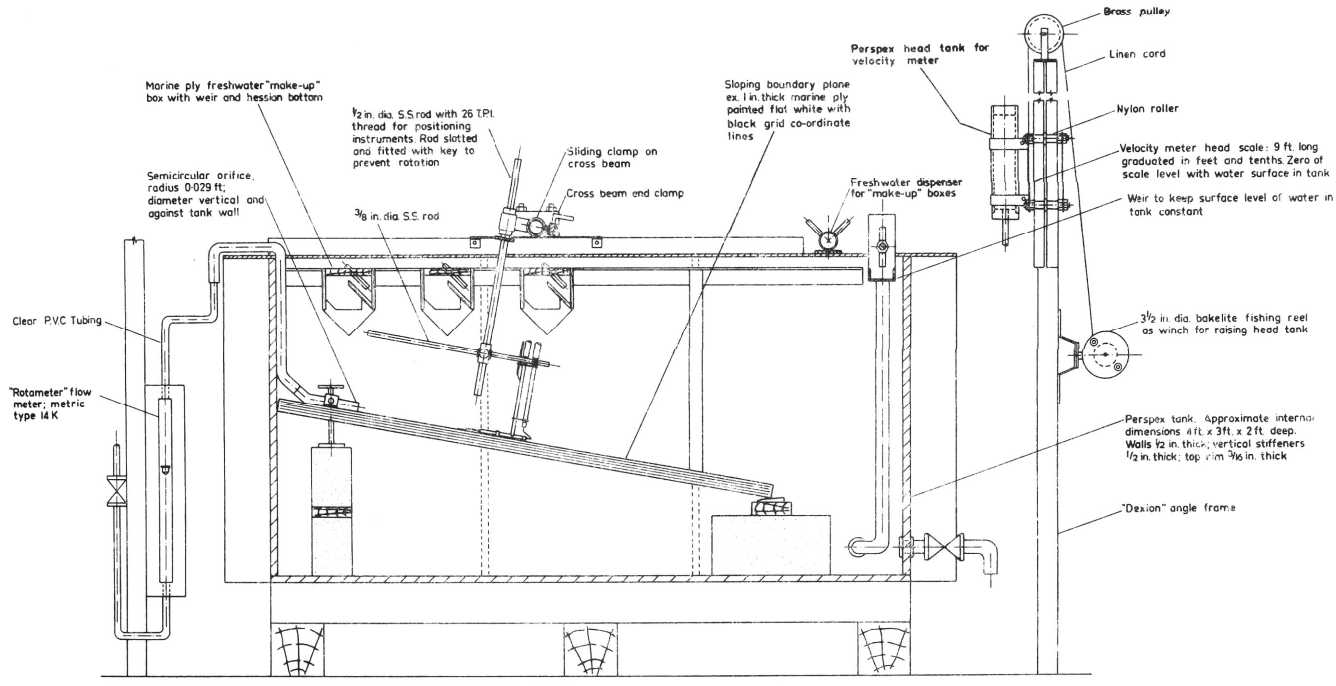

FIGURE 4: TANK DETAILS

dropped from the surface of the water in the tank. The fresh water appeared to be entrained in a direction normal to the sloping floor and s hort circuiting of fresh water between the make-up boxes and the out-flow valves was negligible.

The instruments for measuring velocity and density were held in the suspension system shown in Fig. 4. A round cross beam ran across the tank and this was fitted with a clamp holding a screwed rod which could be traversed normally to the sloping floor. The screwed rod carried a secondary rod to which the instrument being used was clamped. The velocity meter, for example, is shown fixed to the secondary rod in Fig. 4. This system allowed maximum flexibility for positioning an instrument in the tank as it allowed the instrument to be rotated or translated in any direction.

Photographs of the experimental tank in operation are shown in Figs. 5 and 6.

2.3.2 Saltwater Mixing and Supply System

Salt water solutions were prepared by mixing fine salt and fresh water with a commercial food stirrer in the mixing tank shown in Fig. 3. Density control was by glass immersion hydrometer as described in subsection 4.2.2, Chapter 4. The salt water was dyed red with I.C.I. Chlorozol Scarlet dye. The colouring power of Chlorozol Scarlet is not as great as that of an equal weight of potassium

permanganate but it has the advantage that staining of equipment is much less than that resulting from potassium permanangate.

The prepared salt water was then pumped to an elevated marriot syphon type constant head tank for reticulation to the experimental tank. The flow of salt water was measured with a Rotameter calibrated for relative density differences $\left(\frac{\Delta\rho}{\rho}\right)_o$ up to 8 per cent.

2.4 Investigation of Overall Jet Characteristics

2.4.1 General

The initial attempt to model a turbulent three dimensional jet was made by placing the orifice at the top of the downward sloping boundary plane and with its axis coinciding with the longitudinal centreline of the tank. With this arrangement, however, it was apparent that the vertical sidewalls of the tank interfered with the anticipated linear spread of the jet - as shown for a typical jet in Fig. 7.

It was therefore decided to shift the orifice to one side of the tank in an attempt to model one half of a three dimensional jet. A comparison of the lateral spread of a half jet and of a free spreading centrally located jet of the same Richardson Number R_{io} will be made in detail in subsection 2.4.3 below. For the jets compared, it would appear that the lateral spread of a half jet is slightly less than that of a free spreading jet of equal R_{io} value.

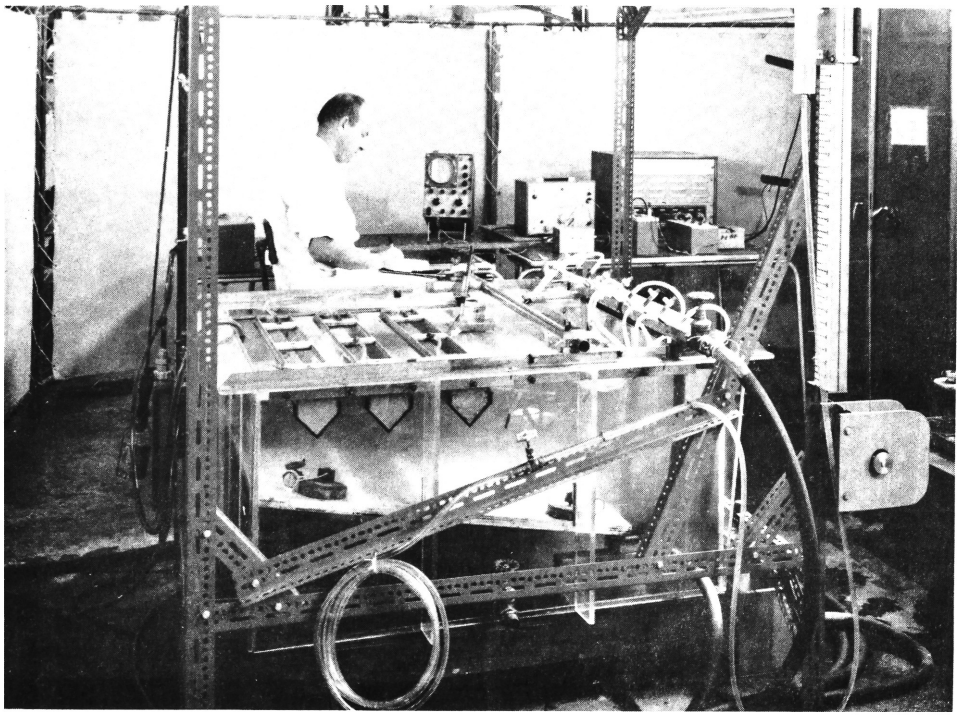

Fig. 5: The Experimental Tank.

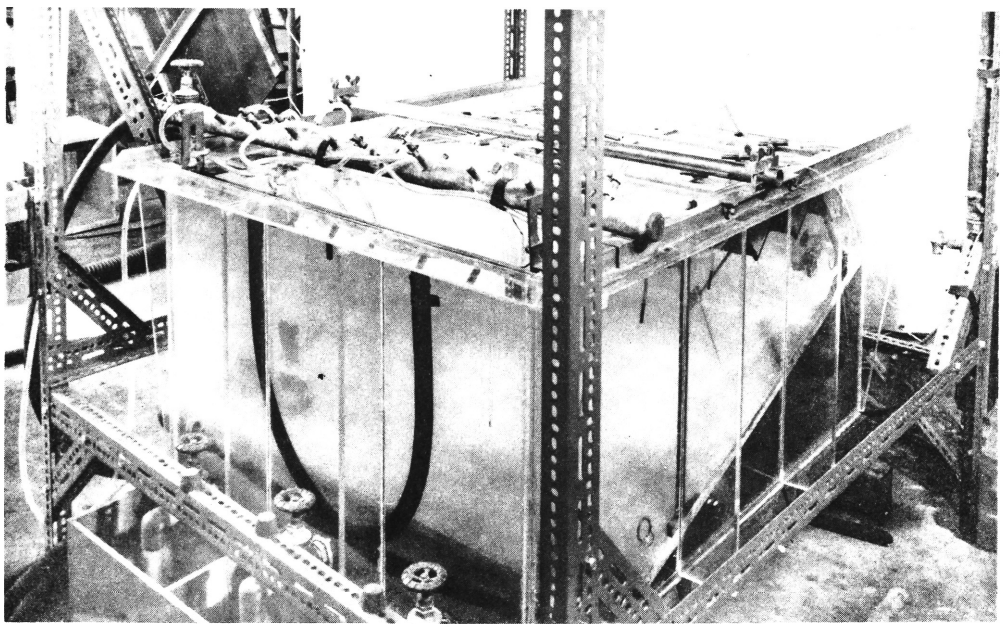

Fig. 6: The Experimental Tank.

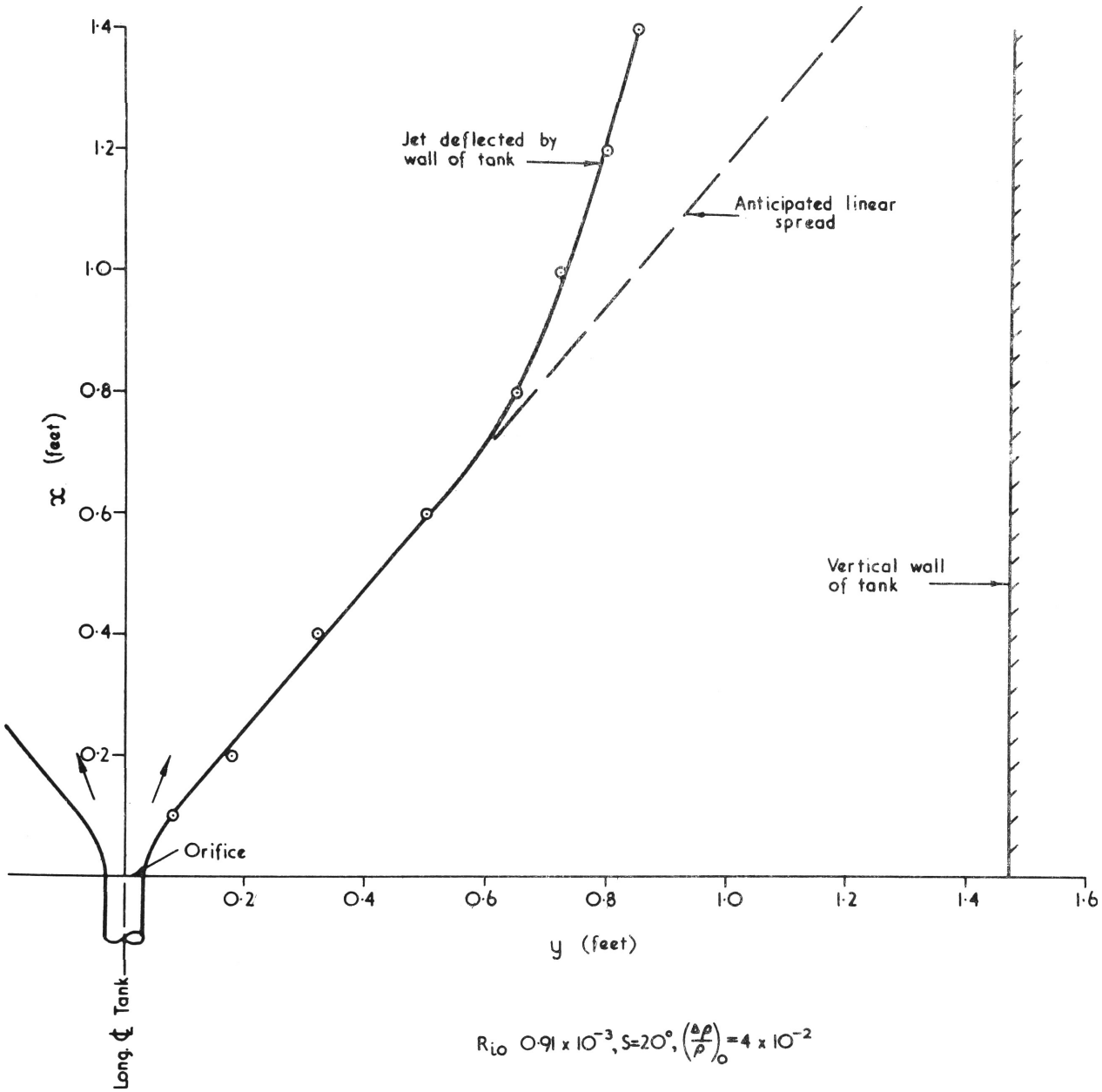

FIGURE 7: EFFECT OF TANK WALL ON LATERAL SPREAD OF A JET ISSUING FROM A CENTRALLY PLACED ORIFICE

The details of the half jets used to determine the overall characteristics of a three dimensional density current are shown in Table 1. The range of tests performed was limited by the equipment available; for instance boundary slopes greater than 20^{o} could not be used in the experimental tank.

2.4.2 Flow Regime

As outlined in Section 1.3 of Chapter 1, the flow in a three dimensional jet may be "slug", "turbulent", or "indeterminate". Three typical jets demonstrating this classification are shown in Fig. 8 As shown in Table 1, all jets on a boundary slope of 20^{o} were turbulent, and slug and indeterminate flows could only be obtained at the lower slope of 10^{o}.

The flow regimes of jets on a boundary of 10^{o} slope are shown plotted on a Richardson Number R_{io} - Reynolds Number R_{eo} field in Fig. 9. It may be seen that slug flows only occur at high values of R_{io}, that is at low injection flow rates or high density differences. At the low values of R_{io} associated with high injection flow rates and/or small density differences, the flow is invariably turbulent. The Reynolds Number R_{eo} only appears to be significant in the zone of indeterminate flow, although a wider range of experiments employing injected liquids of widely different viscosity is necessary to check this aspect of regime classification.

The remaining overall characteristics, such as lateral spread, were investigated by assuming that the effect of varying the Reynolds Number R_{eo} could be ignored and that the Richardson Number R_{io} was sufficient specification for a jet.

2.4.3 Lateral Spread

The lateral spread was determined by dropping large crystals of potassium permanganate on to the boundary plane and observing the deflection by the jet of the downward flowing dye streaks formed by the crystals. This is a rather crude method of investigating jet spread and the accuracy of the lateral angles of spread measured is probably not better than ± 10 per cent. Some typical jet width observations obtained by this method are shown in Fig. 10A. The lateral boundary of the jet appears to be linear in the zone of established flow and the jet may be imagined as emanating from a virtual origin located on the x axis. If a virtual origin is used then the location of the virtual origin x_{Hvo} and the angle of lateral spread θ_H specify the location of the lateral jet boundary.

In Subsection 1.4.1 of Chapter 1, it is shown (equation 13) that $\frac{x_{HVO}}{R_h}$ may be plotted as a function of R_{io} for a particular boundary slope if variation of $\frac{x_{HVO}}{R_h}$ with Reynolds Number R_{eo} and boundary relative roughness $\frac{k}{R_h}$ is ignored. A plot of $\frac{x_{HVO}}{R_h}$ versus R_{io} for the jets examined is shown in Fig. 11. A and B are

TABLE 1: DETAILS OF JETS INVESTIGATED

Test No.	Boundary Slope S (degrees)	Relative Density Difference at Orifice $\left(\frac{\Delta\rho}{\rho}\right)_o \times 10^2$	Injection Flowrate $Q_o \times 10^4$ (cubic feet per second)	Richardson No. at Orifice $R_{io} \times 10^3$	Alternative Richardson No. at Orifice $R_{io-} \times 10$	Reynolds No. at Orifice $R_{eo} \times 10^{-5}$	Flow Regime
A	20	2·0	3·33	1·440	1·031	3·58	Turbulent
C	"	"	6·67	0·907	0·650	7·16	"
E	"	"	13·48	0·567	0·406	14·50	"
F	"	1·0	2·36	1·450	1·038	2·50	"
G	"	"	4·83	0·892	0·639	5·20	"
H	"	"	9·5	0·569	0·407	10·20	"
I	"	8·5	13·48	0·916	0·656	14·50	"
J	"	"	6·67	1·467	1·051	7·16	"
K	"	"	4·83	1·817	1·307	5·20	"
L	10	"	6·83	1·443	1·033	7·35	"
M	"	"	4·83	1·817	1·302	5·20	Indeterminate
N	"	"	3·50	2·254	1·614	3·76	Slug
O	"	2·0	1·67	2·286	1·637	1·76	Slug
P	"	"	2·50	1·745	1·250	2·68	Indeterminate
Q	"	"	3·50	1·394	0·999	3·76	Indeterminate
R	"	"	6·83	0·892	0·639	7·35	Turbulent
S	"	"	13·82	0·558	0·400	14·90	Turbulent
U	"	1·0	1·77	1·745	1·250	1·90	Indeterminate
V	"	"	2·50	1·385	0·992	2·69	Indeterminate
W	"	"	4·83	0·892	0·639	5·20	Turbulent
X	"	"	9·72	0·560	0·401	10·50	Turbulent

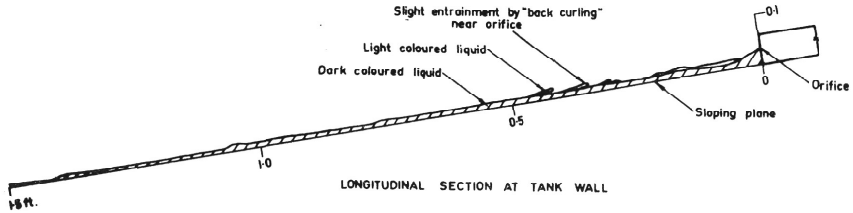

"SLUG" FLOW: TEST O

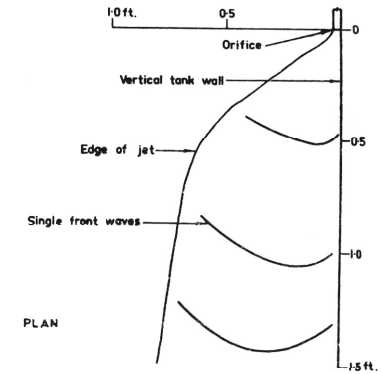

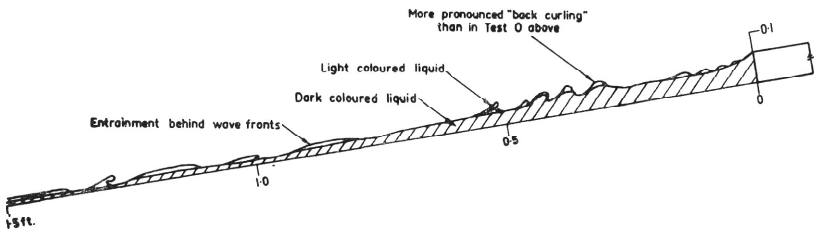

"INDETERMINATE" FLOW: TEST O

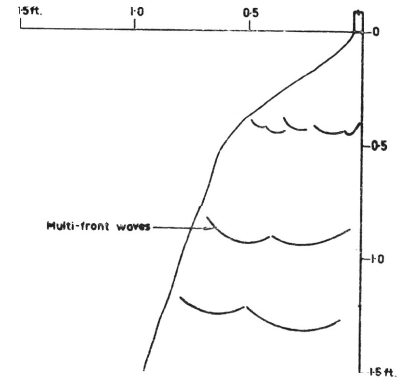

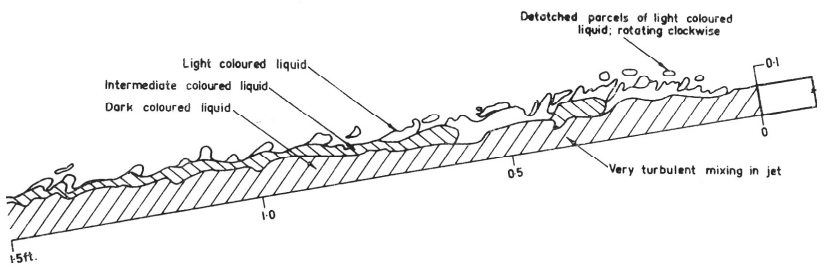

"TURBULENT" FLOW: TEST S

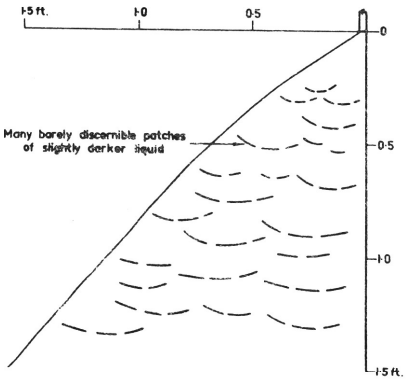

FIGURE 8: CLASSIFICATION OF FLOW REGIME

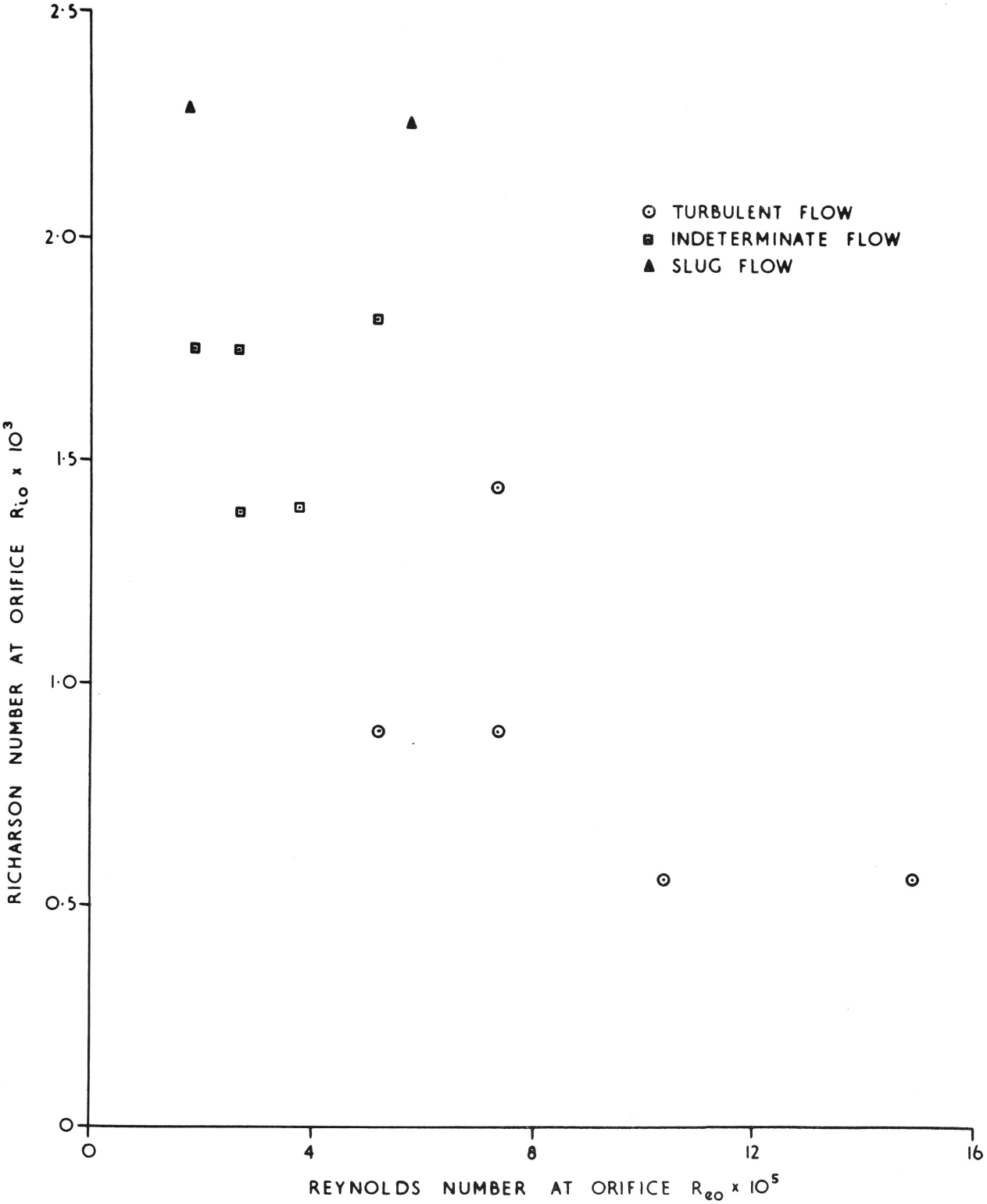

FIGURE 9: FLOW REGIME OF JETS ON PLANE OF SLOPE S=10°

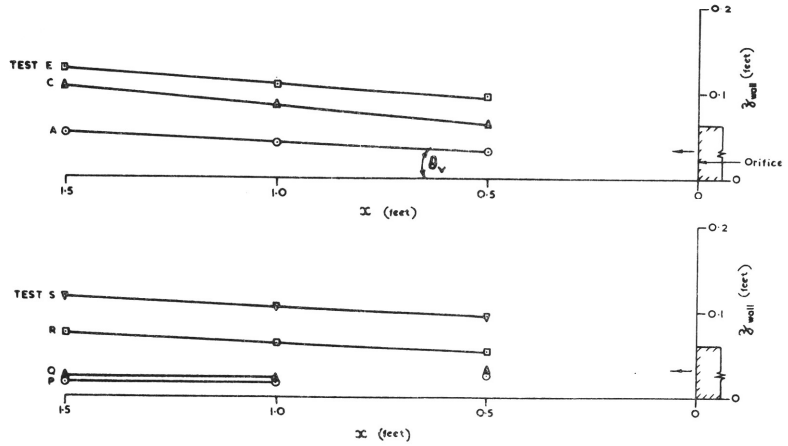

FIGURE 10 B: TYPICAL JET HEIGHT OBSERVATIONS

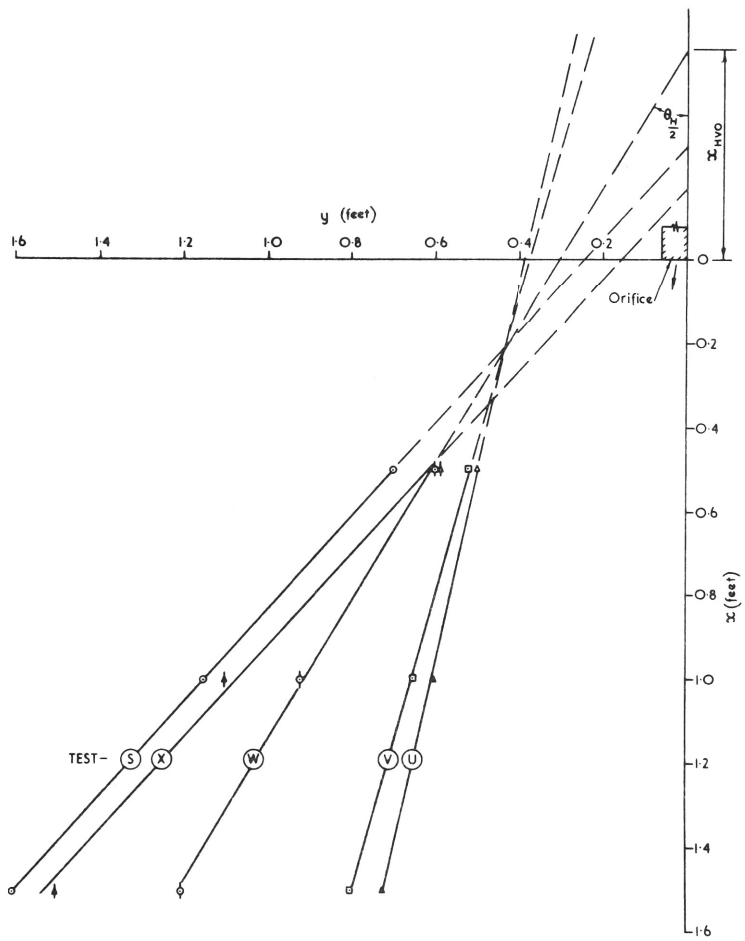

FIGURE 10A: TYPICAL JET WIDTH OBSERVATIONS

FIGURE 10: TYPICAL JET WIDTH AND HEIGHT OBSERVATIONS

lines of best fit for relative density differences $\left(\frac{\Delta\rho}{\rho}\right)_o$ of 1.0 and 2.0 per cent on slopes of 10^o and 20^o respectively. Lines A and B indicate that R_{io} is a reasonable criterion for specifying the position of the virtual origin. C and D are lines of best fit for a relative density difference of 8.5 per cent on slopes of 10^o and 20^o respectively. It is seen that line C, although of roughly the same slope, does not coincide with line A for the smaller relative density differences on the same boundary slope of 10^o. In the dimensional analysis $\left(\frac{\Delta\rho}{\rho}\right)_o$ was assumed to be "small" and only important when combined with g-this is probably not the case with a $\left(\frac{\Delta\rho}{\rho}\right)_o$ of 8.5 per cent and this would account for the lack of coincidence of lines A and C. Similar remarks may apply to lines B and D, although the scatter of points about line D is probably too great to draw any sound conclusion.

The half angle of lateral spread $\frac{\theta_H}{2}$ versus R_{io} is shown plotted in Fig. 12. The same notation for the various relative density differences and slopes tested as used in Fig. 11 has been used. The lines of best fit A and B for small relative density differences might be taken as independent of boundary slope if the accuracy of the method used for determining θ_H is kept in mind. The deviation of points for the jets of relative density difference of 8.5 per cent is again apparent in Fig. 12.

The half angle of lateral spread $\frac{\theta_H}{2}$ of the centrally placed jet shown in Fig. 7 is 40^o while the angle for the half jet of corresponding R_{io} is 33^o from Fig. 12. As pointed out previously, these angles of spread are probably only accurate to within $\pm$ 10 per cent so that for this case at least the angles of spread could coincide. If the accuracy is better than $\pm$ 10 per cent then one might conclude that the vorticity interchange between the jet proper and the boundary layer against the sidewall of a half jet is less than that across the longitudinal vertical (y = 0) plane of a centrally placed jet. If this is correct then use of a half jet to indicate the lateral spread of a centrally placed jet will result in a slight underestimate of θ_H, that is the angles of lateral spread shown in Fig. 12 for half jets could be taken as minimum values for the corresponding centrally placed jets of equal R_{io} value. For a comprehensive laboratory investigation of three dimensional density currents (using centrally located jets which can spread laterally in both the $\pm$y directions) it would appear that a tank at least twice the size of the present tank is necessary.

2. 4. 4 Normal Spread

The spread of a jet normally to the boundary plane is more difficult to determine than lateral spread as the intermittency of the jet boundary appears to be more pronounced in the former case, particularly when the flow is turbulent. The normal spread was estimated by measuring

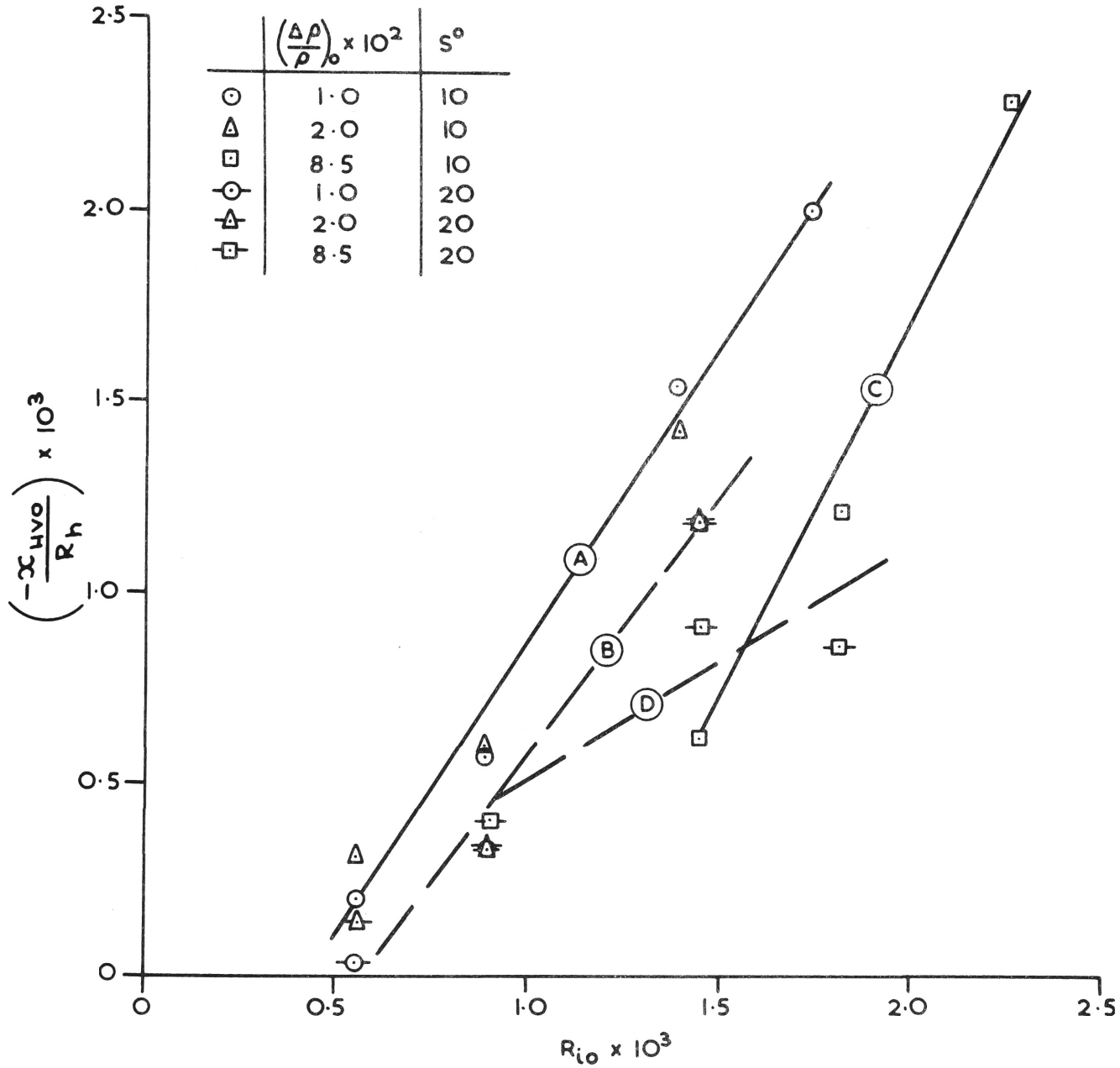

FIGURE II: LOCATION OF VIRTUAL ORIGIN

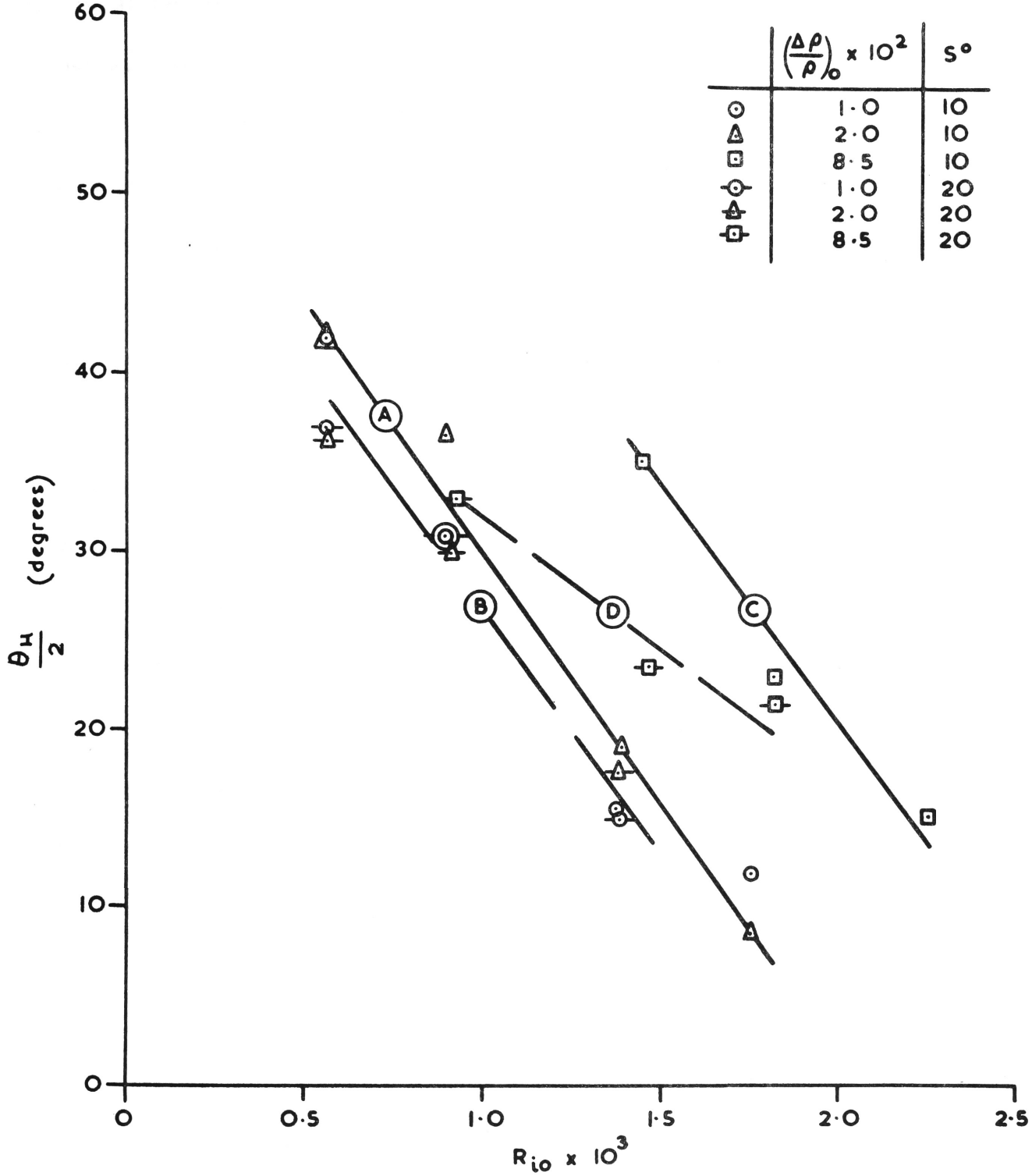

FIGURE 12: ANGLE OF LATERAL SPREAD

the mean height of the intermittent jet boundary at the sidewall at three cross sections; typical measurements are shown in Fig. 10B. The salt water was dyed with a strong solution of potassium permanganate to accentuate the jet boundary for these measurements. The accuracy of the measurements is probably not better than ± 25 per cent and in view of this no attempt was made to estimate the normal co-ordinate z_{VVO} of the virtual origin. It did appear, however, that for all of the jets investigated a virtual origin could be located at a position (x_{HVO}, z_{VVO}) as shown in Fig. 1B. All of the jets observed had finite values of x_{HVO} and z_{VVO}.

The angle of normal spread θ_v versus R_{io} for the jets examined is shown in Fig. 13. The points are far too scattered to draw any firm conclusions, but it may be noted that, for the slug flow jets at high values of R_{io}, θ_v tends to 0^o; while, for turbulent jets at low values of R_{io}, θ_v does not exceed 3^o.

A more accurate, but also more time consuming method of investigating both lateral and normal spread of three dimensional jets would be to utilise density measurements. The boundary of the jet might be defined as the point where the density has fallen to 2 per cent of the maximum value at an x = constant cross section.

2. 4. 5 Streamline Patterns

The pattern of flow close to the boundary plane was visualised by using the dye streaks from crystals of potassium permanganate. This technique has been used for visualisation of flow over a model aircraft wing in a low velocity water tunnel (Ref. 19). At first large crystals were dropped onto the sloping boundary plane but these were soon carried away by the jet when their size decreased as they dissolved. Better results were obtained by anchoring the crystals in modelling clay which was pressed into small holes drilled at the grid intersection points of the plywood floor.

Streakline patterns were obtained for turbulent jets only and a typical pattern is shown in Fig. 14. By drawing lines tangential to the streaklines the streamline patterns shown in Figs. 15 to 17 were obtained. Fig. 15 shows the increasing lateral spread of a jet with decreasing Richardson Number R_{io}, other factors being constant. The streamline patterns of Fig. 15 confirm the lateral boundary spread measurements shown in Fig. 12. Fig. 16 demonstrates the effect on lateral spread of varying the relative density difference $\left(\frac{\Delta\rho}{\rho}\right)_o$ while Richardson Number and slope are held constant. The streamline patterns for the lower $\left(\frac{\Delta\rho}{\rho}\right)_o$ values at 1.0 and 2.0 per cent are practically identical and one may conclude that the Richardson Number R_{io} is a good criterion for specifying a jet if the relative density

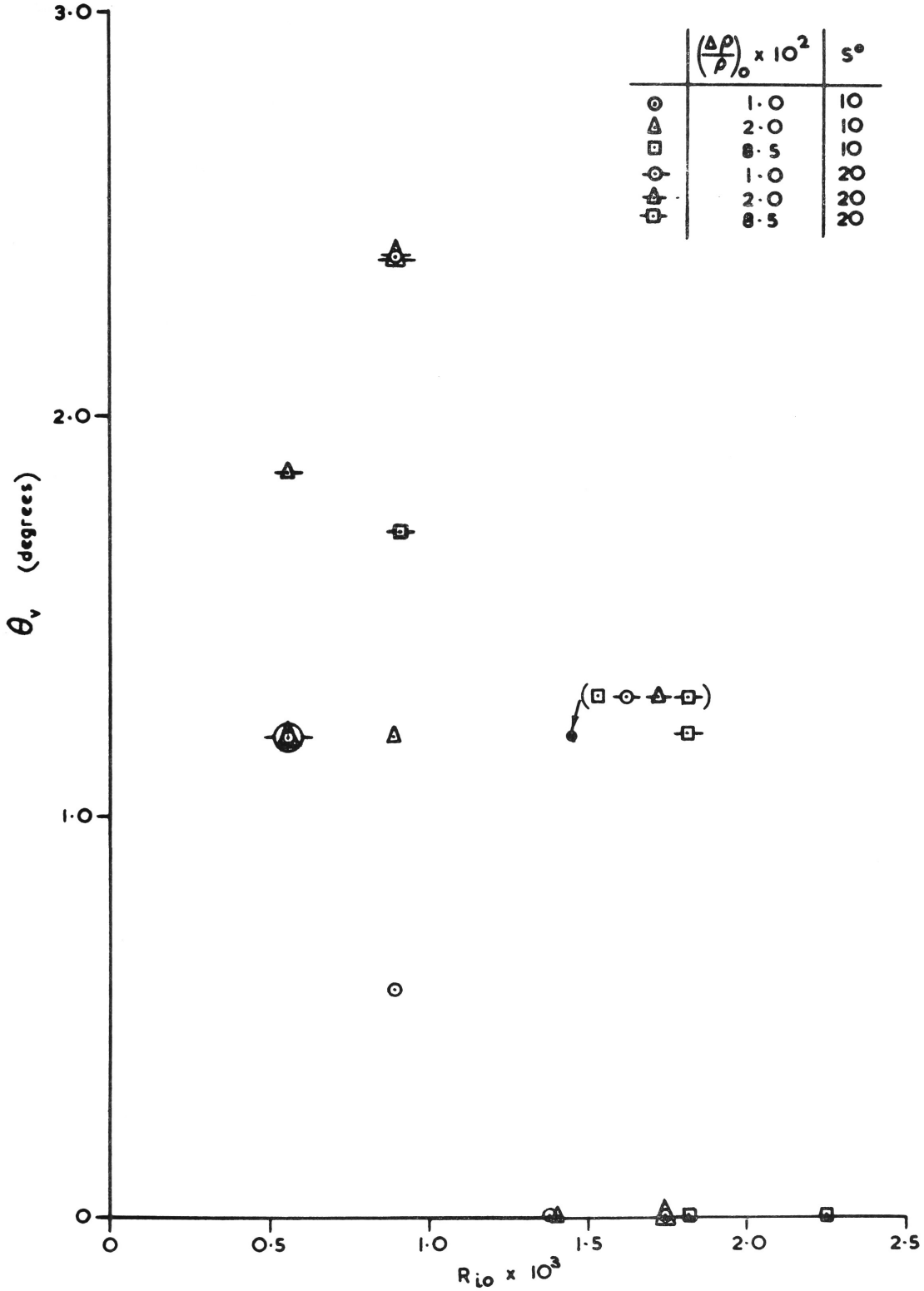

FIGURE 13: ANGLE OF NORMAL SPREAD

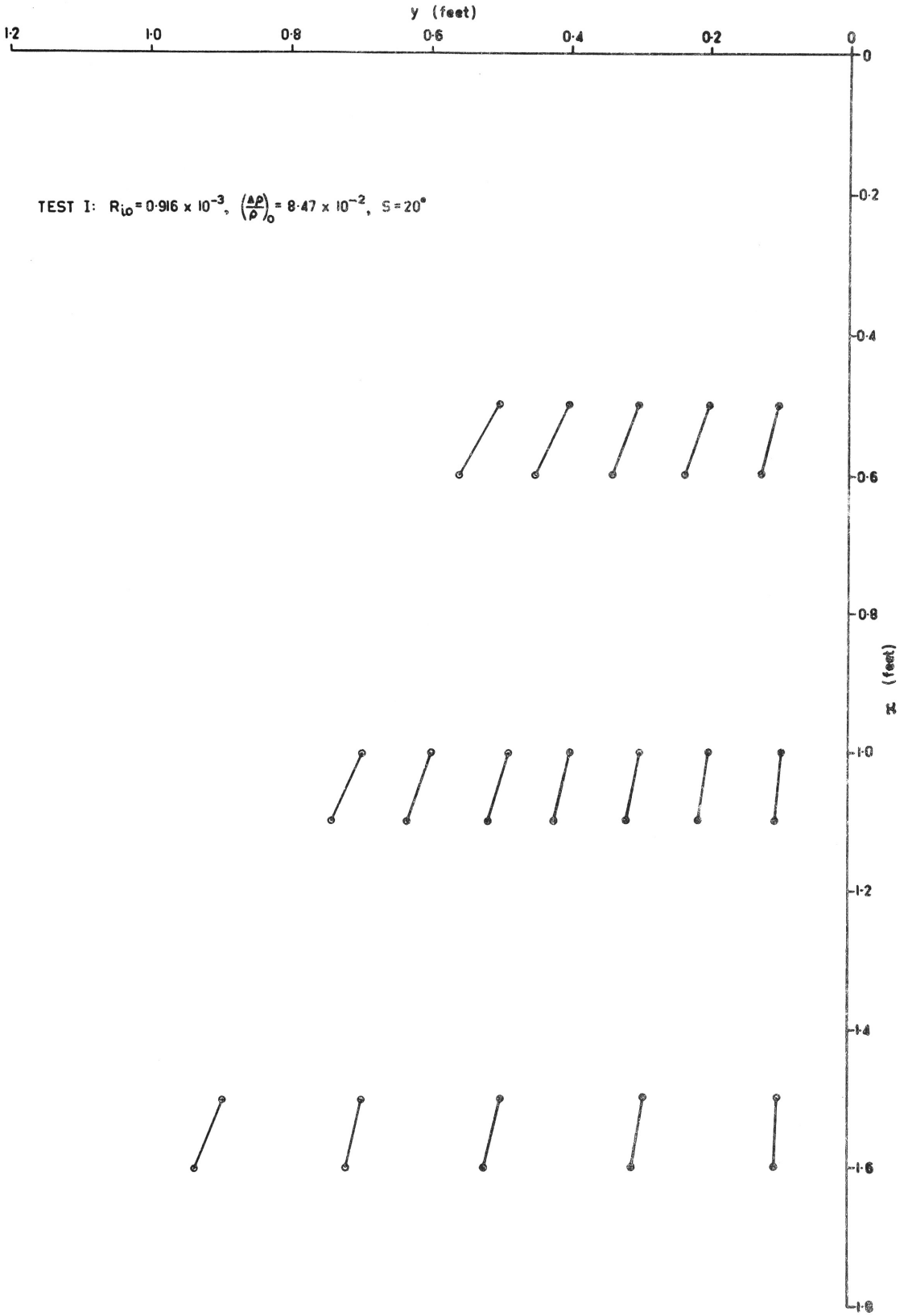

FIGURE 14: STREAKLINE PATTERN FOR A TYPICAL TURBULENT JET

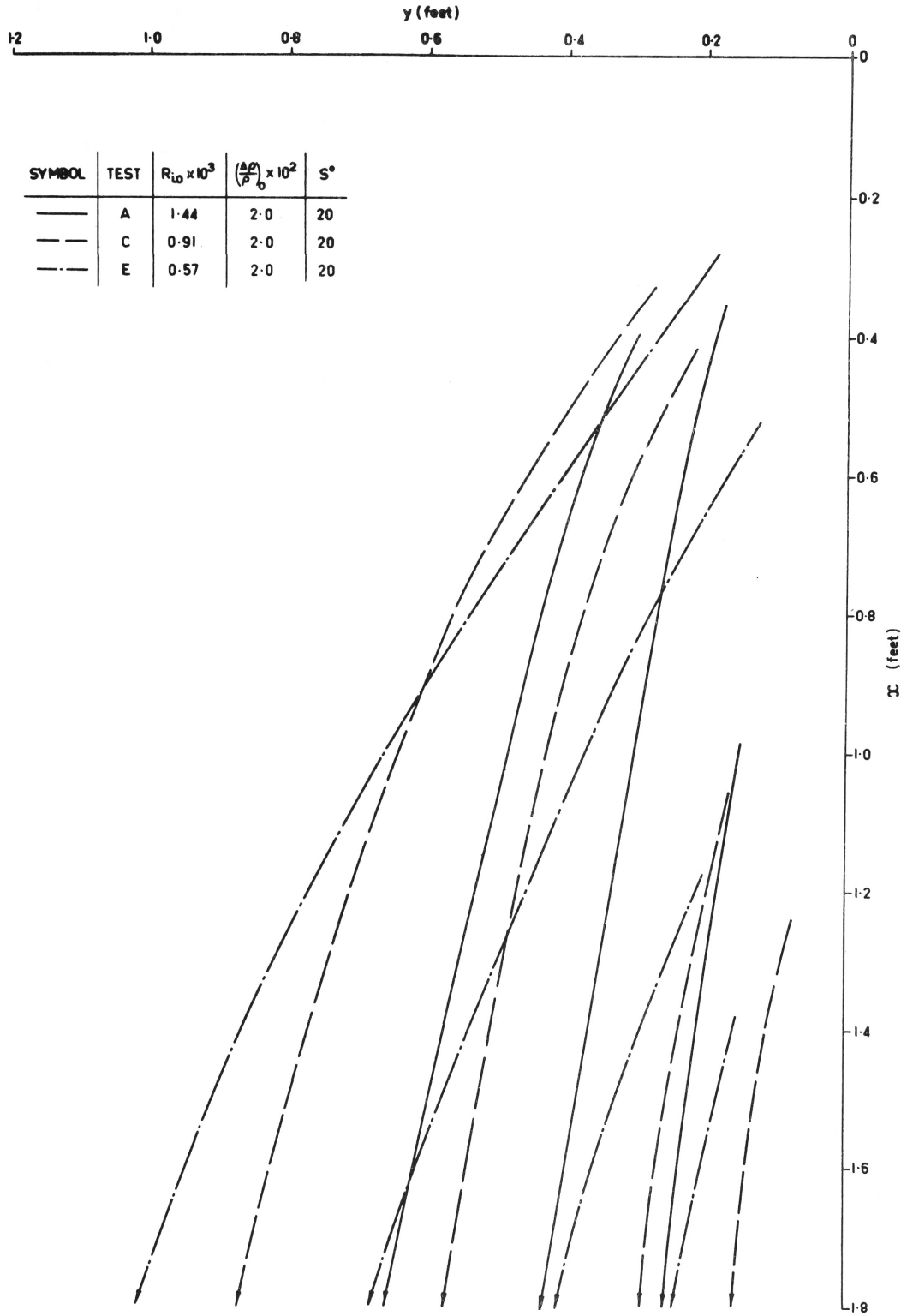

FIGURE 15: EFFECT OF VARYING R_{io} ON THE STREAMLINE PATTERN OF A TURBULENT JET WITH S-CONSTANT AND $\left(\frac{\Delta\rho}{\rho}\right)_o$-CONSTANT

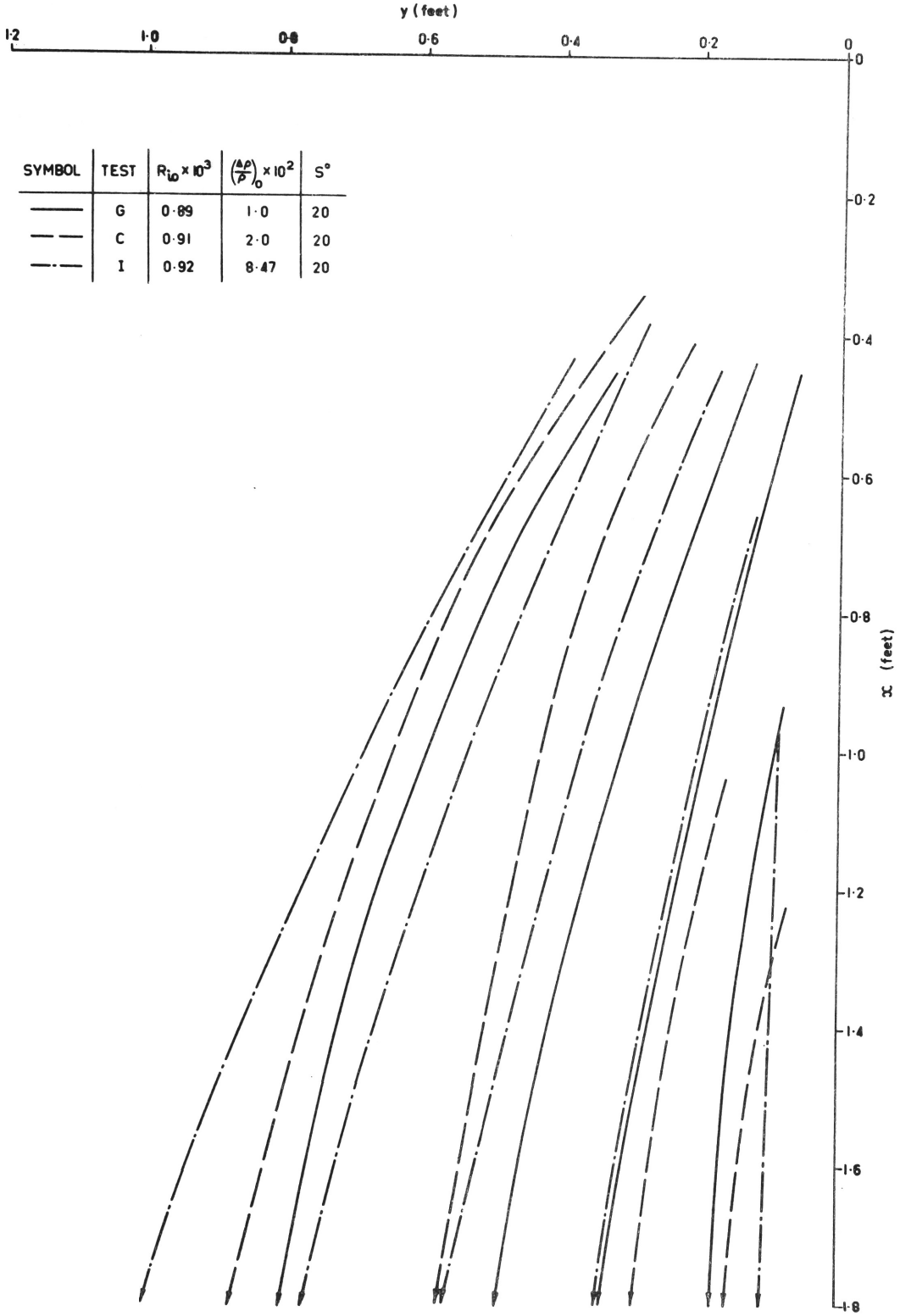

FIGURE 16: EFFECT OF VARYING $\left(\frac{\Delta\rho}{\rho}\right)_o$ ON THE STREAMLINE PATTERN OF A TURBULENT JET WITH R_{io} = CONSTANT AND S = CONSTANT

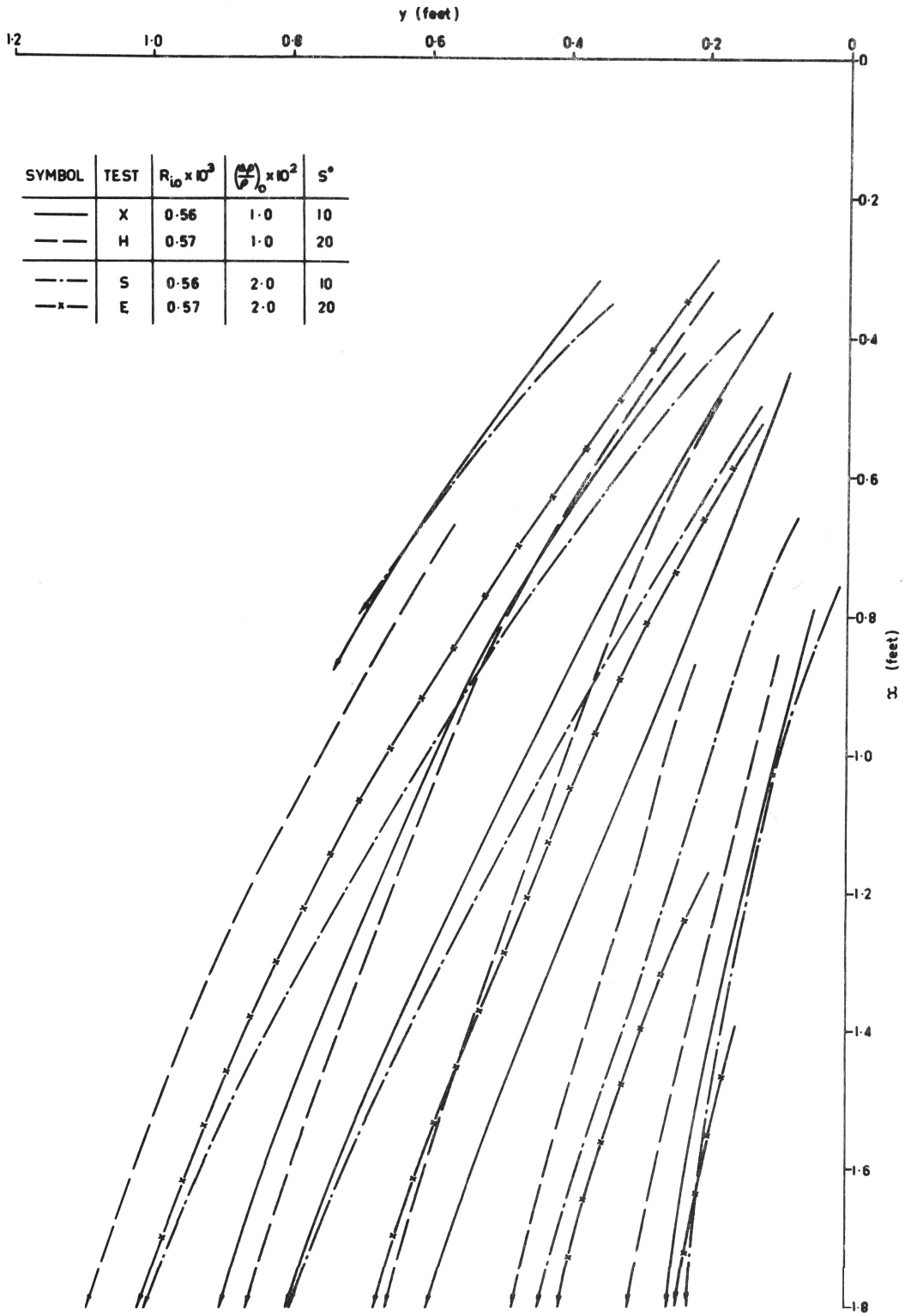

FIGURE 17: EFFECT OF VARYING S ON THE STREAMLINE PATTERN OF A TURBULENT JET WITH R_{io} = CONSTANT AND $\left(\frac{\Delta\rho}{\rho}\right)_o$ = CONSTANT

difference is small. The streamline pattern for a relative density difference $\left(\frac{\Delta\rho}{\rho}\right)_o$ of 8.5 per cent deviates appreciably from the patterns for $\left(\frac{\Delta\rho}{\rho}\right)_o$ of 1.0 and 2.0 per cent. The streamlines for the former compared to the latter appear to spread less near the jet centreline (the x axis) and more near the outer lateral boundary. This confirms the data shown in Fig. 12. It might be considered that the Richardson Number R_{io} is not a sufficient criterion for specifying a jet when the relative density difference $\left(\frac{\Delta\rho}{\rho}\right)_o$ exceeds about 2.0 per cent and that the value of $\left(\frac{\Delta\rho}{\rho}\right)_o$ must also be given.

The effect on lateral spread of varying the boundary slope S while holding other factors constant is shown in Fig. 17. It would appear that increasing the boundary slope from 10^o to 20^o results in a decrease in lateral spread, again confirming the data in Fig. 12.

2.5 Detailed Investigation of a Turbulent Jet

2.5.1 General

Measurements of velocity and density were made at three cross sections of jet number C listed in Table I. The observations were required to check measuring instruments; investigate the self preservation hypothesis; to determine the variation of characteristic property scales (e.g. v_{xmax}, $\Delta\rho_{mean}$ etc.) with distance from the orifice; and to estimate the entrainment and Local Richardson Number at each cross section.

2.5.2 Velocity Measurements

Velocity measurements were made with the Bagnold velocity meter at three cross sections, x = 0.4, 0.7 and 1.0 feet, of jet number C. The velocity profiles on several y = constant planes were obtained at each cross section by traversing the meter normally to the boundary plane as described in Subsection 3.5.5 of Chapter 3. The velocity v at any point was measured with the meter nozzle pointed towards the orifice, that is the nozzle axis was aligned with a radial line from the origin of co-ordinates. The inclination of radial lines to the streamlines shown in Figs. 15 to 17 is in almost all cases less than 10^{o}, and, as the meter is insensitive to yaw up to angles of attack of at least 10^{o}, it follows that the simple procedure used should produce accurate measurements of v. Aligning the nozzle axis with a radial line is much easier than setting it to an inclination determined previously from a streamline pattern.

The x component of velocity was computed from

$$v_x = v \cos\alpha \tag{38}$$

, where α is the inclination of the radial line at a point to the x axis. The profiles at three cross sections of jet number C are shown plotted in Figs. 18 to 20.

Remembering that v_x is slightlyless than v for all profiles shown in Figs. 18 to 20, it is seen that the Bagnold meter will

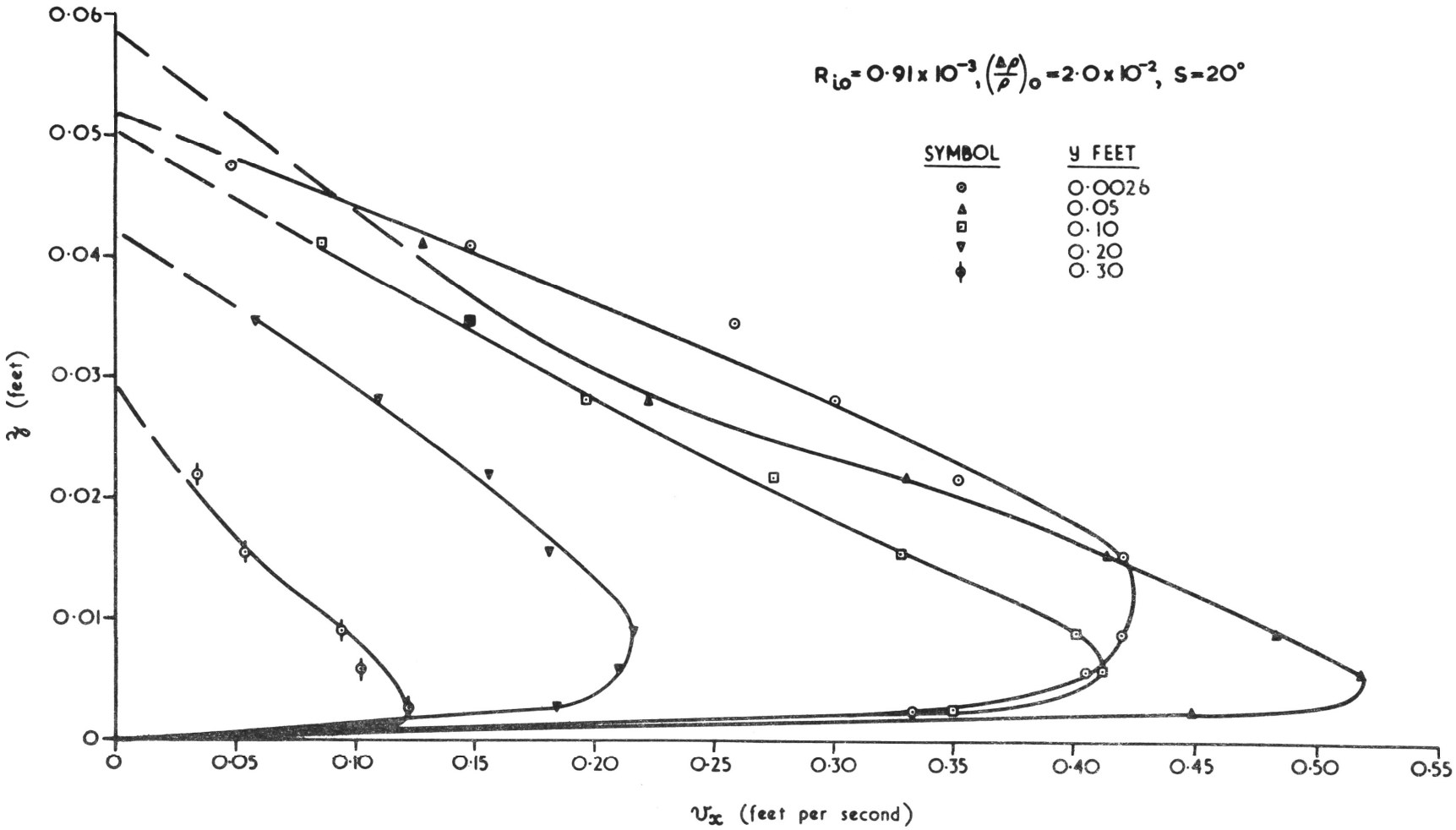

FIGURE 18: v_x PROFILES ON y = CONSTANT PLANES AT x = 0·4 FT. IN A TURBULENT JET

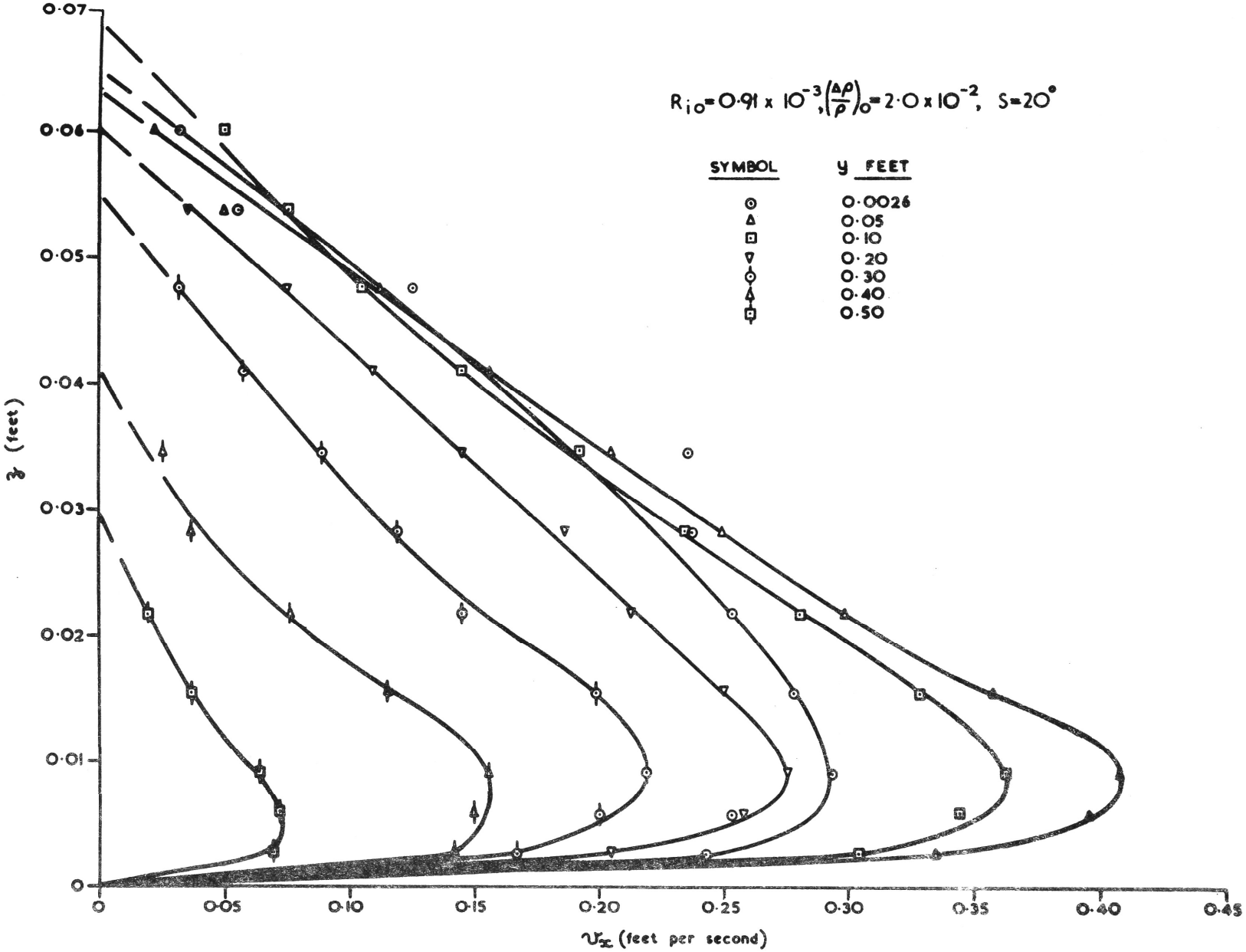

FIGURE 19: u_x PROFILES ON y = CONSTANT PLANES AT x = 0·7 FT. IN A TURBULENT JET

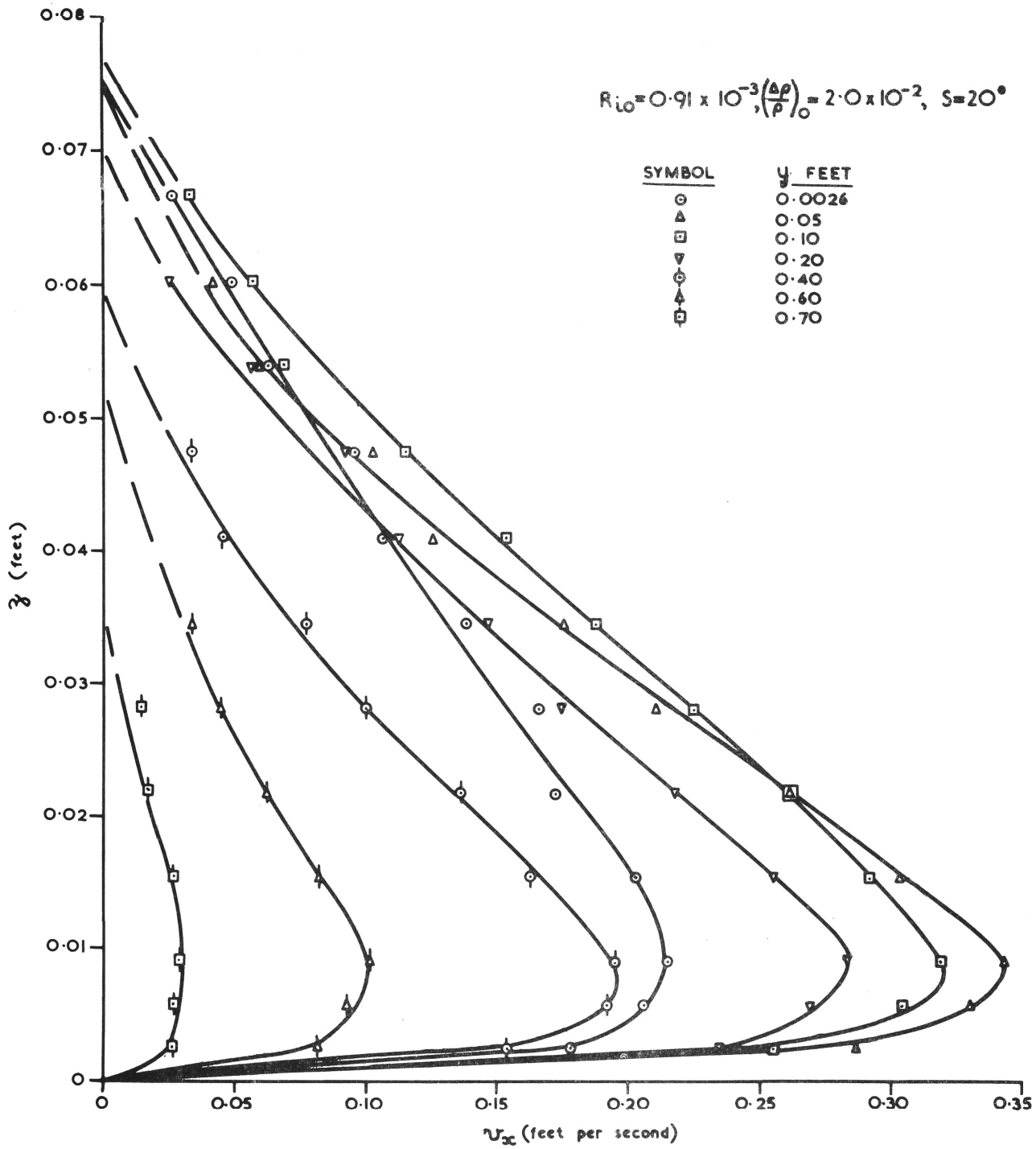

FIGURE 20: u_x PROFILES ON y = CONSTANT PLANES AT x = 1·0 FT IN A TURBULENT JET

comfortably measure velocities in the range 0.025 to 0.5 feet per second. The profiles are similar to those obtained for a two dimensional jet by Ellison and Turner (Ref. 31) in that there is a boundary layer between the boundary and the region of maximum velocity and this is overlain by an almost linear velocity profile. In the case of a three dimensional jet, however, the gradient $\frac{\partial v_x}{\partial z}$ of this linear profile appears to decrease with increasing y. Also in the three dimensional case the linear velocity profile appears to commence at the velocity maximum and not at the somewhat lower velocity shown in Ellison and Turner's profiles. The boundary layer adjacent to the vertical sidewall of the experimental tank is also evident in the profiles shown in Figs. 18 to 20.

2.5.3. Density Measurements

Density measurements were made at the same three cross sections of jet number C at which velocities were measured. The relative density difference profiles shown plotted in Figs. 21 to 23 were obtained by the method of analysis of discrete withdrawn samples which is described in detail in Subsection 4.3.5. of Chapter 4.

Again the measured profiles for the three dimensional case are similar to Ellison and Turner's two dimensional profiles in that the maximum density occurs at the boundary plane. The two dimensional profiles show a well defined layer of high density gradient $\frac{\partial(\frac{\Delta\rho}{\rho})}{\partial z}$ immediately adjacent to the boundary which is overlain by a region where

the density gradient is much lower. The junction of these two regions appears to coincide with the z level of the point of maximum velocity v_{xmax}. In the case of a three dimensional jet, however, the two regions of widely different density gradient are not as pronounced. The higher density fluid appears to be fairly well dispersed across the cross section at x = 0.4 feet and it is only at the x = 1.0 feet cross section that two regions of different density gradient begin to appear. In the three dimensional case therefore the higher density fluid appears to flow in the form of a central core which decreases in height, but increases in width, with distance down the boundary plane.

2.5.4. Instrument Check

In subsection 1.5.1. of Chapter 1 it was shown that the flux of density excess K in the direction of flow (the x direction) of a three dimensional jet must be constant, that is:

$$K = \int_0^{\infty} \int_{-\infty}^{+\infty} v_x \, \Delta\rho \, dy \, dz = \text{Constant} \qquad (24)$$

It is more convenient in the present case to work in terms of flux of relative density excess $\frac{K}{\rho}$ given by:

$$\frac{K}{\rho} = \int_0^{\infty} \int_{-\infty}^{+\infty} v_x \, \frac{\Delta\rho}{\rho} \, dy \, dz = \text{Constant} \qquad (39)$$

as v_x and $\frac{\Delta\rho}{\rho}$ profiles have been plotted in Figs. 18 to 23. $\frac{K}{\rho}$ must also be constant at each flow cross section as the density of the ambient fluid ρ is constant.

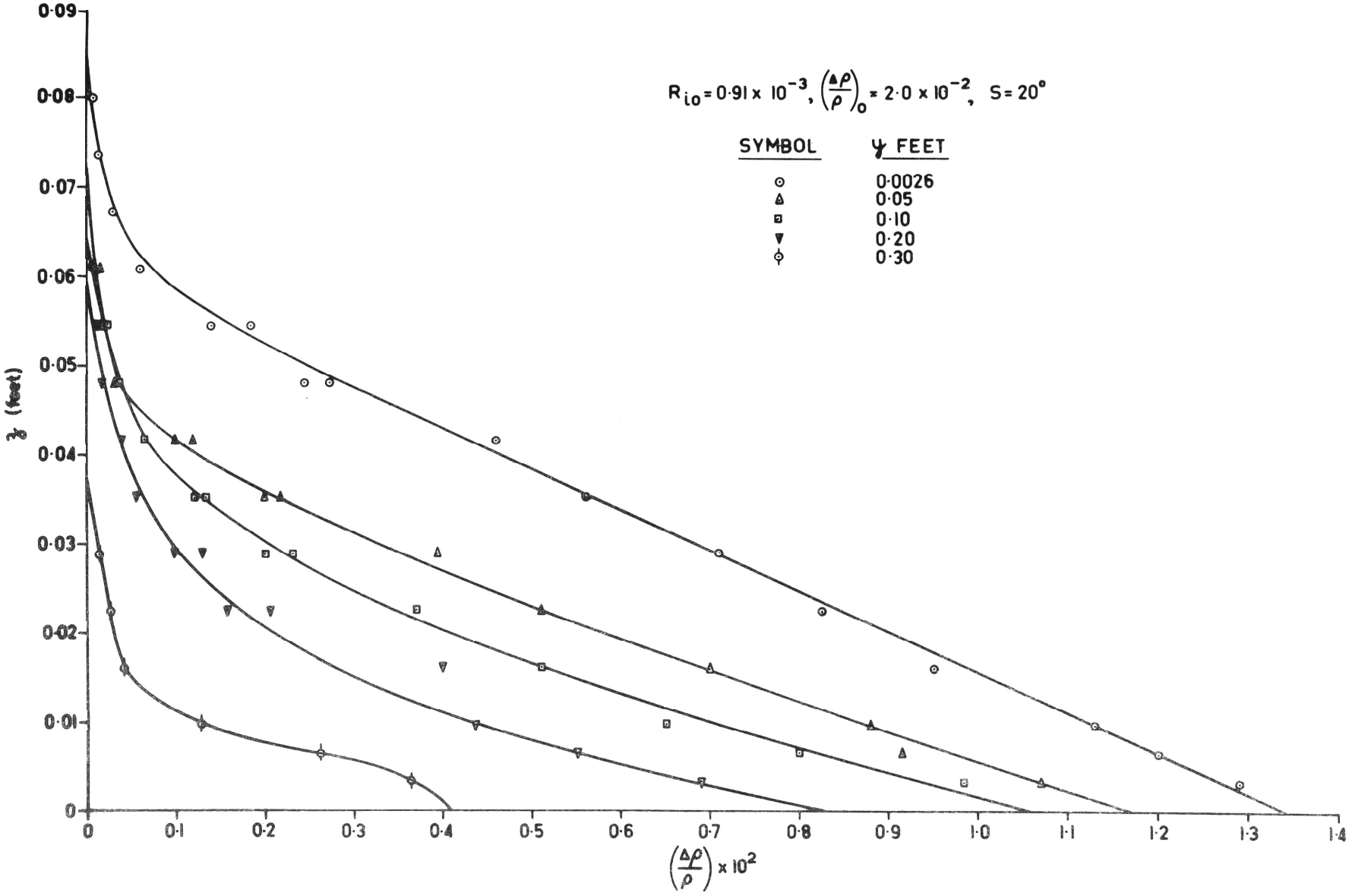

FIGURE 21: $\frac{\Delta\rho}{\rho}$ PROFILES ON ψ = CONSTANT PLANES AT x = 0·4 FT. IN A TURBULENT JET

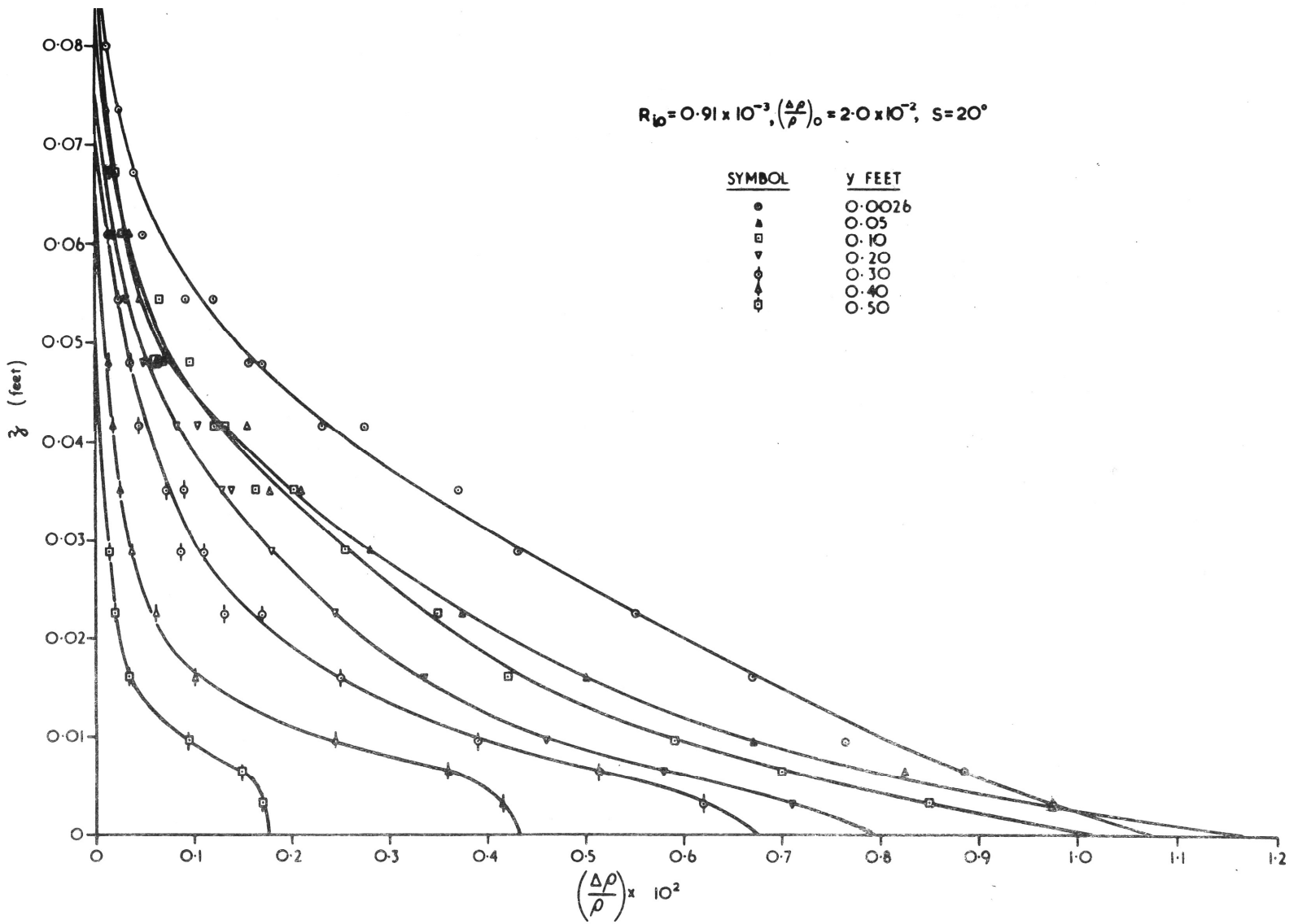

FIGURE 22: $\frac{\Delta\rho}{\rho}$ PROFILES ON y = CONSTANT PLANES AT x = 0·7 FT. IN A TURBULENT JET

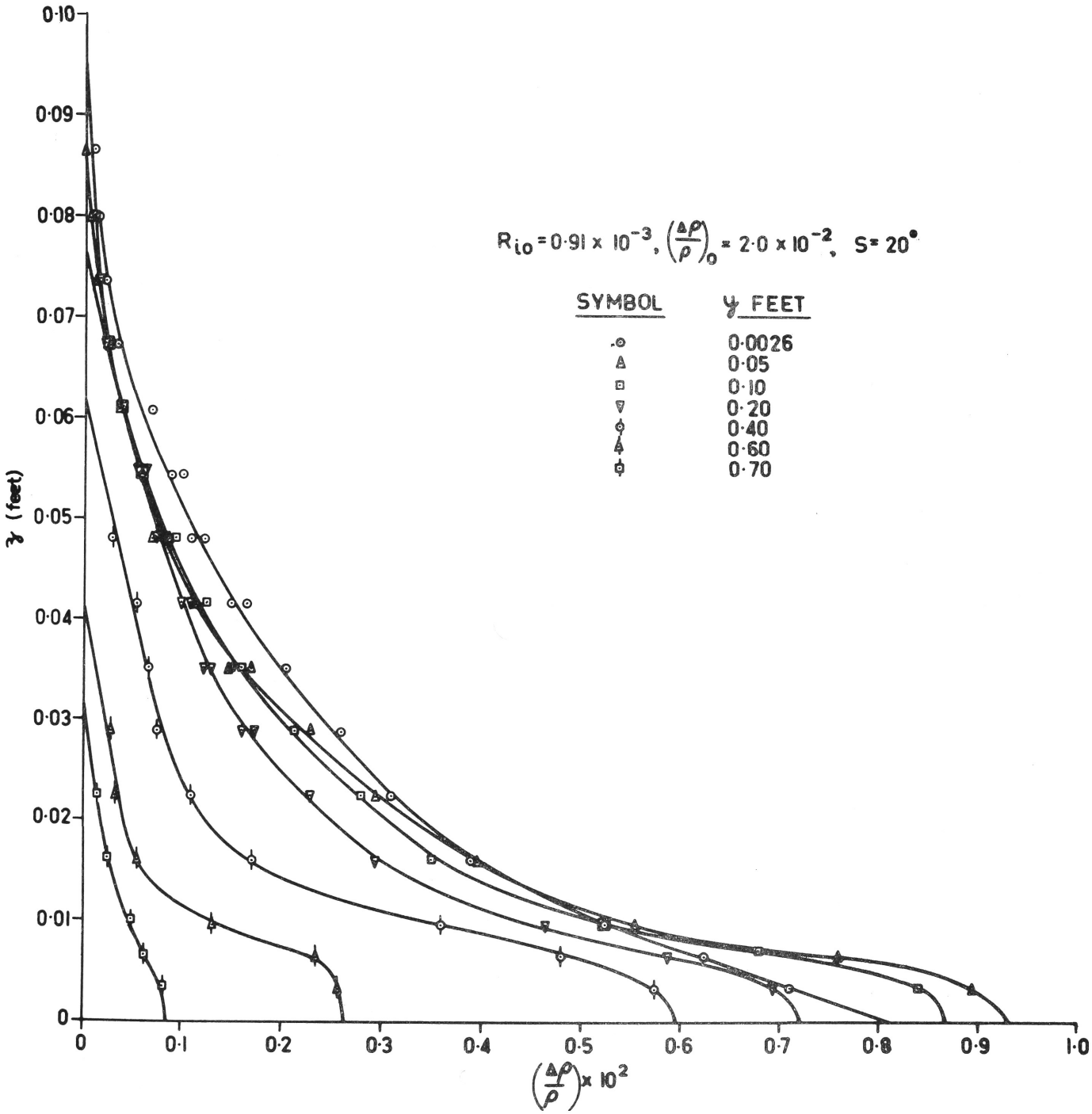

FIGURE 23: $\frac{\Delta\rho}{\rho}$ PROFILES ON y=CONSTANT PLANES AT x=1·0 FT. IN A TURBULENT JET

The right hand side of equation (39) represents the volume enclosed by an x = constant plane and the envelope of normals of length $v_x \frac{\Delta\rho}{\rho}$ erected on that plane. The volume was evaluated by first plotting profiles of $v_x \frac{\Delta\rho}{\rho}$ on z = constant planes for the three flow cross sections as shown in Figs. 24 to 26, and then applying the mean end area formula to areas measured by planimeter. The flux of relative density excess at the orifice was calculated from the data in Table 1, and this is compared with the measured values at the three cross sections in Table 2.

Table 2

Flux of Relative Density Excess $\frac{K}{\rho}$ at Three Cross Sections of Turbulent Jet Number C.

Cross Section, Distance from Orifice x, in ft.	Measured $\frac{K}{\rho}$ x 10^6, in ft.^{3} sec.$^{-1}$	Percentage Error compared to $\frac{K}{\rho}$ at Orifice
0.0	13.36	
0.4	13.46	+0.8
0.7	13.75	+2.9
1.0	13.48	+0.9

The probable cause of the slight over estimate of $\frac{K}{\rho}$ at the three cross sections is treated in detail in the discussion of "Verification of Performance" in Subsection 3.5.5. of Chapter 3. Suffice to say at this stage that the maximum error of +3 per cent in measured $\frac{K}{\rho}$ at a jet cross section is more than satisfactory for an exploratory investigation.

2.5.5. Investigation of Self Preservation

To investigate self preservation of velocity and density difference it is necessary to plot $\frac{v_x}{v_{xmax.}}$ and $\frac{\Delta\rho}{\Delta\rho_{mean}}$ for the three cross sections investigated in terms of the non-dimensional width and height parameters $\epsilon = \frac{y}{b}$ and $\eta = \frac{z}{h}$ respectively. v_{xmax}, $\Delta\rho_{mean}$, b and h are the characteristic velocity, density, width and height scales respectively at a cross section.

v_{xmax} at the cross sections x = 0.4, 0.7 and 1.0 feet was selected from Figs. 27, 28 and 29 respectively, which are v_x profiles on z = constant planes. The value of v_{xmax} for each cross section is shown in Table 3.

Table 3.

Properties of Three Cross Sections of Turbulent Jet Number C.

Cross Section. Distance from Orifice x, in feet.	Velocity Scale v_{xmax}, in ft. sec^{-1}	$\left[\int_0^\infty v_x\,dz\right]_{y\,at\,v_{xmax}} \times 10^3$, in ft.^{2} sec^{-1}	Height Scale $hx10^3$, in ft.	Volumetric Flow-rate $Qx10^4$, in ft.^{3} $sec.^{-1}$	Width Scale $bx10^2$, in ft.	Density Scale $\left(\frac{\Delta\rho}{\rho}\right)_{mean}x10^4$
0.4	0.52	14.04	27.05	25.82	18.39	51.74
0.7	0.41	13.45	32.97	39.25	29.18	34.04
1.0	0.34	11.74	34.2	50.04	42.62	26.70

The height and width scales h and b at a cross section were defined by equations (28) and (29) in Subsection 1.5.2 of Chapter 1:

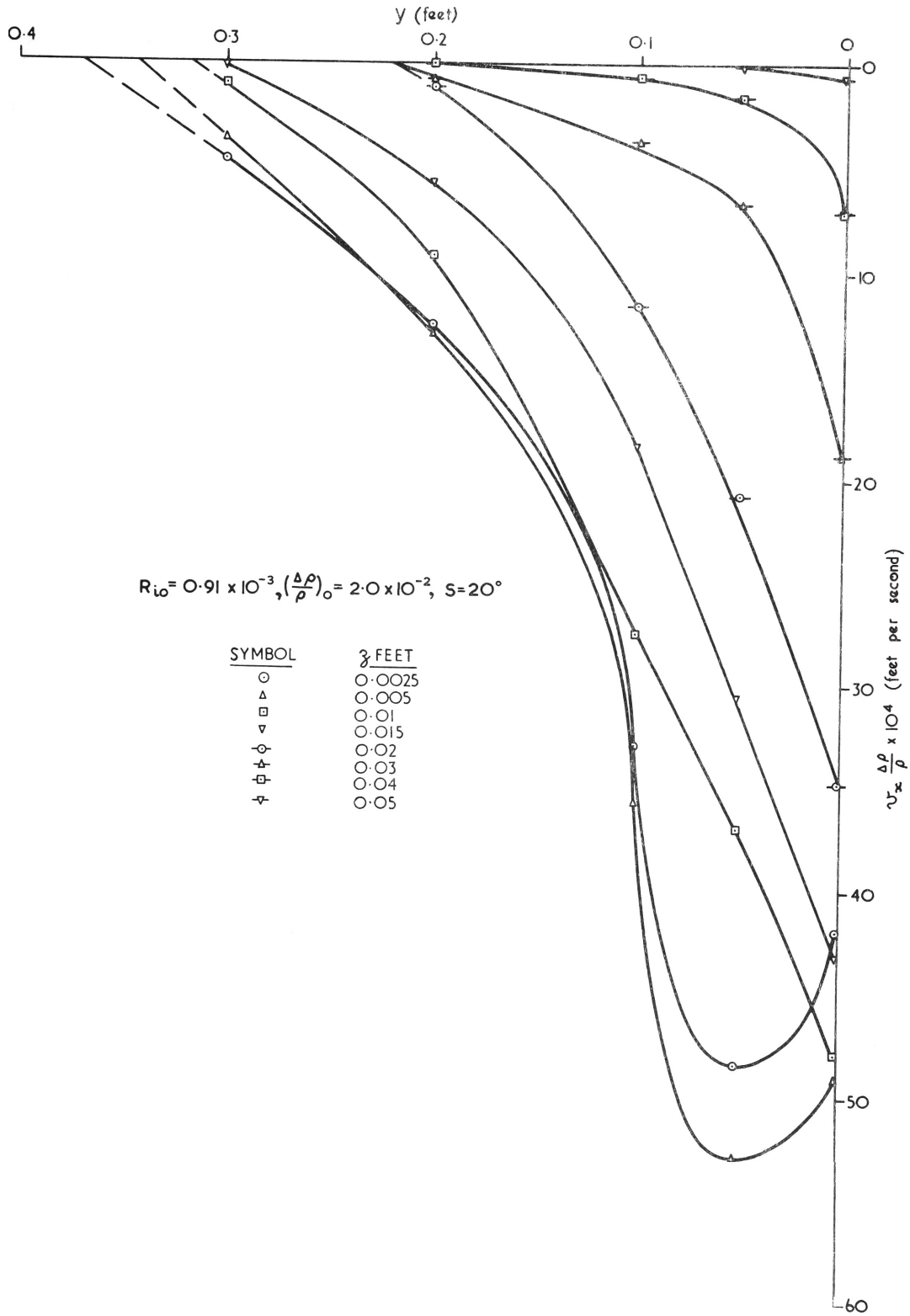

FIGURE 24: $v_x \frac{\Delta\rho}{\rho}$ PROFILES ON z = CONSTANT PLANES AT x=0·4 FT. IN A TURBULENT JET

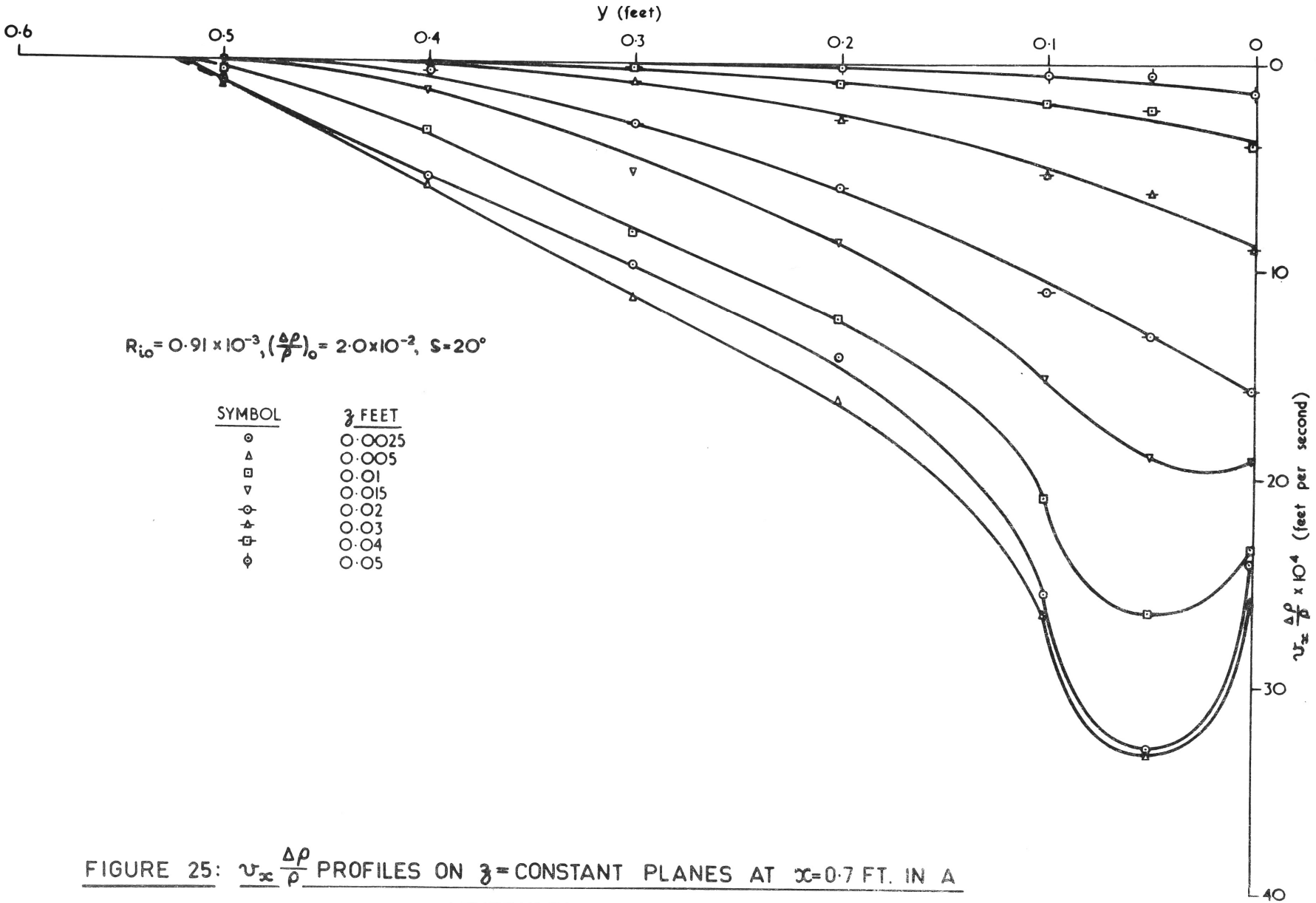

FIGURE 25: $v_x \frac{\Delta\rho}{\rho}$ PROFILES ON z = CONSTANT PLANES AT x=0·7 FT. IN A TURBULENT JET

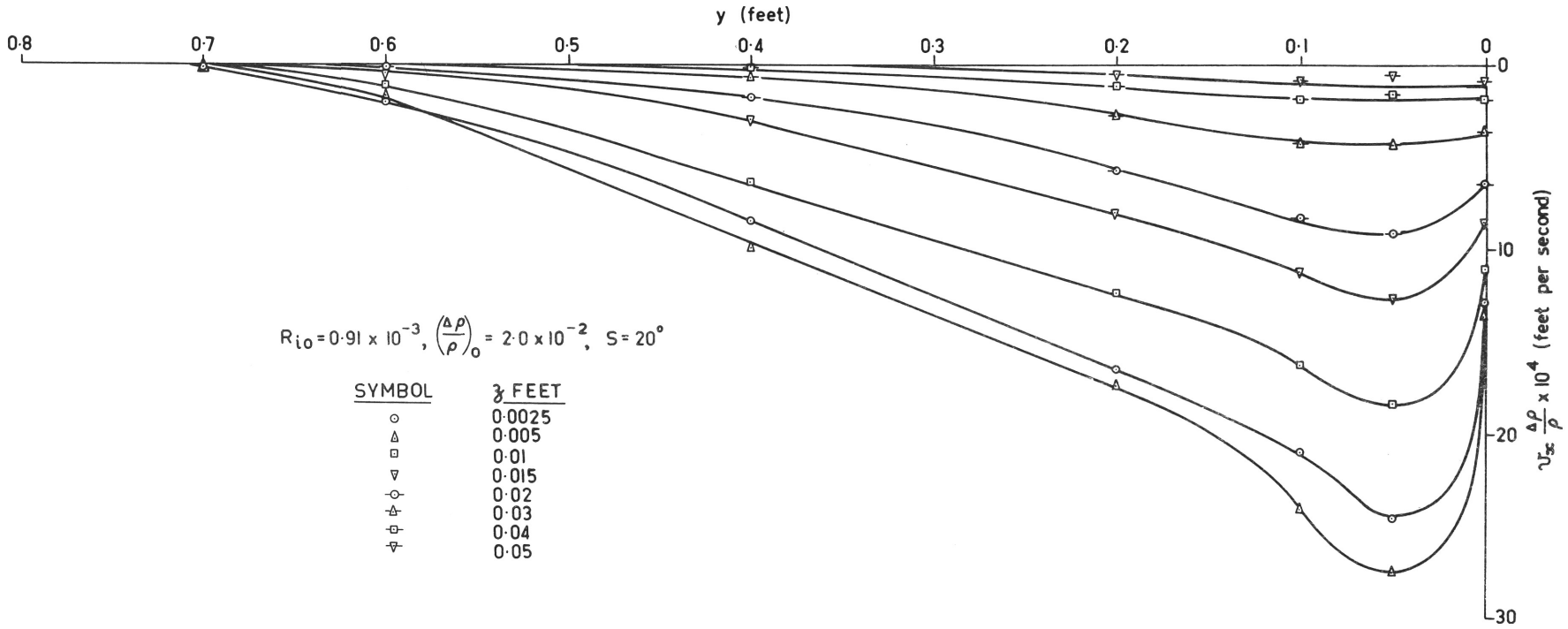

FIGURE 26: $v_x \frac{\Delta\rho}{\rho}$ PROFILES ON z=CONSTANT PLANES AT x=1·0 FT. IN A TURBULENT JET

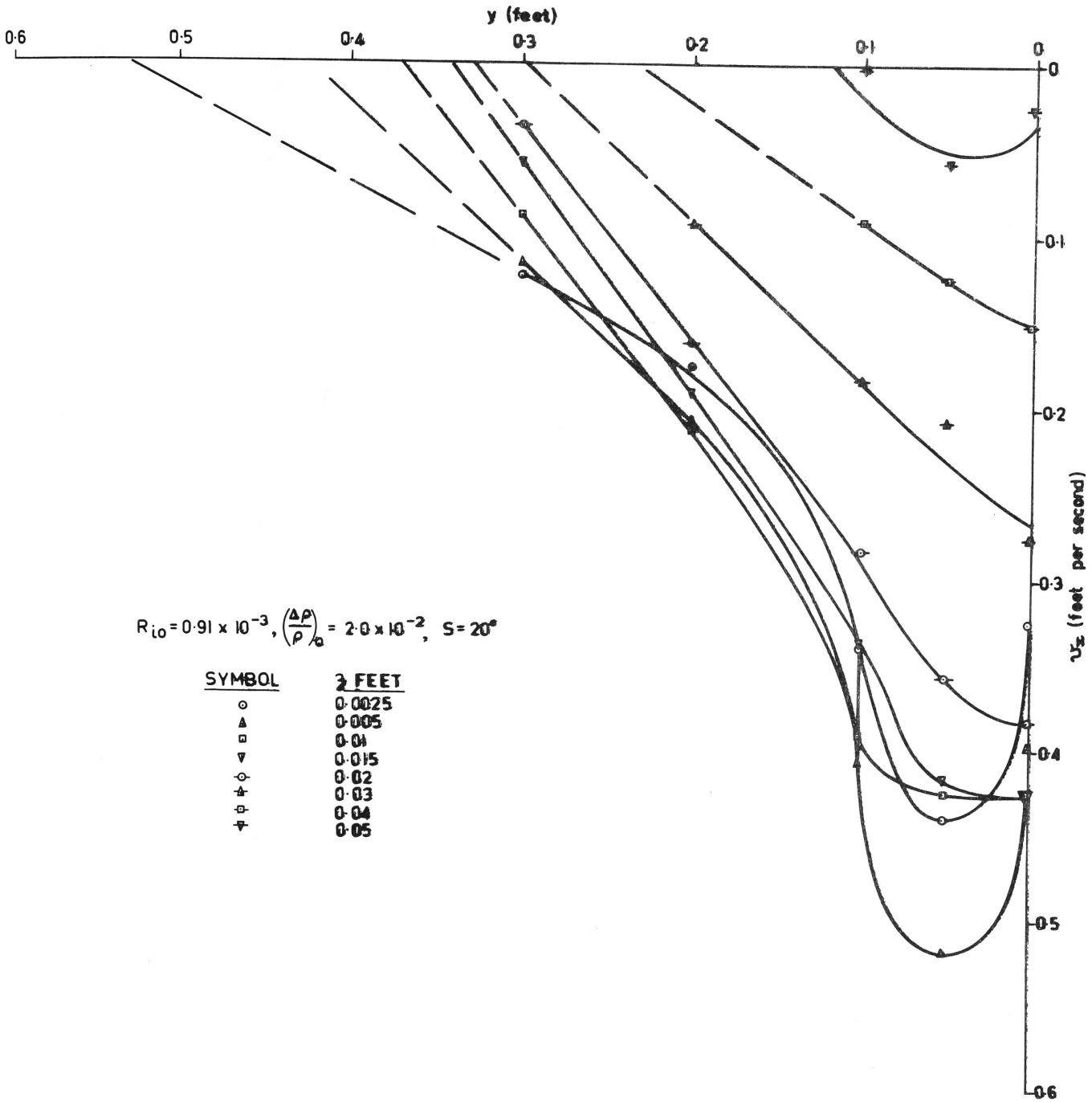

FIGURE 27: v_x PROFILES ON z-CONSTANT PLANES AT x=0·4 FT. IN A TURBULENT JET.

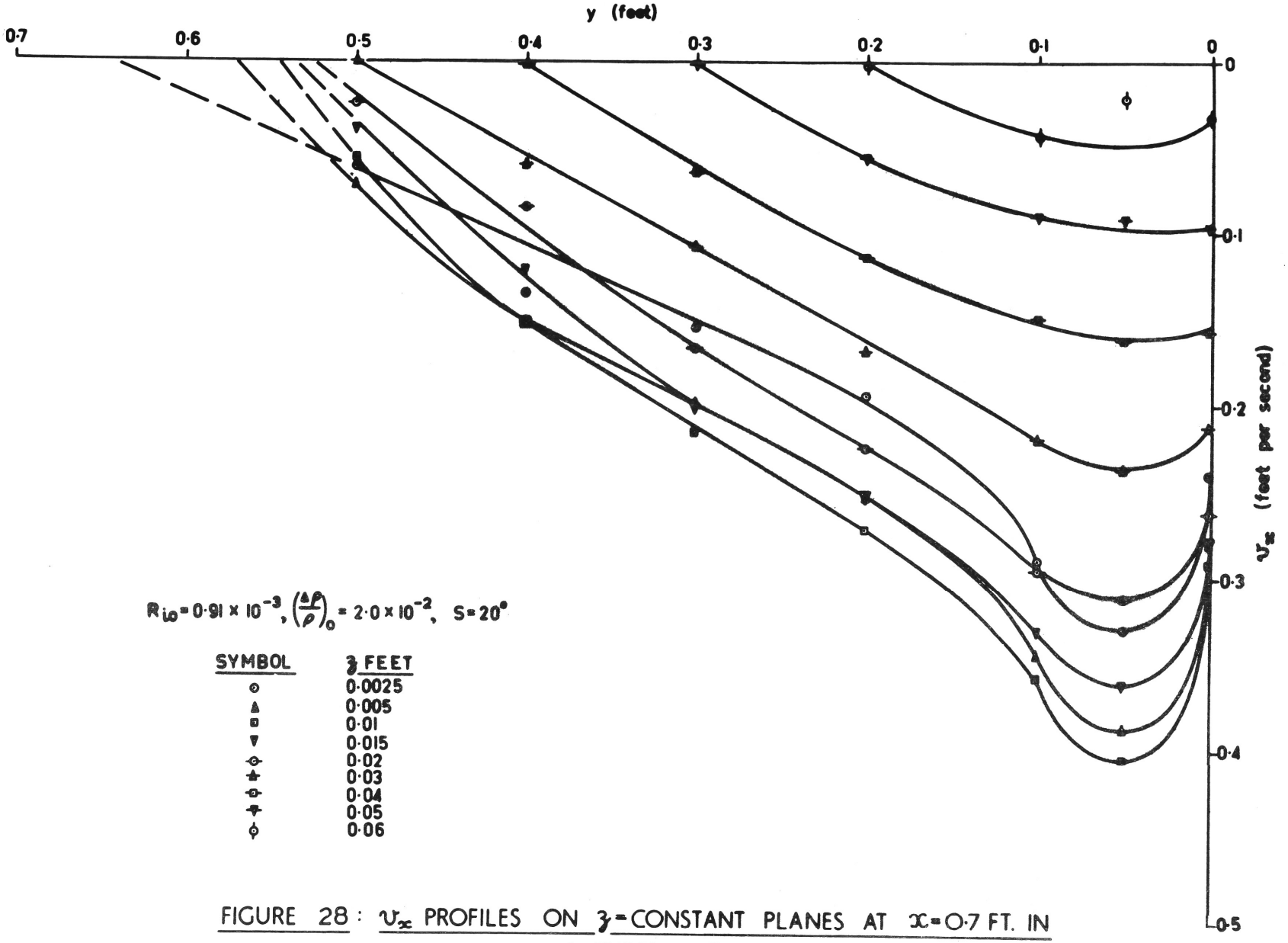

FIGURE 28 : v_x PROFILES ON z = CONSTANT PLANES AT x = 0·7 FT. IN A TURBULENT JET

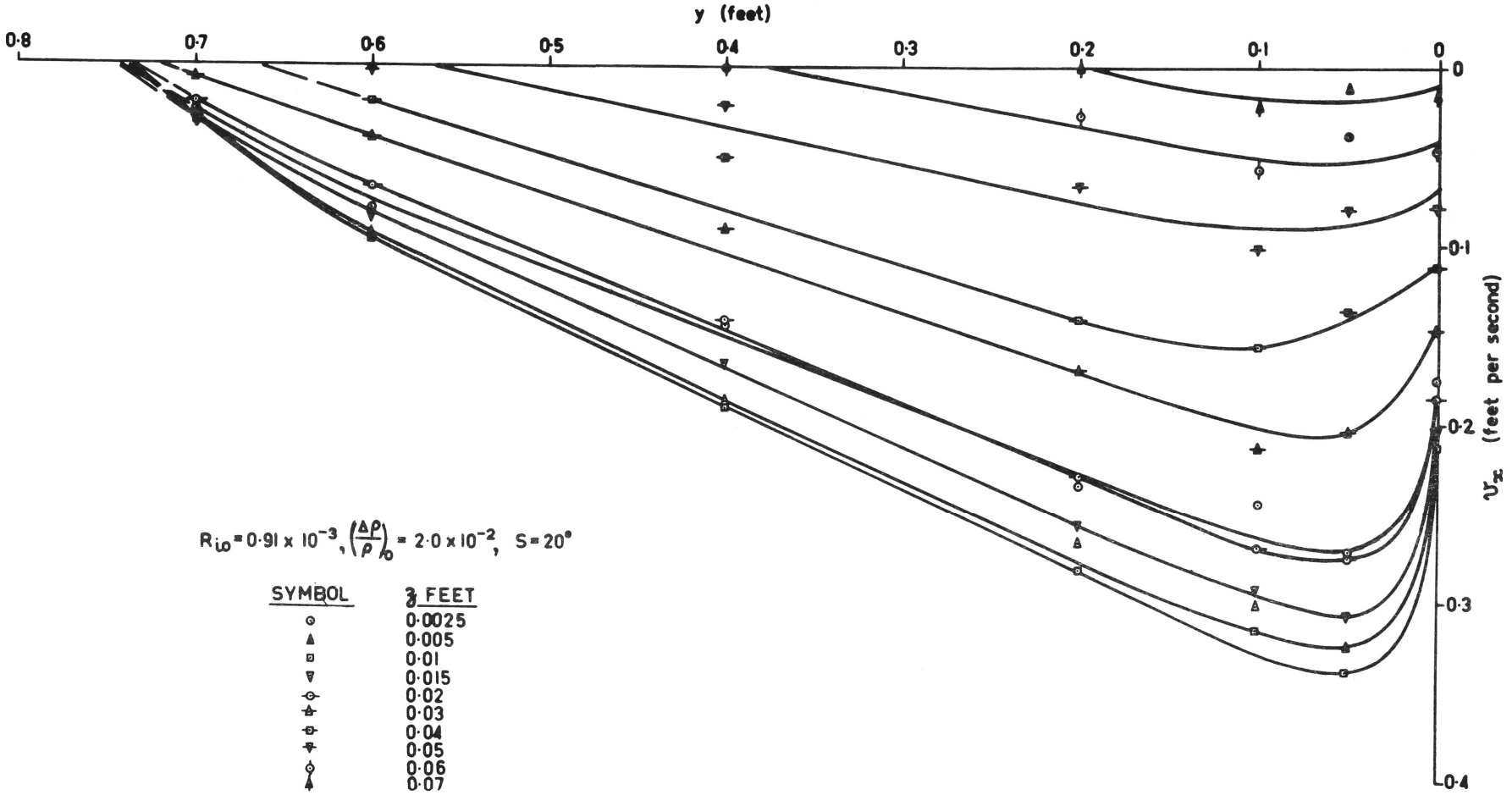

FIGURE 29: v_x PROFILES ON z = CONSTANT PLANES AT x = 1·0 FT. IN A TURBULENT JET

$$h = \frac{\left| \int_0^{\infty} v_x \, dz \right|_{y \text{ at } v_{xmax}}}{v_{xmax}} \qquad (28)$$

$$b = \frac{\int_{-\infty}^{+\infty} \int_0^{\infty} v_x \, dz \, dy}{h \, v_{xmax}} \qquad (29)$$

The integral $\left| \int_0^{\infty} v_x \, dz \right|_{y \text{ at } v_{xmax}}$ for each cross section was obtained by area measurement of the appropriate profile from Figs. 18 to 20 and the results are shown in Table 3. The value of the height scale at each cross section obtained by using equation (28) is also shown in Table 3.

To determine the width scale b at each cross section it is necessary to evaluate $\int_{-\infty}^{+\infty} \int_0^{\infty} v_x \, dz \, dy$ = volumetric flowrate Q, for substitution in equation (29). Q at each cross section was obtained by utilising the v_x profiles on z = constant planes shown in Figs. 27 to 29 and applying the mean end area formula. Again the results for Q and thence b from equation (29) are shown in Table 3.

The mean relative density excess $\left(\frac{\Delta\rho}{\rho}\right)_{mean}$ at each cross section was obtained by using a modified form of equation (30) from Subsection 1.5.2. of Chapter 1, that is

$$\left(\frac{\Delta\rho}{\rho}\right)_{mean} = \frac{\Delta\rho_{mean}}{\rho} = \frac{\frac{K}{\rho}}{Q} \qquad (40)$$

Equation (40) is obtained from equation (30) by remembering that the

fresh water density ρ is constant. It is more convenient to work in terms of $\left(\frac{\Delta\rho}{\rho}\right)_{mean}$ at this stage as $\frac{K}{\rho}$ and Q have already been evaluated for each cross section. The values of $\left(\frac{\Delta\rho}{\rho}\right)_{mean}$ obtained by using equation (40) are shown in Table 3.

Having obtained the characteristic width, height and velocity scales at each cross section, these were combined with the v_x profiles shown in Figs. 18 to 20 to plot non-dimensional velocity diagrams. A typical diagram showing values at grid intersections and lines of equal $\frac{v_x}{v_{xmax}}$ is shown for the cross section at x = 1.0 feet in Fig. 30. Composite diagrams for the three cross sections examined are shown in Figs. 31 and 32. For complete self preservation of velocity profiles the $\frac{v_x}{v_{xmax}}$ lines for the three cross sections should coincide. It is seen that the coincidence is satisfactory in the outer portion of the jet away from the boundary plane and the tank sidewall. The spread of the lines in this region might be accounted for by the error in positioning the velocity meter. In the boundary layer regions close to the boundary plane and the sidewall, however, the spread of the $\frac{v_x}{v_{xmax}}$ lines is too great to be accounted for by positioning errors and the velocity profiles are not self preserving close to a boundary.

Knowing the characteristic width, height and density scales at each cross section and utilising the $\frac{\Delta\rho}{\rho}$ profiles shown in Figs. 21 to 23 the non-dimensional density profiles shown in the Figs. 33 and 34

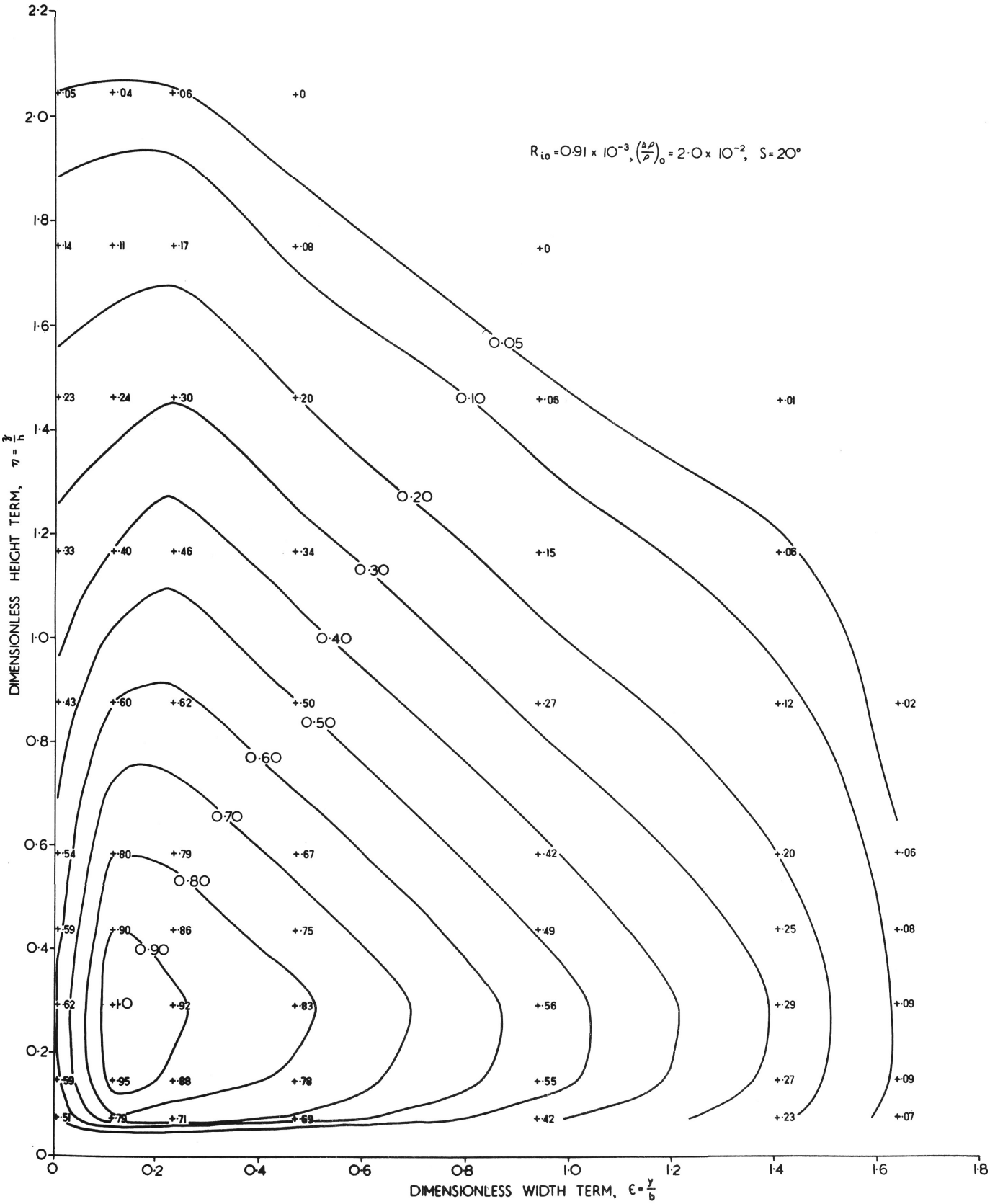

FIGURE 30: LINES OF EQUAL $\frac{v_x}{v_{x\,max.}}$ AT x = 1·0 FT. IN A TURBULENT JET

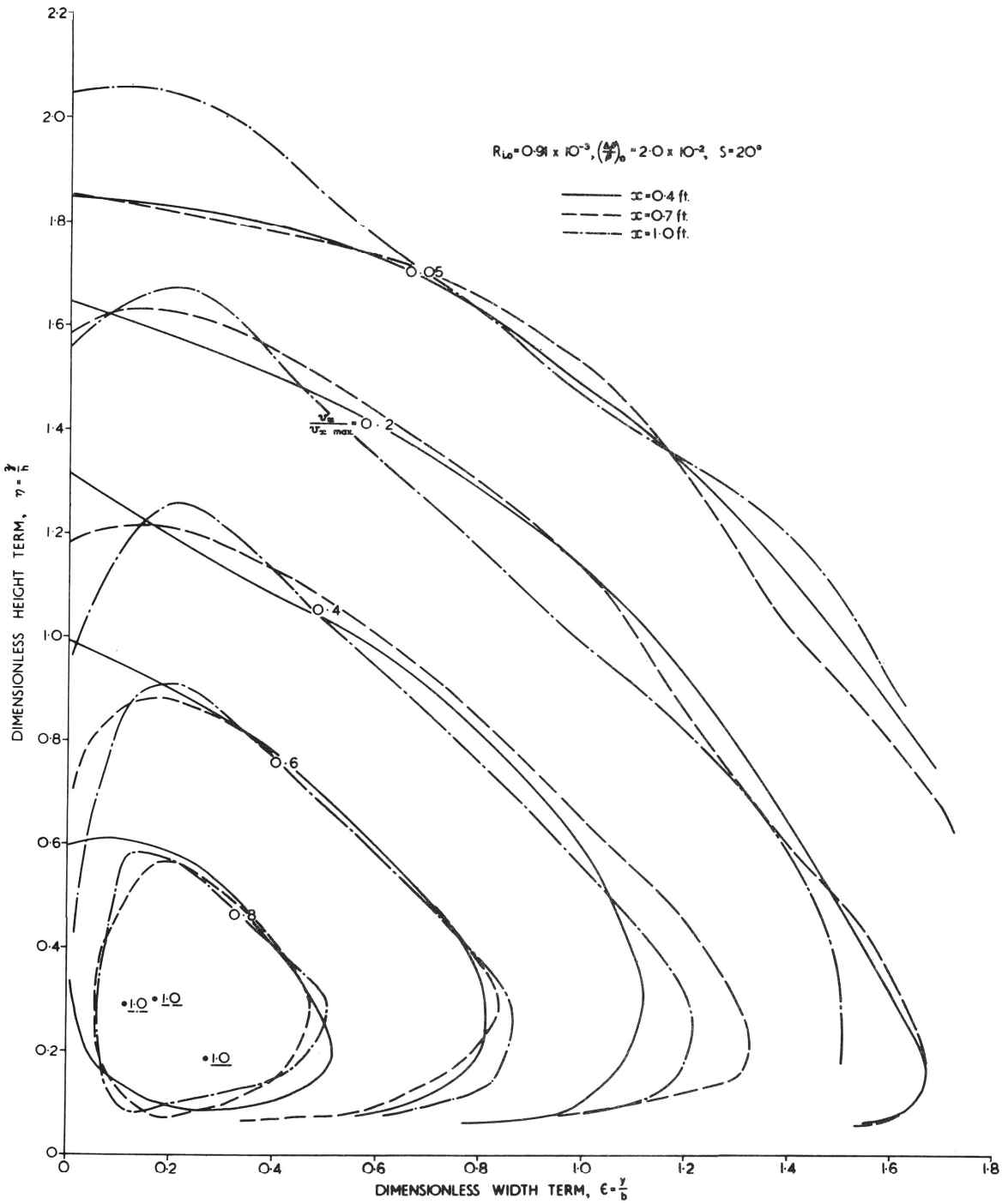

FIGURE 31: LINES OF EQUAL $\frac{v_x}{v_{x\,max}}$ AT THREE CROSS SECTIONS IN A TURBULENT JET

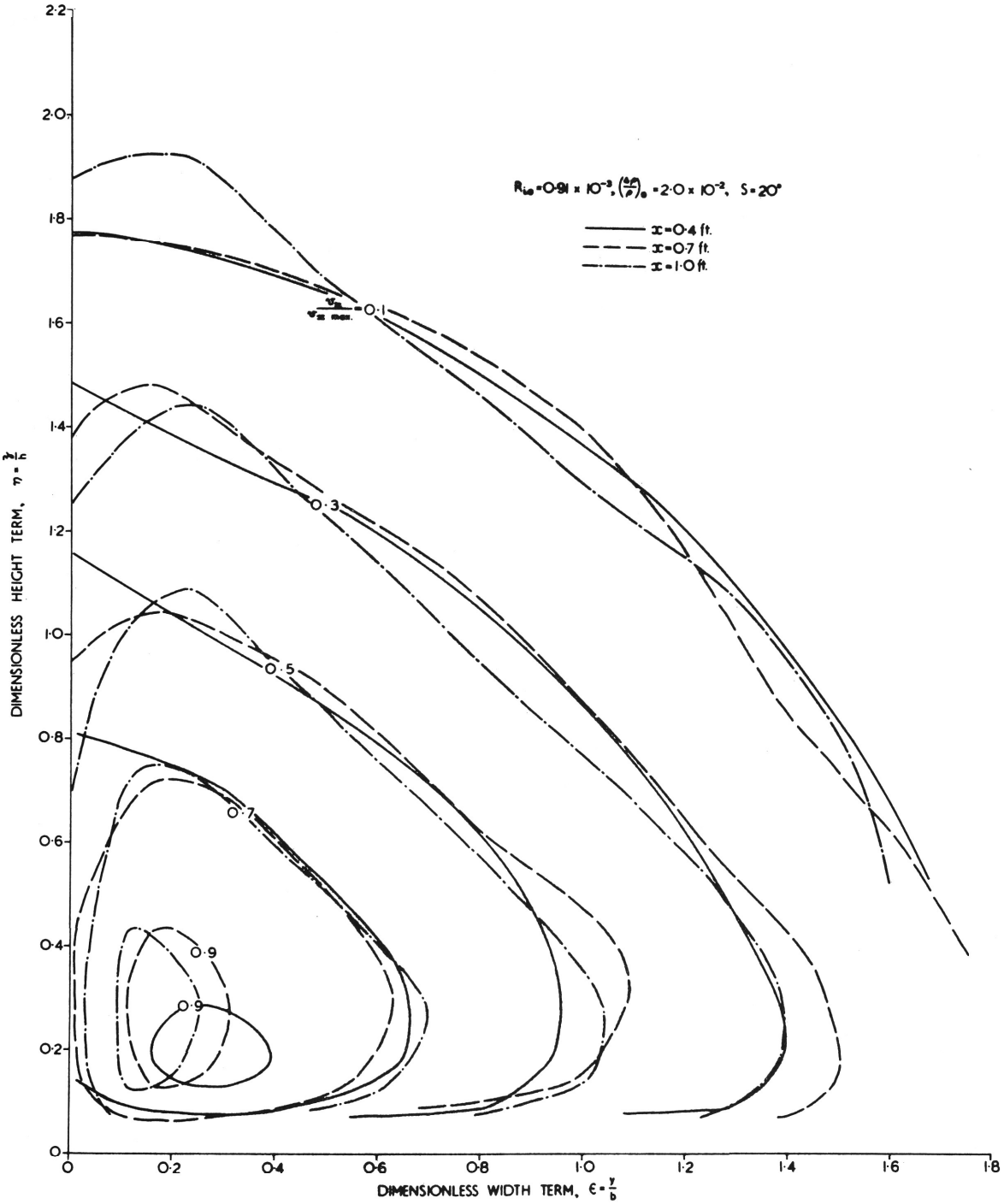

FIGURE 32: LINES OF EQUAL $\frac{v_x}{v_{x\,max.}}$ AT THREE CROSS SECTIONS IN A TURBULENT JET

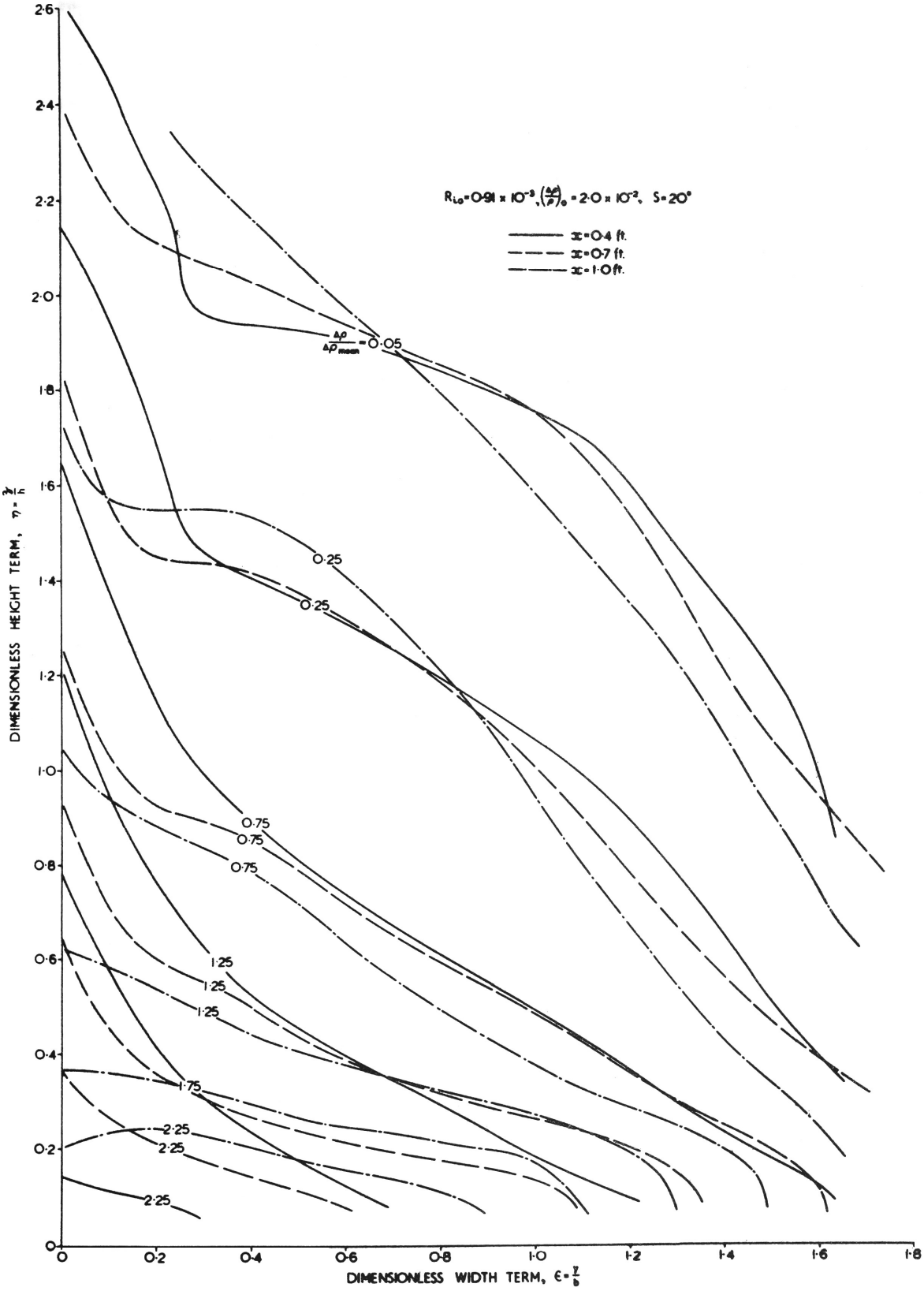

FIGURE 33: LINES OF EQUAL $\frac{\Delta\rho}{\Delta\rho_{max}}$ AT THREE CROSS SECTIONS IN A TURBULENT JET

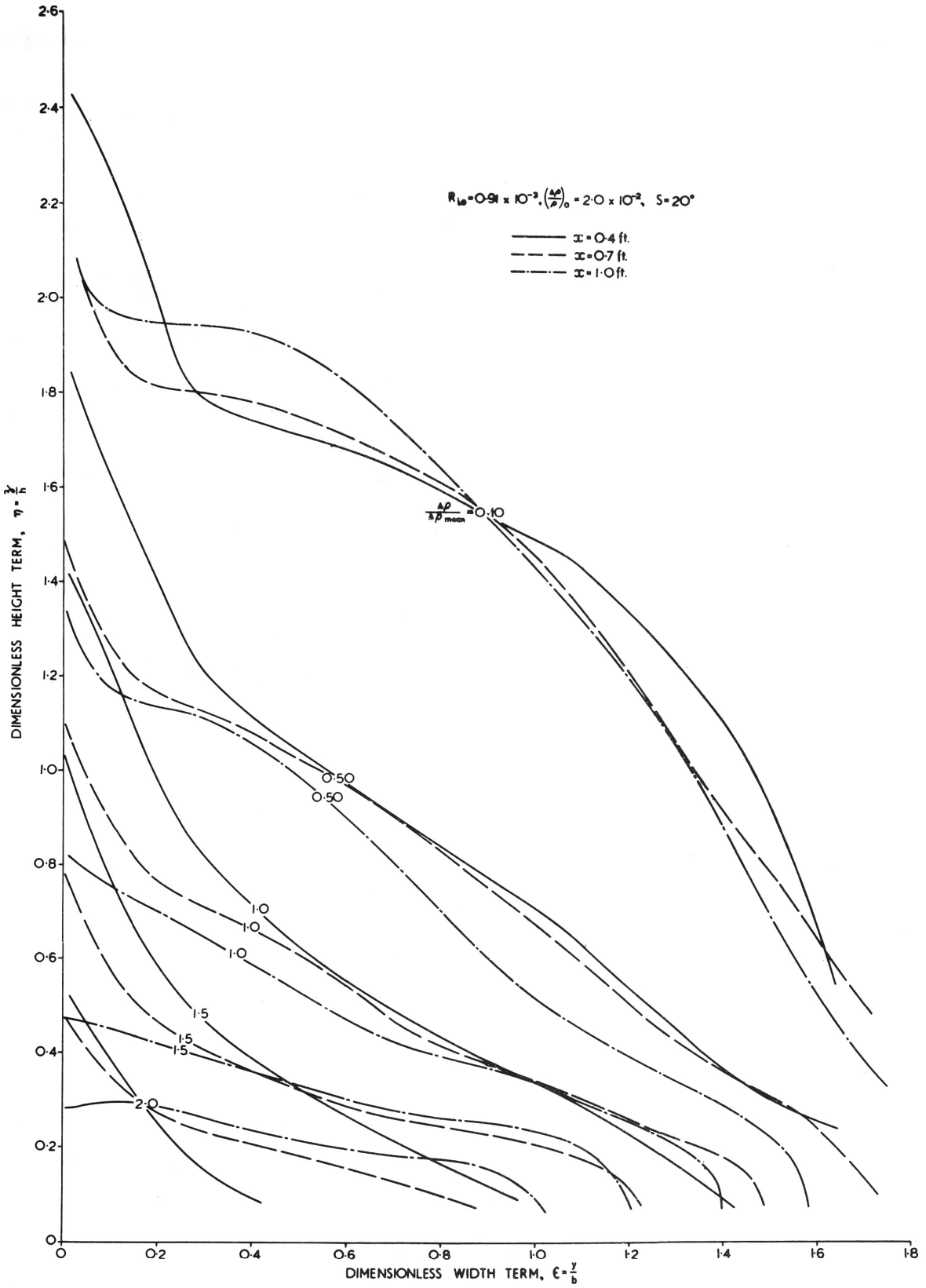

FIGURE 34: LINES OF EQUAL $\frac{\Delta\rho}{\Delta\rho_{mean}}$ AT THREE CROSS SECTIONS IN A TURBULENT JET

were plotted. As with the velocity profiles, the spread between lines is less in the outer portion of the jet away from the boundary plane and the sidewall. Even in this outer region, however, the agreement between lines is not as good as that for the velocity profiles. The positioning error of the nozzle for withdrawing density samples should be less than that of the velocity meter whose nozzle is longer and less rigid. Hence positioning error cannot account entirely for the spread of the lines in the case of the density profiles, and one could not claim with confidence that the density profiles are self-preserving on the basis of the data shown in Figs. 33 and 34.

2.5.6. Variation of Characteristic Scales with Distance from the Virtual Origin

In this Subsection the variation of the characteristic width, height, velocity and density scales with distance from the virtual origin will be compared with the predictions made in Subsections 1.4.2. and 1.5.3. of Chapter 1. The values computed for the characteristic scales at the three cross sections of jet number C are shown in Table 3.

The variation of the width and height scales b and h respectively with distance x down the boundary plane is shown in Fig. 35A. As predicted both b and h appear to be linear functions of x. It may be noted in Fig. 35A that the virtual origin for the height and width scales is located at the centre of the orifice. Also Fig. 35A shows that

$\frac{b}{h}$ is not constant as required by the self preservation assumption but increases in the direction of flow. Fortunately this non independence of X of the $\frac{b}{h}$ ratio does not affect the predictions for v_{xmax} (X) and $\Delta\rho_{mean}$(X) as it is only the powers of b (X) and h(X) which are of interest when making these predictions.

If the virtual origin for the b scale (i.e. at the origin of co-ordinates) is taken as also applying to the velocity and density scales v_{xmax} and $\frac{\Delta\rho_{mean}}{\rho}$ then the log-log plots in Figs. 35B and 35C result for $v_{xmax}(x)$ and $\frac{\Delta\rho_{mean}}{\rho}(x)$ respectively. Note that taking the virtual origin at the origin of the co-ordinates in effect makes the (X, Y, Z) and (x, y, z) co-ordinate systems coincide. The predictions for $v_{xmax}(x)$ and $\frac{\Delta\rho_{mean}}{\rho}$ (x) for a fully turbulent jet from Chapter 1 are also shown as dotted lines in Figs. 35B and 35C respectively.

The measured value of $v_{xmax}(x)$ is $v_{xmax} \propto x^{-0.46}$ while the predicted relation is $v_{xmax} \propto x^{-0.33}$. This discrepancy might be accounted for in two ways; firstly the measurements may have been taken in the zone of unestablished flow. In Subsection 1.4.2 of Chapter 1 it is shown that in the zone of unestablished flow (where both buoyancy and momentum effects are significant) $v_{xmax} \propto x^{a}$, where a lies between -0.33 and -1.0. The fact that the velocity profiles appear to be self preserving, however, tends to show that the cross sections investigated were in the zone of established flow. The second

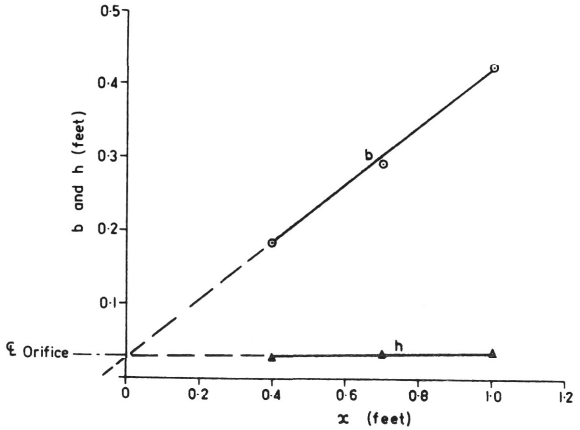

FIGURE 35A. b (x) and h (x)

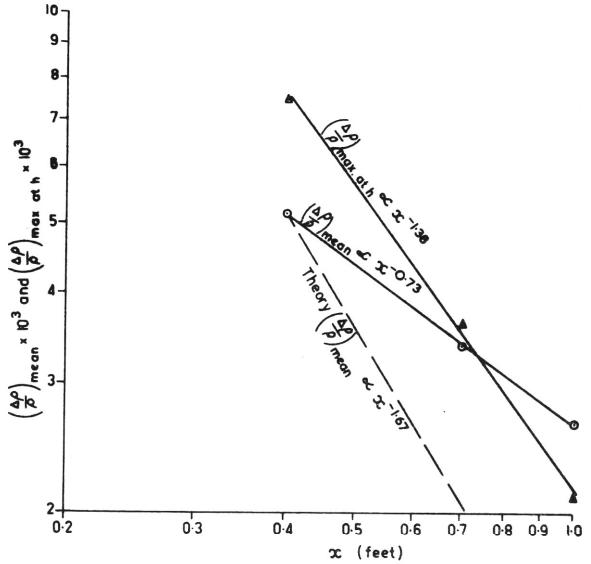

FIGURE 35C. $\left(\frac{\Delta\rho}{\rho}\right)_{mean}$ (x) and $\left(\frac{\Delta\rho}{\rho}\right)_{max.\ at\ h}$ (x)

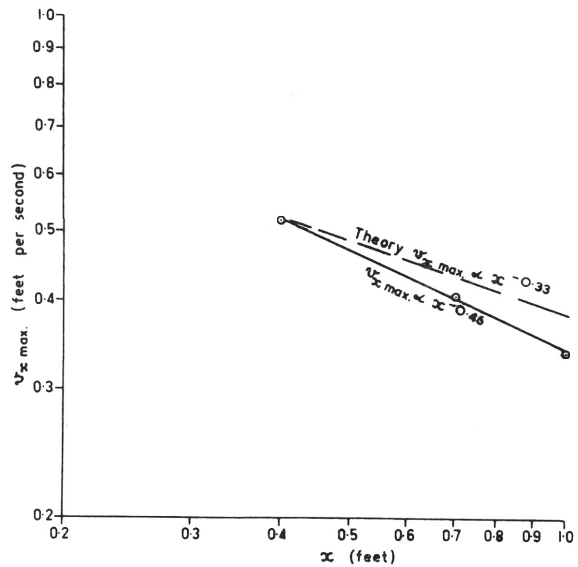

FIGURE 35B. $v_{x\ max}$ (x)

$R_{i0} = 0{\cdot}91 \times 10^{-3}$, $\left(\frac{\Delta\rho}{\rho}\right)_0 = 2{\cdot}0 \times 10^{-2}$, $S = 20°$

FIGURE 35: VARIATION OF CHARACTERISTIC SCALES WITH DISTANCE FROM VIRTUAL ORIGIN

explanation is that the jet is not fully turbulent throughout the flow cross section as assumed in the dimensional analysis. In Figs. 21 to 23 it may be seen that the region adjacent to the boundary is one of steep density gradient and this is overlain by a region of slighter density gradient. It is generally accepted that a steep density gradient has a strong inhibiting effect on the development of turbulence throughout the flow cross section. This would account for the difference between the observed and predicted values of $v_{xmax}(x)$.

In Fig. 35C the measured value of $\frac{\Delta\rho_{mean}}{\rho}(x)$ is $\frac{\Delta\rho_{mean}}{\rho} \propto x^{-0.73}$ which varies greatly from the predicted value of $\frac{\Delta\rho_{mean}}{\rho} \propto x^{-1.67}$. The incomplete turbulence discussed above may possibly account for this discrepancy between the two exponents. To check this a characteristic density scale of $\left(\frac{\Delta\rho}{\rho}\right)_{max}$ at the height h was found for each cross section from Figs. 21 to 23 and these values are shown plotted in Fig. 35C. The variation of $\left(\frac{\Delta\rho}{\rho}\right)_{max}$ at h with x obtained was $\left(\frac{\Delta\rho}{\rho}\right)_{max.\ at\ h} \propto x^{-1.38}$ which shows that the dimensional analysis offers a better prediction of $\Delta\rho$ (x) when the density scale is selected in the region of turbulent flow away from the boundary plane.

Better agreement between predicted and measured values of $v_{xmax}(x)$ and $\Delta\rho_{mean}(x)$ are to be expected for steep boundary slopes where turbulence should be more fully developed across the flow cross section. For turbulent jets on boundary slopes of 20^{o} and less one may

conclude that predictions based on the assumption of completely developed turbulence will slightly underestimate the rate of decrease of v_{xmax} and grossly overestimate the rate of decrease of $\Delta\rho_{mean}$ with distance down the boundary plane. It is probable that a sophisticated theoretical model treating the flow as two separate regions - a higher density boundary layer adjacent to the boundary plane and a lower density, completely turbulent outer mixing region - would allow better theoretical prediction of $v_{xmax}(x)$ and $\Delta\rho_{mean}(x)$ for jets on low to moderate boundary slopes. Also an attempt should be made to measure turbulent intensity of velocity and density fluctuations throughout the flow cross section in any future experiments.

2.5.7 Estimation of Entrainment Constant and Local Richardson Number

The entrainment constant E at a cross section has been defined in Section 1.6 of Chapter 1 as:

$$E = \frac{\frac{d}{dx}(v_{xmax}, bh)}{v_{xmax}(b+h)} \qquad (36)$$

where $v_{xmax}\, bh = Q$ the volumetric flow rate from equation (29). Q(x) is plotted in Fig. 36A which shows that Q appears to vary linearly with x, that is $\frac{dQ}{dx}$ is constant and equal to 4.08×10^{-3} square feet per second. Using the values for v_{xmax}, b and h from Table 3, equation (36) was used to compute E at the three jet cross sections and the results are shown in Table 4.

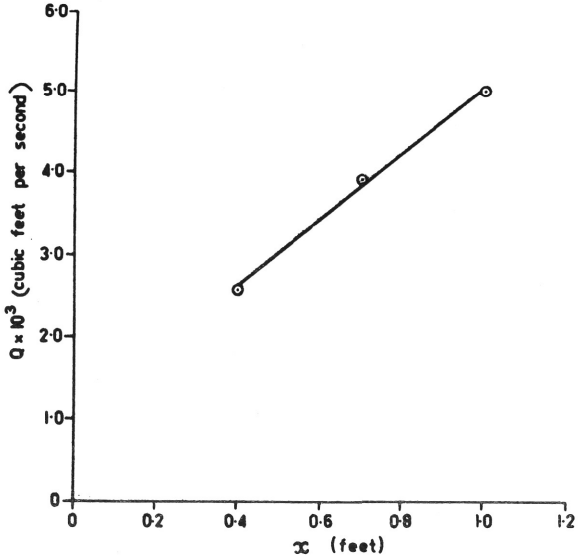

FIGURE 36 A. Q (x)

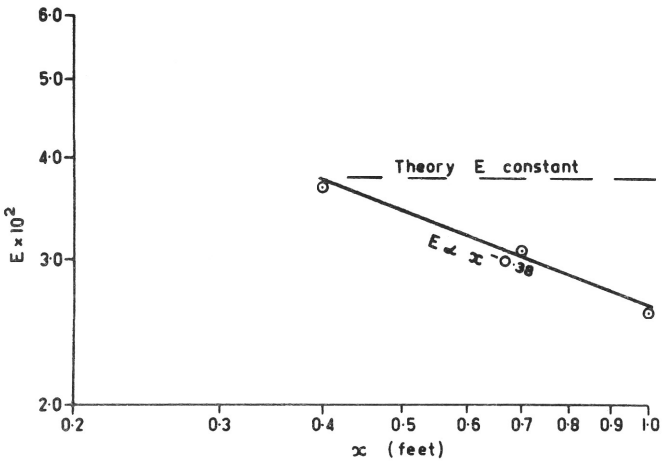

FIGURE 36 B. E (x)

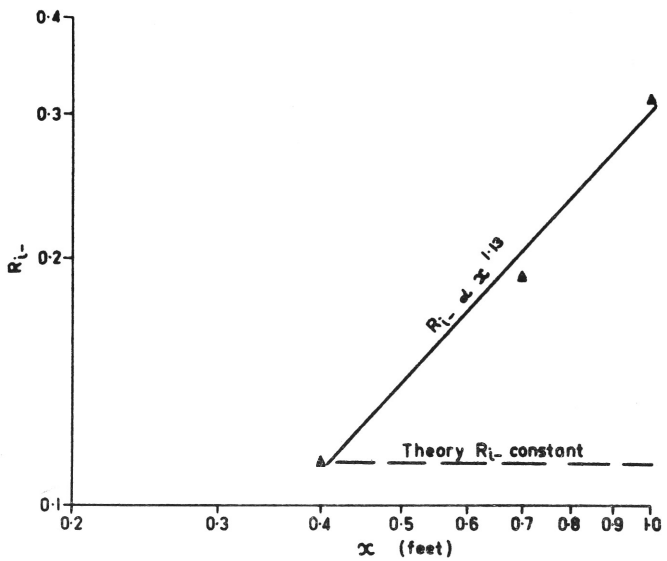

FIGURE 36 C. R_{i-} (x)

$R_{io} = 0{\cdot}91 \times 10^{-3}$, $\left(\frac{\Delta\rho}{\rho}\right)_o = 2{\cdot}0 \times 10^{-2}$, $S = 20°$

FIGURE 36: VARIATION OF VOLUMETRIC FLOWRATE, ENTRAINMENT CONSTANT, AND LOCAL RICHARDSON NUMBER WITH DISTANCE FROM VIRTUAL ORIGIN

Table 4.

Entrainment Constant and Local Stability Parameters at Three Cross Sections of Turbulent Jet Number C.

Cross Section, Distance x from Orifice, in ft.	Entrainment Constant $E \times 10^2$	Local Richardson Number R_{i-}	Local Reynolds Number $R_{e-} \times 10^{-4}$	Width to Height Ratio $\frac{b}{h}$
0.4	3.7	0.113	7.85	6.8
0.7	3.1	0.19	9.8	8.9
1.0	2.6	0.315	11.9	12.4

The Local Richardson Number R_{i-} at a cross section is defined in Subsection 1.4.3 of Chapter 1 as:

$$R_{i-} = \frac{\Delta\rho_{mean}\, g b}{v_{xmax.}^2\, \rho}$$

By utilising the values for $\left(\frac{\Delta\rho}{\rho}\right)_{mean}$ etc. from Table 3 the values of R_{i-} shown in Table 4 were obtained. The measured values of $E(x)$ and $R_{i-}(x)$ are compared with the relations predicted for a fully turbulent jet in Figs. 36B and 36C respectively. The theory predicts that both E and R_{i-} should be constant while the measurements indicate that E decreases and R_{i-} increases with distance down the plane. As outlined previously, the disparity between the observed and predicted values of $E(x)$ and $R_{i-}(x)$ may be due to incomplete development of turbulence across the cross section of the particular jet investigated. Better agreement might be expected for fully

turbulent jets on steep slopes. It is interesting to recall at this point that Ellison and Turner (Ref. 31) contend that in the two dimensional case both E and R_{i-} remain constant throughout the flow.

In Subsection 1.4.3. of Chapter 1 it is shown that:

$$E = \phi_q \left(R_{i-}, \frac{b}{h}, \frac{k}{b}, R_{e-} \right) \qquad (21)$$

, where R_{e-} is the Local Reynolds Number at a cross section defined by:

$$R_{e-} = \frac{v_{x\,max.}\, b \rho}{\mu}$$

, and $\frac{k}{b}$ is the relative boundary roughness. To utilise this relation for a systematic investigation of the dependence of E on the stability parameters R_{i-} $\frac{b}{h}$ etc. would require investigation of a large number of jets. There is no point in attempting to correlate E with R_{i-} for instance, for the three cross sections of the jet investigated as both $\frac{b}{h}$ and R_{e-}, as well as R_{i-}, vary from cross section to cross section as shown in Table 4.

2.6 Application of Model Data to Prototype Cases

Supposing it is required to discharge an industrial effluent into a still lake whose bed slope is 10°. The diameter of the outlet is 4 feet, and the outflow velocity 10 feet per second. If the effluent relative density difference $\left(\frac{\Delta\rho}{\rho}\right)_o$ is 1.0 percent then the Richardson Number at the outlet R_{io} will be 2.73×10^{-2}. This is much larger than the value of R_{io} of 1.7×10^{-3} for model jet number U in Table 1 where slug flows occurred in the jet. Hence it may be concluded

that turbulent mixing, which is desirable for rapid dispersion of the effluent in the lake, is unlikely to occur in this case. For turbulent mixing to occur a much lower value of $\left(\frac{\Delta\rho}{\rho}\right)_o$ is required.

The model data might also be utilised to make a speculative prediction of the spread of hot water on the surface of a thermal power station cooling pond. The boundary plane in this case is the pond surface and the problem is one of the spread of a lighter fluid over a heavier miscible fluid. For a thermal power station of about 500 MW capacity about 1100 cusecs of cooling water are required and the rise in temperature through the condensers is from 12 to 15°F (Ref. 75). If the ambient water is at 50°F and the discharged water at 65°F then this represents a relative density difference $\left(\frac{\Delta\rho}{\rho}\right)_o$ of 0.155 per cent. The heated water is often discharged through an outfall chamber and the appropriate dimensions in this case are width 100 ft. and depth of flow 8.5 feet (Ref. 75). Using this data the Richardson Number at the orifice R_{io} is 0.202, which is very high, so that the heated water might be expected to flow over the surface of the cooling pond in the form of a thin slug flow with little mixing with the underlying cold water. This form of spreading is desirable in recirculated cooling ponds where contamination of the intake water by the heated outlet water is to be avoided.

It would appear that for turbulent flow to occur in a three dimensional jet the boundary slope must be steep, the injected flow rate large and the relative density difference very small. The "artificial" (i.e. engineered by man) prototype cases investigated were slug flows and it is suggested that turbulent flows are only likely to occur in large scale natural phenomena such as movement of air masses in mountainous country, the movement of turbidity currents on steep slopes in the ocean, and the discharge of colder or silt laden water into an alpine lake.

2.7 Summary

The apparatus and experimental techniques used has been described in detail. A larger tank appears to be necessary to allow the model jet to be located centrally in the tank.

The flow regime, lateral spread and normal spread has been examined for a range of jets on boundary slopes of 10^{o} and 20^{o}. The Richardson Number at the orifice R_{io} appears to be an adequate criterion for specifying a turbulent jet, providing the relative density difference $\left(\frac{\Delta\rho}{\rho}\right)_o$ does not exceed 2.0 per cent.

Measurement of velocity and density profiles at three cross sections of a turbulent jet on a 20^{o} slope has been described. The flux of density excess computed from these profiles at each cross section was found to vary by not more than about 3.0 per cent from the flux injected at the orifice, so verifying the accuracy of the

velocity and density measuring instruments.

The velocity profiles for the three cross sections examined were found to be self preserving in the outer region of the jet away from the boundary layers at the sloping floor and the tank sidewall. The density profiles were only approximately self preserving in the outer region of the jet.

The variation with distance down the boundary plane of the measured values of the characteristic scales (b, h, v_{xmax} and $\Delta\rho_{mean}$) describing the velocity and density profiles at a cross section has been computed from the velocity and density measurements. The width and height scales, b and h respectively, were found to vary linearly with x. When the measured functions for $v_{xmax}(x)$ and $\Delta\rho_{mean}(x)$ were compared with those predicted for a fully turbulent jet in Chapter 1 then the agreement in general was poor. It has been suggested the disagreement may be due to the turbulence damping effect of the steep density gradient occurring in the inner region of the flow adjacent to the boundary plane.

The entrainment constant E was found to decrease and the Local Richardson Number R_{i_-} to increase in the direction of flow. This contrasts with the two dimensional case investigated by Ellison and Turner (Ref. 31) who contended that both E and R_{i_-} remain constant throughout the flow.

The experiment data has been used to classify two prototype flows and in both these cases slug flows were predicted.

Chapter 3: Velocity Measurement.

3.1 Introduction

This chapter is an account of the development of a velocity meter for use in trubulent saltwater jets. Firstly, the objectives are stated; the extensive literature review included as Appendix 1 is summarised; and the remainder of the chapter is concerned with the design, manufacture, calibration and operation of two meters selected from the literature review.

3.2 Objectives

3.2.1 Range and Accuracy

An instrument was required to measure point velocities in the range 0.05 to 0.5 feet per second in turbulent salt water jets varying in thickness from 0.02 to 0.1 feet.

An accuracy of $\pm$ 10 per cent was considered to be adequate for an exploratory investigation of the mechanics of turbulent salt water jets.

3.2.2 Other Requirements

The velocity meter should preferably be commercially available or alternatively inexpensive to make and maintain. Freedom from calibration drift and simplicity of operation were also desirable. The meter should be suitable for use on untreated Sydney tapwater which varies in composition and degree of contamination and is also subject to seasonal and diurnal temperature changes.

3.3 Summary of Literature Review

None of the commercially available instruments was suitable but two reported devices appeared to warrant further investigation; these were a miniature cup type current meter and Bagnold's velocity meter.

3.4 Development of a Miniature Cup Type Current Meter

3.4.1 Description

The meter is a miniaturised version of the conventional cup (or Price) type current meter and is shown in detail in Fig. 37, while Fig. 38 is a photograph of the meter and several impellers.

The proposed speed recording system was not proceeded with when, (as outlined subsequently), the meter was found to be unsuitable for the present project. Briefly, it was proposed to mount small mirrors on the impeller and use these to reflect a fine beam of light to a light sensitive semiconductor such as a phototransistor or photo-diode. The output from the light detecting element may then be detected by a commercially available counting unit.

3.4.2 Testing

The meter was fitted with the impeller shown in Fig. 37 and placed in a typical centrally located turbulent saltwater jet in the experimental tank.

The threshhold velocity was about 0.25 feet per second which was much higher than the 0.05 feet per second required. On testing of

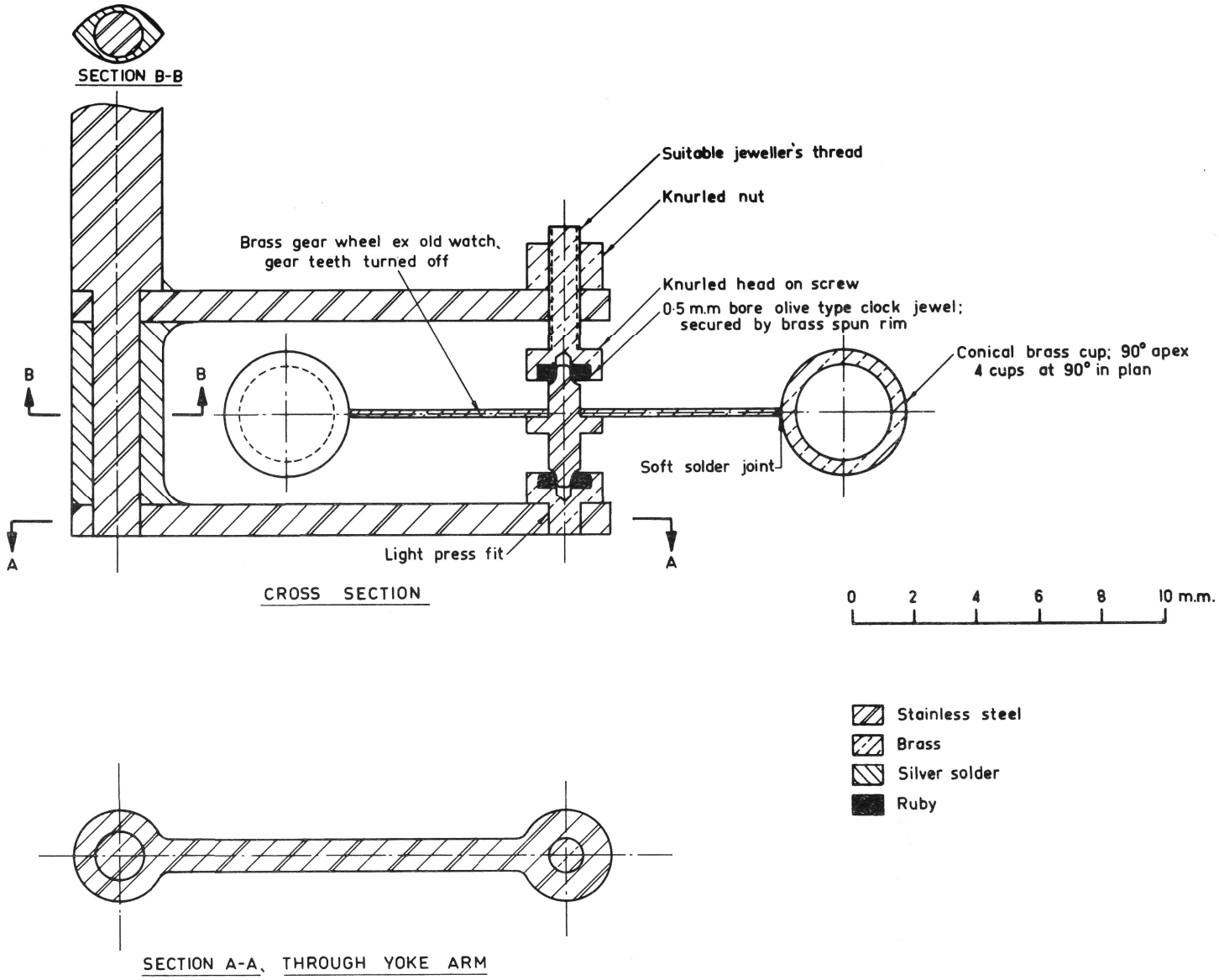

FIGURE 37: MINIATURE CUP TYPE CURRENT METER

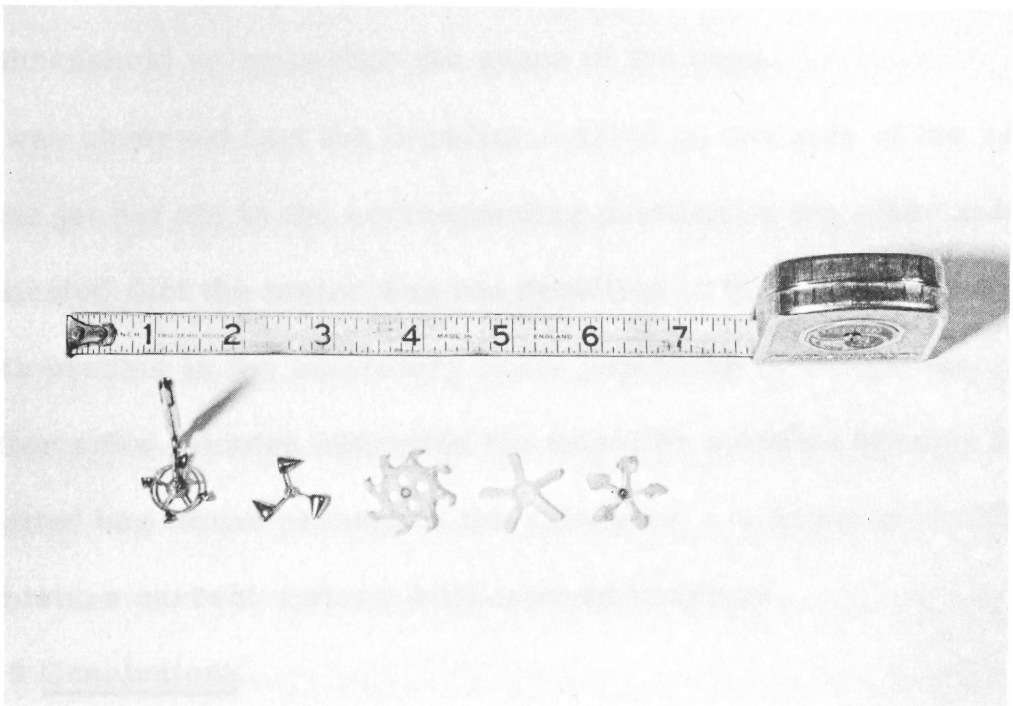

Fig. 38: Miniature Cup Type Current Meter and Various Impellers.

the other impellers shown in Fig. 38 it was found that the lighter perspex impellers had a slightly lower threshhold velocity and that the submerged weight of the impeller appeared to be more critical in determining the threshhold velocity than the shape of the cups.

It was observed that the impeller rotated on one side of the centreline of the jet but not in the corresponding position on the other side. This indicated that the meter was too sensitive to the lateral velocity gradients present in the laboratory scale jets being investigated.

After a few minutes operation the impeller spindles became fouled by elongated bag fibres present in the saltwater - a common problem with miniature current meters with exposed bearings.

3. 4. 3 Conclusions

The threshhold velocity of the meter as designed was too high for use in laboratory scale turbulent saltwater jets, probably because of excessive bearing friction. Also the meter was too sensitive to the lateral velocity gradients present in the jets being investigated and was subject to fouling when used in unfiltered saltwater prepared with bagged salt.

Although the meter was found to be unsuitable for the present project, further development may be justified for its use in the hydraulic laboratory in shallow flow situations where the D. S. I. R. meter cannot be totally immersed. The following alterations are suggested:-

(i) Use of a machined or cast lightweight plastic impeller. The D. S. I. R. Meter is fitted with a machined Cobex plastic impeller which is slightly less dense than water so that bearing friction is minimised.

(ii) Reversal of the bearing system by fitting the jewel bearings in the impeller and the stainless steel spindle in the yoke arms so as to further reduce the weight of the impeller assembly. Fitting a flat thrust jewel bearing under the olive type radial bearing already used may reduce the bearing friction.

(iii) Use of a shroud on the side of the impeller where the cups are travelling upstream should lower the threshhold velocity. Kolupaila (Ref. 63) records that this has been done by Patterson of the U. S. Geological Survey to extend the range of larger price type meters.

The above alterations, together with the optical speed recording system already outlined, should result in a useful instrument.

3. 5 Development and Use of the Bagnold Velocity Meter

3. 5. 1 General Description

The Bagnold velocity meter is named after its inventor R. A. Bagnold who described this novel device for measuring low velocities in water flow in 1951 (Ref. 13). No subsequent mention of the meter in the literature is known to the writer.

The instrument is shown schematically in Fig. 39 where it is depicted in operation in saltwater flow. The stagnation pressure exerted by the saltwater flow at the tip of a long fine bore nozzle is transmitted along the saltwater in the nozzle to a balancing chamber. In the balancing chamber is a saltwater - freshwater interface formed by interaction of the saltwater from the nozzle and an opposing flow of freshwater carried by the opposing flow tube. The latter tube is coaxial with the nozzle and terminates a short distance from the downstream end of the balancing chamber.

The position of the saltwater-freshwater interface is detected by connecting a simple conductivity meter between a ring electrode let into the wall of the balancing chamber and the opposing flow tube which acts as the second electrode. The critical point occurs when the interface coincides with the upstream end of the ring electrode as shown in Fig. 39A; the meter is then said to be in a state of "balance" and the conductivity meter records freshwater conductivity. If the opposing flow of freshwater is too great the interface moves upstream and the meter is said to be in an "overbalanced" condition as shown in Fig. 39B. Unfortunately, with only one ring electrode, it is impossible to differentiate between the balanced and overbalanced conditions as the conductivity meter shows freshwater conductivity when the interface is in a position corresponding to either condition. If the

opposing flow of freshwater is too small, on the other hand, the interface is downstream of the ring electrode and the meter is "underbalanced" as shown in Fig. 39C. The conductivity meter records a conductivity intermediate between that of saltwater and freshwater when the meter is in this condition.

The spent opposing flow of freshwater flows to waste through the bypass holes just downstream of the balancing chamber so that in effect the meter allows a dynamic flow to balance a "static" stagnation pressure. This use of a small liquid flow to balance the stagnation pressure in a pitot nozzle is the most singular feature of the instrument as it is then only a matter of relating the discharge through the opposing flow tube to the oncoming velocity at the nozzle tip in order to calibrate the instrument.

Measurement of the freshwater opposing flowrate, (which is extremely small by hydraulic laboratory standards), is conveniently done by measuring the head loss ΔH through the fine bore head loss tube inserted in the freshwater supply line. The other tubes in the freshwater line are much larger in bore than the head loss tube so that the head loss through the system is effectively confined to the latter. The difference in elevation between the surface level in the freshwater supply tank and the nozzle tip is then an amplified total head. Measuring the head loss between the surface level in the freshwater supply

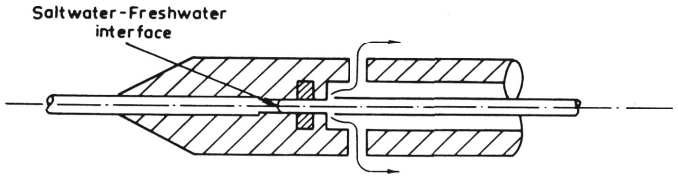

FIGURE 39B: METER "OVERBALANCED"

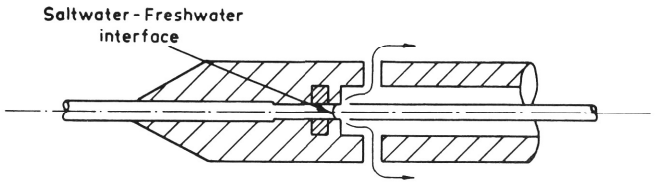

FIGURE 39C: METER "UNDERBALANCED"

FIGURE 39A: METER "BALANCED"

FIGURE 39: SCHEMATIC SKETCH OF BAGNOLD VELOCITY METER

tank and the water surface in the model where the meter is being used compensates for the static pressure at the nozzle tip (providing the streamlines are straight and parallel) and this head loss is then a magnified dynamic head.

The degree of magnification of the dynamic head, and hence the effective range of the instrument, may be varied by using different head loss tubes or varying the gap G_M. Providing the flow through the head loss tube remains laminar the output characteristic of the meter is linear, as shown in Fig. 40.

3.5.2 Design and Manufacture

The meter is composed of three principal parts; the probe, the freshwater supply system and the conductivity meter.

The Probe

The probe is that part of the meter immersed in the flow and consists of a perspex head fixed to a stainless steel supporting elbow. The head details are shown in Fig. 41; the elbow details in Fig. 42; while Fig. 43 is a photograph of the dismantled meter.

The layout of the component parts is similar to that shown in the rough drawing in Bagnold's original paper (Ref. 13). The main modifications are:-

(i) Use of materials resistant to corrosion by saltwater viz. stainless steel, perspex, nylon, gold etc.

(ii) Fitting of a bent nozzle for working close to a boundary.

(iii) Rotation of the opposing flow bypass holes through 45^{o} so that the meter may be used close to a boundary without affecting the escape to waste of the spent opposing flow.

(iv) Fixing of the perspex head to the stainless steel elbow so that the gap G_M between the end of the opposing flow tube and the balancing chamber (see Fig. 39A) cannot be accidentally disturbed.

(v) Use of a spacing sleeve to set the gap G_M instead of the micrometer screw adjustment proposed by Bagnold. Although this latter method is more flexible for initially adjusting the instrument it is not as positive as the former for resetting the gap G_M after the instrument has been dismantled for cleaning.

(vi) Use of epoxy resin for electrical insulation and waterproofing of the lead wire to the ring electrode.

The Freshwater Supply

Details of the freshwater supply system are shown in Fig. 4. The perspex supply tank is attached to a carriage with nylon rollers which is raised by a small hand winch. The carriage runs on the head loss scale which is graduated in feet and tenths and which is adjusted so that its zero mark is level with the surface of the water in the experimental tank. A reading of the head loss, estimated to

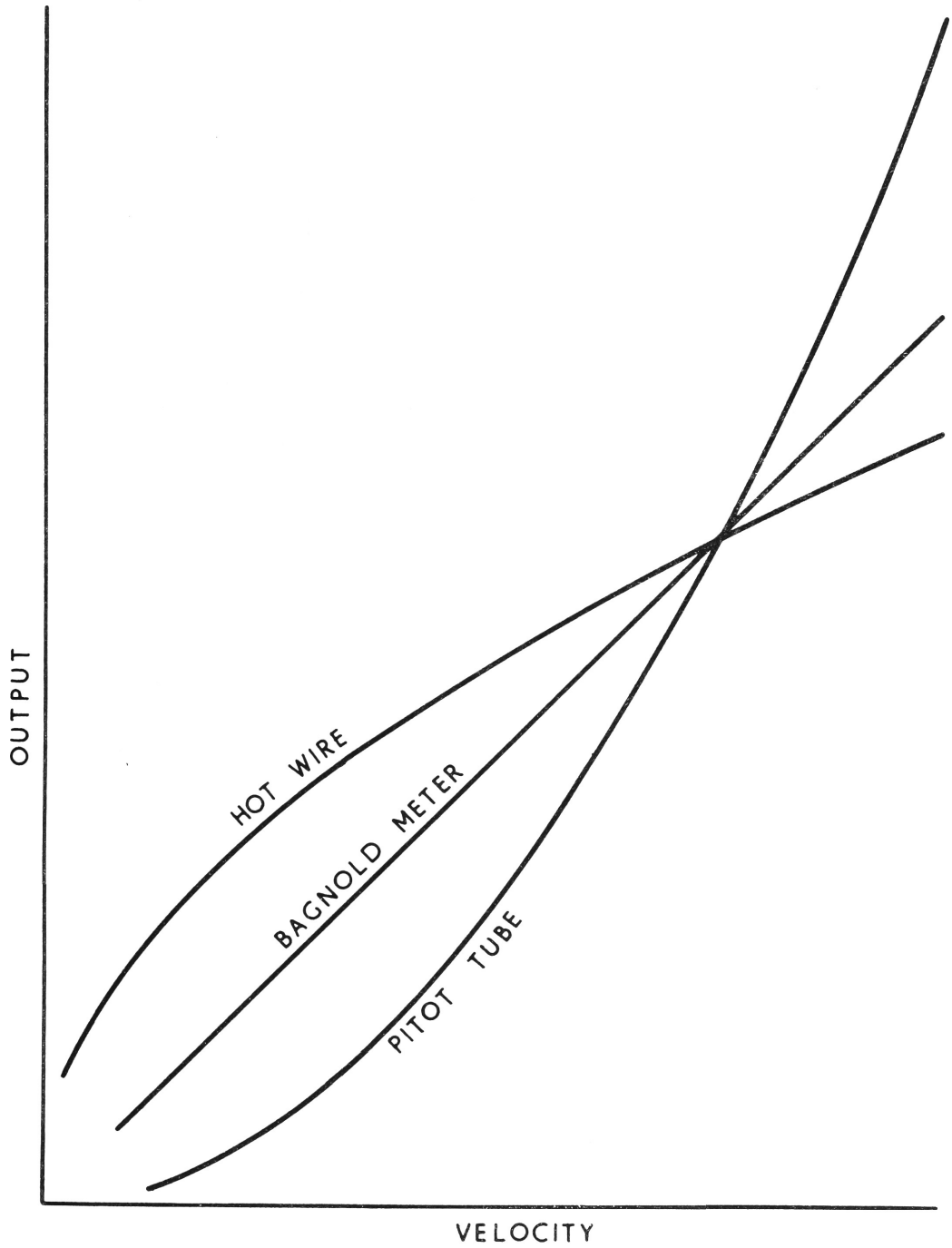

After Corrsin (Ref. 22). Scales arbitrary.

FIGURE 40: OUTPUT CHARACTERISTICS OF VELOCITY METERS

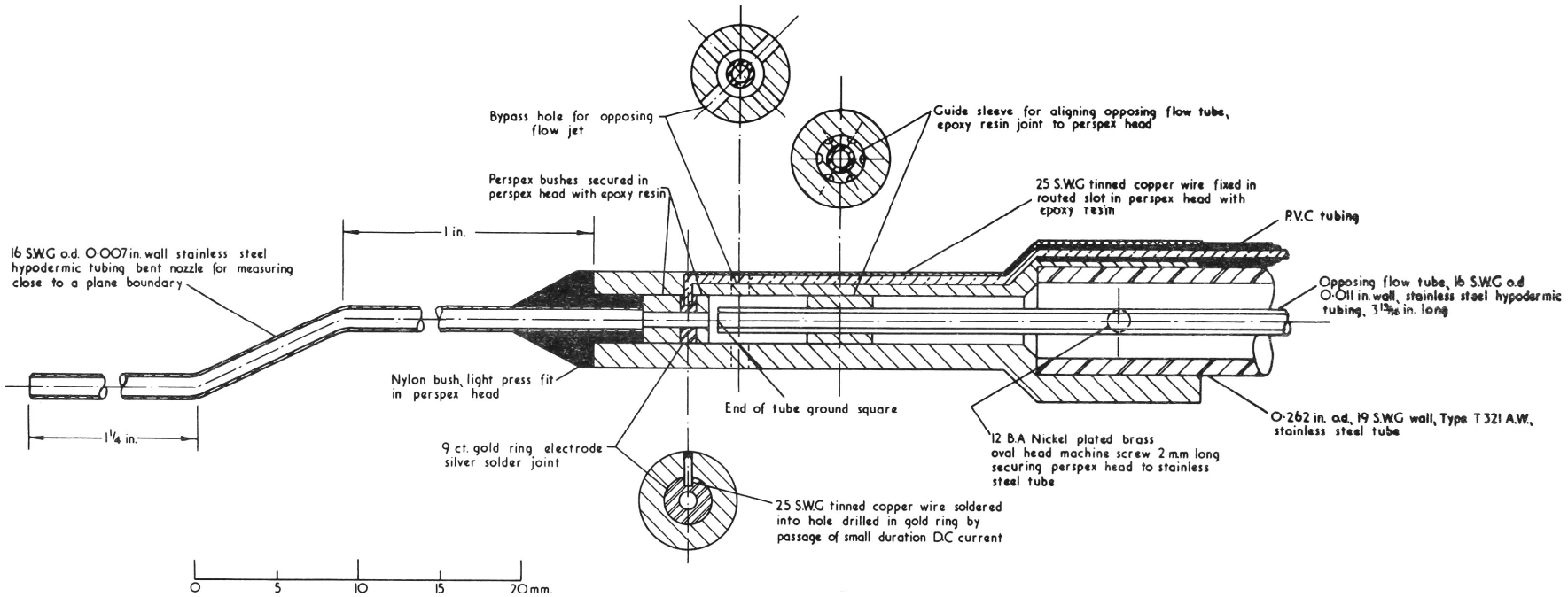

FIGURE 41: VELOCITY METER HEAD DETAILS: LONG. SECTION

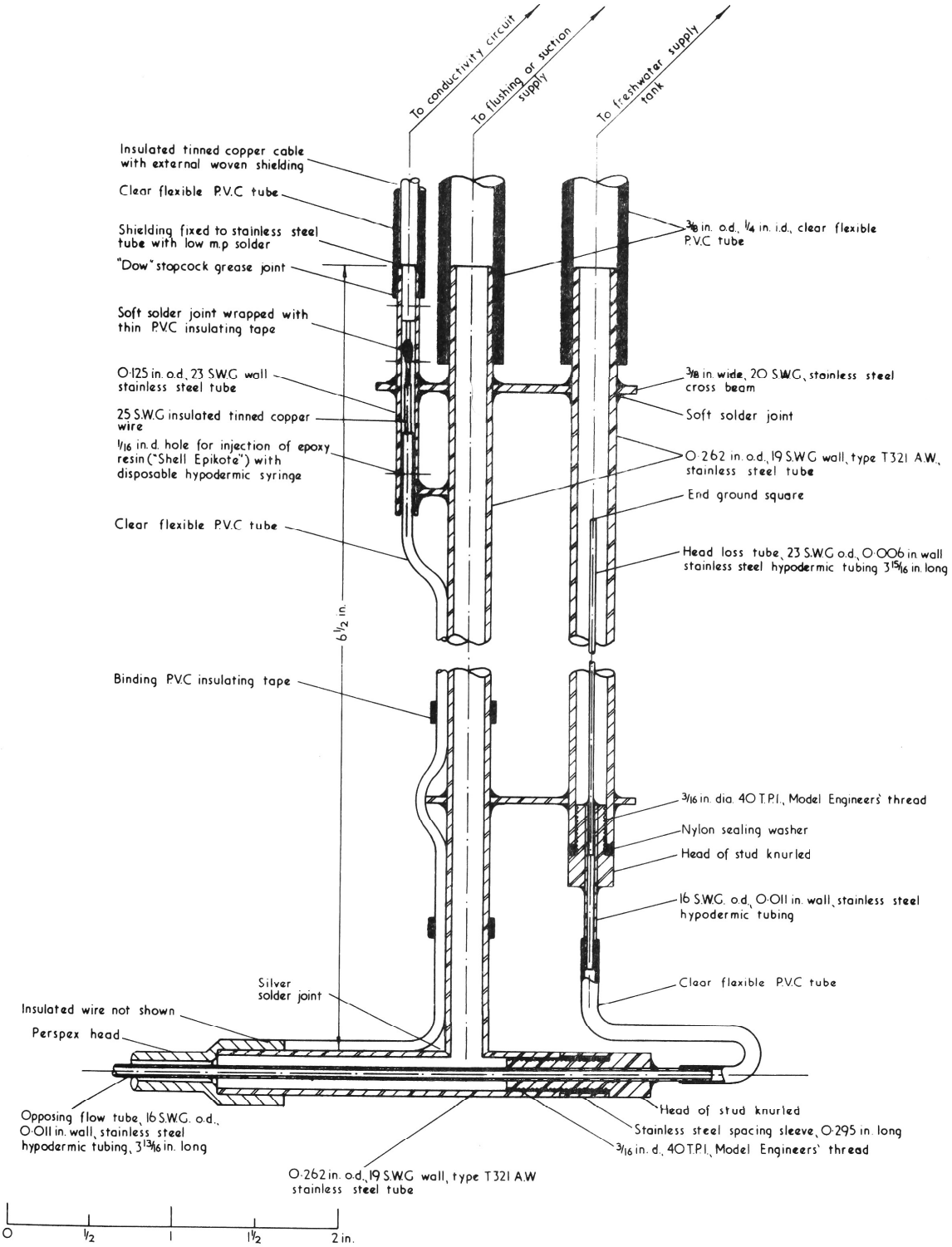

FIGURE 42: VELOCITY METER ELBOW DETAILS: LONG. SECTION

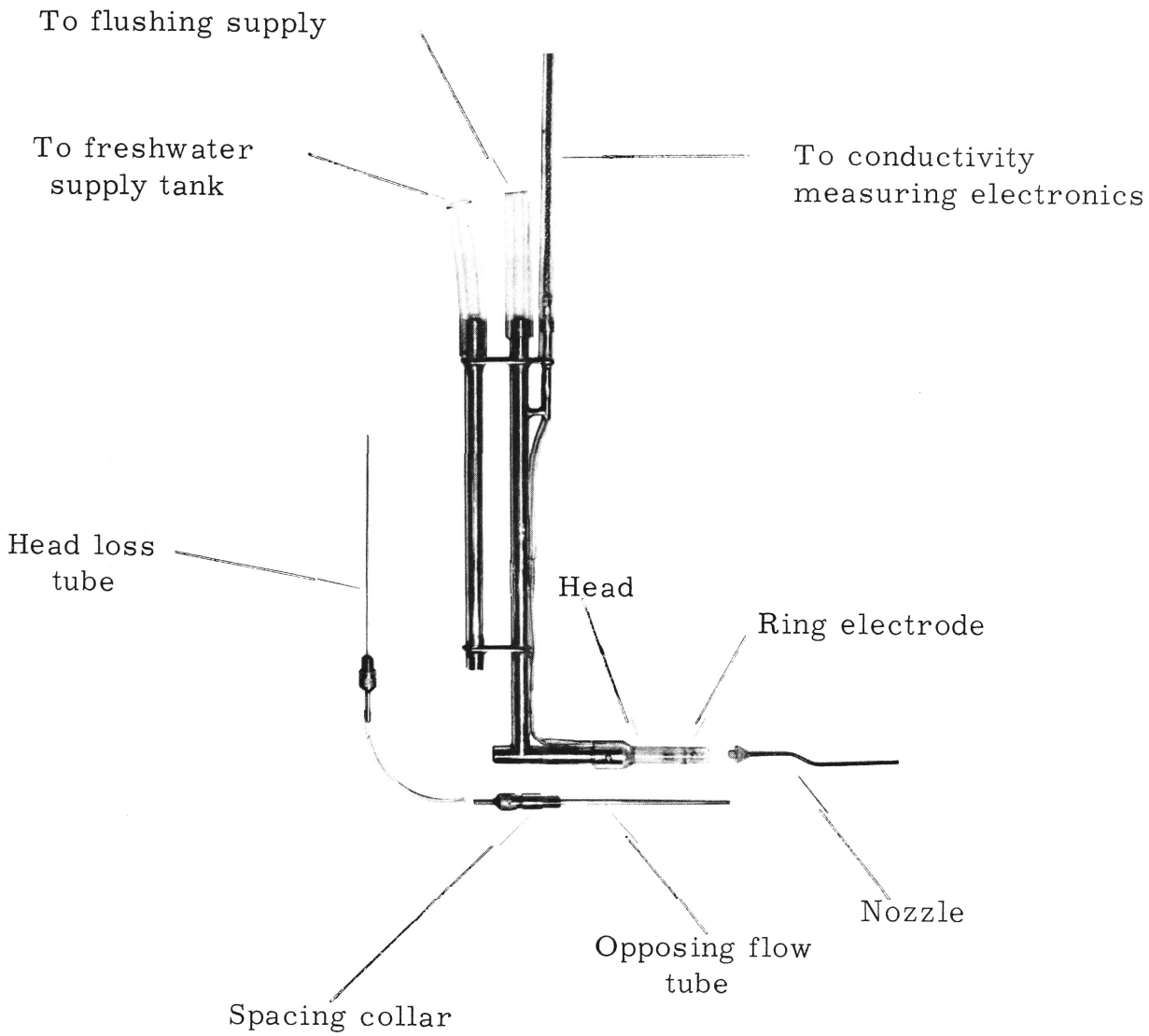

Fig. 43: Dismantled Velocity Meter.

one hundredth of a foot, is taken by sighting through the perspex tank onto the head loss scale. 3/8 inch bore clear, flexible PVC tubing connects the supply tank to the probe and a small needle valve is fitted in the line for initial filling of the tank.

The Conductivity Meter

The conductivity meter circuit is shown in Fig. 44. The circuit is essentially the same as that shown in Chapter 4 for the determination of the conductivity at a point in a turbulent saltwater jet except that the bridge rectifier has been omitted. Omission of the bridge rectifier makes the meter more sensitive to conductivity changes and hence permits more accurate detection of the position of the saltwater - freshwater interface within the balancing chamber. Without the rectifier the CRO display is sinusoidal but this can be tolerated as only the final output voltage corresponding to freshwater conductivity at the point of balance is of interest.

3.5.3 Calibration

The variables affecting calibration may be broadly grouped as follows:-

a. Meter dimensions:

(i) Nozzle internal diameter d_N, external diameter D_N, length L_N and shape.

(ii) The gap G_M between the end of the opposing flow tube and the mouth of the balancing chamber.

(iii) Head loss tube internal diameter d_T and length L.

b. Freshwater supply temperature T_F as it affects the density ρ_F and viscosity μ_F.

c. Density ρ_s of the saltwater flow being measured.

d. Orientation of the meter; the effect of horizontal and vertical yaw.

e. Calibration tank characteristics.

(i) Speed consistency.

(ii) Turbulence.

Most of the above variables are shown schematically in Fig. 39.

Effect of Calibration Variables in Detail

Calibration of the meter was performed in the annular rotating tank described in Appendix 2. The meter was assembled in a bucket of freshwater to ensure that all tubes were free from air bubbles and then positioned in the rotating tank which had been filled with saltwater.

Effect of Nozzle Dimensions and Shape

The internal diameter d_N and the length L_N of the nozzle affect the use of the meter in a turbulent flow but, as the calibration tank was practically free of turbulence, variation of these dimensions had no effect on the calibration graph, (other factors being constant). The

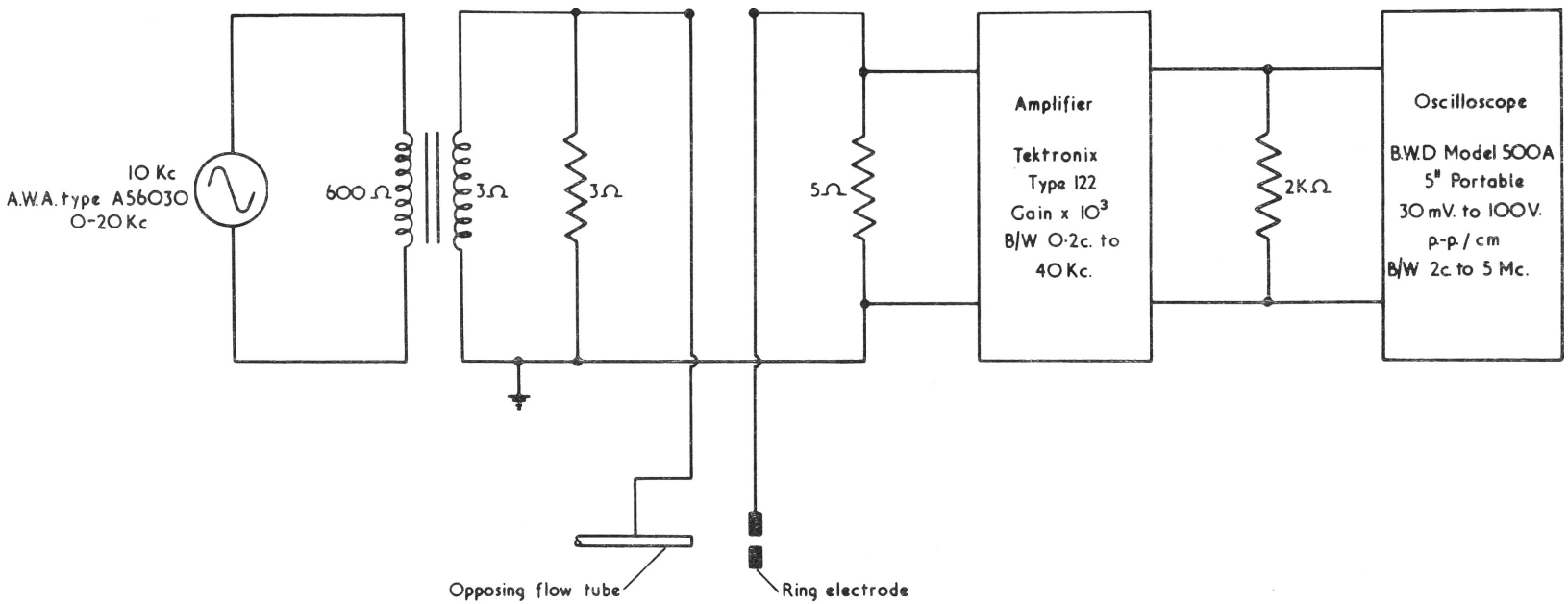

FIGURE 44: VELOCITY METER BALANCE DETECTION: CIRCUIT DETAILS

external diameter D_N of the nozzle becomes significant when working close to a fixed boundary but this effect could not be checked in the calibration tank.

Bent and straight nozzles of equal internal diameter and axial length produced identical calibration graphs.

Effect of the Gap G_M

The effect of varying G_M on the calibration graph is shown in Fig. 45A. It is seen that a slight variation in G_M has a pronounced effect on the calibration graph and in general a slight increase in G_M increases the amplifying power of the instrument. It was found to be more convenient to fix G_M by installing a spacing sleeve at the upstream end of the opposing flow tube and to vary the amplification by using different head loss tubes.

The ratio of the gap G_M to the body diameter D, called the "gap ratio", was fixed at 0.18 in the present case to cover the range of velocities required. Bagnold (Ref. 13) used a gap ratio of about 0.1 to measure velocities down to about .007 feet per second and claimed that the time response was about 20 seconds. Although the effect on time response of reducing the gap ratio was not investigated it is possible that the response of the meter could be improved by reducing the gap ratio.

Effect of Head Loss Tube Dimensions

The head loss tube dimensions determine the shape of the output characteristic (head loss ΔH plotted against mean saltwater velocity $\bar{v}_s$) of the meter. For a desirable linear output characteristic the head loss tube dimensions must be selected so that laminar flow occurs in the head loss tube.

This may be demonstrated theoretically as follows (refer to Fig. 39A for definition of symbols):

The dynamic pressure exerted by the oncoming saltwater flow is $\frac{1}{2}\rho_s \bar{v}_s^2$ and this is transmitted along the nozzle to exert a force on the saltwater-freshwater interface in the balancing chamber of $\frac{1}{2}\rho_s \bar{v}_s^2 \frac{\pi}{4} d^2$.

In the balanced condition the interface is stationary and this force is balanced by the opposing flow force F_{op} due to that portion of the opposing freshwater flow which has entered the balancing chamber, that is:

$$\frac{1}{2}\rho_s \bar{v}_s^2 \frac{\pi}{4} d^2 = F_{op} \qquad (41)$$

F_{op} may be evaluated from the impulse momentum equation:

$$F_{op} = \phi_1 Q_p \rho_F v_F \qquad (42)$$

where ϕ_1 is a function of the geometry of the meter $\phi_1(d, D, G_m, s, D_B)$ as the geometry of the meter affects the flow pattern of the jet issuing from the end of the opposing flow tube. If the geometry of the meter

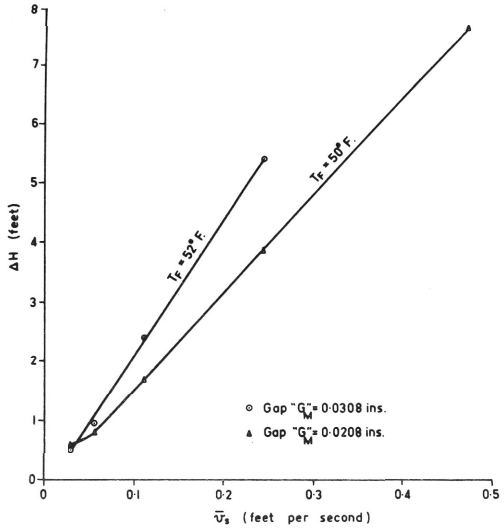

(a) EFFECT OF VARYING GAP "G_M"

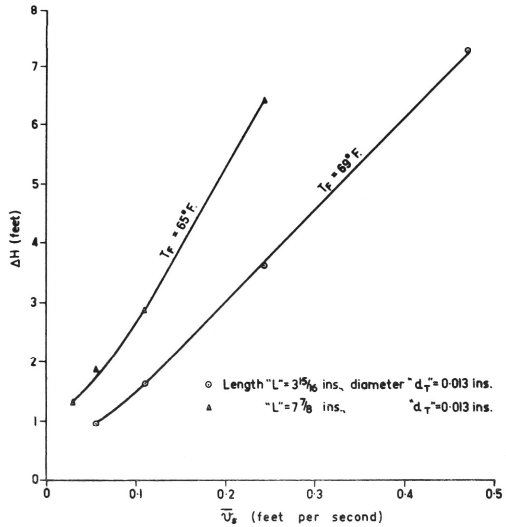

(b) EFFECT OF VARYING DIMENSIONS OF HEAD LOSS TUBE

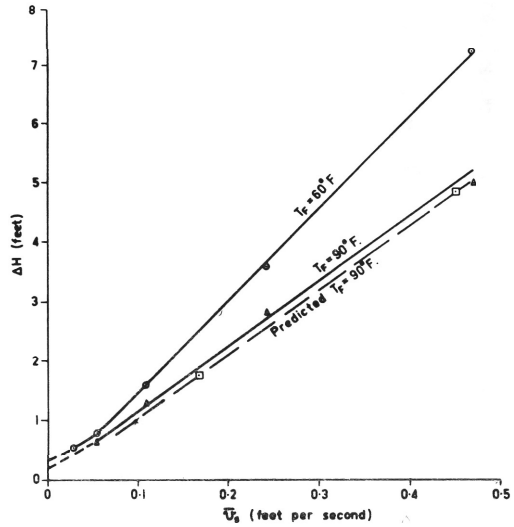

(c) EFFECT OF VARYING FRESH WATER TEMPERATURE "T_F"

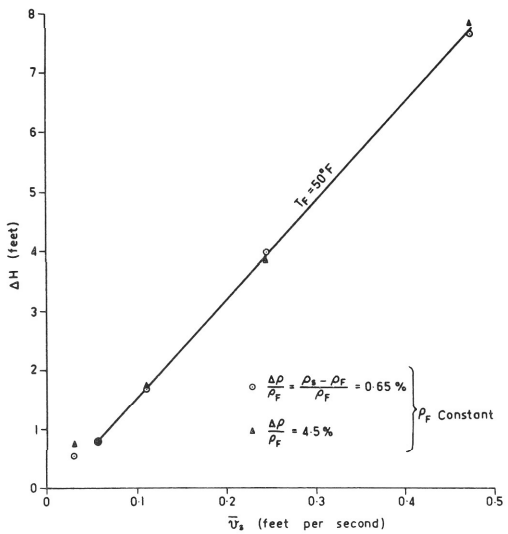

(d) EFFECT OF VARYING SALT WATER DENSITY "ρ_S"

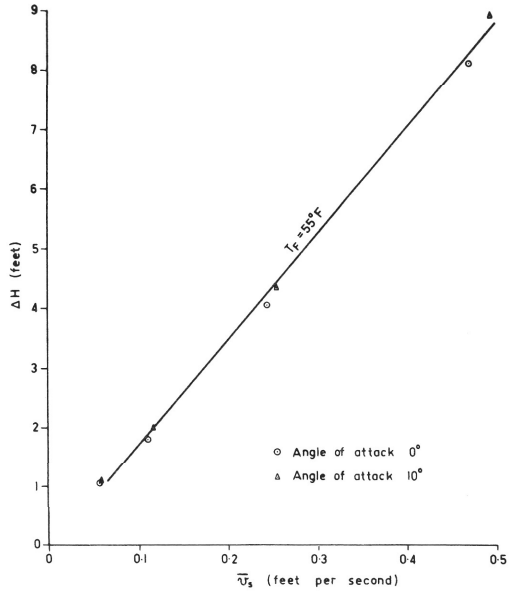

(e) EFFECT OF HORIZONTAL YAW

ALL POINTS PLOTTED INDICATE THE MEAN VALUE OF AT LEAST THREE OBSERVATIONS OF ΔH

FIGURE 45 : EFFECT OF SIGNIFICANT VARIABLES ON CALIBRATION OF VELOCITY METER

remains constant and attention is confined to the balanced state (where the interface is fixed at the upstream end of the ring electrode) then one may assert that ϕ_1 is a constant C_1 so that equation (42) becomes:

$$F_{op} = C_1 Q_p \rho_F v_F \tag{43}$$

Hence from equations (41) and (43):

$$\frac{1}{2} \rho_s \bar{v_s}^2 \frac{\pi}{4} d^2 = C_1 Q_p \rho_F v_F \tag{44}$$

From continuity the discharge through the head loss tube must equal the discharge through the opposing flow tube and substituting for Q_p and v_F in equation (44) yields:

$$\frac{1}{2} \rho_s \bar{v_s}^2 d^2 = C_1 \frac{d_T^4}{d_p^2} \rho_F v_T^2 \tag{45}$$

Then

$$\rho_s \bar{v_s}^2 = C_2 \rho_F v_T^2 \tag{46}$$

where C_2 is a constant given by:

$$C_2 = \frac{C_1}{d^2} \cdot \frac{d_T^4}{d_p^2}$$

From laminar flow through the head loss tube the head loss ΔH is given almost precisely by:

$$\Delta H = \frac{32L}{g d_T^2} \cdot \frac{\mu_F}{\rho_F} \cdot v_T \tag{47}$$

Equation (47) is the Hagen-Poiseville resistance equation for laminar flow in an infinitely long tube with no end effects. Hardy, in a monograph on capillary tube viscometers (Ref. 45), states that inlet

effects may be allowed for by increasing the length term L in equation (47) to $L' = L + n \frac{d_T}{2}$, where n is about 0.6 for the head loss tubes being used. The exit effect is accounted for by inclusion of a velocity head term on the right hand side of equation (47). For the head loss tubes used both the inlet and exit effects may be neglected. This was demonstrated by collecting the discharge from the head loss tube over several minutes under an actual head of 9.0 feet. The measured velocity was then used to compute a head loss of 9.33 feet from equation (47). The difference between the observed and the computed head loss was thus less than 4 pc. which may be neglected.

For constant meter dimensions equation (47) becomes:

$$v_T = C_3 \cdot \frac{\rho_F}{\mu_F} \Delta H \qquad (48)$$

where the constant

$$C_3 = \frac{g d_T^2}{32 L}$$

Then using equation (48) in equation (46):

$$\rho_S \bar{v}_S^2 = C_2 \rho_F C_3^2 \left(\frac{\rho_F}{\mu_F}\right)^2 \Delta H^2$$

i.e.

$$\bar{v}_S^2 = C_2 C_3^2 \frac{\rho_F}{\rho_S} \left(\frac{\rho_F}{\mu_F}\right)^2 \Delta H^2 \qquad (49)$$

or

$$\bar{v}_S = C_4 \Delta H \qquad (50)$$

where C_4 is a constant if freshwater and saltwater properties are constant and the geometry of the meter is constant. Equation (50) states that the output characteristic of the meter will be linear and this

is verified by the calibration graphs of Fig. 45, except for the region near zero velocity. This latter deviation is due to the difference in density between the saltwater and the freshwater opposing flow and will be explained subsequently.

Rewriting equation (50) in full:

$$\bar{v}_s = \frac{\sqrt{C_1 g}}{32 \alpha d_p} \cdot \sqrt{\frac{\rho_F}{\rho_s}} \cdot \left(\frac{\rho_F}{\mu_F}\right) \cdot \frac{d_T^4}{L} \cdot \Delta H \qquad (51)$$

If the freshwater and saltwater properties and the geometry of the meter head are constant then equation (51) becomes:

$$\bar{v}_s = C_5 \frac{d_T^4}{L} \Delta H \qquad (52)$$

where C_5 is a constant.

$C_5 \frac{d_T^4}{L}$ represents the slope of the linear calibration graph (or output characteristic) and indicates the amplification of the instrument. Thus head loss tubes with the same ratio of $\frac{d_T^4}{L}$ will produce identical calibration graphs while varying $\frac{d_T^4}{L}$ varies the amplification of the instrument.

The effect of varying the head loss tube dimensions on the experimental calibration graph is shown in Fig. 45B where it is shown that doubling the length L of the tube approximately doubles the slope of the calibration graph.

A head loss tube of internal diameter d_T = 0.013 inches and

length L = 3.94 inches was selected for the present project as this tube gave adequate amplification, was easy to bleed of air, and was not subject to blockage by the contaminants present in the tapwater used as the freshwater supply.

Effect of Freshwater Temperature

Variation of the freshwater temperature T_F will affect both the density ρ_F and viscosity μ_F. Supposing a calibration curve has been obtained in a saltwater flow of density ρ_s with a freshwater opposing flow of temperature T_{F1}, then for a particular velocity $\bar{v}_s$ the corresponding head loss should satisfy equation (49):

$$\bar{v}_s^2 = C_2 C_3^2 \frac{\rho_{F1}}{\rho_s} \left(\frac{\rho_{F1}}{\mu_{F1}} \right)^2 \Delta H_1^2 \qquad (53)$$

If the freshwater temperature changes to T_{F2} it is required to predict the head loss ΔH_2 corresponding to the same velocity $\bar{v}_s$ in the same saltwater flow. Again using equation (49):

$$\bar{v}_s^2 = C_2 C_3^2 \frac{\rho_{F2}}{\rho_s} \left(\frac{\rho_{F2}}{\mu_{F2}} \right)^2 \Delta H_2^2 \qquad (54)$$

Thence, from equations (53) and (54):

$$\Delta H_2 = \sqrt{\frac{\rho_{F1}}{\rho_{F2}} \cdot \frac{\nu_{F2}}{\nu_{F1}}} \cdot \Delta H_1 \qquad (55)$$

Calibration graphs obtained for $T_F = 60^\circ F$ and $90^\circ F$ are shown in Fig. 45C. (The freshwater supply line was surrounded by a hotwater jacket to obtain the calibration for $90^\circ F$). It is seen that the Bagnold

meter is a temperature sensitive instrument.

Using the calibration graph for 60°F as base, a predicted graph for 90°F was calculated and is shown as a dotted line on Fig. 45C. The agreement between the observed and predicted graphs for 90°F is good, and this implies that for practical purposes a reliable calibration graph might be used as a base for predicting calibrations at other temperatures.

When the meter is wholly immersed in a flow then the temperature of the flow may be taken as the freshwater supply temperature T_F as the flow rate through the immersed freshwater supply line is so small that the freshwater quickly attains the temperature of the surrounding flow.

Effect of Saltwater Density

By following an argument similar to that used in the previous section, it may be shown that the head loss ΔH_2 registered in a saltwater flow of density ρ_{S2} compared to ΔH_1 registered in a flow of ρ_{S1} for the same velocity $\bar{v}_S$ is given by:

$$\Delta H_2 = \sqrt{\frac{\rho_{S2}}{\rho_{S1}}} \cdot \Delta H_1 \qquad (56)$$

For the range of saltwater densities used in density current experiments ($\frac{\rho_S}{\rho_F}$ = 1.005 to 1.01), equation (56) predicts that the effect of varying the density of the saltwater flow being measured on the calibration graph is likely to be negligible. This is verified by the calibration graphs shown in Fig. 45D.

There is another effect on meter calibration due to variation in saltwater density. When the meter is placed in static saltwater a small freshwater flow is required to balance the meter; that is a small dynamic pressure must be added to the static freshwater pressure to obtain a pressure equal to the static saltwater pressure in the balancing chamber. The small freshwater flow at $\bar{v}_s = 0$ will be registered as a small ΔH by the head loss tube and this probably accounts for the slight deviation from a straight line of the calibration graph at very low velocities. As shown in Fig. 45D the higher the saltwater density the greater this deviation.

Deviation of the calibration graph at very low velocities could be avoided when working in a saltwater flow of constant density by using a non-conducting solution (e.g. sugar solution) of equal density as the opposing flow.

Deviation of the calibration graph should not occur when the meter is used in a freshwater flow as the small amount of saltwater necessary to alter the conductivity of the opposing flow will have negligible effect on its density.

Effect of Horizontal Yaw

The tip of the nozzle used was chamfered at 45° to reduce the sensitivity of the nozzle to misalignment with the approaching flow. Folsom (Ref. 33) showed that a square ended tube was insensitive to yaw up to an angle of attack of 10° while an acutely chamfered (60°) tube was insensitive

up to an angle of attack of about 20^{o}. Thus one might expect the present nozzle to be insensitive up to about 15^{o}, which is adequate, but it was suspected that yaw might also affect the flow pattern around the bypass holes in the instrument head and hence alter the calibration.

The effect of horizontal yaw was checked by placing the meter at a maximum possible angle of attack of 10^{o} in the calibration tank. The calibration curve obtained is shown in Fig. 45E which shows that the meter is insensitive to yaw at angles of attack up to 10^{o} at least. This insensitivity to yaw is considered adequate for an exploratory investigation.

Effect of Calibration Tank Characteristics

The speed of rotation of the calibration tank must be consistent both during one revolution and over a long period of operation if a reliable investigation of the variables affecting meter calibration is to be obtained. Speed checks were made initially by timing the tank over several revolutions for the higher speed settings and over different portions of a revolution for the slower speed settings. These measurements indicated that the speed of rotation was uniform. A speed check after about 100 hours operation revealed no variations.

As reported in Appendix 2, the calibration tank performed satisfactorily as far as wake subsidence and intracell circulation was concerned. The tank is virtually free of turbulence except at the higher speed settings where the velocity increases slightly as the probe

tip passes a baffle plate and a slight increase in conductivity is registered by the conductivity meter. This increase represents a change in velocity of about 2 per cent at 0.5 feet per second and is therefore negligible.

3.5.4 Instrument Operation and Response

From the outset it was apparent that the meter was slow to respond to small changes in elevation of the freshwater supply tank, that is to small changes in the head loss ΔH. When the meter is in the under-balanced state (see Fig. 39C) and ΔH is increased by 0.1 feet, say, three to four minutes elapse before the conductivity meter shows a steady reading. At first it was thought that this time delay was due to accelerative effects in the fine bore head loss tube; even though rough calculations indicated the contrary. As a practical check a sensitive rotameter (flow range 0.4 to 5.0 cc per minute) was connected to the downstream end of the opposing flow tube and the time for a steady state to obtain following a change in ΔH observed. Following positive or negative changes in ΔH of up to 0.5 feet it was found that the flow through the freshwater supply system became stable in less than one minute. This delay being less than the overall time delay following a change in ΔH it was apparent that accelerative effects cannot account completely for the overall time delay.

The instrument was reassembled and replaced in the calibration tank which was rotated to produce a nominal velocity of 0.1 feet per

second. The freshwater supply tank was set to coincide with a velocity of about 0.05 feet per second, that is the meter was in an underbalanced state. The rotating tank was switched off and the saltwater in the tank came to rest in less than 10 seconds. A time delay of from three to four minutes occurred, however, before freshwater conductivity was recorded by the conductivity meter. Hence it was concluded that the time delay is associated with the flow conditions in the balancing chamber. In the underbalanced condition the saltwater - freshwater interface is between the mouth of the balancing chamber and the ring electrode and the time delay on increasing the freshwater flow apparently represents the time required for the freshwater to flush the saltwater from the balancing chamber and so shift the interface up to the ring electrode.

As many as five positive adjustments in Δ H may be necessary to bring the meter from the underbalanced to the balanced state so that this represents 15 minutes to obtain a point on a calibration graph or subsequently to use the meter to measure an unknown point velocity. It is necessary to work from the underbalanced to the balanced state carefully because of the danger of overbalancing with the single ring electrode system at present employed. Bagnold was interested in measuring velocities in freshwater flows so he used an opposing flow of a dilute salt solution. He points out that the danger of over-balancing may be avoided in his context as the meter may be calibrated

and used in an underbalanced condition and the saltwater opposing flow never allowed to reach the ring electrode. This method assumes that the freshwater and saltwater conductivities remain nearly constant and would not be applicable to the present case where the conductivity of the oncoming saltwater varies widely.

3.5.5 Use in Turbulent Saltwater Jets

Effect of Turbulence

The meter was calibrated in a turbulence free tank but used in highly turbulent saltwater jets. Hence some estimate of the likely effect of turbulence on the performance of the meter was required. Turbulence may affect performance in two ways; firstly, there is a short term effect due to the low frequency, large scale components which may cause oscillation of the saltwater-freshwater interface in the balancing chamber; and, secondly, there is a long term effect (common to all pitot devices) which is due to the overall intensity of the turbulence which causes the meter to slightly overestimate the mean velocity being measured.

Although the short term effect might possibly be investigated experimentally by using the meter in the wake of a mesh (for which turbulence data are well documented) it was decided to examine the problem theoretically before launching on an elaborate experimental study. Most of the symbols used in the following theory are defined

schematically in Fig. 39A.

At the nozzle tip:

(i) The instantaneous oncoming velocity is $v_s = \bar{v_s} + v_s'$

(ii) The instantaneous static pressure is $p_s = \bar{p_s} + p_s'$

(iii) Turbulent variations in saltwater density ρ_s may be neglected. This is justified when working in turbulent saltwater jets of maximum relative density difference at the orifice of about 8 per cent. In the jet proper variations in ρ_s are 2 per cent or less.

The instantaneous stagnation pressure p_{sT} is given by:

$$p_{sT} = p_s + \tfrac{1}{2}\rho_s v_s^2 = \bar{p_s} + p_s' + \tfrac{1}{2}\rho_s (\bar{v_s} + v_s')^2 \qquad (57)$$

So that the instantaneous total head H_{ST} is

$$H_{sT} = \frac{\bar{p_s}}{\gamma_s} + \frac{p_s'}{\gamma_s} + \frac{\bar{v_s}^2}{2g} + \frac{\bar{v_s} v_s'}{g} + \frac{(v_s')^2}{2g} \qquad (58)$$

Separating mean and turbulent components of H_{ST}:

The temporal mean total head is:

$$\bar{H}_{sT} = \frac{\bar{p_s}}{\gamma_s} + \frac{\bar{v_s}^2}{2g} \qquad (59)$$

The turbulent component of total head is:

$$H_{sT}' = \frac{p_s'}{\gamma_s} + \frac{\bar{v_s} v_s'}{g} + \frac{(v_s')^2}{2g} \qquad (60)$$

With large scale, low frequency turbulence a positive value of $H_{ST}{}^1$ may cause flow in the meter nozzle and result in a shift in the

position of the interface in the balancing chamber so, altering the reading of the conductivity meter. This has been called the short term effect of turbulence. The shift in the interface due to $H_{ST}{}^1$ may be examined with the aid of the following assumptions:

(i) The meter is in a balanced condition under the action of $\overline{H_{ST}}$ prior to the application of $H_{ST}{}^1$ at the nozzle tip; that is the interface is at the upstream end of the ring electrode prior to the application of $H_{ST}{}^1$.

(ii) $H_{ST}{}^1$ is applied as a step function increase in $\overline{H_{ST}}$.

(iii) On application of $H_{ST}{}^1$ the saltwater in the nozzle commences to flow. The flow is laminar and the inlet loss is negligible.

(iv) The interface is a plane normal to the nozzle axis and moves at the instantaneous mean velocity of the saltwater in the nozzle; (this is probably the least justifiable assumption as it is suspected that the interface behaves analagously to an elastic membrane loosely anchored around its periphery).

(v) The time required for the interface to traverse the ring electrode is an indication of the maximum turbulent frequency likely to cause instability of the conductivity meter reading which detects the position of the interface in the balancing chamber.

The problem is essentially one of commencement of laminar flow in a cylindrical tube on impression of a pressure gradient. Szymanski

(Ref. 100) has solved the problem theoretically for an infinitely long tube with neglect of end effects. Szymanski's results are summarised on a dimensionless chart by Schlichting (Ref. 93) and this chart is reproduced in Fig. 46A. Using the present notation $\lambda\ (\nu_s\ , t, r_N)$ is the dimensionless time parameter and it is noted that the maximum centreline velocity v_{Nmax} is only arrived at after an infinite time lapse.

To proceed further, it is necessary to make an estimate of $H_{ST}{}^1$ so that v_{Nmax} may be calculated. The work of Rosler and Bankoff (Ref. 86) may be utilised to obtain an estimate of v_s^1. They measured the maximum intensity of turbulence of a submerged axisymmetric freshwater jet to be 0.3. That is, with the present notation,:

$$\frac{\sqrt{(\overline{v_s'})^2}}{\bar{v}_s} = 0.3 \qquad (61)$$

where $\sqrt{(\overline{v_s^1})^2}$ is the root mean square of all turbulent velocity fluctuations. For a turbulent intensity of 0.3 some of the turbulent fluctuations in velocity v_s^1 must exceed 0.3 and possibly $v_s^1 = 0.5\ \bar{v}_s$ for the largest fluctuations.

The remaining term in equation (60) involves the static pressure fluctuation p_s' . Goldstein (Ref. 40) points out that for a static tube p_s' is a function of the turbulent velocity components normal to the general direction of flow, that is, $p_s'(u_s', w_s')$. For homogeneous turbulence Goldstein relates u_s^1 and w_s^1 to v_s^1 to show that:

$$\overline{p_s'} = \frac{\rho_s \overline{(v_s')^2}}{6} \tag{62}$$

where $\overline{p_s'}$ is the increase in mean static pressure $\bar{p}_s$ registered by a static tube in a homogeneous turbulent flow. Folsom (Ref. 33) summarises work by Fage, who observed for wall taps in turbulent pipe flow that:

$$\overline{p_s'} = \frac{\rho_s \overline{(v_s')^2}}{4} \tag{63}$$

Assuming that the turbulence in a turbulent saltwater jet is intermediate between that of homogeneous turbulence and that of confined pipe flow, and also assuming that the constant of proportionality associated with $\overline{p_s'}$ may be used to relate the instantaneous fluctuation in static pressure p_s' to v_s^1 one arrives at:

$$\frac{p_s'}{\gamma_s} = \frac{(v_s')^2}{5g} \tag{64}$$

(This is a conservative estimate of p_s' as Ippen and Raichlen (Ref. 52) contend that while the terms $\frac{(v_s')^2}{2g}$ and $\frac{p_s'}{\gamma_s}$ in equation (60) are of the same order of magnitude they are normally not in phase. Hence H_{ST}^1 is primarily dependent on the product $\frac{\bar{v}_s v_s'}{g}$ except for low level turbulence.)

Hence equation (60) becomes:

$$H_{ST}' = \frac{\bar{v}_s \cdot 0.5 \bar{v}_s}{g} + \frac{(0.5 \bar{v}_s)^2}{2g} + \frac{(0.5 \bar{v}_s)^2}{5g} \tag{65}$$

and for a mean velocity $\bar{v}_s = 0.5$ feet per second H_{ST}^1 was

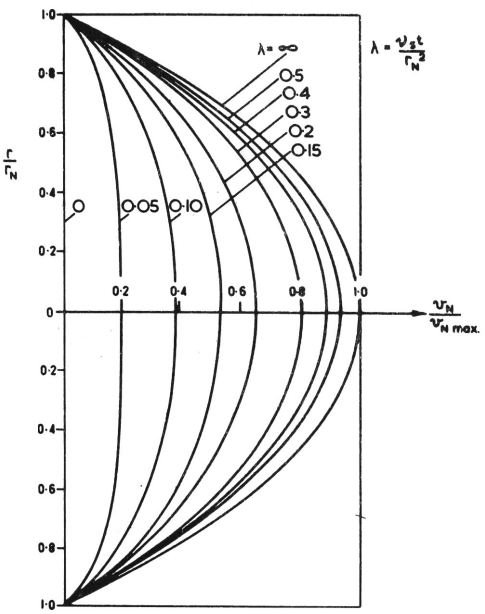

FIGURE 46A: VELOCITY PROFILES DURING COMMENCEMENT OF LAMINAR FLOW IN A LONG CIRCULAR PIPE
(AFTER SZYMANSKI)

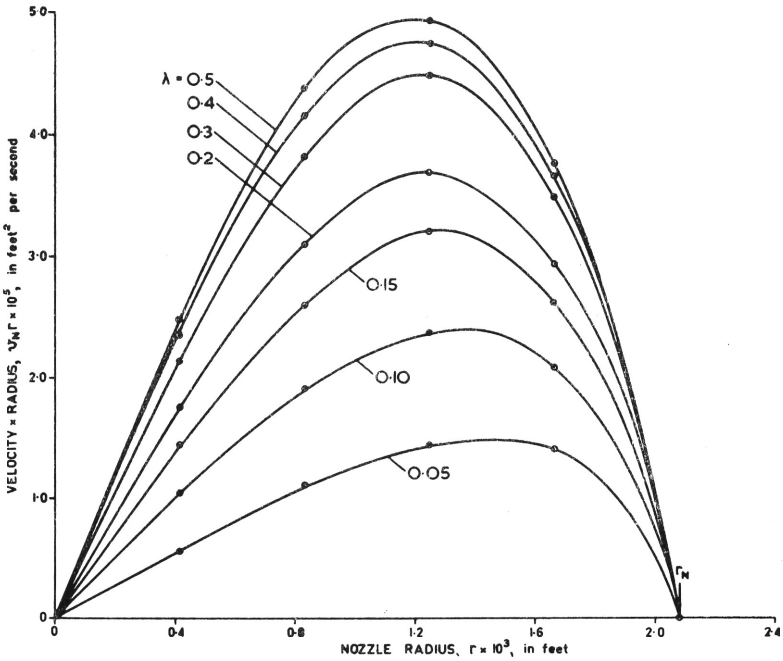

FIGURE 46B: $v_N r$ AS f (r) FOR FINDING MEAN VELOCITIES IN NOZZLE

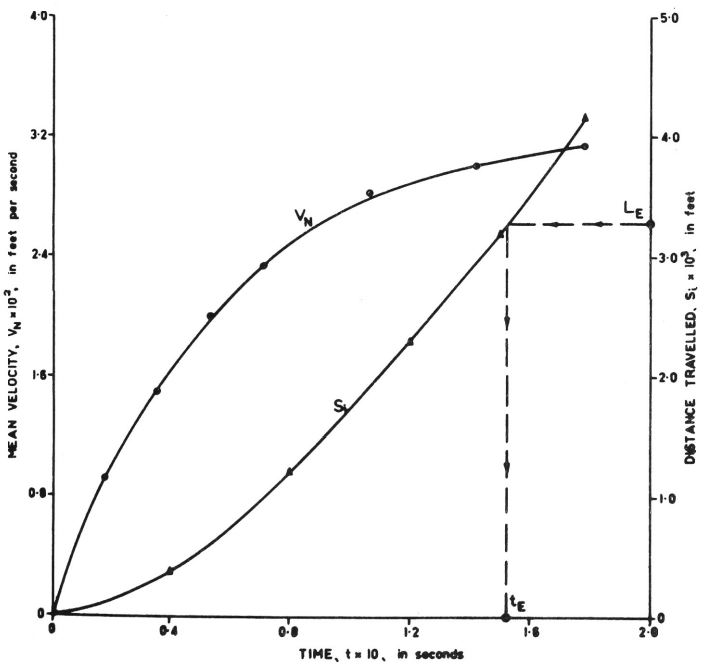

FIGURE 46C: V_N AND S_t AS f (t) IN NOZZLE

FIGURE 46: GRAPHS USED FOR ESTIMATING SHORT TERM EFFECT OF TURBULENCE ON VELOCITY METER

estimated as 0.00525 feet. The Hagen-Poiseiulle equation for steady laminar flow in a long cylindrical tube may be used to compute the maximum mean velocity $V_{Nmax.}$ resulting from the impression of $H_{ST}{}^{1}$ at the nozzle tip:

$$V_{Nmax.} = \frac{H_{ST}{}' \gamma_s d_N{}^2}{32 \mu_s L_N} \qquad (66)$$

where the slight difference between the nozzle bore d_N and the balancing chamber bore d is neglected so that L_N is the distance between the nozzle tip and the ring electrode. The inlet effect at the tip of the nozzle may be allowed for (Hardy Ref. 45) by making an increase of $0.6r_N$ in L_N but as this only decreases $V_{Nmax.}$ by 0.6 per cent in the present case this refinement is unjustified in view of the assumptions already made.

Substituting appropriate numerical values in equation (66) yielded $V_{Nmax.} = 0.0333$ feet per second so that the maximum centreline velocity was $v_{Nmax.} = 0.0666$ feet per second for a parabolic velocity profile. Szymanski's chart (Fig. 46A) was then used to obtain velocity profiles at various values of the time parameter λ and these are shown plotted as $v_N r(r)$ in Fig. 46B. The areas under the curves in Fig. 46B were measured by planimeter to determine the mean velocity V_N in the nozzle at various times t after commencement of flow and the results are shown plotted in Fig. 46C. Graphically integrating the curve $V_N(t)$ yields the distance travelled by the interface $S_i(t)$ and the latter function

is also shown in Fig. 46C. The time t_E for the interface to traverse the ring electrode of length L_E was read from the $S_i(t)$ curve of Fig. 46C and the corresponding critical turbulent frequency was about 3 cycles per second. Repetition of the analysis for $v_s = 0.1$ feet per second yielded a critical frequency of about 0.2 cycles per second.

The above analysis therefore indicated that only the large scale, low frequency turbulent velocity components were likely to cause instability of the freshwater-saltwater interface and that the effect was likely to increase with increase in velocity. When the meter was used in a typical turbulent saltwater jet this short term effect of turbulence was not apparent; probably because the region of maximum velocity close to the sloping boundary plane coincided with a steep density gradient. This steep density gradient inhibits turbulence so that the actual ratio of $\frac{v_s^1}{v_s}$ was probably much less than the value of 0.5 assumed for the preceding analysis and the actual critical frequency therefore less than the computed values. In the outer region of the jet the turbulence is fully developed (as the density gradient is slight) but the velocities are relatively low so that the critical frequency is also low.

If the short term effect of turbulence does affect the interfacial stability of a Bagnold meter then equation (66) indicates that the critical frequency may be easily lowered by fitting a longer or finer

bore nozzle.

The long term effect of turbulence on the velocity meter registration is that which is common to all pitot devices. Over a long time period $H_{ST}{}^{1}$ is given by:

$$H_{ST}' = \frac{\overline{(v_s')^2}}{2g} \tag{67}$$

As the temporal mean values of the other terms on the right hand side of equation (60) are zero. (Note that in equation (67) it is implied that $\frac{\overline{p_s'}}{\gamma_s}$ as measured by a pitot tube is zero; but if measured by a static tube (e.g. Goldstein's work summarised by equation (62)) $\frac{\overline{p_s'}}{\gamma_s}$ has a positive value).

The temporal mean total head registered by the meter $(\overline{H_{ST}})_T$ is then:

$$(\overline{H_{ST}})_T = \bar{H}_{ST} + \frac{\overline{(v_s')^2}}{2g} \tag{68}$$

Substituting for $\overline{H_{ST}}$ from equation (59):

$$(\overline{H_{ST}})_T = \frac{\bar{p}_s}{\gamma_s} + \frac{\bar{v}_s^2}{2g} + \frac{\overline{(v_s')^2}}{2g} \tag{69}$$

$(\overline{H_{ST}})_T$ may be regarded as being generated by the mean static pressure $\bar{p}_s$ and an imaginary "turbulent mean velocity $(\bar{v}_s)_T$" defined by :

$$(\bar{v}_s)_T^2 = \bar{v}_s^2 + \overline{(v_s')^2} \tag{70}$$

Hence the percentage apparent increase in mean velocity due to turbulence $\Delta \bar{v}_s$ per cent is

$$\Delta \bar{v}_s = \frac{(\bar{v}_s)_T - \bar{v}_s}{\bar{v}_s} \times \frac{100}{1} \quad \text{per cent} \qquad (71)$$

Again utilising Rosler and Bankoff's data (Ref. 86) for $\bar{v}_s = 0.5$ feet per second it is found from equations (61), (70) and (71) that $\Delta \bar{v}_s = 4.5$ per cent; while for $\bar{v}_s = 0.1$ feet per second $\Delta \bar{v}_s = 0.5$ per cent.

Effect of Proximity of a Boundary

Daily and Hardison, in a review of the use of stagnation tubes (Ref. 25), concluded that two effects may influence a stagnation tube reading when working close to a boundary.

Firstly there are so called "viscous effects" which cause the measured impact pressure to be too high when the Reynolds Number (based on the probe outside diameter and the mean velocity across the impact face) is less than 200. (Viscous effects are not confined to use of a pitot device near a boundary as they may also occur when the device is used in low velocity and in highly viscous streams). In the present case viscous effects have been compensated for by calibrating the meter at low velocities.

The other effect is termed "displacement of the effective centre" which is the result of two influences. A finite pitot probe in a region of steep velocity gradient, such as a boundary layer, integrates

the stagnation pressure exerted by the flow and the total head registered may be regarded as being concentrated at the centre of pressure of the stagnation pressure prism. In addition the presence of the wall causes an asymmetric displacement of the streamlines around the probe and a further displacement of the effective centre of measurement away from the geometric centre and along the positive normal to the wall. The data gathered by Daily and Hardison indicate that displacement of the effective centre seems to be a function of the external diameter D_N of the probe and the friction velocity of the boundary. In any case the maximum displacement noted by Daily and Hardison was $0.1D_N$ for a circular probe and this may be neglected for the present investigation.

Taking Velocity Measurements

The meter was clamped in the traversing gear shown fitted to the experimental tank in Fig. 4. This system allows rotation or translation of the meter in any direction and is fitted with a screwed traversing rod which allows the meter to be raised in small steps in a direction normal to the sloping boundary plane carrying the saltwater jet.

The meter was carefully positioned so that the underside of the bent nozzle pointed towards the orifice. The tip of the nozzle coincided with the required (x, y) coordinates on the boundary plane as indicated by painted grid lines. The first observation on any y = constant plane was taken with the nozzle touching the boundary and subsequent readings

at equal z increments above the boundary, except in the boundary layer where the increment was halved. Fig. 47 is a photograph of the meter in operation in a dyed saltwater jet.

Once the meter was out of the boundary layer the velocity profile was fairly linear and this allowed anticipation of the likely velocity at a point in this region with a resultant time saving in balancing the meter. It was also found that taking a velocity reading at a new station was expedited if the meter was quickly returned to an underbalanced state (see Fig. 39C) by sucking sharply on the flushing supply tube (see Fig. 42), so filling the balancing chamber with saltwater from the saltwater jet. This procedure was particularly necessary in the outer region of a jet where the saltwater diltution is greatest and balance detection is hampered by the small difference in conductivity between the saltwater in the jet and the freshwater opposing flow.

A thermometer was suspended in the experimental tank and temperature observations made at half hourly intervals during a test. As pointed out previously, this ambient flow temperature may be taken as the temperature of the freshwater opposing flow because of the low flowrate of the latter. Knowing the temperature of the freshwater opposing flow was a prerequisite for selecting the appropriate calibration graph for the meter.

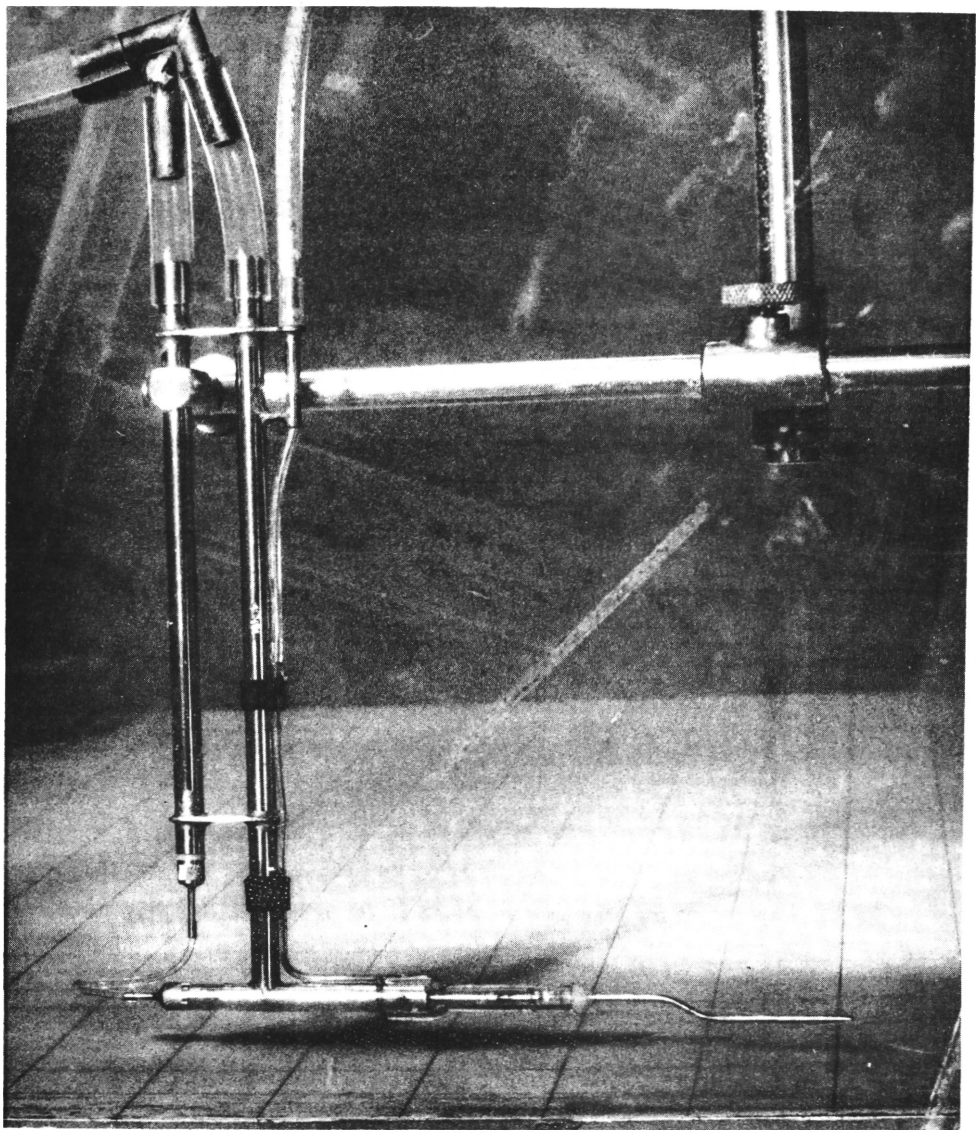

Fig. 47: Velocity Meter in Operation in Saltwater Jet.

Verification of Performance

Verification of the performance of the velocity meter in a turbulent saltwater jet may be undertaken by processing the velocity readings in conjunction with density readings at various cross sections through the jet in order to evaluate the flux of density excess at each cross section. This has been done in Subsection 2.5.4 of Chapter 2 and the flux of density excess at three cross sections of a turbulent jet is compared with the flux at the orifice (known from rotameter and saltwater supply tank density measurements) in Table 2.

The conductivity budge used for determining the density of the discrete samples withdrawn from the jet is claimed by the makers to be accurate within $\pm$ 2 per cent. The maximum error of combined velocity and density readings indicated in Table 2 is about + 3 per cent. It is interesting to note that the velocity was overestimated slightly for all three cross sections investigated and this could be accounted for by the long term turbulence effect discussed previously in this chapter.

It is possible that errors in velocity measurements are compensating in the integration procedure used in compiling Table 2, as failure to detect the maximum velocity on a particular y = constant profile may be balanced by overestimation of velocity in the outer region of the jet. Hence a conservative estimate of accuracy of $\pm$ 5 per cent is adopted for the velocity meter when it is used in turbulent saltwater jets.

3.5.6 Suggested improvements

The following modifications may improve the performance and portability of the instrument -

(i) Use of two electrode systems in the balancing chamber would allow more definite detection of the location of the saltwater-freshwater interface and eliminate the danger of overbalancing. The opposing flow tube would not be used as an electrode with this design but instead two pairs of diametically opposite electrodes would be required. Duplication of the conductivity meter would be desirable so that the conductivity measured by each pair of electrodes could be displayed simultaneously on a double beam oscilloscope.

(ii) Reduction of the body diameter D (See Fig. 39A) may improve the time response when the opposing flow is adjusted.

(iii) Use of a sensitive rotameter for flow measurement in conjunction with a precision needle valve for flow control appears to be an alternative method of supplying the freshwater opposing flow. This system would eliminate the head loss tube and the need to move the freshwater supply tank. In conjunction with a portable conductivity meter a portable instrument should be possible with this arrangement.

3.6 Summary

The literative review indicated two velocity meters apparently suitable for use in turbulent saltwater jets. Only one, the Bagnold meter, proved to be satisfactory.

The Bagnold meter fulfilled most of the requirements outlined in Section 3. 2 of this chapter but suffers from the following disadvantages:

(i) Sensitivity to temperature of the freshwater opposing flow.

(ii) Slow time response after adjusting the freshwater flow.

(iii) The danger of over-balancing.

Nevertheless the meter appeared to be accurate within $\pm$ 5 per cent.

Several design modifications to improve the performance and portability of the instrument have been suggested.

Chapter 4: Density Measurement

4.1 Introduction

Density measurement was required for both control of preparation of salt water solutions and at a point in a turbulent salt water jet. Each of these problems is treated separately although the measurement techniques employed are often suitable for both.

Mixing control and point measurement are described by first stating objectives, then summarising the literature survey, and finally reporting the procedures adopted.

4.2 Control of Preparation of Saltwater Solutions

4.2.1 Objectives

The parameter of interest in the preparation of saltwater solutions for density current experiments is the relative density excess at the orifice $\left(\frac{\Delta\rho}{\rho}\right)_o = \frac{(\rho + \Delta\rho_o) - \rho}{\rho}$, where $\rho + \Delta\rho_o$ is the density of the saltwater being injected into the lighter freshwater of density ρ. Hence a method of measuring both $\rho + \Delta\rho_o$ and ρ was required.

The anticipated range of the parameter $\left(\frac{\Delta\rho}{\rho}\right)_o$ was from 0.05 to 10.0 per cent and an accuracy of ± 10 pc. was considered adequate for an exploratory investigation. For $\left(\frac{\Delta\rho}{\rho}\right)_o$ = 1.0 per cent the percentage error in $\left(\frac{\Delta\rho}{\rho}\right)_o$ will be less than 10 pc. if the specific gravity of the saltwater and freshwater can be determined with a maximum probable

error less than 0.0005. For $\left(\frac{\Delta\rho}{\rho}\right)_o$ = 8.0 pc. the allowable maximum probable error in specific gravity becomes 0.004.

Other Requirements

The method adopted should be quick and give a direct reading. Any instruments used should be resistant to corrosion by saltwater, free from calibration drift and preferably commercially available.

4.2.2 Summary of Literature Review

The literature review (Appendix 3) indicated that use of a constant mass immersion hydrometer appeared to be the most satisfactory method of saltwater mixing control. Direct weighing of a sample in a specific gravity bottle or comparison of a sample with a standard sample using a conductivity bridge appeared to be more time consuming alternatives.

4.2.3 Use of a Constant Mass Hydrometer

Hydrometer Details

The details of three glass constant mass hydrometers used to cover the range of densities required are shown in Table 5.

S60/60°F indicates that the hydrometer measures the ratio of the density of the liquid being measured at 60°F to the density of pure water at 60°F.

Hydrometer A was used for measuring the specific gravity of fresh water as the laboratory ambient temperature was usually above

$60^{\circ}F$. Hydrometer B served for salt water yielding $\left(\frac{\Delta\rho}{\rho}\right)_o$ of 1.0, 2.0 and 4.0 per cent, while hydrometer C was required for 8.0 per cent solutions.

Table 5

Details of Glass Hydrometers

Hydrometer No.	Specific Gravity Range	Least Scale Division	Calibration Temperatures	Maker
A	0.95 to 1.00	0.001	S60/ $60^{\circ}F$	Zeal, London
B	1.00 to 1.05	0.001	S60/ $60^{\circ}F$	Selby, Sydney
C	1.00 to 1.50	0.01	S60/ $60^{\circ}F$	Zeal, London

Errors and Corrections

Random errors are involved in reading the hydrometer and with the sampling and reading procedure outlined subsequently it was estimated that the maximum probable error in reading was 0.25 times the least scale division. Hydrometers A and B therefore measure specific gravity with a maximum probable error of 0.00025 which is half of that allowable for a $\left(\frac{\Delta\rho}{\rho}\right)_o$ accuracy of $\pm$ 10pc. Hydrometer C has a maximum probable error of 0.0025 which is less than the allowable value of 0.004.

The systematic errors involved in using a hydrometer have been outlined by Rands and Bigg (Ref. 80). For precise work corrections

have to be made for:-

1. The scale error at the point of reading.
2. The difference between the surface tension of the liquid being measured and that in which the hydrometer was calibrated.
3. The meniscus height.
4. The difference between the temperature of the liquid being measured and the standard temperature at which the hydrometer was calibrated.

The scale error was not known as the hydrometers had not been independently calibrated (precise hydrometers are supplied with a calibration chart prepared by the DSIR National Physical Laboratory or other organisation independent of the maker).

The surface tension of the liquid in which the hydrometer is immersed causes a meniscus to form around the stem and the resulting downward force increases the depth of immersion of the hydrometer. The net effect is that the hydrometer will underestimate the specific gravity if used in a liquid whose surface tension is greater than that of the liquid in which it was calibrated. The surface tension of a clean surface of saltwater increases linearly with salinity and at a specific gravity of 1.10 is about 7 per cent greater than that of a clean surface of pure water (Fig. 4, Ref. 80). Hydrometers are usually designed so that an increase in surface tension of 7 per cent will result in an

underestimate of specific gravity of about 0.25 times the least scale division. Hence Hydrometer B will underestimate the specific gravity by 0.00013 and hydrometer C by 0.0025 when used in clean saltwater of specific gravity 1.05 and 1.10 respectively.

The above discussion of errors due to surface tension effects assumes a clean liquid surface. The small amounts of contaminants in hydraulic laboratory saltwater solutions can lower the surface tension, however, probably to a value less than that of the pure water in which the hydrometer was calibrated. In this case the surface tension effect will cause the hydrometer to overestimate the specific gravity slightly; the errors involved probably being of similar magnitude to those calculated above for the clean surface case. It was therefore decided that surface tension effects could be ignored providing that the normal cleanliness precautions and manipulation procedure were carried out.

A correction for meniscus height is necessary when a hydrometer is used in an opaque liquid. In the present investigation the hydrometer was read by viewing along the liquid surface through the glass sample jar so no meniscus correction was necessary. When dyed saltwater was required, the dye was not added to the mixing tank until the saltwater density had been adjusted to the desired value. The small quantity of dye used resulted in negligible change in density.

If a hydrometer is placed in a liquid whose temperature is higher than the standard temperature at which the instrument was calibrated, the hydrometer expands slightly and "floats high". This results in an overestimate of specific gravity. The necessary correction may be derived by considering the volumetric expansion of the hydrometer (Ref. 80). The correction c_H to be applied to a hydrometer reading S.G. to give the correct reading $(S.G.)'$ is given by:-

$$c_H = - (S.G.) \alpha (t'-t)$$

where α is the coefficient of volume expansion for laboratory glass = 0.0000167 per ^{o}F

t' is the temperature of observation, and

t the standard temperature of the hydrometer.

Some sample calculations using this formula indicated that the temperature effect was negligible over the range of laboratory ambient temperatures. For example, the specific gravity of a saltwater mix is read as $(S.G.)_s = 1.01$ with hydrometer B at an ambient temperature of $t' = 80^{o}F$. The specific gravity of freshwater (mains supply) at $t' = 80^{o}F$ is S.G. = 0.998 by hydrometer A. The corresponding value of $\left(\frac{\Delta\rho}{\rho}\right)_o$ calculated from indicated values without temperature correction is 1.2026 per cent while with temperature corrections applied $\left(\frac{\Delta\rho}{\rho}\right)_o$ is 1.2021 per cent. Hence the error in $\left(\frac{\Delta\rho}{\rho}\right)_o$ resulting by ignoring temperature effects is in this case 0.04 per

cent which is negligible. The error becomes smaller as $\left(\frac{\Delta\rho}{\rho}\right)_o$ increases.

Sampling and Measurement

Samples of saltwater were obtained from the mixing tank with a 2000 ml. measuring cylinder, care being taken not to include any floating debris. The sample was stirred in the vertical direction with a wire ring stirrer and allowed to stand for a few minutes so that any air bubbles floated to the surface.

The hydrometer stem was wiped clean and the hydrometer introduced carefully into the jar and depressed slightly beyong the anticipated equilibrium value before release. This technique is necessary to ensure consistent meniscus formation. When the hydrometer had stopped oscillating a reading was taken by sighting through the glass jar along the surface of the liquid. The procedure was repeated when final fine adjustments to the saltwater mix were being made. After use the hydrometer was cleaned with methylated spirits.

Check by Direct Weighing

Towards the end of the investigation an automatic electronic balance became available so it was decided to check by direct weighing the $\left(\frac{\Delta\rho}{\rho}\right)_o$ value of a saltwater mix prepared by using hydrometers for density measurement. Saltwater and freshwater samples were weighed direct to 0.0001 gms in a 50 ml. specific gravity bottle and

$\left(\frac{\Delta\rho}{\rho}\right)_o$ computed at 8.45 per cent. The value previously determined by hydrometers was 8.0 per cent which represented a difference of 5 per cent between the two determinations. This represents the maximum probable percentage error as the saltwater mix of $\left(\frac{\Delta\rho}{\rho}\right)_o$ = 8.0 per cent was prepared by using hydrometer C which is the least sensitive. The hydrometer method of saltwater mix control therefore proved to be of sufficient accuracy for an exploratory investigation.

4.3 Measurement of the Mean Density at a Point in a Turbulent Saltwater Jet

4.3.1 Objectives

Range and Accuracy

An instrument was required to measure the mean density at a point in turbulent saltwater jets ranging in thickness from about 0.02 to 0.10 feet. The anticipated density range was from 1.05 to 1.0 times the density of fresh water and an accuracy of $\pm$ 10 pc. was adequate for an exploratory investigation.

Other Requirements

The instrument should be free from calibration drift and simple to operate. Electronic instruments should preferably be commercially available or simple to make. Those portions of the system inserted in the saltwater flow should be corrosion resistant.

4.3.2 Summary of Literature Review

Of the several methods reviewed in Appendix 3 it was decided that

the following warranted further investigation:-

(a) Conductivity measurement with a directly exposed probe and a series type conductivity meter after Lamb et al (Ref. 64).

(b) Analysis of continuously withdrawn samples by conductivity meter.

(c) Analysis of discrete withdrawn samples by conductivity meter.

These techniques are arranged in order of decreasing instrumental complexity but in order of increasing time required to obtain a measurement.

4.3.3 Conductivity Measurement with a Directly Exposed Probe

Principle

The device is composed of two main parts; the probe which is immersed in the turbulent salt water flow and the electronics measuring the conductivity in the vicinity of the probe. Probe details are shown in Fig. 51 and electronic details in Figs. 52 and 53. The system used is similar to that of Lamb et al (Ref. 64) except that the electronics were simplified to determine mean conductivity only and also to match the electronic instruments available.

Briefly the principle of the circuit is to use the varying impedance of the probe due to turbulent conductivity fluctuations in the saltwater jet to amplitude modulate an A. C. carrier wave in a series circuit. Another resistance in this probe series circuit acts as a load resistor

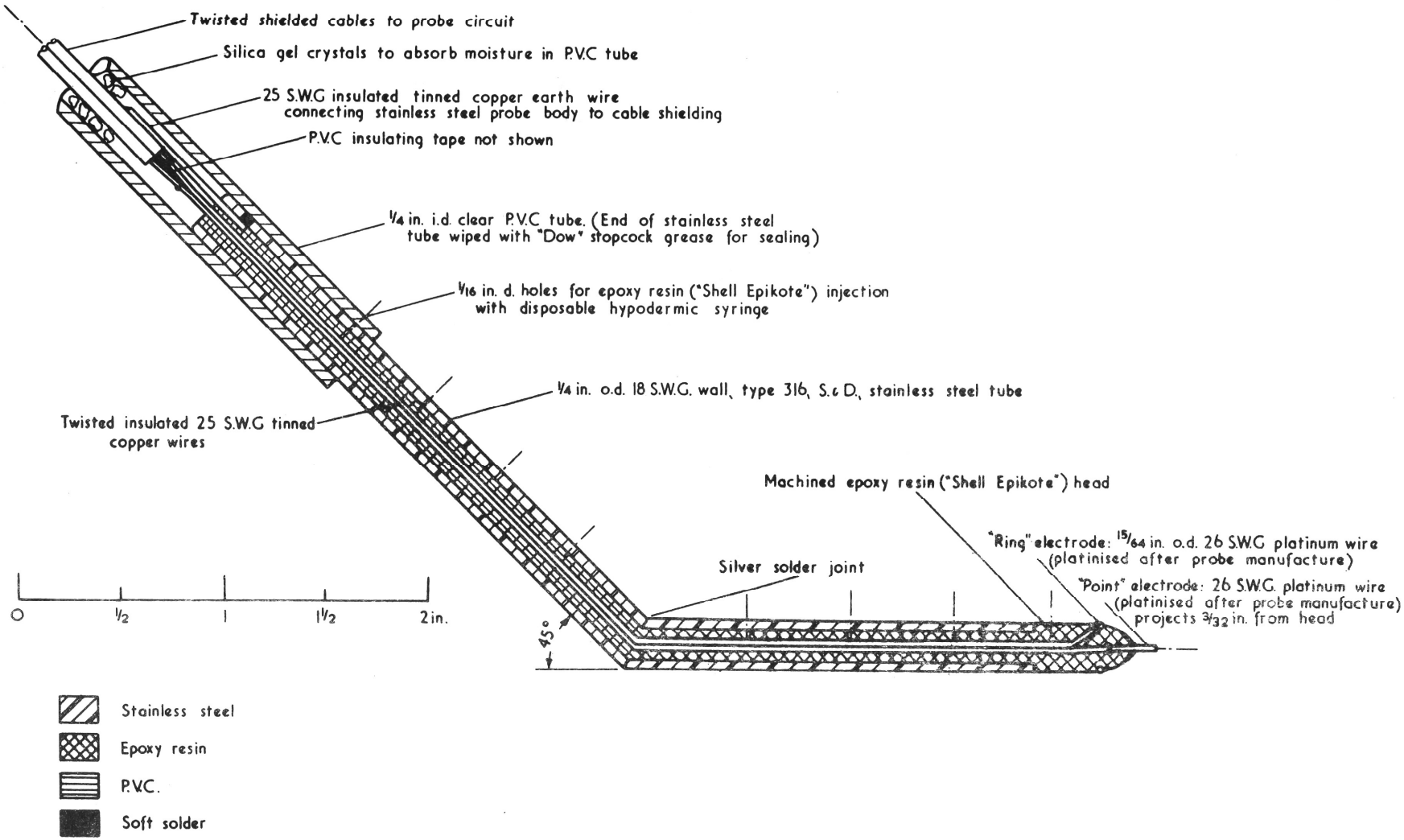

FIGURE 51: CONDUCTIVITY PROBE DETAILS: LONG. - SECTION

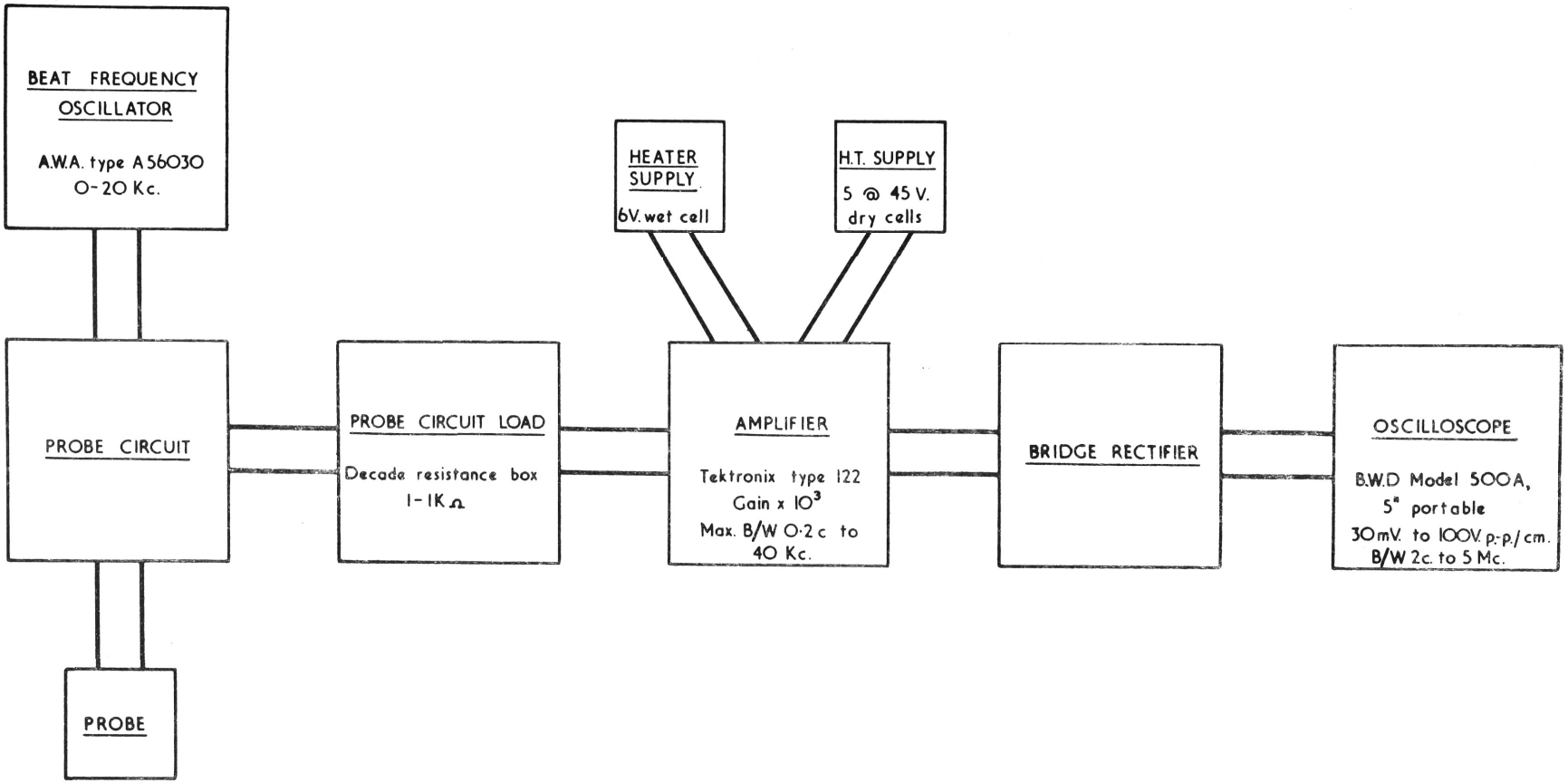

FIGURE 52: SALT WATER CONDUCTIVITY MEASUREMENT: BLOCK DIAGRAM OF COMPONENT ELECTRONIC INSTRUMENTS

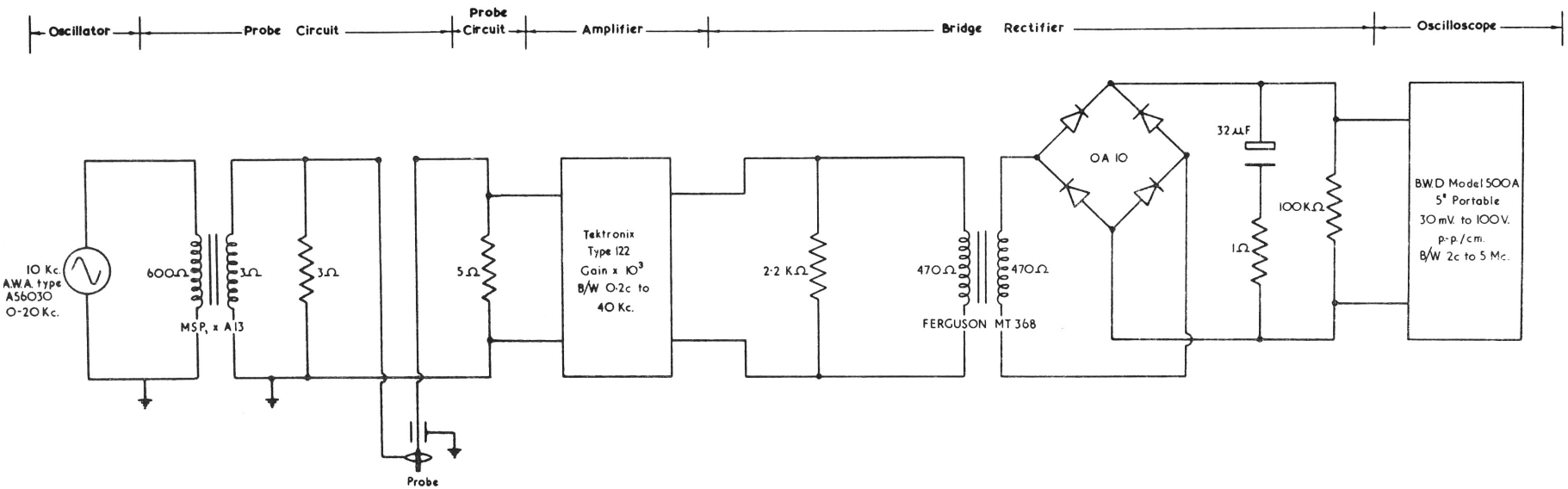

FIGURE 53: SALT WATER CONDUCTIVITY MEASUREMENT: CIRCUIT DETAILS

for obtaining a voltage input for an A. C. amplifier and the output from the amplifier is rectified and measured with a cathode ray oscilloscope.

Design and Manufacturing Details

A detailed drawing of the probe is shown in Fig. 51. The probe is the "point and ring" electrode type after Lamb et al (Ref. 64). This electrode arrangement detects the conductivity of a small volume of saltwater in the vicinity of the smaller point electrode where the electrical flow lines are concentrated so that for practical purposes the conductivity measurement is at a point in the flow. Such a point and ring electrode system has superior spatial resolution to the two electrode system commonly used which detects the conductivity of a larger parcel of fluid between two electrodes of equal area.

Features of the probe design were:-

(1) The use of corrosion resistant materials such as stainless steel and epoxy resin.

(2) The use of a turned epoxy resin head carrying the electrodes. The head was fixed in the probe body by injection of epoxy resin with a hypodermic syringe.

(3) Earthing of the probe body to provide a preferential path to earth for stray electrical currents so minimising the effect of other earthed conductors in the flow being measured.

(4) The use of silica gel crystals to absorb moisture in the

(4) plastic tube carrying the lead wires.
cont'd.

The electrodes were platinised (i.e. coated with a layer of platinum black) using the procedure outlined in the handbook for the Mullard conductivity bridge (Ref. 10). The platinising current was calculated to give an electrode surface current density approximately the same as that used for the Mullard cell electrodes. With a point and ring electrode system, however, a higher platinising current is permissible for the ring electrode of larger surface area compared to that for the point electrode of smaller surface area. If the point electrode is platinised first then the higher current used when subsequently platinising the ring electrode causes part of the platinum black deposit on the point electrode to leave the electrode as a fine powder. This disintegration of the point electrode coating does not occur if the ring electrode is platinised first.

The electronic circuit details are shown in block diagram form in Fig. 52 and in detail in Fig. 53. The probe circuit is a series circuit comprising an A.C. source, the probe, and a load resistor. A.C. excitation is necessary to avoid polarization effects at the electrode surface.

Lamb et al (Ref. 64) have pointed out that linear modulation of the A.C. carrier wave will only occur when:

1. the probe impedence is high compared to the impedences of the

1. cont'd. other components in the probe circuit;

2. the capacitive reactance of the probe at the carrier frequency is an order of magnitude greater than the resistive component of the probe impedance.

The impedance of the probe was determined using an A. C. impedance bridge. The upper arms were comprised of decade resistance boxes (non inductive ± 1 per cent resistors) of equal value while the lower arms were respectively the probe in saltwater solution, and precision decade resistance and capacitance boxes connected in parallel. The bridge was excited by a beat frequency oscillator and balance detected by a cathode ray oscilloscope. The apparatus for determining the probe impedance is shown in Fig. 54. The impedance of the probe at a frequency of 10Kc. was found to range from about 6.5 kilohms to 100 ohms in fresh water and in saltwater of specific gravity 1.10 respectively. The capacitive reactance of the probe was much greater than the resistive parts of the probe impedance in both cases; so satisfying Lamb et al's second criterion for linear modulation.

To satisfy Lamb et al's first criterion for linear modulation, it was decided to make the individual impedances of the elements in the probe circuit about 0.05 times the minimum probe impedance. This required transformer coupling between the beat frequency oscillator

and the probe circuit to reduce the output impedance of the oscillator as seen by the probe circuit from 600 to 3 ohms. A 3 ohm resistor was connected in parallel with the transformer secondary for maximum power transfer between the oscillator and the probe circuit. The probe circuit load resistance was a decade resistance box specially constructed for the purpose as commercially available boxes did not carry a 1 to 10 ohm range.

A small load resistance in the probe circuit for linear modulation carries the penalty, however, of low voltage output. For example, when the probe is immersed in fresh water its impedance is a maximum and the voltage drop across the load resistance about 0.27 millivolts. This voltage drop requires amplification if rectification and oscilloscope measurement is used. A Tektronix type 122 amplifier was found to be suitable, although it was necessary to insert a coupling transformer between the amplifier and the bridge rectifier to eliminate the D.C. component of the amplifier output. The amplifier is provided with a D.C level control but this was a nuisance to adjust and subject to drift.

The A.C. signal from the amplifier then passes through a bridge rectifier to obtain a D.C. signal for display on the cathode ray oscilloscope. The bridge rectifier is similar to that recommended by the Mullard Company and employs OA10 germanium junction diodes.

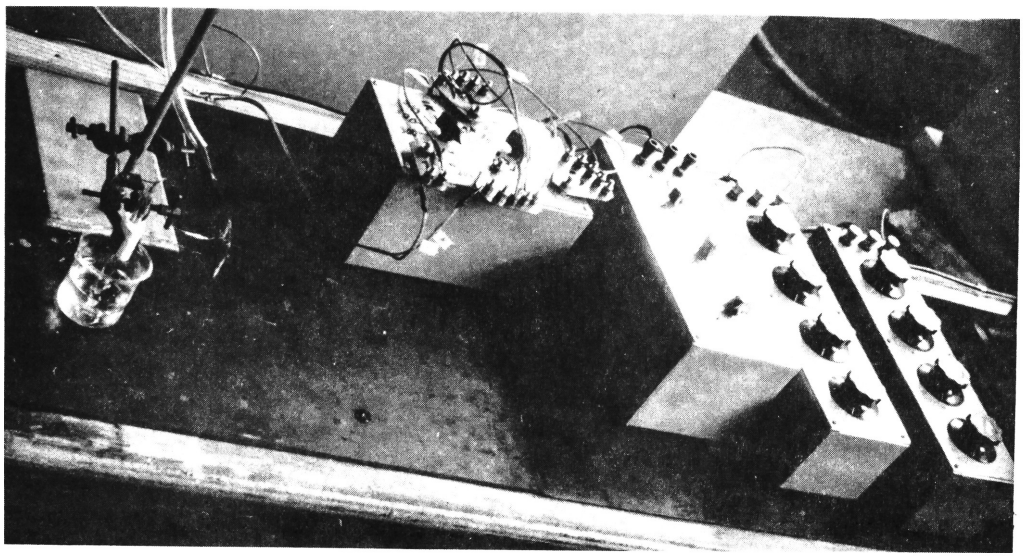

Fig. 54: Electronic Apparatus for Measuring the Impedance of a Conductivity Probe.

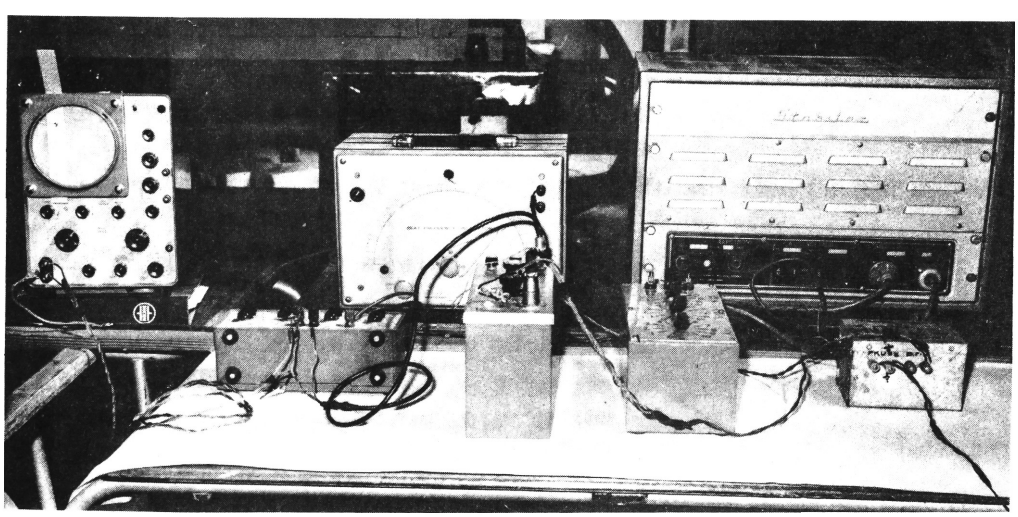

Fig. 55: Electronic Apparatus for Measuring the Conductivity at a Point in a Saltwater Jet.

(Page 113, Ref. 8). A photograph of the assembled electronics is shown in Fig. 55.

Prior to use of the probe in a turbulent saltwater jet the circuit linearity was checked by substituting a precision decade resistance box for the probe. For linear modulation the output voltage measured by the oscilloscope should be inversely proportional to the probe impedance as represented by the substituted resistance. A plot of voltage output versus probe impedance on log-log paper was a straight line for practical purposes, so confirming the circuit linearity.

Testing

The probe was clamped in the suspension device shown in Fig. 4 and lowered into a typical turbulent saltwater jet. The system appeared to faithfully monitor the conductivity fluctuations in the vicinity of the point electrode but the range of fluctuations was too great to obtain a mean reading.

An attempt was made to reduce the range of the fluctuations by installing an R. C. filter system between the bridge rectifier and the oscilloscope but this only lowered the sensitivity to changes in mean conductivity to an unacceptable value.

As additional electronic instruments such as a wave analyser and averaging circuit were not available, it was decided that the alternative of feeding the rectifier output to a chart recorder might

be possible. The recorder trace may be processed to obtain a mean reading although Frankel and Cumming found this task to be very time consuming (Ref. 35). A Both pen recorder was available but could not be matched to the existing circuit without the use of a power amplifier. (A Honeywell "Visicorder" ultra-violet recorder which would be suitable has since become available.)

A further alternative was to connect the heater of a long time constant thermovacuo junction to the bridge rectifier output and to detect the signal with a D.C. millivoltmeter - this in effect is a cheap R.M.S. voltmeter. A long time constant thermo-vacuo junction is a specialised electronic component only made on order in England, however, and the several months delay in obtaining it could not be tolerated.

Conclusions

An attempt to measure the conductivity at a point with a directly exposed probe and simple series type conductivity meter was a failure because the range of the conductivity fluctuations was excessive.

Investigations reported subsequently in any case indicated that the probe calibration was unstable, probably due to excessive current density at the point electrode as a result of over simplification of the electronics.

It was therefore decided to abandon any further attempts to measure conductivity with a directly exposed probe and to proceed with the

alternative method of analysis of continuously withdrawn samples by conductivity meter.

4.3.4 Analysis of Continuously Withdrawn Samples by Conductivity Meter

Principle

Continuous withdrawal sampling is a procedure intermediate between use of a directly exposed probe and analysis of discrete withdrawn samples. The sample is siphoned continuously through a mixing chamber in which the conductivity probe is immersed. The difficulties due to conductivity fluctuations associated with a directly exposed probe are avoided as is the excessive time required by analysis of discrete withdrawn samples.

Design and Manufacturing Details

The conductivity probe and electronic circuitry were the same as described in the previous section 4.3.3 and as shown in Figs. 51, 52 and 53.

The mixing chamber design details are shown in Fig. 56, while Fig. 57 is a photograph of the dismantled device. The important feature of this mixing chamber is the inclusion of two baffle plates through which pass four fine bore tubes of different lengths. The "mechanical" mixing of alternate blocks of liquid of high and low conductivity passing through the chamber may be readily visualised.

The other design details are in keeping with normal hydraulic laboratory requirements of an instrument being corrosion resistant, readily dismantled for cleaning, and not prone to mechanical damage.

Testing

The probe and mixing chamber were assembled and positioned in the experimental tank as shown in Fig. 58. The siphoning rate was adjusted to prevent entrainment of surrounding liquid by the hypodermic tubing nozzle by observing the pickup from a thin slug flow of dyed saltwater on the sloping boundary plane. The saltwater flow rate was then increased to produce a typical turbulent jet and the oscilloscope display observed.

The mixing chamber performed efficiently as the voltage detected by the oscilloscope was steady in the body of the jet. At the wavering jet boundary slight unsteadiness occurred due to low frequency "back-curling" of small parcels of high conductivity liquid. This unsteadiness was not excessive, however, and a mean reading was readily obtained by averaging the oscilloscope fluctuations by eye.

At the slow siphoning rate required through the nozzle to prevent entrainment of surrounding liquid, it was found that the time required to refill the mixing chamber with saltwater at a new station was two minutes. This time lag was determined by checking the time required for freshwater conductivity to be detected by the probe after shutting off

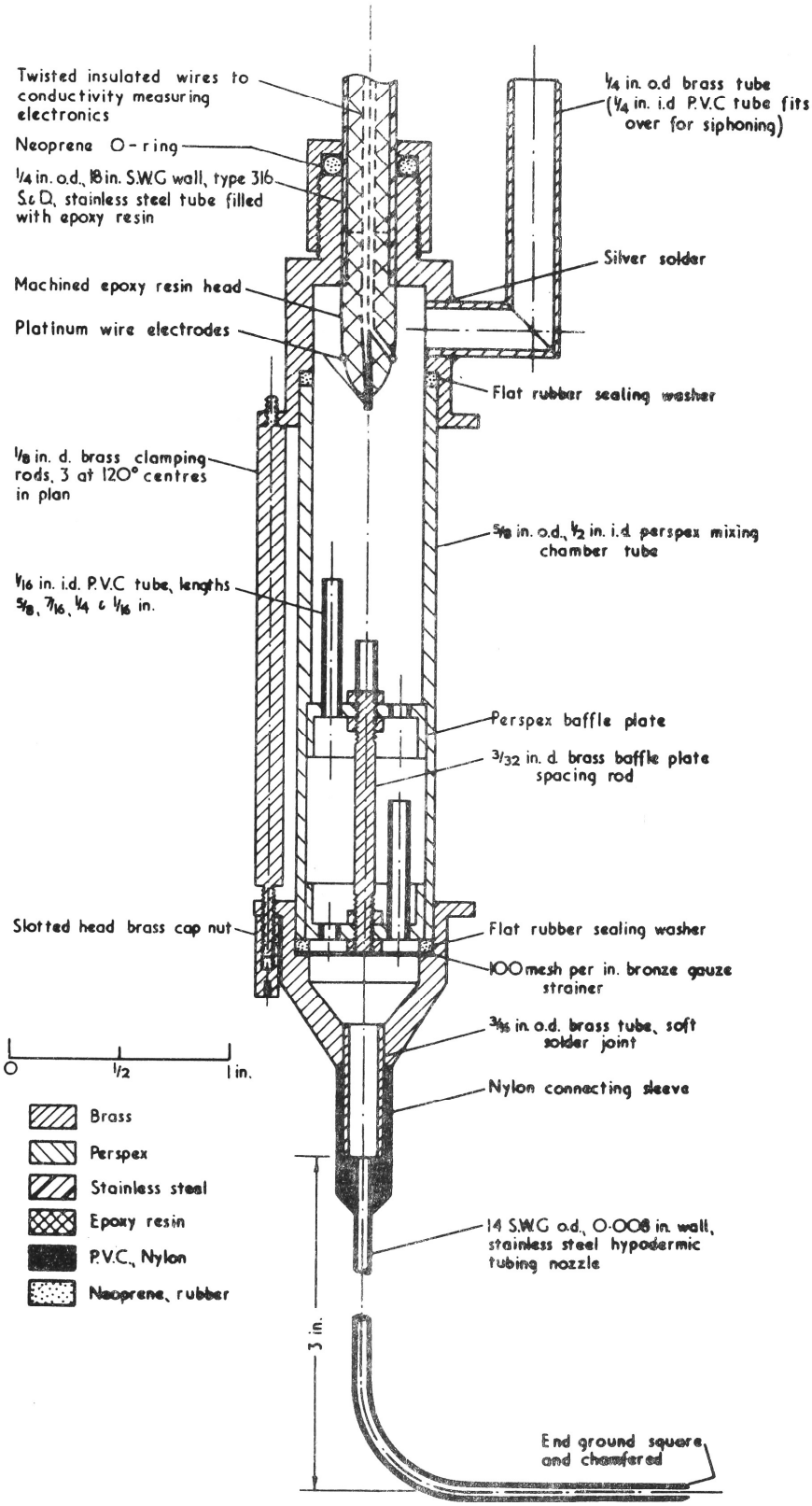

FIGURE 56: MIXING CHAMBER DETAILS : LONG. SECTION

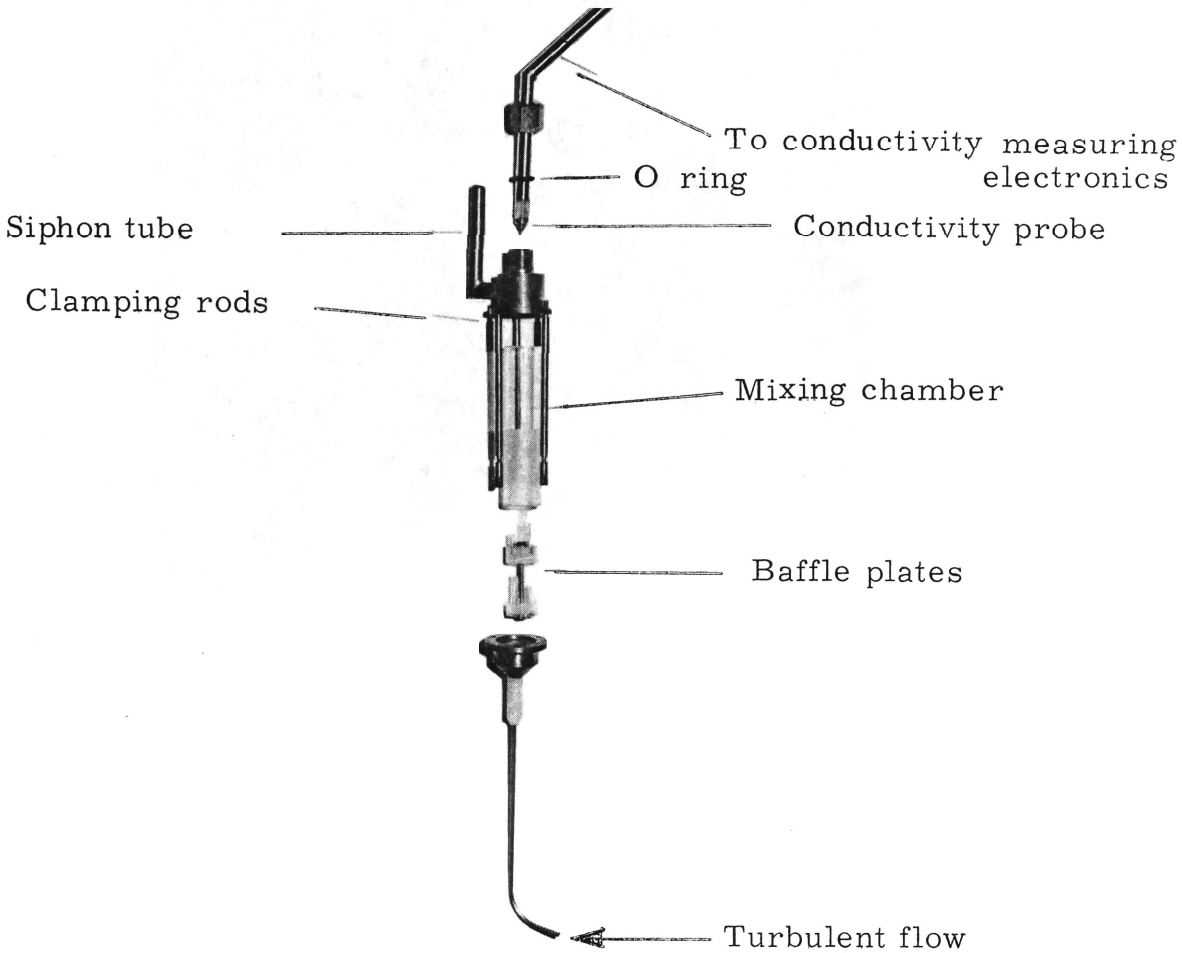

Fig. 57: Dismantled Mixing Chamber

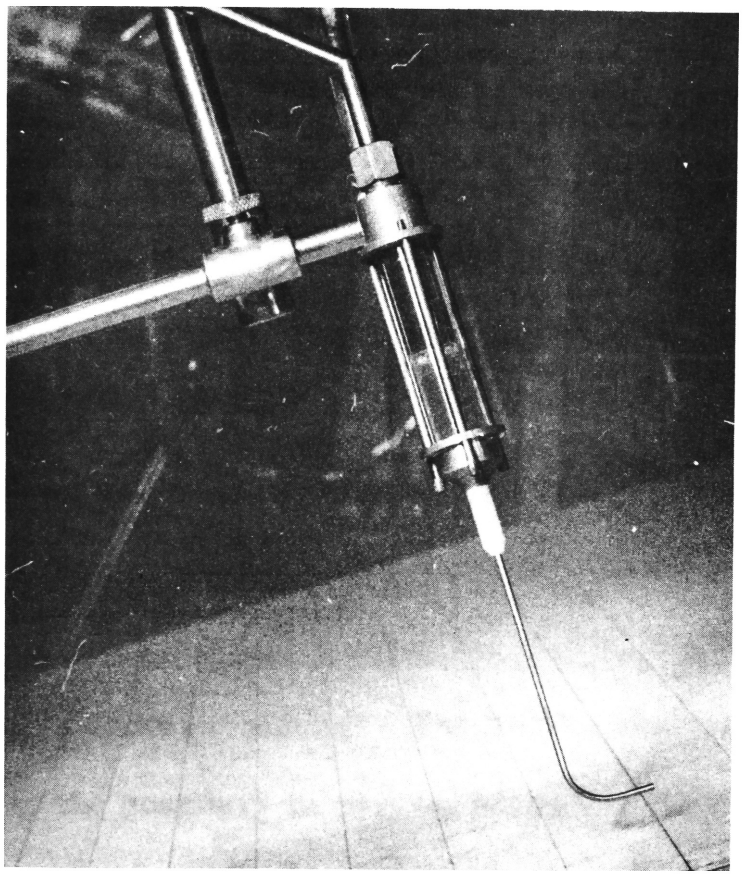

Fig. 58: Mixing Chamber in Operation in a Saltwater Jet.

the saltwater supply. Allowing for adjustment of the suspension screw, oscilloscope reading and observation recording, this means that about two and one half minutes are required to obtain a mean density reading at a point in a turbulent saltwater jet. This is a considerable time saving when compared to the technique of analysis of discrete samples.

The probe calibration was determined by progressive dilution of a saltwater sample using a pipette. A typical nonlinear calibration curve is shown in Fig. 59.

A series of vertical conductivity profiles at a cross section in a turbulent jet were then measured. Each profile was measured by lowering the nozzle so that it just touched the sloping boundary with the tip at the required coordinate marks. The mixing chamber was then raised normally to the boundary in several steps to obtain conductivity readings at several points. The probe was calibrated before and after use in the tank but different calibration curves were obtained: the discrepancy in terms of density amounting to about 40 per cent. This could not be accounted for by the temperature change of less than $5^{o}F$ between calibrations.

Several checks were made in trying to detect the cause of this calibration drift. At first it was thought that stratification was occurring in the saltwater mixing tank even though the mixing tank was thoroughly stirred before filling the elevated constant head saltwater

tank (see Fig. 3 for layout of these tanks). Withdrawal sampling at various depths in the mixing tank after it had stood for 24 hours showed negligible stratification, however.

The electronic circuitry was then rechecked for linearity (by substituting a precision decade resistance box for the probe) and found to be performing satisfactorily. New batteries for the amplifier high tension supply were fitted and the circuit operated for several hours without change.

It was then suspected that calibration drift was occurring in the probe itself. The relatively new material, titanium, reportedly is very resistant to surface attack by saltwater, so it was decided to make a probe using titanium wire electrodes. Titanium is so inert that considerable difficulty was experienced in soldering copper lead wires to the titanium electrodes. The calibration graph for this probe is shown in Fig. 59 which shows that titanium has a lower electrical conductivity than platinised platinum and is electrically a less efficient probe material. The titanium probe electrode was used in the mixing chamber to obtain a vertical density profile in a turbulent saltwater jet. Once again pre and post use calibration checks differed excessively but the effect was not as marked as with platinised platinum electrodes.

It was therefore apparent that the calibration drift was a relatively long term effect occurring during the time interval required to complete

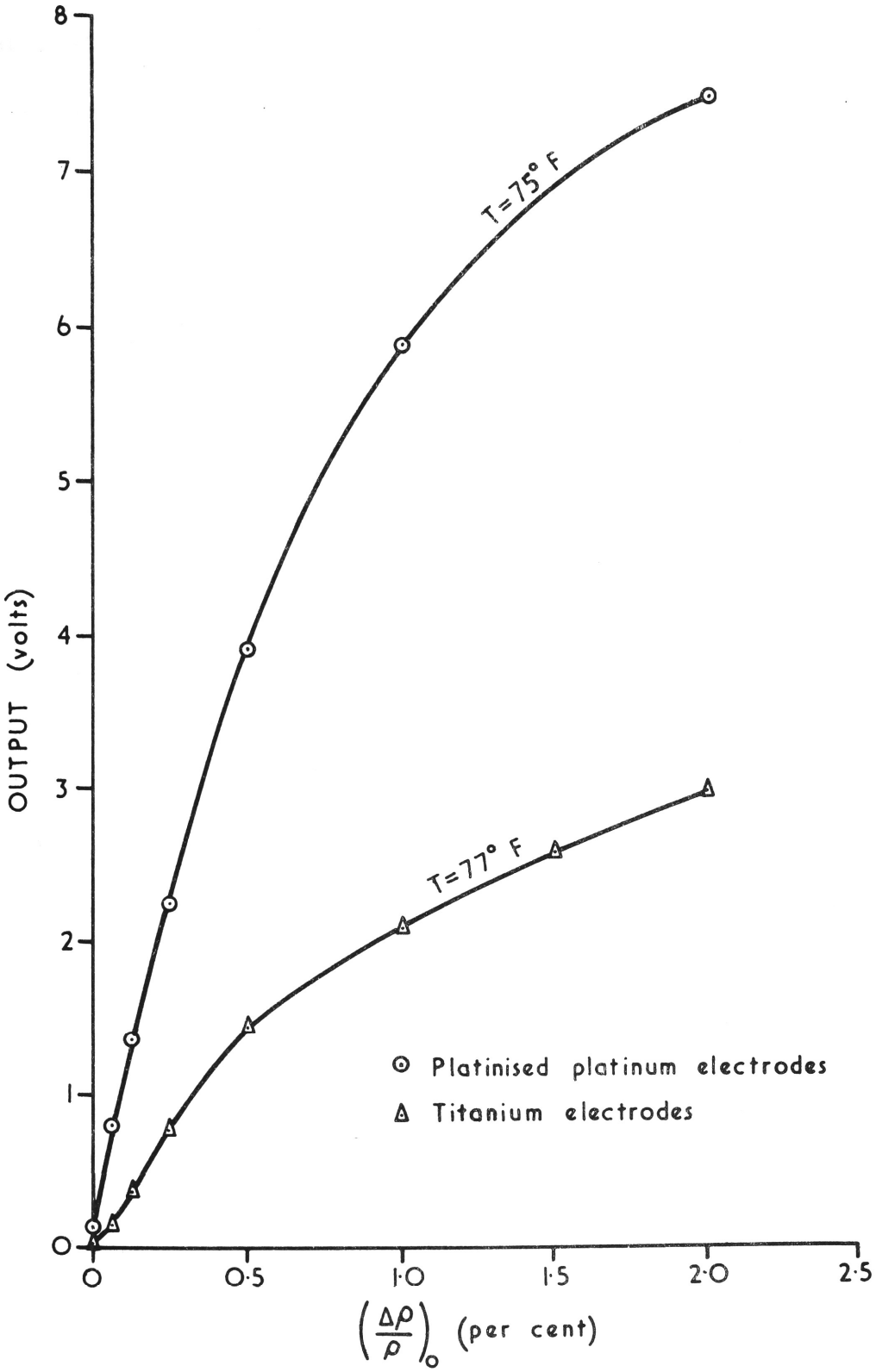

FIGURE 59: CONDUCTIVITY PROBES; TYPICAL CALIBRATION CURVES

a vertical conductivity profile in the jet. To check this the titanium electrode probe was immersed in a saltwater solution and the circuit output voltage measured over a twenty minute period as shown in Fig. 60. An intolerable amount of drift did occur but a more important effect was also detected. When the probe is immersed in freshwater for a few minutes and then returned to the same saltwater solution a sudden increase in conductivity reading results. The conductivity then falls off, appearing to follow a negative exponential curve. A similar effect was found with the platinised platinum electrodes although in general conductivity does not increase following immersion in freshwater but follows the same negative exponential curve. When a probe is used with the mixing chamber to measure several vertical conductivity profiles it is subject to alternate immersion in saltwater and freshwater so that this effect accounts for the observed pre and post measurement calibration differences.

The cause of calibration drift is not known definitely but it is suspected that the electronic circuitry as designed requires excessive electrical current density at the electrode surface. Commercially available conductivity cells have a much larger electrode surface with more sophisticated circuitry and this tends to support this theory.

The use of a proven commercially available conductivity meter in conjunction with the mixing chamber is worth further investigation.

The Radiometer type CDM2 direct reading conductivity meter would be suitable. This is a series type meter which could follow any small conductivity fluctuations not damped by the mixing chamber and which is available with a through-flow cell which could be attached to the top of the mixing chamber.

Conclusions

The mixing chamber designed for analysis of continuously withdrawn samples operated efficiently and allowed detection of a mean density at a point in a turbulent saltwater jet.

The mixing chamber could not be utilised, however, as the conductivity probes used were subject to excessive calibration drift.

Time did not permit manufacture of a more stable probe so it was decided to abandon this technique and to use the third alternative of analysis of discrete withdrawn samples.

The use of the mixing chamber with either a larger electrode probe and the existing electronics or alternatively with a commercially available conductivity meter and through-flow cell warrants further investigation.

4.3.5 Analysis of Discrete Withdrawn Samples

Principle

A discrete sample is collected by slow siphoning through a fine bore nozzle located in the turbulent saltwater flow and the density of the

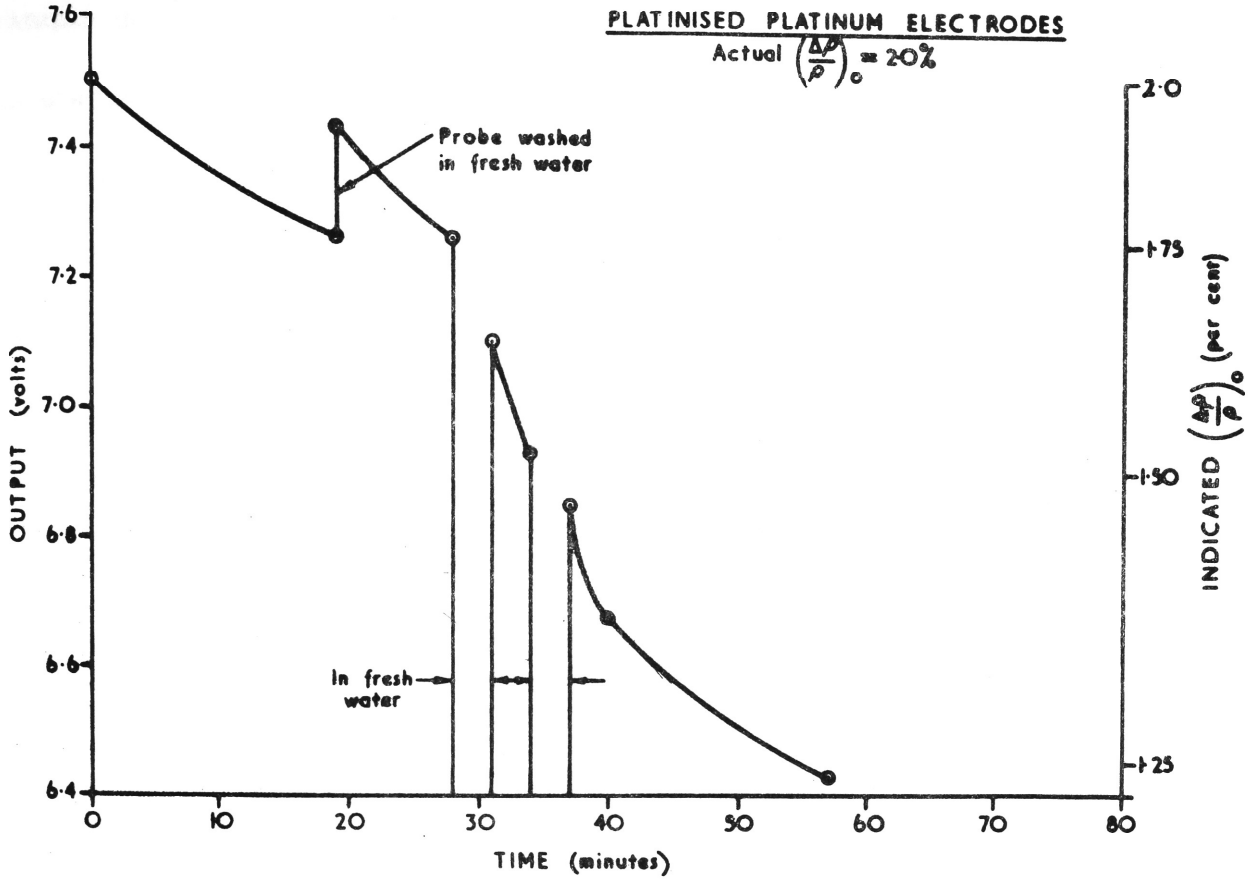

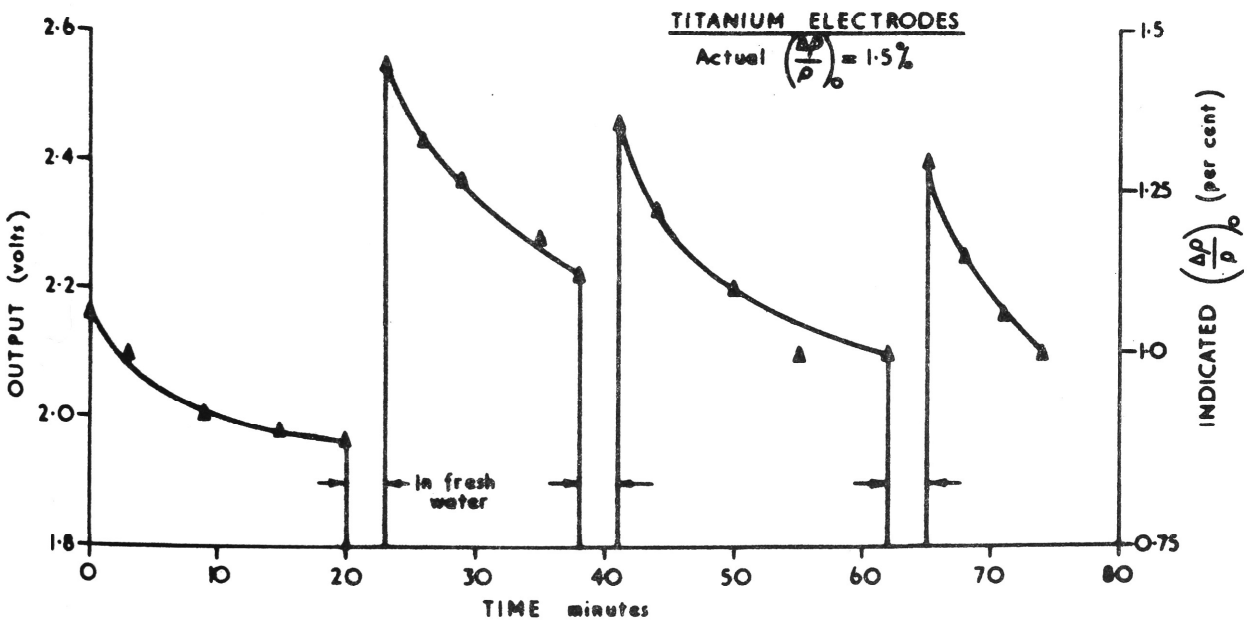

FIGURE 60: STABILITY OF CONDUCTIVITY PROBES

sample is then determined with a commercially available conductivity meter. As discussed in Appendix 3 the nozzle must be small relative to the lateral dimension of the flow to minimise flow disturbance. Also the mean velocity of intake must be less than or equal to the flow velocity at the nozzle tip so that entrainment of surrounding liquid is avoided.

Apparatus Used

The sampling nozzle was made from hypodermic tubing and is shown in operation in a turbulent saltwater jet in Fig. 61.

A length of clear PVC tube approx. 1/16 inch bore was connected to the top of the nozzle assembly to carry the siphoned flow and the sample was collected in the small perspex tubes shown in the rack in the circulated water bath in Fig. 62. The internal diameter of the sample tubes was slightly larger than the external diameter of the conductivity cell and the depth just sufficient to immerse the cell to the specified depth, so that the volume of sample required was minimised.

Conductivity measurement was by "Mullard" conductivity bridge type E7566/3 fitted with laboratory dip cells type E7591/B with platinised platinum electrodes. This instrument is essentially an A. C. excited Wheatstone bridge with amplified bridge out of balance and cathode ray tube ("magic eye") balance detection. The conductivity cell is connected in one arm of the bridge and the bridge balanced by varying the ratio of resistance of two other arms with a precision

calibrated potentiometer. When used in this manner the scale reading multiplied by the cell constant (which varies slightly from cell to cell) gives the absolute specific conductivity which may be measured in the range 0.1 micromhos to 10mhos.

For analysis of samples from turbulent saltwater jets, however, the comparison facility is more convenient. The instrument allows connection of a comparison cell to the fourth arm of the Wheatstone bridge and this cell is immersed in a standard solution of known conductivity. The test cell is connected to the first arm of the bridge as before and this is immersed in the sample whose conductivity is required. When the bridge is balanced the scale reading indicates the ratio of the conductivity of the sample to that of the standard solution in the range 0.1 to 10. The comparison is claimed to be accurate within $\pm$ 2 pc. although this is probably optimistic in the scale intervals from 0.8 to 1.0 and 5 to 10 as the scale has a 2 decade logarithmic calibration.

The bridge output characteristic is almost linear as shown in Fig. 63. Temperature effects were minimised by immersing the standard solution and sample tubes in a water bath with a circulated supply from the experimental tank as shown in Fig. 62. Also the bridge has an inbuilt calibration resistance which allows resetting of the potentiometer cursor for variations in ambient temperature.

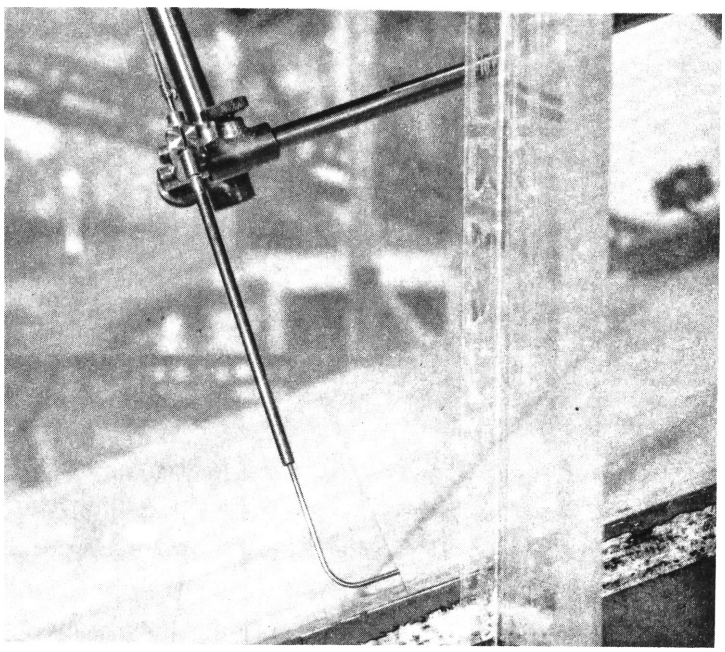

Fig. 61: Probe for Withdrawal of Discrete Samples in Operation in a Saltwater Jet.

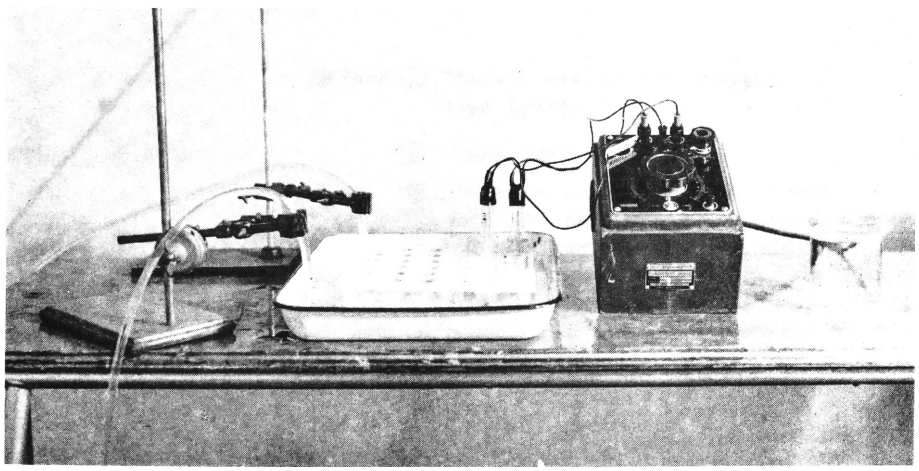

Fig. 62: Apparatus for Measuring the Conductivity of Discrete Withdrawn Samples.

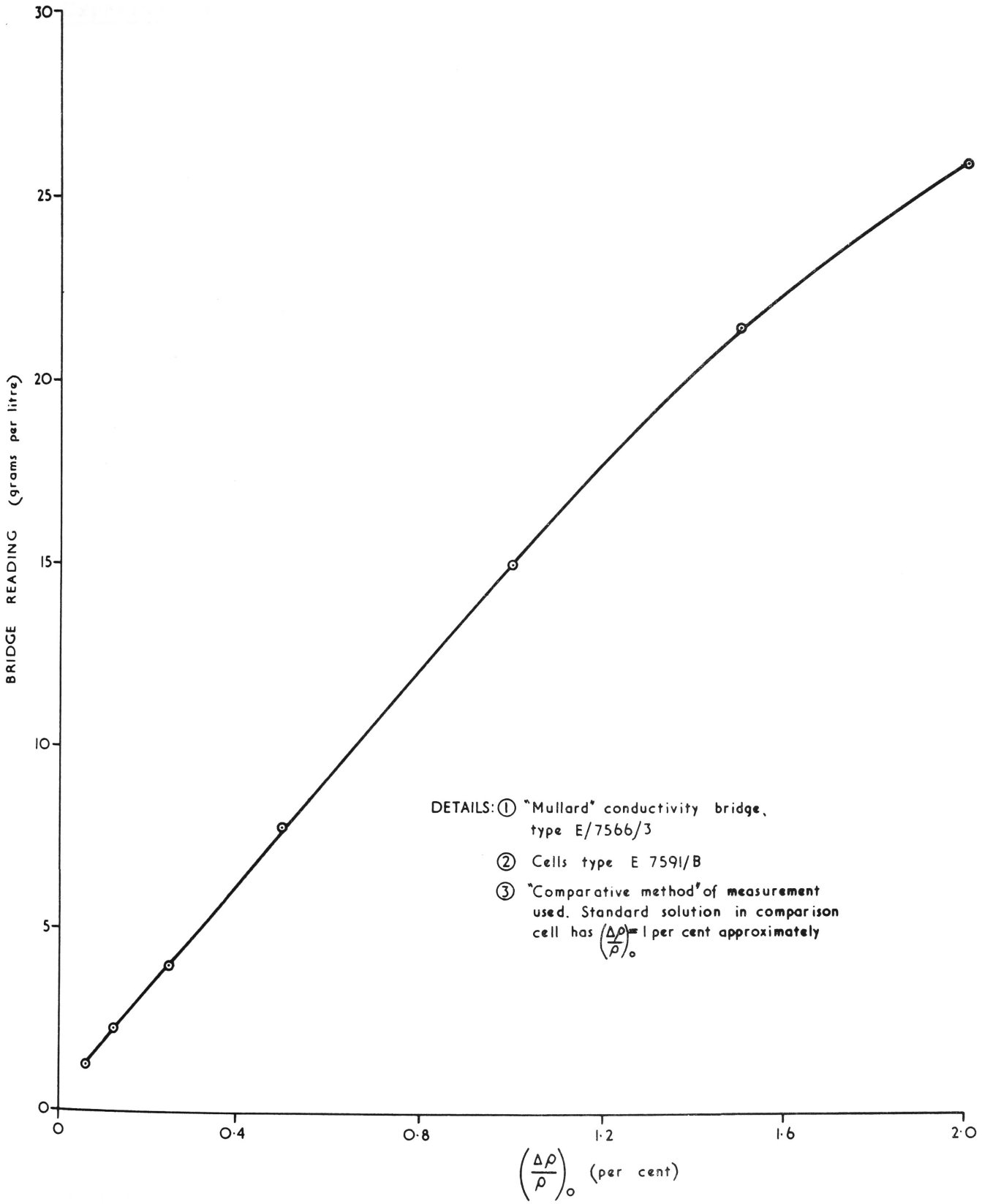

FIGURE 63: CALIBRATION OF "MULLARD" CONDUCTIVITY BRIDGE

Experimental Procedure

The nozzle was fixed in the traversing system clamp (see Fig. 4) in the experimental tank with the nozzle tip at the required boundary grid station. The nozzle was then raised slightly and the siphoning rate adjusted so that pickup from a slug flow jet was not discernible. The nozzle was then lowered to just touch the boundary plane and the saltwater flow rate increased to produce a turbulent jet of the required R_{io} value. The nozzle was then raised in steps to obtain discrete withdrawn samples for analysis with the conductivity meter. The time required to flush the siphoning tube when shifted to a new position was about 1 minute at the low siphoning rate required to avoid entrainment at the nozzle. A time delay of $1\frac{1}{2}$ minutes was therefore allowed as a safety measure before collecting a sample at a new nozzle position.

For relatively high conductivity samples obtained in the body of the jet the comparison cell was immersed in a saltwater solution of $\frac{\Delta\rho}{\rho}$ equal to about one half of the $\left(\frac{\Delta\rho}{\rho}\right)_o$ of the saltwater being injected at the orifice. This standard solution may be prepared by dilution of a sample of saltwater from the constant head tank at the start of the test. This procedure is not essential as it was found to be more convenient to use the same standard sample for all measurements in the body of the jet for the testing period which extended over several days. This particular standard sample was of

nominal concentration 10 gms/litre which is approximately equivalent to a $\frac{\Delta\rho}{\rho}$ of one half of the $\left(\frac{\Delta\rho}{\rho}\right)_o$ = 2 pc. at the orifice of the jet investigated in detail. This latter procedure is justified by checking the bridge calibration at the end of a day's testing by measuring the conductivity of a progressively diluted sample from the saltwater supply tank to obtain a calibration graph as shown in Fig. 63.

For relatively low conductivity samples from the outer region of the jet a standard sample with $\frac{\Delta\rho}{\rho}$ equal to 3.125 pc. of the $\left(\frac{\Delta\rho}{\rho}\right)_o$ of the saltwater injected at the orifice was used with the comparison cell. This was necessary to obtain adequate bridge sensitivity.

When all samples had been collected from a vertical traverse through the jet the conductivity measurements were made by working from the diluted samples obtained from the outer region to the more concentrated samples obtained from near the boundary plane. By using the conductivity cell in this way it is unnecessary to wash the cell in freshwater between readings as contamination of a sample by the liquid adhering to the cell from the previous more dilute sample is negligible.

The total time required to obtain a mean conductivity reading at a point in a turbulent saltwater jet was about 4 minutes. This is greater than the $2\frac{1}{2}$ minutes required to obtain a reading with the

mixing chamber described previously.

Verification of Performance

The "vertical" profiles (i.e. profiles on y = constant planes) of the relative density excess $\frac{\Delta\rho}{\rho}$ at three cross sections in a turbulent saltwater jet are shown plotted in Figs. 21, 22 and 23. Note that for one or two z = constant lines on a vertical profile that two $\frac{\Delta\rho}{\rho}$ observations are plotted; one being determined with the higher conductivity standard solution and the other with the lower conductivity standard solution used for comparisons in the inner and outer jet regions respectively. The agreement between duplicated readings is considered adequate for an exploratory investigation.

The accuracy of the $\frac{\Delta\rho}{\rho}$ determinations can only be assessed when they are combined with velocity measurements to compute the flow rate of density excess at a cross section in the turbulent jet. This has been reported in subsection 3.5.5 of Chapter 3 where it is shown that the maximum error of combined $\frac{\Delta\rho}{\rho}$ and velocity measurements was $\pm$ 3 pc. which is more than adequate for an exploratory investigation.

Conclusions

Analysis of discrete withdrawn samples with a commercially available conductivity bridge proved to be a satisfactory method of obtaining the mean density at a point in a turbulent saltwater jet.

This conclusion has been verified by the investigators reported in the literature review.

The main precautions to be observed in using this method are to adjust the nozzle flowrate to prevent excessive entrainment of surrounding liquid; and to prevent temperature change of the samples during the interval between withdrawal and conductivity measurement.

The main disadvantage of the method is the time required to obtain a point density measurement compared to that required by the more sophisticated methods described previously.

No major improvements to the apparatus or technique used in order to improve accuracy or reduce the time required for measurement can be suggested.

4.3.6 Summary

The determination of mean density at a point in a turbulent salt-water flow was attempted by three methods; use of directly exposed conductivity probe, conductivity measurement of continuously withdrawn samples, and conductivity measurement of discrete withdrawn samples.

The electronic circuitry used was too simple to process the signal from a directly exposed probe. The mixing chamber devised for damping the conductivity fluctuations of continuously withdrawn samples performed satisfactorily but the conductivity probe used was

subject to excessive calibration drift.

Analysis of discrete withdrawn samples with a commercially available conductivity bridge proved to be of adequate accuracy although time consuming. This technique has been described in detail.

APPENDIX 1.

Literature Review of Methods of Measuring Low Velocities in a Turbulent Saltwater Jet.

A1.1 General Remarks

The literature describes a surprising number of ingenious methods of measuring velocity in water flow. Kolupaila (Ref. 63), for instance, lists over one hundred references on the use of pitot tubes alone. On introducing the restrictions of small velocity and saltwater flow, however, the number of apparently suitable methods is drastically reduced.

The procedure adopted in discussing the apparently suitable methods of velocity measurement has been to briefly describe the history and principle, and then to decide whether further investigation is warranted.

A1.2 Classification of Methods

Velocity measurement methods may be classified as:-

1. Pitot tube devices:
   a. Statically balanced:
   b. Dynamically balanced:
   c. Pressure transducers:
2. Hydrometric cords:
3. Hydrometric pendulums:

4. Current meters:

5. Flow tracers:

6. Hot wire and hot film anemometers:

   a. Directly heated;

   b. Indirectly heated.

7. Other methods.

A1.3 Description and Evaluation of Methods

A1.3.1 Pitot tube devices

At a stagnation point in a fluid flow the fluid is forced to stop and kinetic energy is converted to potential energy. In terms of pressures this energy conversion results in an increase in pressure at the nose of a blunt nosed object which is equal to the dynamic pressure $\frac{1}{2} \rho v^2$. The total, or stagnation, pressure p_{st} at the nose of a tube pointing upstream is then $p_{st} = p_s + \frac{1}{2} \rho v^2$,

where p_s is the static pressure at the point.

Henri Pitot observed this effect in 1732 and used a pitot tube in conjunction with a static tube to measure velocities in rivers and canals. If the two tubes are combined in the one instrument, it is known as a pitot-static tube.

The output of a pitot tube device is proportional to the velocity squared, as shown graphically in Fig. 40. The important feature to note in Fig. 40 is the low sensitivity to velocity change of pitot

tube devices at low velocities. Pitot tubes for use in water may be further classified according to the indicating device used, that is as statically balanced, dynamically balanced or pressure transducers.

a. Statically Balanced

This type of pitot device employes the hydrostatic pressure at the base of a static liquid column to balance the stagnation or static pressure in the flow. An open ended piezometer is used with a pitot tube or a differential U tube manometer with a pitot-static tube. The practical lower limit of velocity measurement in water flow with a pitot-static tube and differential U tube manometer is commonly stated to be 0.5 feet per second (Ref. 51). When water is used as the indicating fluid an inverted U tube manometer with air above the water columns is required and a difference in column level of about 0.004 feet results from a velocity of 0.5 feet per second.

The lower limit of measurement of the pitot-static tube was extended by Cole and Cole (Ref. 21) who used a reversible pitot (sometimes called a Cole pitometer) with the static opening facing downstream and immediately behind the pitot tube. Wake effects behind the static tube produce a pressure slightly less than the true static pressure, so increasing the pressure difference registered by the manometer.

The Leon tube, due to Kemp (Ref. 56), is a Cole pitometer coupled to an inverted U tube manometer containing water and another slightly lighter, immiscible liquid. Velocities down to 1.0 feet per second were detected with an accuracy of $\pm 1\frac{1}{2}$ per cent. Velocities down to 0.1 feet per second may be possible, but with reduced accuracy.

Another modification of the Cole pitometer is the Bentzel tube (Ref. 51). The pitometer is connected to an inverted U tube manometer containing water; the downstream leg of the manometer is a slightly tapered cone, expanding downwards, and containing a small buoyant float. The float moves downwards against a calibrated scale as the velocity increases and velocities down to 0.15 feet per second are detectable. Note that this is strictly a through-flow and not a statically balanced instrument.

Returning now to the conventional pitot-static tube; it might appear that the practical lower limit of velocity measurement with this device could be extended by using a micromanometer. The Chattock-Fry tilting micromanometer made by Casella (Ref. 4), for example, will measure head differences in air flow corresponding to 0.001 inches of water. If this micromanometer could be adapted for use with a pitot-static tube in water flow then measurement of velocities as low as 0.0075 feet per second are potentially possible.

Other micromanometers which appear attractive rely on electro-magnetic or interferometric methods of balance detection (Refs. 57, 76).

Cartier (Ref. 16) has outlined some of the difficulties associated with the use of differential liquid micromanometers. It is necessary to consider the following factors:-

(i) The effect of temperature change on the density of manometer indicating liquids. If two immiscible liquids of slightly different density are used to obtain amplification of the differential head then the effect of temperature change is critical as the density difference will vary with temperature. This problem might be overcome by immersing the micromanometer in a constant temperature bath or by making frequent density difference checks.

(ii) The effect of temperature change on the micromanometer components; particularly graduated scales.

(iii) The variation in surface tension at the interface between different indicating liquids.

(iv) Oscillation of liquid columns due to low frequency turbulence in the water flow being measured.

Concerning point (iii) above, Rothfus et al (Ref. 87) state that special precautions were necessary to prevent contamination of the water-monochlorobenzene interface in a U tube manometer used with a pitot-static tube.

Oscillation of liquid columns due to low frequency turbulence in a large permeameter was experienced by Dudgeon (Ref. 28) when using two Casella vernier reading micromanometers coupled together to form a U tube manometer. He found that tedious readjustments were necessary when measuring small head differences. Dudgeon also recorded that the stands supporting the manometer columns were affected by changes in ambient temperature, so necessitating frequent zero adjustment.

Williams (Ref. 106) has discussed the problem of level oscillation in manometers when using a pitot-static tube in pulsating gas flow. The principles outlined probably also apply to measurements in water flow with low frequency, large scale turbulence. Williams demonstrated that the conventional methods of damping pulsations, such as installation of a capacitance or a constriction in the manometer line, can lead to serious errors. He contended that best results were obtained by keeping the connecting lines between the pitot-static tube and the manometer as short as possible and of uniform bore. Any damping should be due to viscous flow in the manometer itself.

In view of the above difficulties, it was decided not to attempt measurement of very small velocities in turbulent saltwater jets with a pitot-static tube coupled to a micromanometer.

b. Dynamically Balanced

In 1951 Bagnold showed that a coaxial opposing liquid jet could be used to balance the stagnation pressure in a pitot nozzle (Ref. 13).

This instrument appeared to warrant further investigation.

c. Pressure Transducers

A transducer converts one type of physical information into another and may be distinguished from modifiers which merely change the scale or form of a physical signal. Lion has summarised the possible transducers and modifiers applicable to fluid mechanics (Ref. 67).

The so called pressure transducer used in hydraulics consists of a mechanical modifier coupled to a mechanical-electrical transducer. A typical example is that of Ippen and Raichlen (Ref. 52) who used a pitot tube leading to one side of a flexible diaphragm whose deflection varies the output of an electrical capacitance, so detecting stagnation pressure variations electronically. (Lion argues that this is not a true pressure transducer which would consist of a capacitance suspended in a chamber connected directly to the pitot tube).

A variable inductance may be used instead of a capacitance in a pressure transducer, as for example in the instruments of Verhagen et al (Ref. 103), Huggins (Ref. 50) and Balakrishna (Ref. 14),

who all used a variable differential transformer on the dry side of a flexible diaphragm. Lion (Ref. 67) also mentions the use of a wire resistance straingauge attached to the dry side of a flexible diaphragm. Eagleson et al (Ref. 29) used a piezo-electric crystal in a chamber connected to a pitot nozzle, so forming a true pressure transducer. This instrument unfortunately is unable to measure mean velocities as it only responds to turbulent velocity fluctuations.

The lower limit of velocity measurement in water flow with presently available pressure transducers appears to be about 0.5 feet per second, so it was decided that such instruments were unsuited to the present investigations.

A1.3.2 Hydrometric Cord

A hydrometric cord measures the drag force exerted on a catenary cord or wire suspended in the fluid flow as an indication of velocity. Kolupaila (Ref. 63) states that the method was originally developed in Germany in the late 19th century for measuring stream-flows. He also refers to work by Perry in 1950, at Wayne University, Detroit, who used straingauges to measure the tension of a fine catinary wire placed across a wind tunnel.

Sharp has reported a hydrometric cord for use in laboratory water flows (Ref. 97). A wire about 0.05 inches diameter and 2.0 inches long is clamped in a yoke, one arm of which is a thin flat

cantilever carrying a strain gauge. Water drag on the catenary deflects the cantilever and the strain gauge reading is related to velocity by calibration. Sharp has recorded velocities down to 0.5 feet per second.

A hydrometric cord was unsuitable for the present investigation because of the transverse velocity gradient in the turbulent jet. The maximum allowable length of catenary wire would be about 0.5 inches and the strain gauge output for such a short wire would be difficult to detect. Also measurements close to a plane boundary are limited by the diameter of the yoke forks supporting the wire.

A1.3.3 Hydrometric Pendulum

A hydrometric pendulum consists of a small body suspended in the liquid flow by a fine flexible filament. The drag force exerted by the flow on the body deflects the filament from the vertical and the angle of deflection is taken as an indication of velocity. The suspended body is often a sphere, but two plates at right angles and streamlined bodies have been used. Bodies of density greater than water are used for measurements from the surface in streams, canals etc. while small buoyant balls have been used by Szalay in laboratory flumes (Ref. 99). Szalay claims that velocities between 0.033 and 0.65 feet per second have been measured.

When large scale, low frequency turbulence is present in the flow, it is difficult to obtain a mean reading with a hydrometric pendulum.

Increase in the submerged or buoyant weight of the body to damp turbulent fluctuations makes the instrument less sensitive to low velocities. Hence, although the hydrometric pendulum is attractive because of its simplicity, it is unsuited for use in a turbulent saltwater jet.

A1. 3. 4 Current Meters

Current meters employing the speed of rotation of an impeller as the velocity measuring device are a standard tool in hydrography. Current meters may be classified as screw(propeller) or cup (Price) types. The screw type consists of a helical bladed propeller which is mounted on a horizontal shaft aligned with the flow. The cup type consists of cups on radial arms which are attached to a vertical shaft aligned normal to the flow.

Prior to 1954, miniaturisation of current meters for hydraulic laboratory work was hampered by friction in the speed recording mechanisms. A typical mechanism up to this time consisted of a slip ring contact on the rotating shaft. In 1954 Dedow and King (Ref. 27) developed a miniature current meter with a frictionless recording device. They measured the speed of rotation of a miniature plastic impeller electronically by detecting the change in resistance between two coaxial electrodes as the propeller blade tip passes. Originally propellers of 0. 4 and 1. 0 centimetres were reported but when the instrument was subsequently manufactured commercially by Armstrong

Whitworth only the latter size was used. The threshhold velocity of this meter is claimed to be 0.075 feet per second although it is doubtful if reliable readings are obtained at this velocity when the flow is very turbulent.

The other commercially available meter using electronic speed detection is the more rugged instrument made by Neyrpic. This meter has an impeller diameter of 3.5 centimetres and a reported threshhold velocity of 0.033 feet per second (Ref. 12). Kolupaila (Ref. 63) lists several other meters using electronic speed detection. Two additional recently developed meters are the Mimosa meter (diameter 1.5 centimetres) of the Delft Hydraulic Laboratory (Ref. 9) and the variable reluctance meter due to Maytin (Ref. 72). It would appear that the minimum practical diameter for a miniature current meter is 1.0 centimetres.

Miniature propeller current meters are accurate in flows where the velocity gradient normal to the shaft is small; this would not be the case if the meter were used in a turbulent saltwater jet or when working close to a fixed boundary. The experimental work of Yarnell and Nagler (Ref. 108) showed that turbulent flow invariably causes a propeller type current meter to under-register. As well as this there is another difficulty when using a meter employing electronic speed detection in a turbulent saltwater flow and this is the turbulent conductivity fluctuations present in

such flows. The Armstrong Whitworth (or D. S. I. R.) meter, for example, senses the change in resistance between two co-axial electrodes as a blade tip passes. If the resistance of the parcel of liquid in the vicinity of the electrodes is changing due to flow turbulence then serious errors will result. A dummy probe is provided with the D. S. I. R. instrument to take account of slight, long term conductivity variations in the flow being measured. It is impossible to mount this probe close enough to the meter head, however, to take account of the large scale conductivity fluctuations occurring in turbulent saltwater jets.

The problem of conductivity fluctuations in turbulent saltwater jets may be overcome by using a frictionless optical speed recording system for the meter. Jonsson has described a miniature meter with an 0.5 centimetric diameter aluminium propeller and optical speed recording system (Ref. 7). The meter was used to measure velocities in a turbulent boundary layer in a rough bed ocean model (Ref. 55). Velocities down to 0.033 feet per second were measured but the performance of the instrument was poor when used close to the rough bed of the model.

The U. S. Corps of Engineers have used a miniature cup type current meter with cups about 0.02 feet in diameter and cup wheel 0.08 feet in diameter (Ref. 5). The threshhold velocity was reported to be 0.05 feet per second. This type of meter would be more suitable than a propeller type meter for use in a turbulent saltwater jet flowing down

an inclined plane as the velocity gradients in the lateral direction are less steep than those in the direction normal to the plane.

An attempt at further miniaturisation of the cup type meter in conjunction with an optical speed recording system was therefore considered to be warranted.

A1.3.5 Flow Tracers

Introduction of small foreign tracers into a fluid flow is a common method of qualitative flow visualisation. The principal requirements of a flow tracer are that firstly it should have a density close to that of the working fluid to minimise path distortion by buoyancy effects and, secondly, that it has high visual contrast with the surrounding fluid to allow photography.

Tracers used in water flow are small solid particles, droplets of an immiscible liquid and small gas bubbles. Solid particles are difficult to introduce into the flow without creating serious flow disturbance while if too many particles are added it is difficult to identify individual particles by photography. Ellison and Turner (Ref. 31) released small plastic beads in a tank of saltwater with an overflowing jet of freshwater in an attempt to measure velocity profiles. The path of the beads was recorded by a movie camera and the positions of single particles plotted frame by frame. The process was abandoned as too tedious after a few experiments. Seddon and Anwar (Ref. 96) utilised

strongly illuminated naturally occurring mineral grams to measure point velocities in a vortex flow in a cylindrical tank. A rotating glass cube was used to intercept the beam of a viewing telescope and so momentarily stop the particles. It is claimed that velocity components in any direction may be determined by aligning the axis of rotation of the glass cube normal to the required component direction. The scale of turbulence in vortex tank flows is much less than that in a turbulent saltwater jet and it is considered that it would probably be impossible to "stop" particles in the latter case. Also the flow to be investigated is three dimensional and three mutually perpendicular velocity components would be required to define the velocity at a point so making the amount of experimental work formidable.

Small droplets of an immiscible liquid have been used by many experimenters for visualisation of water flow. An advantage of liquid drops compared to solid particles is that the former may be introduced at the required point in the flow through a fine bore tube with a minimum of flow disturbance. Frenzen, for example, used droplets made by mixing nitrobenzene and olive oil to measure two dimensional Lagrangian velocities in the region of turbulence decay behind a towed mesh (Ref. 36). Although the analysis of time exposure photographs was partially automated by using an oscillograph scanner with digital output, the time required for data reduction was excessive.

Small gas bubbles have also been used as flow tracers in water flow. The most popular technique at present is to use the hydrogen bubbles generated at a fine wire cathode by the passage of a D.C. current through the flow. This method was invented by Raspet and Geller at Mississippi State College and subsequently improved by Clutter et al (Refs. 19, 20) for qualitative visualisation of flow about aircraft models in a water tunnel. Lukasik and Grosch (Ref. 69) attempted to use hydrogen bubbles to measure velocity profile of laminar flow of water between parallel plates. Their electronic techniques were rather sophisticated but the observed velocities were widely scattered about the known parabolic velocity profile.

Schraub et al attempted to use hydrogen bubbles to investigate a two dimensional boundary layer on a flat plate (Ref. 95). They claimed that the hydrogen bubble technique is valuable in flows where constant current hot wire probes are at their greatest disadvantage. That is, in low speed flows with large scale, low frequency velocity fluctuations or reversals. Among the disadvantages discussed by Schraub et al is the excessive time for data reduction, the necessity for precise strip lighting and the non uniformity of bubble formation. The first disadvantage listed probably accounts for the fact that only one velocity profile was published.

Apart from the formidable amount of work involved in reduction

of flow tracer observations, the work of Hama (Ref. 44) suggests that the results obtained may be strongly suspect. Hama computed numerically the streaklines and pathlines present in a boundary layer perturbed by a constant amplitude sinusoidal wave. He demonstrated that velocities determined by photographing marked particles can be seriously in error and this probably accounts for the difference in results obtained by flow visualisation and other techniques, such as hot wire anemometry.

In view of these two principal disadvantages, it was decided not to attempt velocity measurement by flow visualisation methods.

A1.3.6 Hot Wire and Hot Film Anemometers

The hot wire anemometer was first used in 1894 and this was followed by the classical work of King in 1914 (Ref. 60). Since then hot wire anemometers have become an essential tool in aerodynamic research and several reliable instruments are commercially available.

The hot wire anemometer utilises the fact that the electrical resistance of a conductor varies with its temperature. The temperature of a fine electrically heated wire exposed to a fluid stream depends on the temperature, composition and velocity of the stream. Other factors being constant, a resistance measurement of the wire indicates its temperature, and hence the stream velocity. The output of a hot wire anemometer is approximately proportional to the square root of the stream velocity as shown in Fig. 40.

Compared to a pitot tube - manometer system the hot wire has several advantages: it is sensitive to low velocities, very sensitive to turbulent velocity fluctuations, and the output may be processed electronically to investigate flow turbulence. However, as pointed out in the previous section in the discussion of hydrogen bubbles, hot wires may only yield qualitative results in very low speed flows with large scale, low frequency turbulence or flow reversals.

a. Directly Heated Systems

Hot wire anemometers are usually directly heated instruments in that the hot wire acts as both the heated element and the temperature sensor. Hot wires are operated on either the constant current or constant temperature principle. In the former the current through the wire remains constant and the resistance is measured to indicate velocity. In he latter, the power required to maintain a constant temperature difference between the wire and its surroundings indicates the velocity. The electronics necessary for constant temperature operation are more complex than those for constant current operation but the former is more sensitive to low frequency turbulence.

Hot Wires in Water

Both Kolupaila (Ref. 63) and Corrsin (Ref. 22) refer to use of hot wires in water by Richardson in 1934. Richardson further reported the use of a hot wire in a ship's towing tank in 1948 (Ref. 85). No

mention was made of the usual problems (discussed subsequently) associated with a hot wire in water. Kolupaila (Ref. 63) also quotes work by Maruo and Matsubara, at Yokahama University, who found that it was necessary to clean the wire before every measurement. Stevens et al (Ref. 98) found that hot wires would not maintain a stable calibration when used in water. They recommended use of A. C. heating to prevent polarization effects, use of a protective coating, and thorough filtering of the water being used.

Hot Films in Water

Ling and Hubbard (Ref. 66) invented the hot film anemometer which they claim is superior to the hot wire in that it is more robust, has superior dynamic response, lower signal to noise ratio and less subject to fouling. The probe consists of a platinum film fused to the end of an acutely tapered glass wedge.

Several instances of the use of a hot film probe in water have been recorded. Grant et al (Ref. 42) used a hot film probe fitted with retractable flushing jets in the ocean. They found that fouling by minute marine organisms occurred and readings of only two minutes' duration were obtainable. Tan and Ling (Ref. 101) used a hot film probe in a water tunnel but made no mention of calibration drift. Abbott and Kline (Ref. 2) found that to avoid bubble formation and fouling it was necessary to use filtered, softened and deaerated water.

The minimum mean velocity detected was 0.15 feet per second and the instrument was useless in regions of flow reversal. Gibson and Schwarz (Ref. 38), and Rosler and Bankoff (Ref. 86), have used a hot film in demineralised water.

Runstadler (Ref. 90), and Grant and Kronauer (Ref. 41), have discussed the problems associated with using a hot film probe in water. The main factors affecting stable operation are:-

(i) Dirt Contamination: Even microscopic particles and organisms can cause drift so that filtered water appears to be essential.

(ii) Dissolved Gases: Small bubbles tend to accumulate on the probe surface so effectively insulating the probe from the flow and causing an underestimate of velocity. Not only does the probe sweep out bubbles intercepting it but bubbles also tend to swim towards the hotter water in the vicinity of the probe surface, or come out of solution because of the lowered water density in this region.

Methods of removing dissolved gases in order of efficiency are distillation, application of a vacuum, passage through a convergent-divergent nozzle and long term quiesence.

(iii) Polarization: As with conductivity measuring devices, it is an advantage to use A.C. heating of the probe to prevent electrode polarization.

(iv) Chemical Impurities: Dissolved halogens (e.g. Chlorine) tend to

attack the sponge platinum end connections to the probe and also the probe surface. Scale deposits form on the probe surface when it is used in hard water.

(v) Electrical Conductivity: Water of high conductivity provides a parallel bypass for the electrical current flowing through the hot film. It is necessary to carry out a specific calibration in water whose conductivity exceeds 1 micromho.

(vi) Effect of Boundaries: Wills (Ref. 107) found that when a hot wire anemometer is used close to a heat conducting boundary in air flow that the heat absorbed by the boundary causes the meter to over register. This effect would be more pronounced in water flow as the intervening fluid has a higher thermal conductivity.

(vii) Boiling: If the overheat temperature (the difference in temperature between the probe surface and the surrounding fluid) is too high, a film of insulating steam may form on the probe so causing the meter to under-register. On the other hand, if the overheat temperature is too low, the probe becomes insensitive to small velocity changes.

As it was impractical to treat the quantities of water involved in the proposed experiment to alleviate problems (i), (ii) and (iv) above, and as problem (v) remains when working in saltwater, it was decided not to attempt to use a hot film probe for velocity measurement in the present project.

Thermistors in Water

Hot wire and hot film sensors are usually made from platinum or tungsten alloy but Lumley (Ref. 70) has shown that non-metallic thermistor material has some advantages over metals as a sensing element. Thermistor material has a higher temperature coefficient of resistance than platinum and is therefore potentially more sensitive than platinum as a sensing element. Also the resistance of a thermistor probe is about one thousand times that of the same size platinum probe so that the electronic system may be more robust for the former. Thermistor material is adversely affected by contact with water, however, so a protective coating must be applied to the probe.

Ellison and Turner (Ref. 31) used a commercially available glass enclosed bead thermistor probe for velocity measurement in a turbulent saltwater jet. The thermistor formed one arm of a simple A. C. excited Wheatstone bridge and the bridge out of balance was taken as the velocity indication. The probe was calibrated by placing it in a transparent pipe and timing the passage of a patch of dyed fluid between two marks. Variations in ambient temperature of the water were allowed for by obtaining calibrations at various temperatures. Velocities were measured in the range 0.03 to 0.6 feet per second with an alleged accuracy of $\pm$ 10 per cent. The accuracy was probably considerably less than this, however, as large scale turbulence in the

flow caused the out of balance detecting meter to waver and a mean reading was obtained by "averaging by eye". Also when the velocity observations were subsequently analysed the results were inconclusive and the method was abandoned.

Crow (Ref. 23) attempted to make a directly heated bead thermistor probe by suspending a small bead thermistor between the two arms of a yoke and insulating the whole with rubber solution. A simple Wheatstone bridge circuit was used for resistance measurement and variations in ambient temperature were allowed for by including a dummy thermistor in one arm of the bridge. Crow found that the probe was unsatisfactory as in order to obtain sufficient sensitivity it was necessary to drive the thermistor into its unstable range. Also the probe was too flimsy for use in a hydraulic laboratory.

Rasmussen (Ref. 82) investigated the use of thermistors in moving fluids (in connection with free falling oceanographic probes) by rotating a glass coated bead thermistor in a Dewar jar. For constant current operation he showed that a thermistor probe was practically insensitive to velocity change above 0.2 feet per second; in fact, for simple electronics, the resistance appears to be constant above 0.4 feet per second. He also showed that sensitivity to changes in ambient temperature can only be achieved by using a high overheat temperature

and this probably results in bubble formation and consequent instability. (Rasmussen was unable to observe the phenomenon of bubble formation in the Dewar jar). He also mentioned the likelihood of instability due to fouling if a probe is used in untreated water.

Rasmussen examined theoretically the constant temperature operation of a thermistor probe and showed that the ratio of velocity sensitivity to ambient temperature sensitivity at the same overheat was independent of the method of operation. Constant temperature operation requires more complicated electronics than constant current operation so the latter system is obviously preferred (for determination of mean velocities at least).

Veprek (Ref. 104) has published details of a volumetric flow meter using a thermistor as the velocity detecting element. The thermistor was mounted coaxially in a fine bore tube and the whole apparatus immersed in a constant temperature bath to minimise ambient temperature effects. The rapid decrease in velocity sensitivity above 0.2 feet per second is again apparent in his calibration curves. Veprek mentioned that aged thermistors are necessary to mitigate calibration drift. Crow (Ref. 23) suspected that drift occurred in his thermistor probes but did not check for this effect.

Eagleson and van de Watering (Ref. 30) have designed a non-directional thermistor probe for detecting orbital speeds below the

surface of water waves. The upper limit of the velocity range was extended to 1.5 feet per second by using constant temperature operation and a complex linearising circuit. Calibration curves were obtained for ambient temperatures matching those of the experiments. No mention was made of bubble formation or fouling affecting probe performance, nor was thermistor drift with age considered.

Lumley (Ref. 70) has reported attempts to make a hot film probe for use in water by using thermistor material. He argued that in order to raise the effective velocity range of a thermistor probe it is necessary to use a thin film of thermistor material as the sensing element and not a solid bead. The main difficulty in making thin film thermistor probe appears to be obtaining a thin enough protective coating.

Summarising the above attempts at using a thermistor probe in water:-

(i) Commercially available thermistors are only suitable for measuring velocities in water up to 0.2 feet per second, although complex electronics may allow this range to be extended to 1.5 feet per second.

(ii) Variations in ambient water temperature are critical unless high overheat temperatures are used and this in turn is likely to cause bubble formation in untreated water.

(iii) Fouling of probes and consequent under-registration is likely

in untreated water.

(iv) Thermistor drift with age may necessitate frequent calibration checks.

In view of the above limitations, it was decided not to proceed with the development of a thermistor velocity meter.

b. Indirectly Heated Systems

Contrasting with the directly heated probes described in the previous section is the indirectly heated probe where the heating and temperature detecting systems are separate and electrically insulated from one another.

Reverseau (Ref. 84) has described an indirectly heated probe consisting of a small metal cylinder with an externally wound heating coil and an internally mounted thermistor for temperature measurement. Constant temperature operation was used and the power necessary to maintain an overheat of $5^{o}C$ taken as the measure of velocity. No calibration details were given.

Crow (Ref. 23) attempted to calibrate a probe similar to that of Reverseau but with constant current operation of the heater. The resistance of the thermistor was detected with a Wheatstone bridge with a dummy thermistor in one arm to compensate for ambient temperature variations. The probe was calibrated in a towing tank but the calibration was unstable, mainly because of:-

(i) Variations in ambient temperature in the towing tank. The compensating dummy thermistor was held stationary in the tank but variations in water temperature of 0.5°F along the towing length were sufficient to alter the calibration significantly.

(ii) Accumulation of gas bubbles on the heated coil occurred at the overheat temperatures necessary to obtain adequate sensitivity.

(iii) Accumulation of dirt on the coil surface when the probe was used in untreated water.

Clayton and Farmer (Ref. 18) have published details of an indirectly heated "hot cone" probe for measuring low velocities in air and water flow. A small copper cone was heated with a constant current coil and its temperature measured with a thermopile whose "cold" junctions were exposed to the ambient flow so compensating for variations in ambient temperature. The instrument was calibrated in a small rotating tank over a velocity range of 0.1 to 1.0 feet per second and its sensitivity was adequate up to about 0.6 feet per second.

The published value of thermopile output indicates that an overheat of about 10°C was used and, in the writer's opinion, bubble formation would occur at this overheat, so affecting the reliability of the instrument. Also the instrument as described was 0.25 inches in diameter which precludes it from further consideration for "point"

velocity measurements in turbulent saltwater jets.

A1.3.7 Other Methods

Several other less conventional methods of measuring velocity were noted in the literature:-

a. Ultra-Sonic Meter

Chalupnik and Green (Ref. 17) have used a Doppler shift meter to measure velocities in the ocean. The Doppler shift in frequency between a transmitted beam and a beam reflected by minute naturally occurring scattering particles in the seawater indicated the velocity of the scatterers relative to the instrument.

The reported range of the instruments is from 0.003 to 33 feet per second but the probe is too large and the electronics too costly for the present project.

b. Electromagnetic Meters

Kolin, working under Bakhmeteff in 1944, (Ref.62) used an electromagnetic meter to obtain velocity profiles in an 0.67 inch diameter glass pipe. The pipe was surrounded by a large electromagnet which generated an alternating magnetic field and a miniature probe allowed measurements to be taken within 0.02 inches of the pipe wall in the range 0.2 to 7.5 feet per second. Kolin mentions that precautions are necessary to prevent polarization and fouling of the electrodes.

Kolin also describes a miniature meter with the electromagnet wound integral with the sensing probe which allows measurements to be taken in large flows. Exact constructional and calibration details of this probe were not given.

Grossman and Charwat (Ref. 43) used an electromagnetic velocity meter to determine mean and turbulent velocity components in water flow in a 1.73 inch diameter pipe. A D.C. external magnet provided the magnetic field but the low signal to noise ratio (up to 1.0) was not encouraging.

Bowden (Ref. 15) used an electromagnetic meter for turbulence measurements in the ocean. The overall diameter of the instrument was about 4 inches which immediately eliminates it from further consideration.

c. Electrolytic Methods

Eskinazi (Ref. 32) has reported preliminary work on an electrolytic velocity meter which utilises the distortion of the current path between two electrodes when they are placed in a flow of electrically conducting fluid as the measure of velocity.

Ranz (Ref. 81) investigated electrolytic methods and concluded that the chemical reactions involved were too unstable for consistent calibration to be obtained.

Recently Reiss and Hanratty (Ref. 83) attempted to relate

turbulent velocity fluctuations in the laminar sublayer to the fluctuating mass transfer rate in the vicinity of a small electrode placed flush with the inside of a pipe wall. Their results indicated that the method requires further development to be reliable.

It would appear that electrolytic methods of measuring velocity are too unreliable at their present stage of development.

d. The Quartz Fibre Anemometer

Tritton (Ref. 102) has used a small cantilevered quartz fibre for mean and turbulent velocity measurements in air flow. The difficulties involved in observing a quartz fibre in a large tank of water are probably insurmountable.

A1.4 Recent Methods of Velocity Measurement

Some new developments in measuring low velocities in water have been noted since completing the above literature review.

a. The Thermal Pulse Meter

Piquemal and Truchasson (Ref. 77) have devloped a meter which times the passage of a small patch of heated water between a heater and a pair of conductivity measuring electrodes. A pair of dummy conductivity electrodes upstream of the heater compensates for changes in ambient temperature.

The instrument is inapplicable to measurement in turbulent saltwater jets as the conductivity probe would be unable to distinguish

between conductivity changes due to heating and those due to salinity.

b. The Quartz Coated Hot Film Anemometer

Thermo-Systems Inc. (Ref. 11) have developed a cylindrical platinum hot film probe with a thin quartz protective coating. The sensor is similar in shape and size to a conventional hot wire and it is claimed that the problems of current bypass and electrolysis are eliminated while surface contamination by dirt and dissolved gases is reduced. The problems of fouling by elongated particles and over-registration when working close to a heat conducting boundary still remain.

The makers recommend that the probe should only be used in water treated to remove dissolved gases and filtering is probably also necessary if the probe is to be used for long term measurements. This device appears to be the most reliable presently available for measuring mean and turbulent velocities in treated water.

c. The Cold Tip Velocity Meter

Many of the problems arising from the use of heated probes in water are overcome if the heat flow is reversed, that is if the heating of a cool probe by a water flow is taken as the measure of velocity. Harris (Ref. 48) has reported preliminary work on a cold tip velocity meter which uses a thermoelectric refrigerator to cool a conical tipped probe whose temperature is measured by a separate thermocouple.

The instrument is still in the process of development but appears promising.

d. The Tandel Sensor

Veprek (Ref. 105) has invented a new di electric component which he claims is more sensitive to velocity changes in a flowing fluid than a thermistor. If applicable to water flow this Tandel sensor would allow lower overheats to be used and more stable calibrations would probably result.

APPENDIX 2.

Details of the Rotating Tank for Calibrating the Bagnold Velocity Meter.

A2.1 Methods of Calibrating Velocity Meters

Velocity meters may be calibrated in a number of ways:-

a. By towing at a known speed in a tank of still water.

b. By holding the meter stationary in a rotating tank of water.

c. By placing the meter at a point in a flow where the velocity can be predicted from previous experiments.

d. By comparison with readings from a calibrated meter at the same point in a flow.

Evaluating each method in detail:

a. Towing Tanks

A straight towing tank must be fairly long (say at least 50 feet) if a steady velocity is to be obtained over a sufficient period. Also the towing carriage and running rails must be vibrationless for accurate calibrations and the carriage should be large enough to house the ancillary systems of the meter being calibrated. When a meter is towed through the tank the resulting disturbance to the water in the tank should have been damped out by viscous dissipation before the next run is made. For this reason conventional hydrographic current meters are usually calibrated in large ship model towing tanks.

Longitudinal temperature gradients in the water in a long straight tank may affect the calibration of temperature sensitive meters. Crow, for example, recorded variations of 1.3°F in a relatively short (26 feet long) indoor towing tank at the Water Reseach Laboratory (Ref. 23).

Circular towing tanks are usually preferred for calibrating miniature current meters. The D.S.I.R. meters used at Wallingford are calibrated in an annular tank 12 feet in diameter and a similar tank is in use at the Public Works Department Hydraulic Laboratory at Manly Vale. A small annular tank has the advantages that temperature gradients are negligible and the water can be readily changed. The main disadvantage of towing a meter in an annular tank is that the instrument ancillary systems must rotate with the meter. To calibrate a Bagnold meter in an annular towing tank, it would be necessary to provide slip ring contacts for electrical connections to the conductivity meter and a rotating siphon in the freshwater supply tank.

b. Rotating Tanks

Holding the meter stationary in an annular rotating tank has the advantages that the meter ancillary systems are also stationary and minor adjustments to the meter are possible without stopping the tank.

The main hydraulic requirements of an annular rotating tank are:-

(1) The liquid should rotate at the same speed as the tank. Radial

baffle plates are usually fitted for this purpose.

(ii) The circulation within and between the cells formed by the baffle plates should be small.

(iii) The tank rotation should be smooth so that the water is turbulence free for practical purposes.

(iv) The wake produced by the meter should decay in less than one revolution of the tank.

c. Use of a Flow of Known Velocity

Bagnold calibrated the original meter by inserting the nozzle in a converging orifice (Ref. 13). The only reference to velocity profiles in a converging orifice noted in the literature was in a paper by Kolin (Ref. 62) who measured a few profiles with his electromagnetic velocity meter. No comprehensive details of velocity profiles for various flow regimes could be found so that it would probably be necessary to calibrate an orifice with the velocity meter (to obtain relative velocities and then integrate the velocity profile to match it with the discharge) before it could be used to calibrate the meter.

Ellison and Turner (Ref. 31) calibrated a thermistor velocity meter by placing it in a transparent pipe and timing the passage of a patch of dyed liquid between two marks. Providing a wall tapping for insertion of the Bagnold meter in a pipe would have been difficult.

d. Calibration Against Another Meter

This method was inapplicable as no other meter of adequate range was available.

Of the above methods for calibrating the velocity meter a small annular rotating tank appeared to be the most attractive.

A2. 2 Design Details of a Rotating Calibration Tank

The main details of the rotating tank used are shown in Fig. 48 while Fig. 49 is a photograph of the tank in operation.

The main features of the design are:-

(i) Use of a central bearing in the form of a bicycle wheel hub for smooth running. The outside of the rim of the wheel also serves as a large diameter pulley for the driving belt.

(ii) The stepped pulley system for speed selection. The stepped pulleys are fitted on a swinging arm which dispenses with a jockey pulley for maintaining drive belt tension. The stepped pulleys are designed to produce tangential velocities of 1. 0, 0. 5, 0. 25, 0. 1, 0. 05 and 0. 03 feet per second at a point in the tank midway between the vertical sides of the U slot in the baffle plates.

(iii) Isolation of the motor drive unit from the tank base with rubber bushes on the connecting bolts and the use of a rubber tube motor coupling to inhibit vibration. Also the tank base and drive unit were set up on sponge rubber blocks for the same purpose.

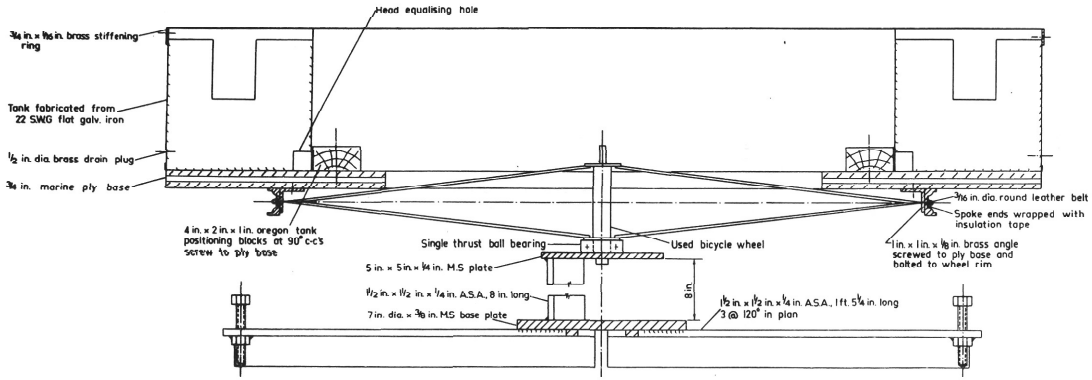

ROTATING TANK – CROSS SECTION

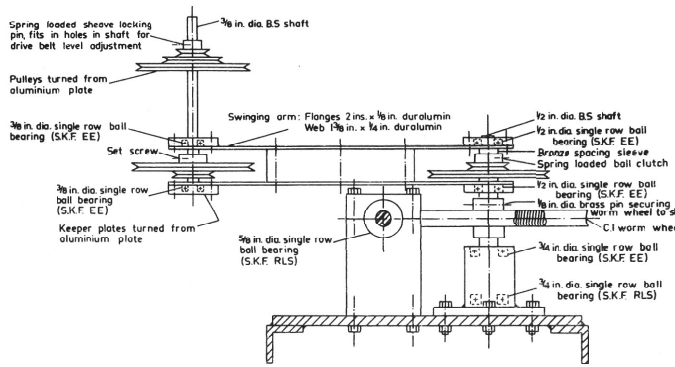

SWINGING ARM DETAILS – ELEVATION

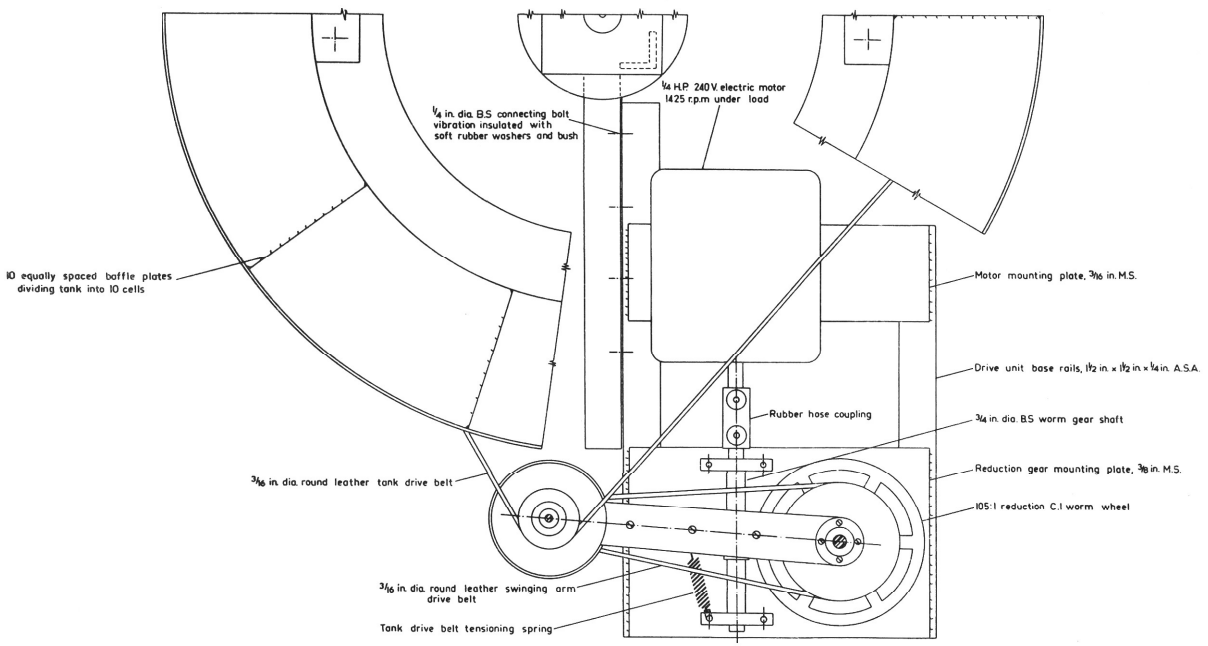

DRIVE UNIT – PLAN

Mild steel
Bright mild steel
Brass
Marine plywood
Oregon

FIGURE 48: VELOCITY METER CALIBRATION TANK

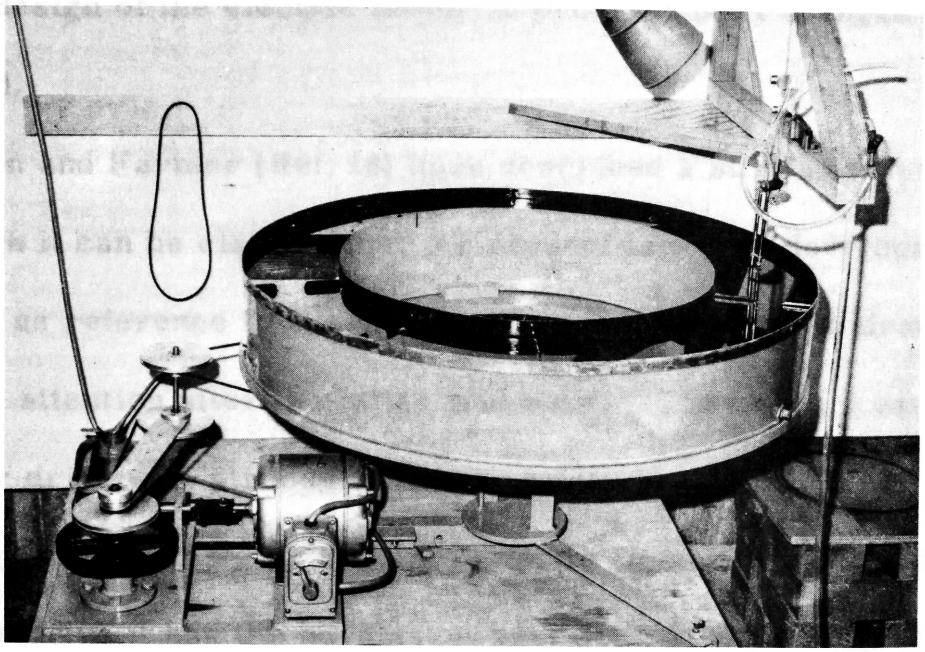

Fig. 49: Velocity Meter Calibration Tank.

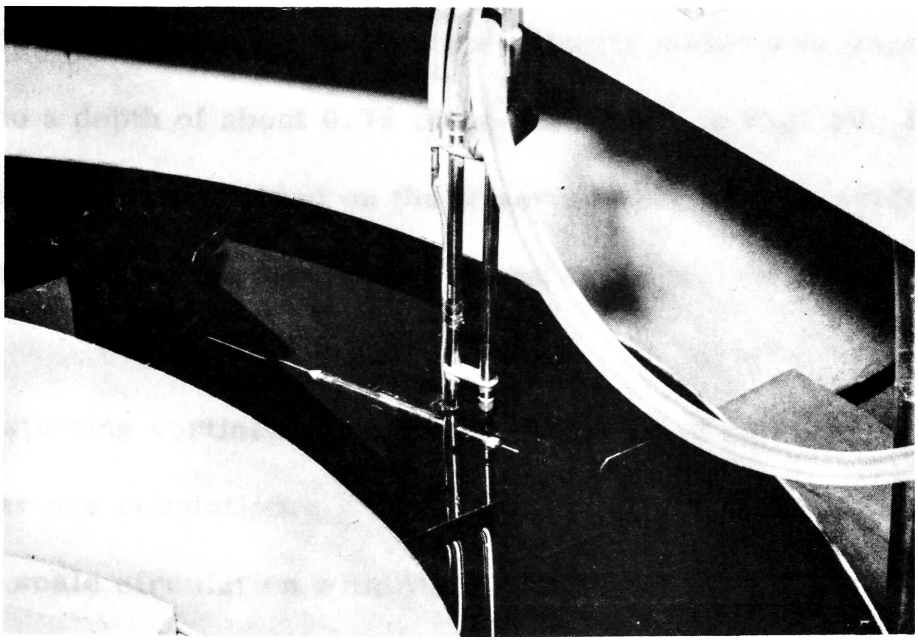

Fig. 50: Velocity Meter in Position in Calibration Tank.

(iv) Over design of the electric motor to prevent speed changes with varying load.

Clayton and Farmer (Ref. 18) have described a similar rotating tank although it can be claimed that the present tank was developed independently as reference to Clayton and Farmer's paper was drawn to the writer's attention after the latter was built. They used a variable speed motor drive with stroboscopic speed detection. Although a belt drive by a stepped pulley system is not as flexible as a variable speed motor drive it has the advantages that drift in motor speed is eliminated and speed adjustment is simplified.

A2.3 Performance of the Tank

The tank was filled with saltwater to a level about 0.125 inches below the top of the baffle plates and the velocity meter was immersed in the tank to a depth of about 0.75 inches as shown in Fig. 50. Small pieces of paper wire sprinkled on the water surface and the surface flow patterns observed at the various speed settings. It was noted that:

(i) Small starting vortices occurred on the start of rotation but these died out after one revolution.

(ii) Large scale circulation within and between cells was negligible at all speeds. At the highest speed of 1.0 feet per second the paper markers rotated in the lee of the baffle plates at the rate of two to

three revolutions per revolution of the tank but this was not serious as the velocity meter cannot be used in this zone.

(iii) The wake behind the meter was small and died out in one quarter of a tank revolution at the maximum tank speed.

No variation in tank speed was detectable after about one hundred hours of operation.

APPENDIX 3.

Literature Review of Methods of Density Measurement for Control of Preparation of Saltwater Solutions and at a Point in a Turbulent Saltwater Jet.

A3. 1 General Remarks

Density measurement was required for control of preparation of saltwater solutions as well as at a point in the turbulent saltwater jet.

For engineering experiments the accuracy required for density measurement is much less than for other purposes. For example, the techniques for density measurement used in oceanography are far too precise for the present project.

A3. 2 Description and Evaluation of Methods for Control of Preparation of Saltwater Solutions

A3. 2. 1 Direct Weighing

A known volume of the saltwater solution is accurately weighed and the density computed directly. A glass "specific gravity" bottle with drilled and ground stopper is commonly used. Ellison and Turner, for example, used this method for a laboratory study of two dimensional turbulent saltwater jets (Ref. 31).

The specific gravity bottle is calibrated to contain a specified volume at a stated temperature e.g. 50 ml. at 20^{o}C. Change in volume due to variations in temperature may be estimated from the volumetric change equation (Ref. 80) but this change in volume is negligible for practical purposes over the normal range of hydraulic laboratory

temperatures. For control of saltwater mixes quick accurate weighings are necessary; an automatic electronic balance will perform such weighings but none was available at the start of the project.

A3. 2. 2 Application of Archimedes' Principle

The density of a liquid may be determined by adjusting the mass of a buoyant hydrometer to immerse a specified volume. This is called a constant volume hydrometer and consists of a normal hydrometer with a pan attached to the stem (Ref. 80). Weights are added to the pan to immerse the stem to a graduated mark but the balancing process is time consuming and the instrument is not direct reading.

The constant mass hydrometer is preferred to the constant volume type as the volume immersed is shown on the graduated stem which indicates density directly. Although the hydrometer is made of glass, and is hence fragile by hydraulic laboratory standards, it is cheap and readily replaced. Use of a constant mass hydrometer was considered to warrant further investigation.

A third method is to weigh a non-buoyant sinker in the liquid whose density is required. Specialised balances are available for this purpose. Hart, for example, used a Westphal balance of least count 1×10^{-4} grams per ml. for saltwater mixing control in a jet discharge experiment (Ref. 49) while Frankel and Cumming used a Sartorius balance for mixing control of sugar solutions in an ocean

outfall model (Ref. 35). Alternatively a conventional analytical balance with bridge or base plate hole may be used. Schoeneck and Wanninger have described this latter technique and showed that when the necessary corrections are applied an accuracy of $\pm$ 1 x 10^{-4} gm. per ml. is possible (Ref. 94). Saunders has used this technique for preparing saltwater solutions (Ref. 91). Lack of a suitable balance eliminated the hydrostatic balance method from further consideration.

A3. 2. 3 Other Methods

Analysis of samples by chemical titration has been used for mixing control of very dilute saltwater ($\left(\frac{\Delta\rho}{\rho}\right)_o$ = 0. 06 pc.) solutions by Frankel and Cumming (Ref. 35). A. S. T. M. Standard Method A using mercuric nitrate for titration of chloride ion was claimed to yield an accuracy within $\pm$ 2 pc (Ref. 6). Chemical titration was considered to be too time consuming a method of density control.

The Public Works Department Hydraulic Laboratory at Manly Vale uses conductivity measurement for saltwater mixing control in tidal models. A sample of the saltwater being mixed is compared with a standard sample (prepared by titration) of known density by means of a conductivity bridge with a comparison facility. The density of the freshwater still remains to be determined by some other method, however. It was decided that mixing control by conductivity measurement would warrant investigation if control by hydrometer proved to be

unsatisfactory.

A3. 3 Description and Evaluation of Methods of Measuring the Mean Density at a Point in a Turbulent Saltwater Jet

A3. 3. 1 Analysis of Discrete Samples Withdrawn from the Flow

In turbulent saltwater jets the density at a point varies widely and randomly. The mean density at a point may be determined by analysing a discrete sample obtained by slow siphoning through a fine bore tube so that the time of collection of the sample is much greater than the period of the density fluctuations.

The density of the withdrawn samples may be determined by a variety of means. A common method is to use a commercially available conductivity bridge which relies on the correlation between sodium chloride concentration and electrical conductivity. Such bridges are refinements of the classical bridge used by Kohlrausch in 1898 and referred to by Keulegan (Ref. 58). The common conductivity bridge is essentially an A. C. excited Wheatstone bridge which measures the impedance of a sample of aqueous solution between two exposed metallic electrodes in a cell which forms one arm of the bridge. Most commercially available bridges claim an accuracy of ± 2 pc. or better. Aagaard and van Haagen have described an apparently superior bridge which utilises the aqueous solution as an inductive link between two protected toroidal coils but unfortunately this bridge

is not commercially available (Ref. 1). Analysis of discrete samples from turbulent saltwater flows by conductivity bridge has been used by Ippen et al, Lofquist, Macagno and Rouse, and Prych et al (Refs. 53, 68, 71, 79).

The U. S. Corps of Engineers have analysed discrete samples by chemical titration in a tidal estuary model (Ref. 5). A. S. T. M. Standard Method B using sodium nitrate titration of relatively high chloride ion concentrations was found to be suitable (Ref. 6). Ippen et al also tried this method but changed to conductivity bridge measurement after a few tests as the former was too time consuming (Ref. 53). Apart from the time required to perform titrations it was felt that the precision glass burettes etc. necessary for this type of analysis were too fragile for use in an hydraulic laboratory.

The main advantage of the withdrawal sampling method is that a mean density reading is obtainable with relatively simple apparatus. The more complex methods of point density measurement usually rely on withdrawal sampling as an independent check on instrumentation.

The main disadvantage of withdrawal of discrete samples in conjunction with density measurement by conductivity bridge is the time required to obtain a sample of sufficient volume for use with typical immersion type conductivity cells. The outside diameter of the withdrawal probe immersed in the flow should be small to minimise flow

disturbance, while the velocity of withdrawal should not exceed the flow velocity at the probe tip if "point" sampling is to be obtained. The net result of these two conditions is a very small flow rate through the siphoning line so that the sample collection time is appreciable - typically two to three minutes. Also there is a similar time delay when the probe is shifted to a new station as the siphoning tube must be completely flushed before collection of another sample.

Also it is necessary to ensure that the temperature of the samples does not change between the time of withdrawal and the time of conductivity measurement. This is because the specific conductivity of saltwater increases by about 2 pc. per ^{o}C (Ref. 58). Sample jars should therefore be immersed in a bath with a water supply circulated from the model being tested.

To summarise, it would appear that withdrawal of discrete samples is a proven method of obtaining the mean density at a point in a turbulent saltwater flow. This method is used as a check for more sophisticated techniques. It was decided that withdrawal sampling in conjunction with conductivity measurement could be used as a standby if less time consuming methods failed.

A3. 3. 2 Analysis of Continuously Withdrawn Samples

Instead of collection of discrete samples, it is possible to monitor the conductivity of a sample continuously withdrawn from the flow

through a siphoning probe moved from station to station.

Continuous withdrawal sampling was used by Lincoln et al in oceanographic models (Ref. 65). The conductivity cell was made from perspex tube inlaid with annular silver electrodes and the cell was connected in series with an A. C. voltage source and a load resistance whose output was amplified, rectified and displayed on a cathode ray oscilloscope. This is a circuit typical of direct reading or series type conductivity meters. Conductivity fluctuations in oceanographic models are of an order of magnitude less than those in turbulent salt-water jets so it is doubtful whether this system would work without modification in the latter case.

The U. S. Corps of Engineers siphoned continously through a small bore tube into a chamber containing a commercial conductivity cell connected to a recording meter (Ref. 5). They were testing a tidal river model where conductivity fluctuations were small compared to those in a turbulent saltwater jet and the conductivity recordings were used to monitor tidal reversals.

Ellison and Turner siphoned samples through a simple conductivity cell consisting of two lengths of stainless steel hypodermic tubing joined by a sleeve of polythene so that there was a small gap between the ends of the tubes (Ref. 31). The hypodermic tubes were connected in series with an A. C. voltage source and a current meter so forming

an elementary series type conductivity meter. No mention was made of fluctuations in meter reading when this system was used in a turbulent saltwater jet. It is probable that the meter was very sensitive to the wide fluctuations in conductivity present in such jets and that an estimate by eye of the mean meter reading was required.

It was decided that continuous withdrawal sampling in conjunction with conductivity measurements warranted further investigation as this method is quicker than the analysis of discrete samples.

A3.3.3 Conductivity Measurement with a Directly Exposed Probe

The quickest method of obtaining a mean density traverse in a turbulent saltwater jet is to measure the conductivity with a small conductivity cell or probe exposed directly to the flow. The probe must be small relative to the dimensions of the saltwater flow being investigated for two reasons. Firstly to minimise flow disturbance and secondly for low spatial resolution; that is the probe must sense the conductivity of a relatively small volume of liquid if "point" density measurements are to be obtained. Probes small enough for use in hydraulic laboratory models are not commercially available and have to be made for the particular project in hand.

The impedance of the probe is measured by either a conductivity bridge or series type conductivity meter; both these systems have been described previously.

Exposed Probe with Conductivity Bridge

Several investigators have used a directly exposed probe in conjunction with a conductivity bridge. Lofquist used a probe with two fine platinum wires connected to a recording conductivity bridge but made no attempt to analyse the recorder trace to obtain mean point densities (Ref. 68). Harleman et al used a probe made by fixing small platinised platinum electrodes to a 1/16 inch diameter stainless steel tube for a model estuary investigation (Ref. 46). The probe formed one arm of a simple Wheatstone bridge circuit with A. C. excitation while another arm acted as the load resistance for a recording oscillograph. The bridge was balanced at a station where a vertical profile of density was required at the maximum density for that station. The bridge was thrown out of balance at other points on the profile of density less than the maximum and the bridge output was recorded by the oscillograph. This is the "out of balance" method of operating a conductivity bridge with a directly exposed probe. A check on density readings was obtained by withdrawing discrete samples at the mid depth at each probe station. No details were given of the processing of the wavering trace on the oscillograph chart but it is suspected a mean density reading was obtained by averaging by eye. It is doubtful whether this procedure would be suitable for recordings from a turbulent saltwater jet where the conductivity fluctuations are

of an order of magnitude greater than in an estuary model.

Harleman et al mention several other important effects when using a directly exposed probe. They found that the probe electrodes had to be platinised to mitigate polarization effects (this is common practice with commercially available conductivity cells). They also noted that conductivity readings were reduced when working close to a boundary due to interference of the electrical current flow lines between electrodes. The experimental flume in which they were working with several probes simultaneously contained aluminium screens which provided a low resistance current path between probes and resulted in interference between probe readings. This interference was eliminated by grounding the screens and this caused an increase in apparent conductivity by a factor of about two.

Harleman et al also reported that they checked the probe calibration after each vertical traverse at a particular station. This leads one to suspect that considerable calibration drift was occurring, probably due to excessive current flow between electrodes which was necessary with the simplified electronics employed.

Rumer has described a conductivity probe with bridge detection used in a study of dispersion of dilute saltwater through a porous column (Ref. 89). Two square platinum foil electrodes were attached by protruding wires to a perspex supporting rod to form the probe. The probe

formed one arm of an A. C. bridge and the bridge out of balance was detected by a recording oscillograph. The level of conductivity fluctuations in this situation was low so that the oscillograph trace was practically steady. Probe calibration was performed in situ by filling the porous column with salt solutions of various densities and the calibration curve was linear for the very small salt concentrations ($\left(\frac{\Delta\rho}{\rho}\right)_o$ = 0.15 pc.) used. The probe calibration during a test was checked by measuring the conductivity of a few samples withdrawn from the vicinity of the electrodes with a commercial conductivity bridge.

Frankel and Cumming attempted to use a directly exposed probe with stainless steel electrodes and conductivity bridge detection in an ocean outfall model (Ref. 35). The conductivity measurements were made in the jet formed by discharging freshwater into a tank of saltwater of $\left(\frac{\Delta\rho}{\rho}\right)_o$ = 2.5 per cent. They found that drift in probe calibration and temperature effects prevented reliable correlation between density and conductivity measurement. They were forced to abandon this fluid system and to discharge a jet of fresh water containing a very small concentration of salt as a tracer ($\left(\frac{\Delta\rho}{\rho}\right)_o$ = 0.03 per cent) into a tank of sugar solution. Although probe instability is overcome, sugar solutions have two objectional features; firstly they take some days to clear after mixing and, secondly, they are subject to clouding bacterial growths. Probe calibration remained constant at this lowered

salinity although temperature variations were found to affect the conductivity readings. It is interesting to note that Frankel and Cumming claimed that conductivity varied by 10 pc. per ^{o}C and not 2 pc. per ^{o}C as generally accepted. The conductivity bridge output was amplified and fed to a chart recorder. The recorder traces were processed on a semi automatic GOATchart scanning device to obtain mean readings and a cumulative frequency distribution of density fluctuations. Even with the chart scanning device the amount of work involved to obtain a mean density reading at a point was considerable. As the level of turbulence in Frankel and Cumming's model was probably close to that in the proposed model, it was apparent that the amount of work involved to obtain a series of mean density profiles would be formidable.

Gibson and Schwarz have reported a system for determining the fluctuating component of conductivity at a point in a turbulent salt-water flow (Ref. 37). Their "single electrode" probe consisted of a very fine platinum wire (0.002 to 0.0004 inch diameter) fixed in a glass holder with a tapered epoxy resin tip. The exposed cross section of the wire acted as the point electrode and it was platinised to avoid polarization effects. An earthed wall of the experimental water tunnel acted as the distant electrode so that the system detected conductivity fluctuations in a very small volume of liquid surrounding the probe tip. Detection of conductivity fluctuations

was by a bridge circuit in conjunction with other sophisticated commercial electronic instruments. The apparatus was used for an investigation of equilibrium spectra behind a square mesh in a water tunnel (Ref. 38). Dilute saltwater of $\left(\frac{\Delta\rho}{\rho}\right)_o$ about 0.2 per cent was introduced through fine holes in the mesh and the conductivity fluctuations were taken as the scalar measure of turbulence. No details of calibration or probe stability were given.

Gibson and Schwarz's circuitry could probably be modified to yield mean point densities but the electronic instrumentation would be too expensive for the present investigation.

Exposed Probe with Series Type Conductivity Meter

Keulegan has described a preliminary investigation of a conductivity probe with copper electrodes monitored by an elementary series type conductivity meter (Ref. 58). The probe was connected in series with an A.C. source and ammeter while a voltmeter was connected in parallel with the probe. This circuit was used for calibrating the probe in saltwater solutions but the performance of the probe in a practical model was not tested. Keulegan found that the probe was reasonably stable once a layer of reddish-brown compound had been allowed to form on the electrode surfaces. The conductivity of saltwater was found to vary by 2 pc. per ^{o}C.

Prausnitz and Wilhelm developed a miniature conductivity probe

and associated electronics for measuring both the mean and turbulent components of a small volume of electrolyte in the vicinity of the probe electrodes (Ref. 78). This was the forerunner of a similar but superior system developed by Lamb et al so only the latter work will be reviewed in detail (Ref. 64).

Lamb et al used a miniature probe with a "point and ring" electrode system. The point electrode consisted of the cross sectional end of a 26 gauge platinum wire while the ring electrode was a platinum wire ring of exposed area 0.04 square inches. The point electrode wire was coaxial with the polar axis of the ring electrode while both were held in position by polymer resin compound. The lead wires from the electrodes were passed through a stainless steel tube which was earthed to provide a preferential path to ground of any stray current and so minimise the effect of any earthed conductors in the vicinity of the probe. This point and ring electrode system measures the conductivity of a very small volume of fluid in the vicinity of the point electrode where the electrical current lines are concentrated so that, for practical purposes, the conductivity measurement is at a "point".

The electronics system was rather sophisticated. Briefly, the probe was connected in series with an A.C. source providing a carrier wave and a load resistor to form the probe circuit. Variations

in conductivity of the liquid in the vicinity of the point electrode then resulted in amplitude modulation of the carrier wave. The output from the probe circuit was amplified, demodulated and then processed to provide a mean conductivity and a mean square conductivity reading. Some of the electronic instruments, for example the wave analyser, used in the circuitry were not available for the present investigation. Lamb et al investigated the spatial resolution of the probe but did not report any practical use or calibration drift investigation.

Kiser has outlined in brief a conductivity measuring system similar to that of Lamb et al (Ref. 61). His conductivity probe was a "single electode" type similar to that of Gibson and Schwarz which utilises the grounded wall of the metal model tank as the distant electrode. The electronic circuitry was similar to that of Lamb et al except that the components required for measuring the turbulent component of conductivity fluctuations were omitted as only mean point densities were required. Nevertheless some of the commercial electronic instruments used were expensive and not available for the present project. The apparatus was used in a model of an axisymmetric submerged jet of very dilute saltwater released in a tank of saltwater of slightly lower density so that density difference effects were negligible. No calibration details were given.

The literature reviewed indicated that the use of an exposed

probe to detect mean conductivity at a point in a turbulent saltwater jet would be either tedious or require complex electronics. If a simple conductivity bridge such as that of Frankel and Cumming is used then the processing of recorder chart traces is formidable. Also the simplified electronics require high electrical current densities at the probe electrode surfaces which lead to calibration drift. On the other hand, if a series type conductivity meter such as that of Lamb et al is used to detect the conductivity sensed by the probe then expensive instruments are required to process the signal electronically in order to obtain a mean reading.

The series type conductivity meter system has the advantages, however, that a mean density reading at the probe location is obtained quickly and directly and this is desirable for performing a series of traverses through a turbulent saltwater jet. In view of these advantages, it was decided that an attempt to simplify the electronics of Lamb et al would be justified.

A3. 3. 4 Other Methods

The addition of a foreign tracer, such as a dye, is sometimes used in saltwater-freshwater mixing studies for detection of mean point densities.

Keulegan, for example, withdrew discrete samples in the vicinity of the interface of a stream of freshwater flowing over a pool

of dyed saltwater (Ref. 59). The samples were placed in a crude colorimeter consisting of a parallel sided glass jar, a light source, and a photoelectric cell connected to a milliammeter. The colorimeter was calibrated by using samples of known dilution. Andre, in a discussion of salt dilution methods of stream gauging, has pointed out that this simple type of colorimeter has many disadvantages (Ref. 3). The instrument is relatively insensitive and subject to errors due to drift in lamp brilliance and instability of the photoelectric cell and galvanometer. A more complex colorimeter which compensates for these sources of error is commercially available but costs approx. £ 400.

Ippen et al and Schiesser and Lapidus have used colorimetric analysis of discrete withdrawn samples in studies involving zero density difference i.e. freshwater-freshwater mixing processes. (Refs. 53, 92).

Hart reported colorimetric analysis of discrete withdrawn samples in an ocean outfall model (Ref. 49). A dark blue ink was added to the freshwater jet being discharged into a model tank containing saltwater ($\left(\frac{\Delta\rho}{\rho}\right)_o$ = 2.5 per cent). Samples comprised of 1 pc. dyed freshwater and 99 pc. saltwater were readily detectable by a commercial colorimeter.

The fluorescent dye Rhodamine B has been used by Csanady in a turbulent diffusion study in Canada (Ref. 24). A concentrated dye

solution was released continuously in a lake and the resulting dye plume sampled from a boat. The sample was drawn continuously through a Turner fluorometer equipped with a chart recorder. The minimum dye concentration recorded was about 0.02 mgm. per litre although this was by no means the minimum sensitivity of the instrument as the plume could not be followed far enough to utilise the highest sensitivity range. According to Andre Rhodamine B has certain disadvantages as a flow tracer (Ref. 3). It is unstable when exposed to sunlight and, more importantly, causes permanent discolouration of even normally inert materials such as glass, stainless steel and aluminium. This latter disadvantage probably precludes Rhodamine B from use in an hydraulic laboratory.

Radioactive isotopes are probably the most efficient tracer material. Glaser and Lichensten have used a radioactive tracer in a laboratory study of fluid dispersion and time residence in a packed column (Ref. 39). They claim that the main advantage of radioactive tracers compared to salts and dyes is the ease with which peak to background ratios from 100 to 1 to 5,000 to 1 may be readily measured. On the other hand, radioactive tracers have several disadvantages; they are costly, they require special handling and disposal techniques, and also require complex electronic detection equipment.

It was decided that the addition of a flow tracer for density measurement would only be attractive when very small, zero, or negative density difference existed between the receiving liquid and the turbulent saltwater jet. There is no point in using a dye tracer, say, when the electrical conductivity of the saltwater jet may be readily detected as the measure of density at a point in the flow. In any case, for very small, zero, or negative density difference between the jet liquid and the receiving liquid then a system using saltwater as the jet liquid and sugar solution as the receiving liquid (such as used by Frankel and Cumming) is probably better than the use of dye tracers with colorimetric detection. A saltwater-sugar solution liquid system allows density measurements in the usual fashion by conductivity detection.

APPENDIX 4

Main Symbols.

b	Width scale at a jet cross section
C_1, C_2, C_3 etc.	Various constants
D	Internal diameter of body of Bagnold meter
D_B	Diameter of bypass holes of Bagnold meter
D_N	External diameter of nozzle of Bagnold meter
d	Internal diameter of balancing chamber of Bagnold meter
d_N	Bore of nozzle of Bagnold meter
d_p	Bore of opposing flow tube of Bagnold meter
d_T	Bore of head loss tube of Bagnold meter
E	Overall entrainment constant at a jet cross section
E_y	Entrainment constant for inflow in the y direction
E_z	Entrainment constant for inflow in the z direction
F_{op}	Opposing flow force of Bagnold meter
f	Function of
G	Flux of unit weight excess at a jet cross section
G_m	Gap between end of opposing flow tube and mouth of balancing chamber of Bagnold meter
$\frac{G_m}{D}$	Gap ratio of Bagnold meter
g	Acceleration due to gravity

H_{st}	Instantaneous total head at nozzle tip of Bagnold meter
$\bar{H}_{st}$	Temporal mean total head at nozzle tip of Bagnold meter
H'_{st}	Turbulent component of instantaneous total head at nozzle tip of Bagnold meter
$(\bar{H}_{st})_t$	Temporal mean total head registered by pitot tube in turbulent flow
h	Height scale at a jet cross section
K	Flux of density excess at a jet cross section
$\frac{K}{\bar{\rho}}$	Flux of relative density excess at a jet cross section
k	Equivalent sand grain roughness of boundary plane
$\frac{k}{R_h}$	Relative roughness of boundary plane
L	Length of head loss tube of Bagnold meter
L_E	Length of ring electrode of Bagnold meter
L_N	Axial length of nozzle of Bagnold meter
p_s	Instantaneous static pressure at nozzle tip of Bagnold meter
$\bar{p}_s$	Temporal mean static pressure at nozzle tip of Bagnold meter
p'_s	Turbulent component of instantaneous static pressure at nozzle tip of Bagnold meter
$\bar{p}'_s$	Increase in $\bar{p}_s$ registered by a static tube in turbulent flow
p_{ST}	Instantaneous stagnation pressure at nozzle tip of Bagnold meter
Q	Volumetric flow rate at a jet cross section

Q_o Volumetric flow rate of injected denser fluid at the orifice

Q_p Volumetric flow rate through opposing flow tube of Bagnold meter

Q_t Volumetric flow rate through head loss tube of Bagnold meter

R_{eo} Reynolds number at the orifice

R_{e-} Local Reynolds number at a jet cross section

R_h Hydraulic radius of the orifice

R_i Local Richardson number at a jet cross section

R_{io} Richardson number at the orifice

R_{io-} Alternative Richardson number at the orifice

r Radius at a point in Bagnold meter nozzle

r_N Internal radius of nozzle of Bagnold meter

S Angle of inclination of sloping boundary plane to the horizontal

S_i Distance travelled by interface in balancing chamber of Bagnold meter

s Space between mouth of balancing chamber and ring electrode of Bagnold meter

T_F Temperature of freshwater supply for Bagnold meter

t Time after application of H'_{st} at nozzle tip of Bagnold meter

t_E Time for interface to traverse ring electrode of Bagnold meter

V_N Mean velocity in nozzle of Bagnold meter

$V_{Nmax.}$	Ultimate mean velocity in nozzle of Bagnold meter
v	Mean velocity in a three dimensional jet flow
v_F	Mean velocity in opposing flow tube of Bagnold meter
v_i	Inflow velocity of ambient fluid into jet
v_N	Centreline velocity in nozzle of Bagnold meter
$v_{Nmax.}$	Ultimate centreline velocity in nozzle of Bagnold meter
v_s	Instantaneous velocity of oncoming saltwater at nozzle tip of Bagnold meter
$\bar{v}_s$	Temporal mean velocity of oncoming saltwater at nozzle tip of Bagnold meter
$(\bar{v}_s)_T$	Temporal mean velocity registered by a pitot tube in turbulent flow
v_s' , u_s' , w_s'	Turbulent components of velocity of saltwater at nozzle tip of Bagnold meter
$\sqrt{(\bar{v_s'})^2}$	Root mean square of turbulent velocity components of oncoming saltwater at nozzle tip of Bagnold meter
v_t	Mean velocity in head loss tube of Bagnold meter
$v_x v_y v_z$	Mean velocity components in direction indicated by subscript
v_{xmax}	Velocity scale at a jet cross section
X, Y, Z	Cartesian co-ordinates, origin at virtual origin of jet
x, y, z	Cartesian co-ordinates, origin at orifice
x_{Hvo}	Distance in x direction from orifice to virtual origin of jet
z_{vvo}	Distance in z direction from boundary plane to virtual origin of jet

γ_s	Unit weight of saltwater at nozzle tip of Bagnold meter
ΔH	Head loss through head loss tube of Bagnold meter
$\Delta \bar{v}_s$	Increase in $\bar{v}_s$ registered by a pitot tube in turbulent flow
$\Delta\rho_{mean}$	Density scale at a jet cross section
$\frac{\Delta\rho}{\rho}$	Relative density excess at a point in the jet
$\left(\frac{\Delta\rho}{\rho}\right)_o$	Relative density excess at the orifice
ϵ	Dimensionless width parameter locating a point in jet
η	Dimensionless height parameter locating a point in the jet
θ_H	Angle of lateral spread of jet
θ_v	Angle of normal spread of jet
λ	Dimensionless time parameter for commencement of laminar flow in a cylindrical tube
μ	Viscosity of ambient fluid
μ_F	Viscosity of freshwater supply for Bagnold meter
μ_s	Viscosity of saltwater at nozzle tip of Bagnold meter
ν_F	Kinematic viscosity of freshwater supply of Bagnold meter
ν_s	Kinematic viscosity of saltwater at nozzle tip of Bagnold meter
ρ	Density of ambient fluid
ρ_F	Density of freshwater supply of Bagnold meter
ρ_s	Temporal mean density of saltwater at nozzle tip of Bagnold meter
$\rho+\Delta\rho$	Density at a point in jet

$\rho + \Delta\rho_o$ Density of injected denser fluid

ϕ Function of

APPENDIX 5

References.

1. Aagaard E. E., and van Haagen R. H., "A Probe Type Induction Conductivity Cell". Marine Sciences Instrumentation, Vol. 2, Inst. Soc. of America, 1962, pp. 11-17.

2. Abbott D. E., and Kline S. J., "Experimental Investigation of Subsonic Turbulent Flow over Single and Double Backward Facing Steps". Trans. A. S. M. E. V. 84, Series D, 3, Sept. 1962, pp. 317-325.

3. Andre H., "Hydrometrie Pratique des Cours d'Eau, Jaugeages par la Methode de Dilution". (In French), E. N. S. E. H. R. M. A., Section Hydraulique, Faculte de Sciences de Grenoble, Certificat de Potamologie, 1964, 88 pp.

4. Anon., "Thermometers, Hydrometers and Scientific Instruments". Catalogue No. 808, C. F. Casella and Co., London, 1955, 176 pp.

5. Anon., "Hydraulic and Salinity Verification, Report No. 1, Delaware River Model Study". TM2-337, Corps of Engineers U. S. Army, Waterways Experiment Station, Vicksburg, May 1956, 25 pp. + 74 plates.

6. Anon. "Manual on Industrial Water and Industrial Waste Water" A. S. T. M. Spec. Tech. Publn. No. 148-E, 2nd Edn. 1960, 653 pp.

7. Anon., "Progress Report No. 1. "Coastal Engineering Laboratory, Tech. Univ. of Denmark, Jan. 1961.

8. Anon., "Reference Manual of Transistor Circuits". Mullard-Australia Pty. Ltd., Sydney, 2nd Edn. 1961, 308 pp.

9. Anon., "Description of the Propeller Current Meter and the Mimosa Apparatus." Publn. 30, Hyd. Lab. Delft, Aug. 1963, 7 pp.

10. Anon., "Mullard Conductivity Bridge Type E. 7566/3; Equipment Manual". Mullard Equipment Ltd. London, circa 1963, 20 pp + 1 circuit.

11. Anon., "Applications of the Heat Flux System in Low Temperature Gases and Liquids". Tech. Bull. No. 4, Thermo Systems Inc., Minneapolis, Minn., Circa 1964, pp. 1-42.

12. Anon., "Midget Current Meter". Data Sheet M2134, Etablissements Neyrpic, Grenoble, 2 pp.

13. Bagnold R. A., "Measurement of Very Low Velocities of Water Flow." Nature, N. 4260, June 23, 1951, pp. 1025-1027.

14. Balakrishna S., and Srinathkumar S., "Pressure Transducers using Linear Differential Transformer". Nat. Aer. Lab., Bangalore, TN SE-3-63, July 1963, 7 pp + 6 figs.

15. Bowden K. F., "Measurements of Turbulence Near the Sea Bed in a Tidal Current." J. Geophys. Res., V. 67, N. 8, July 1962, pp. 3181-3186.

16. Cartier R. J., "Precision Liquid Manometry". Insts. and Control Systems, V. 35, N. 4, April 1962, pp. 114-115.

17. Chalupnik J. D., and Green P. S., "A Doppler Shift Ocean Current Meter." Marine Sciences Instrumentation, Vol. 1, Inst. Soc., of America, 1962, pp. 194-199.

18. Clayton B. R., and Farmer E. G., "An instrument for Measuring Low Fluid Velocities." J. Sci. Insts., V. 40, 1963, pp. 579-582.

19. Clutter D. W., Smith A. M. O., and Brazier J. G., "Techniques of Flow Visualization using Water as the Working Medium". Report No. ES29075, Douglas Aircraft Co., El Segundo, April 1959, 83 pp.

20. Clutter D. W., and Smith A. M. O., "Flow Visualization by Electrolysis of Water." Aerospace Eng'g., V. 20, N. 1, Jan. 1961, pp. 24-27, 74-76.

21. Cole E. S., and Cole E. S., "Pitot Tubes in Large Pipes". Trans. A. S. M. E., V. 61, 1939, pp. 465-473.

22. Corrsin S., "Turbulence: Experimental Methods." Chapter in "Encyclopedia of Physics," Vol. VIII/2, Fluid Dynamics II, Springer-Verlag, Berlin, 1963, pp. 524-590.

23. Crow T. W., "The use of Thermistors to measure the Velocity of Flowing Water." Unpubl. B. E. Thesis, School of Civil Engineering, The University of New South Wales, Jan. 1962, 78 pp.

24. Csanady G. T., "Turbulent Diffusion in Lake Huron". J. F. M. V17, Pt. 3, Nov. 1963, pp. 360-384 + 4 plates.

25. Daily J. W., and Hardison R. L., "Rigid Particle Suspensions in Turbulent Shear Flow: Measurement of Total Head, Velocity and Turbulence with Impact Probes." M. I. T. Hydrodynamics Lab. Rep. 67, April 1964, 73 pp + 59 pp. Appendices.

26. Davar K. S., and Cermak J. E., "Characteristics of Diffusion Plumes for a Point Source within a Turbulent Boundary Layer." Air and Water Pollution, V. 8, N. 6/7, July 1964, pp. 339-354.

27. Dedow H. R., and King R. F., "Miniature Liquid Flow Meter". Engineering, V. 178, N. 4626, 24th Sept. 1954, pp. 396-398.

28. Dudgeon C. R., "Flow of Water through Coarse Granular Materials" Report No. 76, Water Research Laboratory, The University of New South Wales, Dec. 1964, 109 pp.

29. Eagleson P. S., Huval C. J., and Perkins F. E., "Turbulence in the Early Wake of a Fixed Flat Plate." M. I. T. Hydrodynamics Lab., T.R. No. 46, Feb. 1961, 65 pp.

30. Eagleson P. S., and van de Watering W. P. M., "A Thermistor Probe for Measuring Particle Orbital Speed in Water Waves". M. I. T. Hydrodynamics Lab., Rep. 61, Sept. 1963, 50 pp.

31. Ellison T. H., and Turner J. S., "Turbulent Entrainment in Stratified Flows." J. F. M., V. 6, Pt. 3, Oct. 1959, pp. 423-448.

32. Eskinazi S., "Turbulence Measurement in Electrically Conducting Fluids." Phys. Fluids, V. 1, N. 2, March-April 1958, pp. 161-162.

33. Folsom R. G., "Review of the Pitot Tube". Trans. A. S. M. E. V. 78, N. 7, Oct. 1956, pp. 1447-1460.

34. Foster D. N., and Stone D. M., "Ocean Disposal of Ash." Uni. N. S. W., Water Research Laboratory Report No. 65, Jan. 1963, 130 pp.

35. Frankel R. J., and Cumming J. D., "Turbulent Mixing Phenomena of Ocean Outfalls." Univ. of California, Hyd. Eng. Lab. Rep. HEL-3-1, Berkely, Feb. 1963, 71 pp + 40 figs.

36. Frenzen P., "A Laboratory Investigation of the Lagrangian Autocorrelation Function in a Stratified Fluid." ANL. Report 6794, Argonne National Lab., Illinois, Nov. 1963, 168 pp.

37. Gibson C. H., and Schwarz W. H., "Detection of Conductivity Fluctuations in a Turbulent Flow Field." J. F. M., V. 16, Pt. 3, July 1963, pp. 257-364.

38. Gibson C. H., and Schwarz W. H., "The Universal Equilibrium Spectra of Turbulent Velocity and Scalar Fields." J. F. M. V. 16, Pt. 3, July 1963, pp. 365-384 + 2 plates.

39. Glaser M. B., and Lichensten I., "Interrelation of Packing and Mixed Phase Flow Parameters with Liquid Residence Time Distribution." A. I. Ch. E. Journal, V. 9, N. 1, Jan. 1963, pp. 30-34.

40. Goldstein S., "Modern Developments in Fluid Dynamics" Vol. I, 1st Edn., Oxford University Press, 1938.

41. Grant H. P., and Kronauer R. E., "Fundamentals of Hot Wire Anemometry." A. S. M. E. Hyd. Div. Proc. Symp. "Measurement in Unsteady Flow," Worcester, Mass. May 1962, pp. 44-53.

42. Grant H. L., Stewart R. W., and Moillet A., "Turbulence Spectra from a Tidal Channel." J. F. M., V. 12, Pt. 2, 1962, pp. 241-268.

43. Grossman L. M., and Charwat A. F., "The Measurement of Turbulent Velocity Fluctuations by the Method of Electromagnetic Induction." Rev. Sci. Insts., V. 23, N. 12, Dec. 1952, pp. 741-747.

44. Hama F. R., "Streaklines in a Perturbed Shear Flow". Phys. of Fluids, V. 5, N. 6, June 1962, pp. 644-650.

45. Hardy R. C., "NBS Viscometer Calibrating Liquids and Capillary Tube Viscometers" NBS Monograph 55, Dec. 1962, 22 pp.

46. Harleman D. R. F., McDougall D. W., Galvin C. J., and Hoopes J. A., "An Analysis of One-Dimensional Convective Diffusion Phenomena in an Idealised Estuary." M. I. T. Hydrodynamics Lab. Tech. Rep. 42, Jan. 1961, 32 pp.

47. Harris G. S., "An Inclined Plume." Proc. A. S. C. E., V. 91, N. EMI, Feb. 1965, pp. 7-18.

48. Harris G. S., "A Cold Tip Velocity Meter." J. Sci. Insts., V. 42, 1965, (in press).

49. Hart W. E., "Jet Discharge into a Fluid with a Density Gradient." J. Hyd. Div. Proc. A. S. C. E., V. 87, N. HY6, Part I, Nov. 1961, pp. 171-200.

50. Huggins L. F., "A Microdifferential Pressure Transducer" Ag. Eng'g. V. 43, N. 9, Sept. 1962, pp. 529-531.

51. "Hydraulic Models", A. S. C. E. Manuals of Engineering Practice No. 25, A. S. C. E., 1942, 110 pp.

52. Ippen A. T., and Raichlen F., "Turbulence in Civil Engineering; Measurements in Free Surface Streams" J. Hyd. Div. Proc. A. S. C. E., V. 83, N. HY5, Oct. 1957, pp. 1392-1 to 1392-27.

53. Ippen A. T., Harleman D. R. F., and Lin J. D., "Turbulent Diffusion and Gravitational Convection in an Idealized Estuary." M. I. T. Hydrodynamics Lab. Tech. Rep. 38, March 1960, 33 pp.

54. Johnson M. A., "Physical Oceanography - Turbidity Currents." Science Progress, V. 2, N. 198, April 1963, pp. 257-273.

55. Jonsson I. G., "Measurements in the Turbulent Wave Boundary Layer". Proc. 10th Congress, I. A. H. R., London, Vol. I, 1963, pp. 85-92.

56. Kemp J. F., "The Leon Tube; An Instrument for Measuring Flow Speeds in Water". J. Sci. Insts., V. 34, Oct. 1957, pp. 390-392.

57. Kemp J. F., "Liquid Manometer with Electromagnetic Balance Indicator." J. Sci. Insts., V. 36, Feb. 1959, pp. 77-81.

58. Keulegan G. H. "The Determination of Salinities in Tests on Density Currents". 4th Progress Report on Project 48, Model Laws for Density Currents, U. S. Dept. Commerce, Nat. Bur. St'ds. Report 6. 5P-48, Oct. 1949, 46 pp. + 15 figs.

59. Keulegan G. H., "Interfacial Instability and Mixing in Stratified Flows". U. S. Dept. Commerce, Nat. Bur. St'ds. Res. Pap. RP2040, V. 43, Nov. 1949, pp. 487-500.

60. King L. V., "On the Precision Measurement of Air Velocity by Means of the Linear Hot Wire Anemometer." Phil. Mag., V. 29, Series 6, 1915, pp. 556-577.

61. Kiser K. M., "Material and Momentum Transport in Axisymmetric Turbulent Jets of Water." A. I. Ch. E. Journal, V. 9, N. 3, May 1963, pp. 386-390.

62. Kolin A., "Electromagnetic Velometry, I. A Method for the Determination of Fluid Velocity Distribution in Space and Time." J. Appl. Phys., V. 15, N. 2, Feb. 1944, pp. 150-164.

63. Kolupaila S., "Bibliography of Hydrometry." Univ. Notre Dame Press, Indiana, 1961, 975 pp.

64. Lamb D. E., Manning F. S., and Wilhelm R. H., "Measurement of Concentration Fluctuations with an Electrical Conductivity Probe." A. I. Ch. E. Journal, V. 6, N. 4, Dec. 1960, pp. 682-685.

65. Lincoln J. H., Paquette R. G., and Rattray M., "Microsalinometer for Oceanographic Model Studies." Dept. Oceanography Tech. Rep. 26, Univ. Washington, March 1954.

66. Ling S. C., and Hubbard P. G., "The Hot-Film Anemometer: A New Device for Fluid Mechanics Research." J. Aer. Sci., V. 23, Sept. 1956, pp. 890-891.

67. Lion K. S., "Pressure Transducer Survey". A. S. M. E., Hyd. Div., Proc. Symp. "Measurement in Unsteady Flow", Worcester, Mass., May 1962, pp. 9-14.

68. Lofquist K., "Flow and Stress Near an Interface between Stratified Fluids." The Physics of Fluids, V. 3, N. 2, Mar.-Apr. 1960, pp. 158-175.

69. Lukasik S. J., and Grosch C. E., "Velocity Measurements in Thin Boundary Layers". TM. No. 122, Davidson Lab., Stevens Inst. of Tech., New Jersey, Oct. 1959, 30 pp.

70. Lumley J. J., "The Constant Temperature Hot-Thermistor Anemometer." A. S. M. E. Hyd. Div. Proc. Symp. "Measurement in Unsteady Flow", Worcester, Mass. May 1962, pp. 75-82.

71. Macagno E. O., and Rouse H., "Interfacial Mixing in Stratified Flow". J. Eng. Mech. Div. Proc. A. S. C. E., V. 87, N. EM5, Oct. 1961, pp. 55-80.

72. Maytin I. L., "Development of a Variable Reluctance Velocity Meter". J. Hyd. Div. Proc. A. S. C. E., V. 87, N. HY1, Jan. 1961, pp. 95-102.

73. Morton B. R., Taylor G. I., and Turner J. S., "Turbulent Gravitational Convection from Maintained and Instantaneous Sources." Proc. Roy. Soc. London, V. 234, Series A, N. 1196, Jan. 1956, pp. 1-23.

74. Morton B. R., "Forced Plumes." J. F. M., V. 5, Pt. 1, Jan. 1959, pp. 151-163.

75. Parnell J. P., Johnson A. E. and Raymont J. E., "An Investigation into the Effects of Warmed Water from Marchwood Power Station into Southhampton Water". Proc. I. C. E., V. 23, Sess. 1961-2, Sept. 1962, pp. 35-62.

76. Peube J. L., "On a Differential Manometer of High Sensitivity and its Applications." (in French), C. R. Acad. Sci. Paris, V. 259, Nov. 7, 1964, pp. 3180-3182.

77. Piquemal J., and Truchasson C., "Principle of a New Method of Measuring Velocities and its Application to Water." (in French) C. R. Acad. Sci. Paris, V. 259, Group 2, 14 Sept. 1964, pp. 1808-1809.

78. Prausnitz J. M., and Wilhelm R. H., "Turbulent Concentration Fluctuations Through Electrical Conductivity Measurements." Rev. Sci. Insts., V. 27, N. 11, Nov. 1956, pp. 941-943.

79. Prych E. A., Harty F. R., and Kennedy J. F., "Turbulent Wakes in Density Stratified Fluids of Finite Extent". M. I. T. Hydrodynamics Lab. Rep. 65, July 1964, 65 pp.

80. Rands J. B., and Bigg P. H., "Hydrometers and Hydrometry". Notes on Applied Science No. 25, National Physical Laboratory. H. M. S. O., 1961, 31 pp.

81. Ranz W. E., "Electrolytic Methods of Measuring Water Velocities." A. I. Ch. E. J., V. 4, N. 3, Sept. 1958, pp. 338-342.

82. Rasmussen R. A., "Application of Thermistors to Measurements in Moving Fluids." Rev. Sci. Insts., V.33, N. 1, Jan. 1962, pp. 38-42.

83. Reiss L. P., and Hanratty T. J., "An Experimental Study of the Unsteady Nature of the Viscous Sublayer." A. I. Ch. E. J., V. 9, N. 2, March 1963, pp. 154-160.

84. Reverseau J., "The Use of Thermistors to Measure Very Low Velocities in Liquids." (in French), Le Genie Civil, 15 Sept., 1959 (Water Research Laboratory Translation).

85. Richardson E. G., "Measurements of Water Flow and Pressure Set up by Ships in Motion." Trans. N. E. Coast Instn. Eng's. and Shipbuilders, V. 64, 1948, pp. 273-288, D141 - 144.

86. Rosler R. S., and Bankoff S. G., "Large Scale Turbulence Characteristics of a Submerged Water Jet." A. I. Ch. E. J., V. 9 N. 5, Sept. 1963, pp. 672-676.

87. Rothfus R. R., Walker J. E., and Whan G. H., "Correlation of Local Velocities in Tubes, Annuli and Parallel Plates." A. I. Ch. E. J., V. 4, N. 2, June 1958, pp. 240-245.

88. Rouse H., Yih C. S., and Humphreys H. W., "Gravitational Convection from a Boundary Source." Tellus, V. 4, N. 3, Aug. 1952, pp. 201-210.

89. Rumer R. R., "Longitudinal Dispersion in Steady and Unsteady Flow." J. Hyd. Div. Proc. A. S. C. E., V. 88, N. HY4, Part I, July 1962, pp. 147-172.

90. Runstadler P. W. Jr., "Stable Operation of Hot Film Probes in Water." A. S. M. E. Hyd. Div. Proc. Symp. "Measurement in Unsteady Flow," Worcester, Mass., May 1962, pp. 83-84.

91. Saunders P. M., "Penetrative Convection in Stably Stratified Fluid". Tellus, V. 14 N. 2, 1962, pp. 177-194.

92. Schiesser W. E., and Lapidus L., "Further Studies of Fluid Flow and Mass Transfer in Trickle Beds." A. I. Ch. E. Journal, V. 7, N. 1, Mar. 1961, pp. 163-171.

93. Schlichting H., "Boundary Layer Theory." McGraw Hill, New York, Edn. 4, 1960, 647 pp.

94. Schoeneck H., and Wanninger W., "Rapid and Accurate Determination of Liquid Densities with Hydrostatic Balances." (In German). Wissenschaftliche Abhandulgen der Physikalisch-Technischen Bundesanstalt, V. 12, N. 2, 1960, pp. 175-178. (C. S. I. R. O. Translation No. 5709.)

95. Schraub F. A., Kline S. J., Henry J., Runstadler P. W. Jr., and Littell A., "Use of Hydrogen Bubbles for Quantitative Determination of Time Dependent Velocity Fields in Low Speed Water Flows." Report MD10, Thermosciences Div., Dept. Mech. Eng'g., Stanford University, Feb. 1964, 55 pp.

96. Seddon A. E., and Anwar H. O., "Measuring Fluid Velocities Optically." Engineering, V. 196, N. 5081, 6 Sept. 1963, pp. 318-319.

97. Sharp B. P., "A Flow Measuring Device Depending on the Drag Developed on a Wire Suspended in Water." Report CER62BBS73, Colorado State University, Civil Engineering Dept., Dec. 1962, 39 pp.

98. Stevens R. G., Borden A., and Strausser P. E., "Summary Report on the Development of a Hot Wire Turbulent Sensing Element for use in Water." U. S. Navy Dept., David W. Taylor Model Basin, Res. and Dev. Rep. 953, Dec. 1956, 18 pp.

99. Szalay M., "Laboratory Measurement of Water Velocity with Spheres". (In Hungarian). Hidrologiai Kozlony (Hydrological Organ), V. 40, N. 3, 1960, pp. 204-206 (C. S. I. R. O. Trans. No. 5739).

100. Szymanski F., "Quelques Solutions Exactes des Equations de L'Hydrodynamique de Fluide Visqueux dans le cas d'un Tube Cylindrique". Proc. 3rd Intern. Congr. Appl. Mech., Stockholm, I, 1930, p. 249. (Not available in Australia).

101. Tan H. S., and Ling S. C., "Final Stage Decay of Grid Produced Turbulence." TAR-TR 628, Therm Inc. Adv. Res. Div., Ithica, July 1962, 22 pp.

102. Tritton D. J., "The Use of a Fibre Anemometer in Turbulent Flows". J. F. M., V. 16, Pt. 3, June 1963, pp 269-281.

103. Verhagen C. J., Palm J. P., Van Der Ster J., Van Genderen W., and Veltman B. P. "Construction and Properties of Subminiature Pressure Pickups." Appl. Sci. Res., Sect. B, V. 3, N. 6, 1954.

104. Veprek J. A., "A Thermistor Flow Meter". J. Sci. Insts., V. 40, 1963, pp. 66-68.

105. Veprek J. A., "The Tandel; a New Element for Measuring Thermal Conductivity, Pressure and Velocity of Gases". J. Sci. Insts., V. 42, N. 4, April 1965, pp. 252-255.

106. Williams T. J., "Pulsation Errors in Manometer Gauges". Trans. A. S. M. E., V. 78, N. 7, Oct. 1956, pp. 1461-1469.

107. Wills J. A. R., "The Correction of Hot-Wire Readings for Proximity to a Solid Boundary." J. F. M., V. 12, N. 3, March 1962, pp. 388-396.

108. Yarnell D. L., and Nagler F. A., "Effect of Turbulence on the Registration of Current Meters." Trans. A. S. C. E., V. 95, 1931, pp. 765-795.

Errata.

Page	Line	Correction
(v)	7	Figure 26 follows page 45
(vi)	25	Figure 53 follows page 102
	27	Figure 54 follows page 105
6	12	Change than the to than of
58	1	Change experiment to experimental
59	4	Change trubulent to turbulent
62	13	Change price to Price
71	18	Change Poiseville to Poiseuille
73	11	Insert inverse between the and slope
85	1	Change Poiseiulle to Poiseuille
91	10	Change budge to bridge
93	2	Change literative to literature
129	19	Change catinary to catenary
133	13	Change centimetric to centimetre
138	13	Change he to the
150	16	Change devloped to developed

KEY WORDS: density current; density measurement; hydraulics; hydraulic model; self similarity; velocity measurement

ABSTRACT: The results from a hydraulic laboratory model of a three dimensional density current were presented. Overall flow characteristics were investigated for 21 density currents on slopes of 10^{o} and 20^{o}. Velocity and density measurement techniques were described in detail. Detailed measurement of one turbulent density current were used to examine an extended self similarity hypothesis and the variation of characteristic cross section properties in the direction of flow.

REFERENCE: Fietz, T.R. "The Measurement of Characteristics of a Three Dimensional Density Current", Rep. 85, Water Research Laboratory, University of New South Wales, April 1966, 19 pp. + 63 figs.

KEY WORDS: density current; density measurement; hydraulics; hydraulic model; self similarity; velocity measurement

ABSTRACT: The results from a hydraulic laboratory model of a three dimensional density current were presented. Overall flow characteristics were investigated for 21 density currents on slopes of 10^{o} and 20^{o}. Velocity and density measurement techniques were described in detail. Detailed measurements of one turbulent density current were used to examine an extended self similarity hypothesis and the variation of characteristic cross section properties in the direction of flow.

REFERENCE: Fietz, T.R., "The Measurement of Characteristics of a Three Dimensional Density Current". Rep. 85, Water Research Laboratory, University of New South Wales, April 1966, 19 pp. + 63 figs.

KEY WORDS: density current; density measurement; hydraulics; hydraulic model; self similarity; velocity measurement

ABSTRACT: The results from a hydraulic laboratory model of a three dimensional density current were presented. Overall flow characteristics were investigated for 21 density currents on slopes of 10^{o} and 20^{o}. Velocity and density measurement techniques were described in detail. Detailed measurements of one turbulent density current were used to examine an extended self similarity hypothesis and the variation of characteristic cross section properties in the direction of flow.

REFERENCE: Fietz, T.R., "The Measurement of Characteristics of a Three Dimensional Density Current". Rep. 85, Water Research Laboratory, University of New South Wales, April 1966, 19 pp. + 63 figs.